LINEAR AND NONLINEAR VISCOELASTIC CHARACTERIZATION OF PROTON EXCHANGE MEMBRANES AND STRESS MODELING FOR FUEL CELL APPLICATIONS

Kshitish A. Patankar

Dissertation submitted to the faculty of the Virginia Polytechnic Institute and State University in partial fulfillment of the requirements for the degree of

Doctor of Philosophy

In

Macromolecular Science and Engineering

David A. Dillard, Chair

Michael W. Ellis, Co-Chair

Scott W. Case

Yeh-Hung Lai

Robert B. Moore

Herve′ Marand

02 July 2009
Blacksburg, VA

Keywords: proton exchange membrane fuel cell, hygrothermal viscoelastic characterization, mechanical durability, hygrothermal stresses, fracture energy of proton exchange membranes, nonlinear viscoelasticity, Schapery modeling

Linear and Nonlinear Viscoelastic Characterization of Proton Exchange Membranes and Stress Modeling for Fuel Cell Application

Kshitish A. Patankar

ABSTRACT

In this dissertation, the effect of temperature and humidity on the viscoelastic and fracture properties of proton exchange membranes (PEM) used in fuel cell applications was studied. Understanding and accurately modeling the linear and nonlinear viscoelastic constitutive properties of a PEM are important for making hygrothermal stress predictions in the cyclic temperature and humidity environment of operating fuel cells. In this study, Nafion® NRE 211, Gore-Select® 57, and Ion Power® N111-IP were characterized under various humidity and temperature conditions. These membranes were subjected to a nominal strain in a dynamic mechanical analyzer (DMA), and their stress relaxation behavior was characterized over a period of time. Hygral master curves were constructed noting hygral shift factors, followed by thermal shifts to construct a hygrothermal master curve. This process was reversed (thermal shifts followed by hygral shifts) and was seen to yield a similar hygrothermal master curve. Longer term stress relaxation tests were conducted to validate the hygrothermal master curve. The Prony series coefficients determined based on the hygrothermal stress relaxation master curves were utilized in a linear viscoelastic stress model.

The nonlinear viscoelastic behavior of the membranes was characterized by conducting creep tests on uniaxial tensile specimens at various constant stress conditions and evaluating the resulting isochronal stress-strain plots. The nonlinearity was found to be induced at relatively moderate stress/strain levels under dry conditions. To capture the

nonlinearity, the well known Schapery model was used. To calculate the nonlinear parameters defined in the Schapery model, creep/recovery tests at various stress levels and temperatures were performed. A one-dimensional Schapery model was developed and then validated using various experiments.

The fracture properties were studied by cutting membranes using a sharp knife mounted on a specially designed fixture. Again, various temperature and humidity conditions were used, and the fracture energy of the membranes was recorded as a function of cutting rate. Fracture energy master curves with respect to reduced cutting rates were constructed to get some idea about the intrinsic fracture energy of the membrane. The shift factors obtained from the fracture tests were found to match with those obtained from the stress relaxation experiments, suggesting that the knife cutting process is viscoelastic in nature. The rate and temperature dependence for these fracture energies are consistent with the rate, temperature, and moisture dependence of the relaxation modulus, suggesting the usefulness of a viscoelastic framework for examining and modeling durability of fuel cell membranes. The intrinsic fracture energy was initially thought to be a differentiating factor, which would separate various membranes tested in this study from one another. However, it was later found that all the membranes tested showed similar values at lower cutting rates, but showed significant variation at higher reduced cutting rates, and thus was thought to be a more meaningful region to differentiate the membranes for durability understanding.

While the preceding work was undertaken to characterize as-received commercial PEMs, it is possible to modify material properties through treatment processes including thermal annealing and water treatment. The transient and dynamic viscoelastic properties

of water-treated Nafion membranes revealed unusual behavior. Such unusual properties might have originated from irreversible morphological changes in PEM. Besides the constitutive viscoelastic properties, another set of properties useful for the stress modeling is the hygral strain induced as a function of relative humidity (RH) The effect of pretreatment on hygral strains induced as a function of RH was also investigated. These studies suggest that pretreatment significantly changes the mechanical properties of proton exchange membranes.

Acknowledgement

I wish to thank my advisor Dr. David Dillard firstly for accepting me in his group and giving me a chance to work in an intellectually stimulating environment. I thank him for everything he has offered in the past three and half years to cultivate my interests in exploring many things. He is a great mentor, colleague and friend. I especially acknowledge his encouraging attitude and commending of my work at every step of this process. I would also like to thank my co-advisor Dr. Michael Ellis for his constant support, encouragement and guidance. He and Dr. Scott Case have always been a source of many ideas, for which I am grateful to. I thank Dr. Yeh-Hung Lai for his continuous support and guidance. I especially want to thank him for numerous candid discussions on problems I encountered. I also thank Dr. Robert Moore and Dr. Herve Marand for numerous helpful discussions and for their interest in my work.

I am grateful to the rest of the GM-VT fuel cell membrane research team for the teamwork that has fostered the exceptional interdisciplinary work. I'm truly proud of being part of the team. Thanks must go to the Fuel Cell Research Lab of General Motors R&D for valuing this work and providing financial support. Special thanks to Yongqiang Li for numerous discussions and suggestions on a number of issues, and being a liaison for Virginia Tech after he graduated.

I would also like to thank Melissa Nipper and Beverly Williams for keeping our lives a little more organized. Many thanks to the machine shop folks Dave Simmons and Darrell Link for their help on numerous occasions.

Finally I want to appreciate and thank my family for their constant encouragement and words of wisdom throughout my career.

Table of Contents

List of Figures

List of Tables

CHAPTER 1: Introduction

In recent years, the demand for environmentally friendly and cost effective alternatives to traditional power sources has grown significantly. As a result many industries have invested considerable resources in finding new methods of power production. One of the new technologies that has been under investigation for quite some time is fuel cell technology (FC). Proton exchange membrane-based fuel cells (PEMFCs) are being investigated with great interest by various automotive industries as a primary or secondary (hybrid) vehicle power-train component due to their fast start-up time, clean by-product (water), and favorable power-to-weight ratio. In spite of potentially being more environmentally friendly and efficient, there are a number of barriers which must be overcome in order to utilize the potential of PEMFCs. Besides cost, the durability of various components, especially that of proton exchange membranes (PEMs) poses major concerns for their implementation. The PEM must be sufficiently robust to keep the reactant gases separated throughout the life of the fuel cell stack. The resistance to gas-crossover may decay over time as the membrane thins due to local compression in a fuel cell stack, as cracks and pinholes develop due to repetitive mechanical stress and as the polymer network break-down due to fluoride release. The durability of PEMs is directly related to their mechanical properties. Various ex-situ and in-situ tests have been proposed and used to characterize different aspects of the mechanical properties of PEMs. In this dissertation, we attempt to establish a viscoelastic framework wherein the mechanical durability of PEMs can be examined and modeled. The majority of dissertation consists of five chapters (chapters 3 through 7) prepared for journal publication.

When a proton exchange membrane (PEM) based fuel cell is placed in service, hygrothermal stresses develop within the membrane and vary widely with internal operating environment. These stresses associated with hygrothermal contraction and expansion at the operating conditions, are believed to be critical in the overall performance of the membrane. Understanding and accurately modeling the viscoelastic constitutive properties of a PEM is important for making hygrothermal stress predictions in the cyclic temperature and humidity environment present in operating fuel cells. Therefore both linear and nonlinear viscoelastic properties are extremely important while considering the short and long term durability of the membranes. Such constitutive properties relating stress, strain, temperature and moisture content are necessary to understand and analyze the failure modes; improving design features; and optimizing design features. Linear viscoelastic behavior was studied by subjecting the membranes to a small (maintaining linearity) uniaxial strain, and allowing them to relax in a dynamic mechanical analyzer (DMA) at various temperature and humidity conditions. The hygral and thermal master curves were constructed recording shift factors to construct a hygrothermal master curve. The thermal shift factors were fit using the well-known WLF equation, while the hygral shift factors were fit with a polynomial in temperature and relative humidity (RH). The hygrothermal master curve was fit with a Prony series that could later be used in the recursive stress prediction program as well as in the finite element modeling. Dynamic tests were also conducted in conjunction with the transient stress relaxation tests, and were found to match the modulus predicted by the stress relaxation tests. In order to support the relaxation modulus data obtained as well as to establish confidence in procedure, the creep tests were conducted. Creep compliance

obtained from such tests was compared with stress relaxation modulus obtained under the same conditions using a simple viscoelastic transformation. A side study was conducted to show the evidence of physical aging in Nafion under dry conditions. No aging phenomenon was observed when the relaxation tests were conducted under humid conditions. Discussion of this work on Gore®Select 57 and Nafion® NRE 211 membranes will follow in chapters 3 and 4 respectively.

Nonlinear viscoelastic effects are likely to play a key role when the nominal stresses in membranes exceed linear range and/or in damage localization. Nonlinear effects may also be induced at discontinuities such as cracks or layer terminations. Thus, in order to account for these nonlinear effects, a nonlinear viscoelastic characterization study was performed on PEMs. Constructing isochronal plots based on creep tests established a limit of nonlinearity. It was found that small strain levels could induce nonlinearity in PEMs under dry conditions. Such limit will likely be pushed to higher strain levels at higher humidity conditions and/or higher temperatures. The well-known nonlinear viscoelastic Schapery model was found to capture nonlinearity. The model consists of various nonlinear terms, which were determined by running creep/recovery tests at various stress loading conditions and temperatures. The experimentally determined parameters were then used in a uniaxial model that was validated by a comparison with results from a series of loading-unloading cycles. Good agreement was found between the experimental data and model predictions. Discussion of this will be presented in chapter 5.

Pinhole formation in PEMs may be thought of as a process of flaw formation and crack propagation within membranes exposed to cyclic hygrothermal loading. This crack

propagation process is thought to occur in a slow time-dependent manner under cyclic loading conditions, and is believed to be associated with limited plasticity. The intrinsic fracture energy has been used to characterize the fracture resistance of polymeric materials with limited viscoelastic and plastic dissipation. Insight into of the intrinsic fracture energy may be useful in characterizing the durability of PEMs and particularly their resistance to the formation of pinhole defects. A knife-slit test was applied to collect fracture data with limited plasticity under various temperature/ RH conditions. The fracture energies were also measured for membranes immersed in water. The time temperature moisture superposition principle was used to generate fracture energy master curves plotted as a function of reduced cutting rate based on the humidity and temperature conditions of the tests. Details of the fracture energy study can be found in chapter 6.

Researchers investigating various properties of PEMs often treat the membranes by thermal annealing or water soaking in order to remove the low molecular weight impurities and erase any thermal and morphological history in PEMs. In chapter 7, we investigate transient and dynamic viscoelastic properties of treated PEMs under dry conditions. Such membranes were prepared by heating them in water at various temperatures, followed by drying in vacuum oven. A very unusual viscoelastic behavior was observed as a result of transient and dynamic loading, in the sense that the modulus (both storage and relaxation) was seen to increase until a certain temperature and to decrease for all temperatures above this particular temperature. Possible morphological changes at certain temperatures when the membrane was exposed to water might have triggered the unusual viscoelastic behavior. The effect of pretreatment on hygral strains

induced as a function of relative humidity (RH) changes was also investigated. These studies suggest that pretreatment significantly changes the mechanical properties of proton exchange membranes. In this chapter, we discuss the hygral strains developed in the membranes as a function of the RH. The membranes, when subjected to humid conditions, take up large amount of water and expand significantly. The coefficient of hygral expansion, β (CHE) was measured in the DMA under a nominal creep mode with a preload force of 0.5 mN. The membranes were subjected to various humidity levels at a given temperature, and then at various temperatures. The CHE was measured at a given temperature, and was fit with a cubic polynomial as a function of temperature.

Preconditioning the membranes before conducting stress relaxation or creep tests significantly changes their properties. Details of this investigation can be found in Appendix 1.

In chapter 2, we give a brief literature review pertaining to general aspects of PEMFC, including various properties of PEM (mainly Nafion®). Chapters three through seven also have a background section in which specific literature pertaining to the chapter are discussed.

CHAPTER 2: Literature Review

2.1 Introduction

As natural resources grow scarcer and the environmental constraints on industry grow tighter, it is imperative to find environmentally friendly and cost effective alternative to the traditional power production method. Fuel cell technology has been around for almost two centuries. As early as 1839, Sir William Grove discovered the operating principle of fuel cells by reversing electrolysis of water to generate electricity with hydrogen and oxygen. Francis T. Bacon revisited the experiment performed by Sir Grove in 1939. Bacon modified the design of the fuel cell apparatus to solve liquid flooding and gas bubbling problems between 1946 and 1955, and built a 6 kW fuel cell stack in 1959 [1]. NASA has been using fuel cells in their shuttle program since the 1950s. However, only recently has this technology received attention from the scientific community as a viable power source. The features that brought fuel cells to the forefront of research for the automotive industry include high power density, reduced emissions, fast room temperature start-up, elimination of corrosion problems, noise free operation and lower operating cost [2]. A fuel cell is defined as an electrochemical device that converts chemical energy into electrical energy (and some heat) for as long as fuel and oxidants are supplied. All fuel cells function in the same basic way, i.e., fuel is oxidized at the anode while oxygen is reduced at the cathode, ions are conducted through the ion-conducting but electrically insulating electrolyte while electrons travel through an external circuit to do useful work. The common types of fuel cells, characterized by electrolyte, are alkaline (AFC), proton exchange membrane (PEMFC), phosphoric acid (PAFC), direct methanol (DMFC), molten carbonate (MCFC), and solid oxide (SOFC).

Among these, the first four belong to the low temperature category and typically operate below 200°C, while the remaining two belong to the high temperature category and typically operate at 600°C-1000°C [3, 4]. A summary of different types of fuel cells and their applications can be found in a review paper by Carrette et al. [5].

2.2 Proton Exchange Membrane Fuel Cells (PEMFCs)

PEMFCs are considered to be a promising alternative to rechargeable batteries and to internal combustion (IC) engines. PEMFC vehicles can provide a driving range and refueling time comparable to conventional IC engine powered vehicles. In the terrestrial applications PEMFCs run on air with ambient or slightly higher pressure, and use a sulfonated solid polymer as the electrolyte. They are suitable for transportation applications due to high power density, low temperature operation, easy construction, and elimination of corrosion and electrolyte leakage problems [6].

Generally speaking, a PEMFC is composed of current collector, gas distributor and membrane electrode assembly (MEA). The current collector is usually of common metals such as copper or aluminum. The gas distributor, in the form of a monopolar plate in a single cell and a bipolar plate in a stack, is usually injection molded from a graphite plate with grooved gas channels to transport the reactant gases to the reaction sites. The MEA is an assembly where the electrochemical reaction takes place. The components of a MEA are listed below:

A. Gas diffusion layer (GDL) is often made from carbon fiber or carbon cloth and functions to wick away liquid water, transports reactants, and conducts electrons. It is about 200-300 μm thick. The microporous sublayer (MSL) is a more recent addition to the PEMFC. This layer is composed of small carbon particles and a

fluoropolymer. The MSL is placed between the catalyst layer and the GDL. Varying the loading (thickness) and composition within the MSL can change the performance of a fuel cell drastically [7].

B. Catalyst layer is the region where electrochemical reactions take place. It allows ion conduction and transport of electrons at the same time. Catalyst layer and gas diffusion layer together constitute the electrode. The typical thickness of catalyst layer is about 10 μm.

C. Membrane is the heart of a PEMFC. It should have enough mechanical, chemical and electrical stability to withstand the stringent operating conditions in the fuel cell. It transports the hydrogen ions through the thickness in the presence of water, but is ideally impermeable to gas and electrons. Typical thicknesses for the range of membranes used in fuel cells vary between 18μm-50μm.

The following shows the most accepted reaction mechanism involving hydrogen oxidation and 4-electron reduction for a PEMFC [8]:

Anode:

$2\ Pt\ (s) + H_2 \rightarrow Pt\text{-}H_{ads} + Pt\text{-}H_{ads}$ *slow adsorption*

$Pt\text{-}H_{ads} \rightarrow H^+ + e^- + Pt\ (s)$ *fast reaction*

Cathode:

$Pt\ (s) + O_2 \rightarrow Pt{\cdot\cdot}O_2$ *fast adsorption*

$Pt{\cdot\cdot}O_2 + H^+ + e^- \rightarrow Pt{\cdot\cdot}O_2H$ *rate determining step*

$Pt{\cdot\cdot}O_2H + 3H^+ + 3e^- \rightarrow Pt(s) + 2\ H_2O$ *fast step*

Overall Reaction:

$2\ H_2 + O_2 \rightarrow 2H_2O$

2.2.1. Durability of PEMs

The durability requirement for a PEMFC stack in automotive application is about 5000 hours, in bus applications it is about 20,000 hours, and in stationary applications it is about 40,000 hours [9, 10]. A durability study of the PEMFC involves the theoretical analysis and experimentation. Both are equally important and complimentary. It has been noted that the degradation of the performance of fuel cell is primarily due to the decay of the MEA [11]. In operation, membranes are subjected to a strong acidic environment (pH~2), mechanical compression in the stacks, contamination, high temperature (90°C or so for automotive and stationary applications), and dynamic loading cycles. Along with the membrane, various components of the fuel cell may age, leading to changes in almost all of the system variables; activity and active surface area, exchange current density, membrane proton conductivity, interfacial resistance to name a few [11]. We limit ourselves to discussing the mechanical durability issues of the PEM within a framework of viscoelasticity.

The membrane durability issue has attracted extensive attention in recent years. The early failure of the PEMs (service life < 1000 hours), is usually attributed to structural failure of the membranes resulting from the cracking, tearing, puncturing, mechanical stresses, inadequate humidification and reactant pressure [12]. Tang et al. [13] studied the durability and degradation behavior of Nafion NR 111 under various mechanical, chemical and polarization conditions. They found that the safety limit of the cyclic stress or fatigue strength for NR 111 is about 1.5 MPa, which is about $1/10^{th}$ of the tensile strength. They also showed that cyclic stresses and dimensional changes induced by the water uptake can be substantial and are the main cause of mechanical degradation and failure of the membrane. Hydrogen peroxide (H_2O_2) has been proposed to be another

important factor that leads to the degradation of fuel cell membranes [14]. Peroxide was proposed to form in two different ways, one being oxygen reduction at the cathode according to the following reaction [14]:

$O_2 + 2H^+ + 2e^- \rightarrow H_2O_2$

The presence of H_2O_2 accelerates the degradation of membranes, as they become unstable due to strong oxidative characteristics of H_2O_2. Much of the prior research on chemical degradation has focused on the effect of H_2O_2 on the deterioration of a membrane, typically Nafion, in the presence of counterions such as Ti(III), Fe(II) and Cu(II) [15-17] and halogen ions [18] using ex situ or in situ [19] accelerated degradation protocols. Membranes were characterized for thinning, loss of fluoride, and reduction in proton conductivity using various techniques. Durability studies over a period of one month also revealed the evident membrane degradation ascribed to the decomposition of sulfonic acid groups in the pendent side chains [20].

The behavior and the properties of the membrane depend on the structure of the membrane. For example, the earlier polystyrene sulfonic acid (PSSA) based membranes were found to degrade faster as compared to inert Nafion-type membranes, due to peroxide intermediates attacking tertiary hydrogen at the α-carbon of a PSSA chain, leading to the loss of aromatic rings and sulfonic acid ($SO_3^-H^+$) groups [21]. Stucki et al. [22] proposed a detailed membrane thinning mechanism for fluorinated membranes. They showed that the dissolution of PTFE backbone mainly occurs at the anode side. The gaseous oxygen molecules first dissolve in the membrane, diffuse through the membrane from cathode to anode side and react with hydrogen molecules chemisorbed on platinum surface and generate H_2O_2. Thus the membrane degradation mechanism is influenced by

the permeation of oxygen through the membrane. Also the higher moisture conditions facilitate the transport of oxygen, accelerating the degradation mechanism. However, reducing the operating humidity or low water content can lead to lower proton conductivity, hygral shrinkage, and higher mechanical stresses in the membranes. Having discussed the basics of fuel cell technology and other relevant issues, we move on discuss the membrane materials before we plunge into the viscoelasticity and other fundamental aspects that were studied during this dissertation.

2.2 Proton Exchange Membrane Materials

The following materials were chosen for study: DuPont™ Nafion® NRE 211, Gore™ Gore®Select 57, and Ion Power™ N111-IP. These membranes are all essentially Nafion-type materials, the chemical structure of which is shown in Figure 2.1.

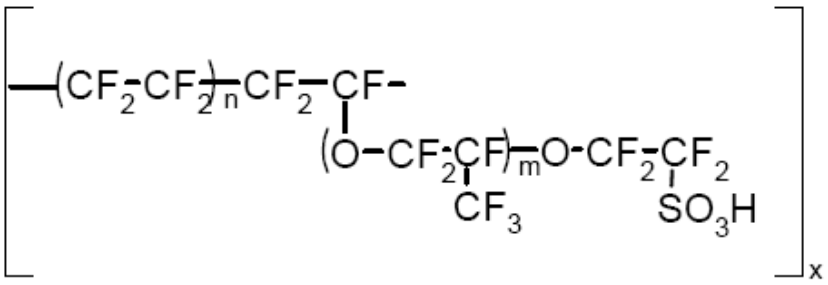

Figure 2.1 The chemical structure of Nafion® type of membrane.

DuPont™ Nafion® NRE 211 membranes are non-reinforced dispersion-cast films based on chemically stabilized perfluorosulfonic acid/PTFE copolymer in the acid (H^+) form. N111-IP membranes are manufactured by the Ion Power, Inc by extrusion process; on the other hand, Gore-Select®57 contains an expanded PTFE mesh as a reinforcing layer. Nafion is widely used in automotive applications where the operating range is about 80°C. While the exact nature of water transport in the PEM is very much an area of active

research, the following explanation is well accepted in the literature. As a result of hydration, negatively charged sulfonated sites are formed, and positive sites such as protons created by hydrogen oxidation reaction, can jump from site to site, permeating through the membrane [23-25]. Liu [6] provides a thorough and comprehensive summary of modeling and experimental research efforts on transport phenomena in PEMFCs. Several representative PEMFC models and experimental studies have been discussed in greater depth. As mentioned earlier, proton conductivity through a membrane depends strongly on its water content. Thus the membrane needs to be hydrated, but at the same time, flooding of the porous electrodes and GDL should be avoided so that reactants can be transported effectively. There are three mechanisms of water transport in the membrane: electro-osmotic drag, diffusion and hydraulic permeation. Liu et al. [26] discuss a good water management scheme that involves controlling these fluxes so that the membrane is kept well hydrated while avoiding flooding. The moisture uptake and drying behavior of Nafion type of membranes has been studied extensively, and the corresponding activation energies measured. The results of the moisture uptake studies on Nafion are summarized in Uan-zo-Li's thesis [27]. Water uptake also depends on the drying process preceding the experiment [28]. The membrane samples that were dried at room temperature showed higher content compared to the samples dried at 105°C, whereas the time required to reach the equilibrium was almost the same. The authors explained this phenomenon by ionic cluster formation and disintegration. The water absorption behavior of sulfonated poly(styrene-ethylene/butylenes-styrene), or commonly known as Dais® membranes was studied by Weiss et al. [29]. They concluded that the water uptake increased with temperature and the extent of sulfonation.

It has been recognized that the water absorbed in hydrophilic polymers does not display the same thermal, diffusive or relaxation characteristics as bulk water [30]. The investigation of water-swollen hydrogels has led researchers to define three states of water: (1) non freezable, bound water. This water is strongly bound to the copolymer and shows no thermal transitions by DSC. This water is principally responsible for a T_g depression of the copolymer; (2) freezable water- water that is loosely bound with the copolymer, but still displays thermal transitions in DSC measurements; (3) free water- water that has the same transitions of bulk water [31]. The characteristics of water absorbed in hydrogels were also investigated by McConville and Pope [32], using ^{1}H NMR T_2 relaxation technique, showed that their results showed two pools of protons, one with long correlation times ("slow" water species) and one with short correlation times ("fast" water species). These two pools of protons are analogues to the concept of free (fast) and bound (slow) water. Kim et al. [33] extended the previous DSC studies by investigating water plasticization of the proton exchange membranes. Transitions around 0°C were observed corresponding to free and frozen bound water, but thermograms were extended to high temperatures to observe the depression in T_g by the absorbed water (Figure 2.2). In Figure 2.2, features of each of the three states of water are visible. The T_g depression caused by tightly bound, non freezable water is denoted by the vertical lines intersecting each scan between 160°C for dry Nafion 1135 and fully hydrated Nafion around 100°C. The presence of bound freezable water becomes apparent at about 11.7% water content where a broad melting peak is observed around 0°C. Free water with a sharp melting peak at 0°C is evident at full hydration.

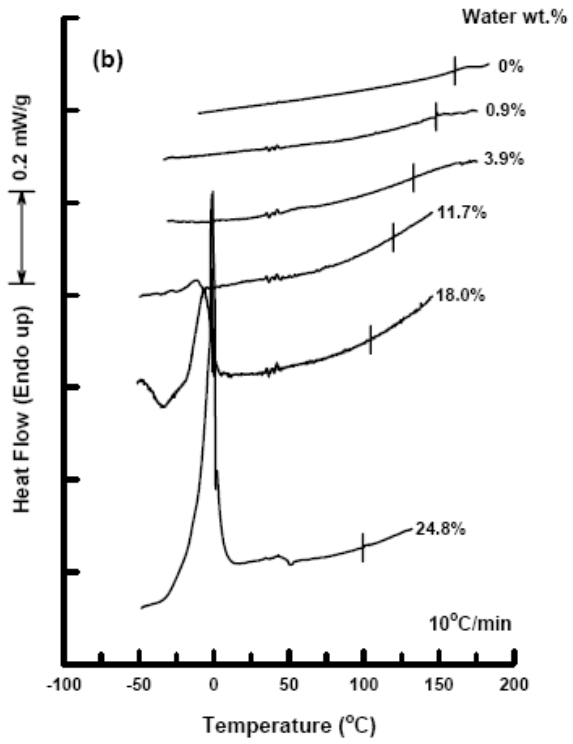

Figure 2.2 DSC thermograms of Nafion 1135 at various water contents [33].

Perflourosulfonate ionomers (PFSIs) are copolymers containing tetrafluoroehtylene and generally less than 15 mol % of perfluorovinyl ether units that are terminated with a sulfonic acid exchange site. The polar perfluoroether side chains containing the ionic sulfonated groups have been shown to organize into aggregates, leading to nanophase-seperated morphology where the ionic domains are distributed throughout the PTFE matrix [34]. In addition, the runs of tetrafluoroehtylene of sufficient length are capable of organizing into crystalline domains having unit cell dimensions identical to those of pure PTFE [35, 36]. The phase-separated morphology containing crystalline and ionic domains has been the focus of several investigations, and the thermo-mechanical behavior of these membranes has been discussed at greater length as

well. An excellent resource on the morphology of Nafion is a review paper by Mauritz and Moore [37]. Numerous morphological studies of Nafion have focused on the small-angle x-ray scattering behavior. With electron density difference between the ionic domains and the PTFE matrix, a scattering maximum appears at $q = 1\text{-}2\ nm^{-1}$, which has been termed as the "ionomer peak" [38]. Several structural models have been proposed in the literature in order to explain the origin of the ionomer peak in Nafion [34, 35, 38-40]. As regards to mechanical and thermal properties, ionomer domains are generally accepted to provide physical cross-links that can inhibit segmental mobility.

A number of differential scanning calorimetry (DSC) studies of dry neutralized PFSI materials have revealed two endothermic peaks below 300°C in the initial heating scan of these materials [41-44], which have been correlated to two distinct mechanical relaxations in Nafion observed at temperatures T_β and T_α [45]. A recent DSC study on the thermal behavior of Nafion membranes revealed two endothermic peaks upon first heating, occurring at 120°C and 230°C. The peak at 120°C did not appear upon reheating, but appeared gradually as the sample was annealed. This peak was thought to occur due to order-disorder transition inside the clusters, while the peak at 230°C was attributed to the melting of the crystallites in Nafion [46]. Mauritz and co-workers [44, 47, 48] used DSC and dielectric spectroscopy to study the Dow PFSIs. They examined the effect of annealing on the DSC and dielectric relaxation of the PFSIs. The DSC thermograms revealed three endotherms that were attributed to the matrix-glass transition temperature, $T_{g,m}$ (215°C-240°C), the ionic domain glass transition, $T_{g,c}$ (282°C) and the melting of crystallites, T_m (332°C-338°C). Changes in DSC thermograms upon annealing at different

temperatures were ascribed to microstructural reorganizations in the matrix and/or the cluster phase.

Eisenberg and co-workers [45, 49] studied the effect of ionization and neutralization on the DMA of Nafion polymers. In early studies, three relaxation peaks ($\alpha > \beta > \gamma$), in the temperature range from -160°C to 150°C, were observed for the acid form of Nafion. Both α and β relaxations were observed to increase by over 100°C when neutralized with alkali salts, while the low temperature relaxation (γ) remained unaffected by neutralization. Because of the strong dependence of water on the β relaxation, the peak was assigned to ionic domain relaxation, while α and γ relaxations were attributed to the glass transition temperature of the fluorocarbon matrix and short-range motions of the $-CF_2-$ backbone, respectively [49]. In a later study, the assignments of α and β relaxations were reversed, while the assignment of γ relaxation remained the same [45]. Having discussed the morphological and water uptake properties of Nafion, we discuss the principles of viscoelasticity. Nafion, being a polymer, is viscoelastic in nature. Thus in order to understand the constitutive properties, one must understand the fundamental aspects of viscoelasticity. Certainly, the subject of viscoelasticity has been around for almost a century. In this review, we intend to discuss the basic ideas of viscoelasticity.

2.3 Principles of Linear Viscoelasticity

Many engineering materials such as polymers and elastomers exhibit time dependent stress and strains. Such flow is accompanied by the dissipation of energy due to some internal loss mechanism. The materials exhibiting such response are viscoelastic in nature, as they exhibit both elastic and viscous properties [50, 51]. The time-dependent strain is characterized by creep compliance and is defined as the ratio of time dependent strain to the applied stress. On the other hand, a ratio of time-dependent strain to the

strain input is referred to as the relaxation modulus. The relaxation and creep phenomenon can occur in tension, compression, or bulk (shear or volumetric) deformations. Combining spring (representing elastic part) and dashpot (representing viscous part) has been thought to be an approximate way to model the behavior of a polymer. A combination of these elements in series is referred to as Maxwell model; while a combination of these elements in parallel is referred to as Voigt or Kelvin model. The differential equation describing linear viscoelastic behavior of a polymer is often used to connect stress and strain, and is given by:

$$\sigma + p_1 \cdot \dot{\sigma} + p_2 \cdot \ddot{\sigma} + \ldots = q_0 \cdot \varepsilon + q_1 \cdot \dot{\varepsilon} + q_2 \cdot \ddot{\varepsilon} + \ldots \quad (1)$$

The number of constants p_i and q_i will depend on the viscoelastic response of the particular material under consideration. It might be sufficient to represent the viscoelastic response over a limited time scale by considering only few terms on each side of Equation 1.

To predict the response of the material to an arbitrary stress or strain history (i.e. stress or strain as a function of time), constitutive equations have been developed. Due to the entropic changes that take place in a viscoelastic system perturbed by a stress/strain field, the response does not vanish when the perturbation field ceases. A consequence of this fact is that the deformation depends not only on the current mechanical state (stress or strain) but also on the previous mechanical history [50-52]. Under the linear viscoelastic behavior, the responses to different perturbations superimpose. This fundamental principle in linear viscoelasticity is called Boltzmann superposition principle. For an isothermal deformation in 1-D and assuming linear viscoelastic behavior, following equations can be given:

$$\varepsilon(t) = \int_0^t D(t-\tau)\frac{d\sigma(\tau)}{d\tau}d\tau \tag{2}$$

where it is understood that the lower limit includes the jump discontinuity in stress at the origin and the stress is expressed as a step function.

$$\sigma(t) = \int_0^t E(t-\tau)\frac{d\varepsilon(\tau)}{d\tau}d\tau \tag{3}$$

where it is understood that the lower limit includes the jump discontinuity in strain at the origin and the strain is expressed as a step function. In Equation (2) and (3), *D* and *E* refer to the creep compliance and relaxation modulus respectively. Similar expressions can be written in terms of shear or bulk modulus or corresponding compliances [52]. These equations are important as they lead to the generalization of the superposition principle. The generalized stress-strain relationship in linear viscoelasticity can be directly obtained from the generalized Hooke's law, by using the correspondence principle. This principle establishes that if an elastic solution to a stress analysis exists, then the corresponding viscoelastic solution can be obtained by substituting for the elastic quantities the s-multiplied Laplace transforms [53-55]. A generalized 3-D relationship between the stress and strain tensors is given by:

$$\sigma_{ij}(t) = 3\delta_{ij}\int_0^t K(t-\tau)\frac{de(\tau)}{d\tau}d\tau + 2\int_0^t G(t-\tau)\frac{de_{ij}(\tau)}{d\tau}d\tau \tag{4}$$

where *e* is defined as an average dilatational strain, K and G refer to the bulk and shear moduli respectively, and δ_{ij} is the Kronecker delta.

Dynamic perturbations typically give responses that are quicker than the transient responses by a couple of decades. Because of the effect of delayed elasticity and viscous

flow in the viscoelastic material, the stress and strain will be out of phase [56]. For example, the strain and stress can be described by a sine function:

$$\varepsilon = \varepsilon_0 \sin(\omega t) \text{and } \sigma = \sigma_0 \sin(\omega t + \delta) \quad (5)$$

where ω is the angular frequency and δ is the phase lag. Based on these equations, storage modulus (E'), loss modulus (E'') and tan δ can be expressed as:

$$E' = \frac{\sigma_0 \cos\delta}{\varepsilon_0}, E'' = \frac{\sigma_0 \sin\delta}{\varepsilon_0}, \tan\delta = \frac{E''}{E'} \quad (6)$$

The complex modulus is given by:

$$E^* = E' + iE'' \quad (7)$$

The real part of complex modulus (E') that is in phase with the strain is referred to as storage modulus as it is associated with the energy stored in the specimen due to applied strain. The imaginary part of complex modulus (E'') that is out of phase with the strain is referred to as loss modulus as it defines the dissipation of energy, and forms the part of energy dissipated per cycle.

2.3.1. Time Temperature Superposition Principle

Before discussing the time temperature equivalence, the regions of an amorphous polymer on a modulus-temperature plot are worth a mention. Amorphous polymeric materials exhibit five different regions of viscoelastic behavior: a glassy region, a glass-rubber transition, a rubbery plateau, a rubbery flow region and a liquid flow region. Glassy region is characterized by only a short range rotations and vibrations of the molecular motions. The glass-rubber transition is characterized by initiation of long range molecular motions (10-50 atoms). The region where the modulus has a greatest dependence upon temperature (maximum magnitude of slope) is called the transition

region [56]. The corresponding temperature, or a narrow temperature range, is referred to as the glass transition temperature (T_g). The other definition will be discussed in reference with the free volume later in the review. Christiansen [53] gives a thorough thermodynamic treatment of the glass transition. He maintains that classical second order transitions commonly observed in metals for example, cannot be used as a model for glass transition in polymers because the reasoning is based on equilibrium thermodynamics, while polymer are dissipative and their behavior is governed by the irreversible thermodynamics [57].

Although linear viscoelastic theory deals with isothermal and homogeneous materials, it is of interest to consider the effect of temperature, pressure and composition on the time-dependent properties of the material. Amongst these, temperature is extremely important, as the viscoelastic response depends heavily on temperature. We shall not discuss the effect of pressure or composition in this review, although excellent treatment can be found in a paper by Tschoegl [54, 55]. An increase in temperature facilitates the conformational transitions about the skeletal bonds, thus allowing the chains to comply with the external perturbation, thereby increasing the free volume of the system, and reducing the friction between the moving segments of the molecular chains. These processes lead to the conclusion that higher temperature increases the free volume and lowers the retardation or relaxation times. In general cases, t and T are considered two independent variables. Figure 2.3 shows the plot of shear modulus as a function of temperature. Shear modulus decays with time at shown at various temperatures.

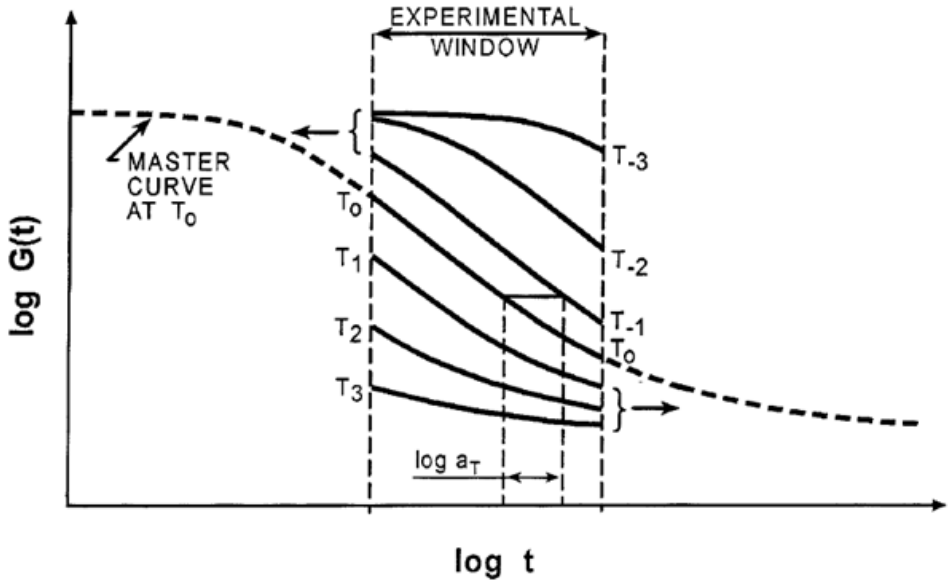

Figure 2.3 Loss of shear modulus of a polymer with time at different temperatures giving rise to the principle of time temperature superposition (TTSP), generating a thermal master curve [55].

A convenient and highly popular shortcut is available if we assume that the effect of temperature on the response times is to change all of them in the same proportion. This is the fundamental basis of a thermorheologically simple material (TSM). In that case, the ratio of the i^{th} response time at the temperature of measurement (T) to the same response time at a reference temperature (T_0) is the same for all the relaxations; or mathematically

$$\frac{\tau_i(T)}{\tau_i(T_0)} = a_T \tag{8}$$

The term a_T is referred to as thermal shift factor. An increase in temperature shortens the response time. Thus, when $T > T_0$, $a_T < 1$. Based on the free volume equation proposed by Doolittle and Doolittle [58], a well known William-Landel-Ferry (WLF) equation was proposed [56], and is given by

$$\log_{10} a_T = \frac{-C_1(T - T_0)}{C_2 + (T - T_0)} \tag{9}$$

where C_1 and C_2 are the constants which can determined experimentally. The shift factors allow the data collected at any temperature to be shifted into superposition with the data recorded at the reference temperature to form a master curve, while the WLF equation provides a fit of the shift factors. It needs to be noted that the WLF equation is applicable to a TSM, and cannot be applied to a multicomponent time-dependent systems, such as block co-polymers or composites, where each component may follow a separate or independent WLF equation. Typically the WLF equation is applicable above the T_g of a polymer, while the Arrhenius equation is more appropriate at temperature below T_g. However, many researchers believe that the superposition manifests itself from the molecular basis, and therefore formulate equations based on activation energy (E) such as Arrhenius equation:

$$\log_{10} a_T = -2.303 \frac{E}{R}\left(\frac{1}{T_0} - \frac{1}{T}\right) \tag{10}$$

where R is the gas constant, T the temperature at which a_T is desired, and T_0 the reference temperature. In the process of constructing a master curve, one more variable must be taken into account [56]. There is a change in the density of the material associated with the change in temperature. Therefore, in order to construct a more accurate master curve, it is necessary to shift the data vertically as well as horizontally to accommodate for a vertical shift that corresponds to a modulus change, and given by $\frac{T_0 \rho_0}{T \rho}$. In regions where the modulus or compliance changes rapidly, it is possible to match the adjacent curves empirically whether they were first shifted vertically In accordance with the factor

$\frac{T_0\rho_0}{T\rho}$ or not shifted at all. In regions where the viscoelastic function is flat, the influence of a vertical shift is much more apparent, and has been demonstrated in cases that such a shift is necessary for satisfactory matching. To best of our knowledge, there have been no references in the literature concerning the vertical shifting in case of Nafion type membranes. Wenbo et al. [59] studied the creep behavior of HDPE under various stress levels and constructed a compliance master curve by applying both horizontal and vertical shifts. Van Gurp et al. [60] claim that the vertical shifts may provide some information about chain stiffness and branching. Although the TTSP was originally developed for amorphous polymers, Nielsen and Landel [61] maintained that it could be applied to semicrystalline polymers, as long as vertical shift factors, also strongly dependent on temperature, are employed. Also the vertical shift factors are largely empirical with little theoretical validity. In case of semicrystalline polymers, a part of vertical shift factor results from the changes in the modulus of elasticity resulting from the change in the degree of crystallinity with temperature [61]. Ward [62] maintains that the TTSP could not be applied to crystalline materials, however Faucher [63] argues that the principle of TTS can be applied to the crystalline domains if their structure is maintained and under sufficiently low strain and the shift factors typically conform to Arrhenius equation. In their work on the frequency and temperature dependence of the dynamic mechanical properties of HDPE, Nakayasu [64] concluded that a simple horizontal shift along the horizontal axis is not sufficient to accurately superimpose dynamic loss compliance data at different temperatures, and vertical shifts were required for the purpose. On the other hand Mark and Findley [65] reported a successful nonlinear creep master curve obtained by only horizontal shifts of LDPE. A linear relationship

between the inverse of temperature and shift factors indicated Arrhenius relationship. Harper and Weitsman [66] stated that the viscoelastic properties of thermorheologically complex (TCM) can be shifted suitably using both horizontal and vertical shift factors. Miller [67] suggested that change in internal structure of the polymer during testing requires adjustment along both horizontal and vertical axes while shifting its viscoelastic properties. Djoković et al. [68] reported that the introduction of a two-process model for stress relaxation in the standard time temperature procedure made possible a distinct study of the viscoelastic properties of the crystalline and amorphous fractions of polyethylene and propylene. By considering the modulus values and the molecular origin of α- and β-relaxations, they concluded that the amorphous phase is thermorheologically simple and crystalline phase is complex. Although the method of TTSP has been shown to be useful in characterizing the rheological properties of a large class of amorphous polymers over a wide range of time, it can only be applied to a much shorter range of time for many crystalline polymers such as Nylons or polyvinyl alcohol (PVA) for example [69]. In case of PVA films, the stress relaxation modulus was plotted against logarithm of time. It was observed that the relaxation curves at various temperatures could not be superimposed even with the vertical shifts along the modulus axis along with the horizontal shifts along the time axis. In case of Nylon 6 films, the relaxation curves below 50°C could be superimposed horizontally to form a smooth master curve, but those above 50°C, could not be superimposed with horizontal translation.

2.3.2. Free Volume and Physical Aging

Even with no applied stress, the mechanical properties of polymers may vary during time due to changes occurring in the molecular structure. Variations due to changes in molecular packing are called physical aging and changes due to modification

of the inter/intra-molecular bonding are referred to as chemical aging. Physical aging effects are thermoreversible while chemical aging effects are not [70]. In this review, we focus only on physical aging.

Physical aging can be explained by invoking the free volume theory, which when put in a simple terms, states that, in order to have molecular motions, there needs to be free volume or "holes" between the chains. According to Sperling [71], the free volume at the T_g (f_g) is constant for all the viscoelastic materials and is 2.5%. The value of f_g really depends on the constant C_1 in the WLF equation. These values were originally taken to be universal for all amorphous polymers with C_1 = 17.44 and C_2 = 51.6. It was later found that C_1 value was indeed approximately constant for all systems but C_2 varied quite widely. This means that f_g is approximately constant at a value of 2.5%. When a polymer is formed or quenched in a glassy state, the chains are randomly packed, especially long chains, or chains with sterically hindered structures pack more loosely, giving rise to higher free volume. As the polymer "ages", the chains tend to pack in an orderly manner, giving rise to lower and lower free volume. The process of shrinkage of free volume is referred to as physical aging (Figure 2.4).

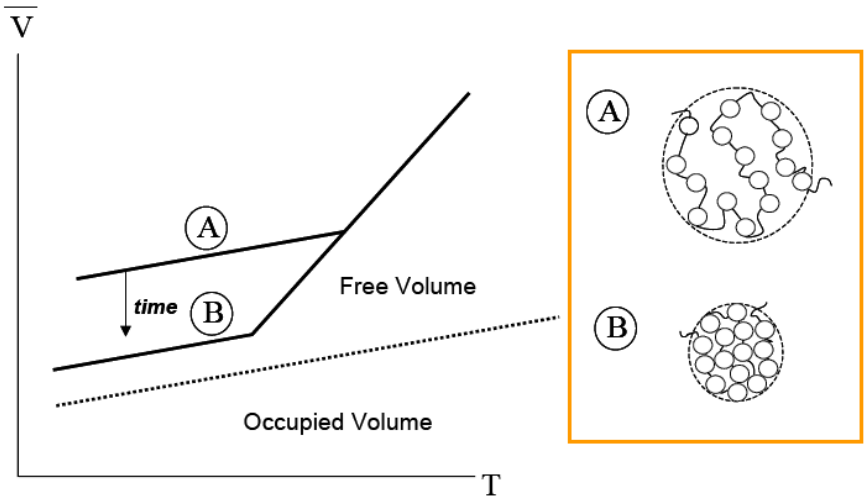

Figure 2.4 Physical aging in a polymer.

Physical aging affects the time scale of the mechanical relaxation properties of glassy systems. Viscoelastic rate processes slow down with aging time. Thus, transient viscoelastic functions such as stress relaxation and creep compliance shift toward longer times when plotted as a function of logarithm of time [72, 73]. In general, the importance of physical aging increases as the temperature approaches the transition temperature. Horizontal shifts of the isotherms obtained in the aging processes combined with suitable vertical shifts give master curves that permit the prediction of the viscoelastic behavior of aged systems over a wide interval of time. When the temperature of the aged glass is increased above the glass transition temperature, the aging effects are erased, making the aging process reversible. In ideal conditions, a change in temperature causes each retardation (or relaxation) time to be shifted by the same amount and the amount of shift due to change in temperature is independent of that due to the departure from the equilibrium [74]. It was noted that at aging temperature far below T_g, the aging continues for the duration of experiments, and at temperature closer to T_g, the aging seemed to

cease at some time t^* that might be expected to be an equilibrium time for the glass [73, 75].

2.3.3. Thermorheological Simplicity and Complexity

There is a special type of temperature dependence of mechanical properties which is amenable to analytical description of TTSP and which applies to a wide variety of materials. This class of materials is referred to as being thermorheologically simple (TSM) [50, 53, 76]. When temperature shift factors are a function of temperature only, resulting in a master curve by shifting the entire relaxation modulus data horizontally parallel to the time axis, the polymer is referred to as a TSM. For a TSM, a change in temperature is equivalent to a shift of behavior on the log time or log frequency axis, and a constitutive relationship is given by a Boltzmann integral. In essence, the assumption of TSM behavior requires that all viscoelastic relaxations are accelerated by the same amount by a given increase in temperature. Haddad [50] and Christensen [53] give a detailed mathematical description of a TSM under constant and non-constant temperature states. Of special consequence and relevance to thermal and humidity cycles in PEM, is the mathematical treatment on non-constant temperature states. Under non-constant temperature state, the effects cannot be described by the first order linear theory. Although this idealization is a useful concept and often applies across several decades of material response, the concept often fails to apply across the full spectrum of viscoelastic relaxations, which inevitably involve molecular motions on different length scales. For example, the activation energy for long chain motion associated with an alpha transition is often larger than that associated with shorter range motion involved in the beta or gamma relaxations. Thus a material can behave as a TSM over a narrow time window, but may fail to do so over a wider range [76]. For a thermorheologically complex

material (TCM) response, the temperature dependence cannot be incorporated through a single shift factor and the curves do not overlap. For a TCM, shift factors are not just functions of temperature but also of time, in that short time response may shift differently than long time response [77].

A TCM is the class of viscoelastic materials whose temperature dependence of mechanical properties is not particularly responsive to the analytical description through the TTSP. Schapery [78] proposed two classes of such materials, namely TCM-1 and TCM-2. TCM-1 materials would be a composite system consisting of two or more TSM phases. The case of a TCM-1 under a constant temperature has been studied by Halpin [79] and Fesco and Tschoegl [77]. The case of a TCM-1 under transient temperature is complicated, and has been discussed to a greater extent in papers by Schapery [78, 80]. The TCM-2 class of materials is defined by the following uniaxial constitutive relationship for the cases of constant or transient temperature [81]:

$$\varepsilon(t,T) = D_0(T)\sigma_0 + \int_0^t \Delta D\left(\xi - \xi'\right)\frac{d}{dt'}\left[\frac{\sigma}{a_G(T)}\right]dt' \qquad (11)$$

where $D_0(T)$ is the initial value of creep compliance, $a_G(T)$ is a new shift factor for the class of material defined and ξ, ξ' are reduced time parameters. This theory paved way to a well-known universal theory of nonlinear viscoelasticity proposed by Schapery.

2.4 Nonlinear Viscoelasticity

There is a long line of researchers working in the field of nonlinear viscoelasticity, and an excellent resource is a book by Findley, Lai and Onaran [82]. However, we do not discuss various theories proposed by researchers before Schapery in this review. Schapery [78, 80, 81, 83, 84] formulated a universal nonlinear viscoelastic

model. This model assumes the nonlinear stress dependent behavior of a material may be characterized in a manner similar to the traditional TTSP used for linear viscoelastic materials. The stress dependence is shown by a systematic compression or expansion of the time scale. Schapery's theory assumes that the nonlinear stress or strain dependent behavior may be characterized in a manner similar to the traditional TTSP where the applied stress, or strain systematically compresses or expands the time scale. He has provided a review of experimental results, and has presented the theoretical results for a variety of nonlinear viscoelastic materials. These results support the validity of the derived constitutive equations. Based on his thermodynamic theory, Schapery formulated nonlinear constitutive equations. When stress is treated as an independent variable, the theory yields the following equation:

$$\varepsilon(t) = g_0 D_0(t)\sigma(t) + g_1 \int_0^t \Delta D\left(\psi - \psi'\right) \frac{d\left(g_2 \sigma(\tau)\right)}{d\tau} d\tau \tag{12}$$

where $D_0(t)$ and $\Delta D(\psi)$ are the components of creep compliance. The reduced time variables ψ and ψ' are defined as:

$$\psi = \psi(t) = \int_0^t \frac{dt'}{a_\sigma} \text{ and } \psi = \psi(\tau) = \int_0^\tau \frac{dt'}{a_\sigma} \tag{13}$$

The nonlinear parameters are functions of stress and temperature (could also be a function of humidity). At sufficiently small values of stress, all these parameters take the value of unity.

Smart and Williams [85] compared Schapery's method to the modified superposition principle (MSP) and to the Bernstein-Kearsley-Zapas (BKZ) theory [86]. The MSP theory separates creep behavior into time dependent and stress dependent parts.

The time dependence of applied load is factorable from the load dependence; specifically, the modulus is multiplied by a damping function. The damping function has a value of unity for small loads, representing linear viscoelastic behavior, and decreases as the applied load increases. The MSP theory is simple to implement, but the predicted stress output based on input strain history is poor. Popelar et al. [87] analyze a comprehensive data obtained from stress relaxation and constant strain tests. The relaxation datasets are used to develop the nonlinear model, and the nonlinear response is characterized by Schapery's model. At low strains, the nonlinear model based on relaxation data predicts the stress-strain response in agreement with the experimentally measured response. The discrepancies at higher strain rates are possibly due to viscoplastic effects that are not incorporated into the model. A special case of the Schapery model is the 'free-volume' approach by Knauss and Emri [88, 89] The underlying assumption is that the free volume, although not explicitly defined in the papers, controls the molecular mobility, directly affecting the time scale of the material. Knauss and Emri describe the shift factor in terms of temperature, solvent concentration and mechanical dilatation by:

$$a = a(T, c, \theta) \tag{14}$$

where T, c and θ stand for temperature, concentration and mechanical dilatation respectively. Assuming that the change in fractional free volume due to these variables is additive, and with further mathematical manipulation, the cumulative shift factor can be expressed as:

$$\log_{10} a(T, c, \theta) = \frac{-B}{2.303 f_0} \frac{\alpha\Delta T + \gamma c + \delta\theta}{f_0 + \alpha\Delta T + \gamma c + \delta\theta} \tag{15}$$

where α, γ, δ are in general constants, but could be functions of T, c and θ. Instead of using the Doolittle equation, which the abovementioned theories used, Shay and

Carruthers [90] used a thermodynamic equation of state to establish the interrelation between temperature, specific volume and pressure. Thus, in all the above cases, free volume serves as a unifying parameter describing the nonlinearity through the reduced time. These free volume based model predict that the shear behavior should always be linear, which clearly is not the case. Popelar and Liechti [91, 92] proposed a distortion-modified free volume theory, which takes into account the distortional effects in the inherent time scale of the material along with the dilatational effects. Accepting that shear and distortional contributions to the reduced time is appropriate and necessary, they extended the free volume concept to allow for the reduced time to be sum of dilatational and distortional effects.

In this review, we have tried to discuss various aspects of PEMs as well as fundamentals of linear and nonlinear viscoelasticity. In chapters 3 through 7, we will review some specific aspects of Nafion type PEM that are relevant to the chapter.

CHAPTER 3: Hygrothermal Characterization of the Viscoelastic Properties of Gore-Select® 57 Proton Exchange Membrane

Manuscript prepared for Mechanics of Time-Dependent Materials

3.1 Abstract

When a proton exchange membrane (PEM) based fuel cell is placed in service, hygrothermal stresses develop within the membrane and vary widely with internal operating environment. These hygrothermal stresses associated with hygral contraction and expansion at the operating conditions are believed to be critical in membrane mechanical integrity and durability. Understanding and accurately modeling the viscoelastic constitutive properties of a PEM are important for making hygrothermal stress predictions in the cyclic temperature and humidity environment of operating fuel cells. The tensile stress relaxation moduli of a commercially available PEM, Gore-Select® 57, were obtained over a range of humidities and temperatures. These tests were performed using TA Instruments 2980 and Q800 dynamic mechanical analyzers (DMA), which are capable of applying specified tensile loading conditions on small membrane samples at a given temperature. A special humidity chamber was built in the form of a cup that encloses the tension clamps of the DMA. The chamber was inserted in the heating furnace of the DMA and connected to a gas humidification unit by means of plastic tubing through a slot in the chamber. Stress relaxation data over a temperature range of 40-90°C and relative humidity range of 30-90% were obtained. Thermal and hygral master curves were constructed using thermal and hygral shift factors and were

used to form a hygrothermal master curve using the time temperature moisture superposition principle. The master curve was also constructed independently using just one shift factor. The hygrothermal master curve was fit with a 10-term Prony series for use in finite element software. The hygrothermal master curve was then validated using longer term tests. The relaxation modulus from longer term data matches well with the hygrothermal master curve. The long term test showed a plateau at longer times, suggesting an equilibrium modulus.

Keywords: Proton exchange membranes, polymer electrolyte membranes, fuel cell, viscoelastic characterization, mechanical durability, hygrothermal stresses, dynamic mechanical analyzer, Gore-Select®57, stress relaxation, time temperature moisture superposition principle, doubly shifted master curve

3.2 Introduction

Proton exchange (or polymer electrolyte) membrane fuel cells (PEMFCs) have received considerable attention from various government and private organizations interested in developing a cleaner source of energy for portable and automotive applications, and to a lesser extent, for stationary installations. PEMFCs offer significant advantages in terms of energy and power density, higher efficiency and cleaner power [93, 94]. However, there are still a number of barriers that must be overcome in order to utilize the full potential of PEMFCs in automotive applications. According to US Department of Energy targets for year 2010, PEM-based fuel cells for transportation applications should perform consistently and reliably for 5000 hours at operating temperatures ranging from -40°C to 80°C [9]. This requirement imposes stringent conditions on the durability of automotive fuel cells [13].

In an operating fuel cell, the PEM must readily allow proton transport through the membrane, while preventing the reactant gases from mixing. Proton exchange membranes are very hydrophilic, as they must be sufficiently hydrated for efficient proton transport. Commercial membranes may expand 22% in volume when fully hydrated [2], with concomitant dimensional changes. When constrained in a fuel cell, substantial hygrothermal stresses develop as moisture and temperature vary during operation. These stresses are believed to significantly affect the durability of the membrane. Accurately predicting the stresses in proton exchange membranes in operating fuel cells is a challenging barrier to wider commercialization of PEM fuel cells.

In a conventional fuel cell stack, the membranes are compressed between layers of bipolar plates and gas diffusion media, effectively constraining them against lateral movement. With in-plane shrinkage and swelling in a non-constrained membrane ranging from -4% to 10%, significant and nominally equal biaxial in-plane stresses will result when such membranes are constrained in a fuel cell stack [95]. Accurate constitutive characterization of the PEM is essential for making stress predictions in the transient humidity and temperature environment of an operating fuel cell. An understanding of these hygrothermal stresses in the PEM is important for developing life prediction models to estimate durability and improve operation.

One concern from a durability standpoint is pinhole formation, which can lead to crossover of reactant gases, localized heating, failure of the membrane, and ultimately failure of the fuel cell stack [96-98]. The mechanisms surrounding formation of these pinholes are complex and not yet fully understood. Nonetheless, these pinholes could form as a result of the combination of mechanical stresses in a constrained membrane due

to humidity and temperature cycles and chemical dissolution of the ionomer [95]. This emphasizes the need for appropriate constitutive models to accurately predict the stresses that develop in operating fuel cells. Several references cited in the literature, have focused on enhancing the mechanical durability of the PEM at higher temperatures and reducing the swelling, such as by adding inorganic fillers and crosslinking [99-101]. Such membranes show some improvement at room temperature and ambient humidity. However, durability at high temperature and humidity levels is still questioned [102].

Bauer *et al.* [102] measured the mechanical properties of the Nafion® 117 using a dynamic mechanical analyzer (DMA) at elevated temperatures and higher humidity conditions. They concluded that although water acts as a plasticizer, at elevated temperature it stiffens the membrane by forming hydrophilic clusters. Some of the early work measuring the viscoelastic properties of the PEM includes the measurement of loss tangent tan δ as a function of water content [103]. Bauer *et al*. [104] and Young *et al.* [105] reported the mechanical properties of dry Nafion® with inorganic fillers using the DMA, and found high stiffness and low loss tangent at elevated temperatures.

The time temperature superposition principle (TTSP) is well established and has been successfully applied to a wide range of polymeric materials, although exceptions do exist [56]. Time is the most common quantity used for shifting viscoelastic properties, but other factors such as diluents concentration, stress level, and blend ratios have also been successfully used for shifting behavior in log time [70]. The use of multiple shifting variables to create a "doubly shifted" master curve has been used and reported in literature. Diamant *et al*. [106] reported the stress-strain properties of butadiene rubber with various filler content loading by changing temperature and strain rate. Doubly

shifted master curves with respect to temperature and strain rates were constructed for breaking stress. A similar study was performed by Sumita *et al*. on nylon 6 with varying filler content. The yield stress as defined by authors, was measured as a function of temperature and filler content [107]. Onogi *et al*. [69] studied the viscoelastic behavior of semicrystalline poly (vinyl alcohol) and nylon using tensile stress relaxation tests over a range of temperature and humidity conditions. Relaxation modulus versus time curves were shifted along the log time axis using temperature and relative humidity as variables. Superposition of these variables was found applicable except for extremely low or high humidities and temperature. The study then concluded that time moisture superposition was valid when temperature was close to the polymer transition temperature [69]. Emri *et al*. [108] studied the mechanical response of poly (vinyl acetate) (PVAc) under torsion at temperatures from 20-36°C and moisture mass contents of 0-3%. Doubly shifted master curves demonstrated the applicability of time temperature moisture superposition of PVAc for the given conditions [108]. Kohan [109] studied the temperature humidity equivalence for yield stress of various nylons under various temperature and humidity conditions. Each of the polymers showed similar trends in behavior with regard to temperature and humidity. Shepherd and Wightman [110] investigated the effects of temperature and moisture on the fracture energy of a silicone sealant peeled from various substrates. Doubly shifted master curves were constructed, allowing the prediction of crack growth rate as a function of fracture energy, temperature, and relative humidity of the silicone sealants. Dillard *et al*. [111] took an approach to characterize the formation of the pinholes in proton exchange membranes in fracture mechanics sense, and studied the time dependent crack propagation using the knife slit test. Fracture energy master curves

were constructed based on values recorded at different temperatures and relative humidities. Patankar *et al.* [112, 113] conducted a study on the hygrothermal viscoelastic characterization of Nafion® NRE 211 and developed hygrothermal master curve, and Prony series coefficients. Harper *et al.* [114] studied the stress relaxation behavior of polyimide at various temperatures and humidity levels, and found that the plasticizing effect of moisture on the stress relaxation above 50% of moisture levels could not be described by the simplifying assumptions of TTSP. Therefore they concluded that the moisture has different effect on transient ($E(t)$) and equilibrium modulus (E_∞).

3.2.1 Hygrothermal Viscoelastic Characterization of the PEM

Polymers are time, temperature, and in many cases, moisture dependent. When thermal shift factors are a function of temperature only, resulting in a master curve by shifting the entire relaxation modulus data horizontally parallel to the time axis, the polymer is referred to as a thermorheologically simple material (TSM) [50]. For a TSM, a change in temperature is equivalent to a shift of behavior on the log time or log frequency axis [50, 51, 82, 115].

$$E(t,T) = E(\frac{t}{a_T}, T_{ref}) = E(t', T_{ref}) \quad (1)$$

where E, t and T are the relaxation modulus, time, and temperature, respectively. The relaxation modulus, defined as the ratio of time-dependent stress to the magnitude of strain applied as a step function, is often obtained using stress relaxation experiments. Thus, the tensile stress relaxation modulus used herein is given by $E(t) = \frac{\sigma(t)}{\varepsilon_0}$ where ε_0 is the amplitude of the applied step strain. Engineering definitions of stress and strain were used since the strains were limited to 0.5%. The reduced time, t', may be

determined using a thermal shift factor (a_T) determined based on the reference temperature, T_{ref} ,using [50, 116].

$$t' = \int_0^t \frac{d\xi}{a_T[T(\xi)]} \tag{2}$$

If the viscoelastic response curves can be superimposed to form a master curve by means of only horizontal translations, then the associated property would depend only on temperature and time through the reduced time parameter. In essence, the assumption of TSM behavior requires that all viscoelastic relaxations are accelerated the same amount by a given increase in temperature. Although this idealization is a useful concept and often applies across several decades of material response, the assumption often fails to apply across the full spectrum of viscoelastic relaxations, which inevitably involves molecular motion on different length scales. For example, the activation energy for long chain motion associated with an alpha transition is often larger than that associated with shorter range motion involved in the beta or gamma relaxations. For a thermorheologically complex material (TCM) response, the temperature dependence cannot be incorporated through a single shift factor and the curves do not overlap [51]. It has also been cited in the literature that a material can behave as a TSM over a narrow time window, but fails to do so over a wider range [50, 51]. For a TCM, shift factors are not just functions of temperature but also of time [53]. In addition to the time and temperature dependence of constitutive properties, significant moisture dependence is seen in many polymers, especially for hydrophilic materials. With significant moisture sorption, the viscoelastic response of PEMs also depends strongly on moisture content. Thus if thermal and hygral shift factors (a_T and a_H respectively) are functions only of

temperature and moisture, accelerating all relaxation processes consistently, the polymer can be referred to as a hygrothermorheologically simple material (HTSM). The effect of temperature and moisture may be combined for a hygrothermorheologically simple material (HTSM) which follows hygral and thermal shift factors to form a hygrothermal master curve. The reduced time in the case of a HTSM may be given by [117]:

$$t' = \int_0^t \frac{d\xi}{a_H[\lambda(\xi)]a_T[T(\xi)]} \tag{3}$$

where $\lambda(\xi)$ refers to the humidity conditions or moisture uptake.

In this paper, we discuss the viscoelastic characterization of commercially available Gore-Select® 57 PEM (referred to as GoreSelect 57 henceforth) with a thickness of 18μm (W.L.Gore and Associates, Newark, DE). This membrane is based on DuPont's Nafion® ionomer but is reinforced with an expanded poly(tetrafluoroehtylene) (PTFE) layer. A humidity chamber was custom designed to enclose the tension clamps on the DMA and contain the moist air coming in from a humidifying unit. We discuss the environmental chamber, sample mounting, and results from the viscoelastic stress relaxation experiments at various temperatures and humidity levels.

3.3 Experimental Procedure

The experiments were conducted in both 2980 and Q800 dynamic mechanical analyzers built by TA Instruments. Standard tensile clamps were used to load slender specimens cut from GoreSelect 57 proton exchange membrane. The instruments were fit with a humidity chamber to allow for testing over the range of temperatures and humidity levels of interest. The chamber was humidified using a Fuel Cell Technologies™ two-channel low flow gas humidification system (Albuquerque, NM).

3.3.1 Design of Humidity Chamber

The humidity chamber was conceived as a simple cylinder that would enclose the tension clamps, contain the humid air, and prevent the moist air from escaping and damaging the DMA furnace. Additionally the DMA units have sensitive drive electronics (displacement encoder and drive motor) below the specimen mounts, which must be protected. The air flowing up through the air bearings provides such a protection. Considering these requirements and through discussions with TA Instruments representatives, the base shown in Figure 3.1 was designed. The base was heated to minimize the water condensation inside the chamber. The chamber was designed in such a manner that the DMA furnace would nearly close around the chamber, leaving only a 20 mm gap at the bottom through which inlet and outlet tubes were passed. Special actions were needed to bypass the furnace closure switch on the DMA 2980 and Q800 to allow for operation in the partially closed position. Two holes are drilled into the base to provide an inlet for the hot, moist air and an outlet drain port which also lets the spent air exit. Plastic tubes were used to carry the humidified air in the chamber from the humidifier. The tubes were not heated, so the tube length was minimized to reduce condensation of water.

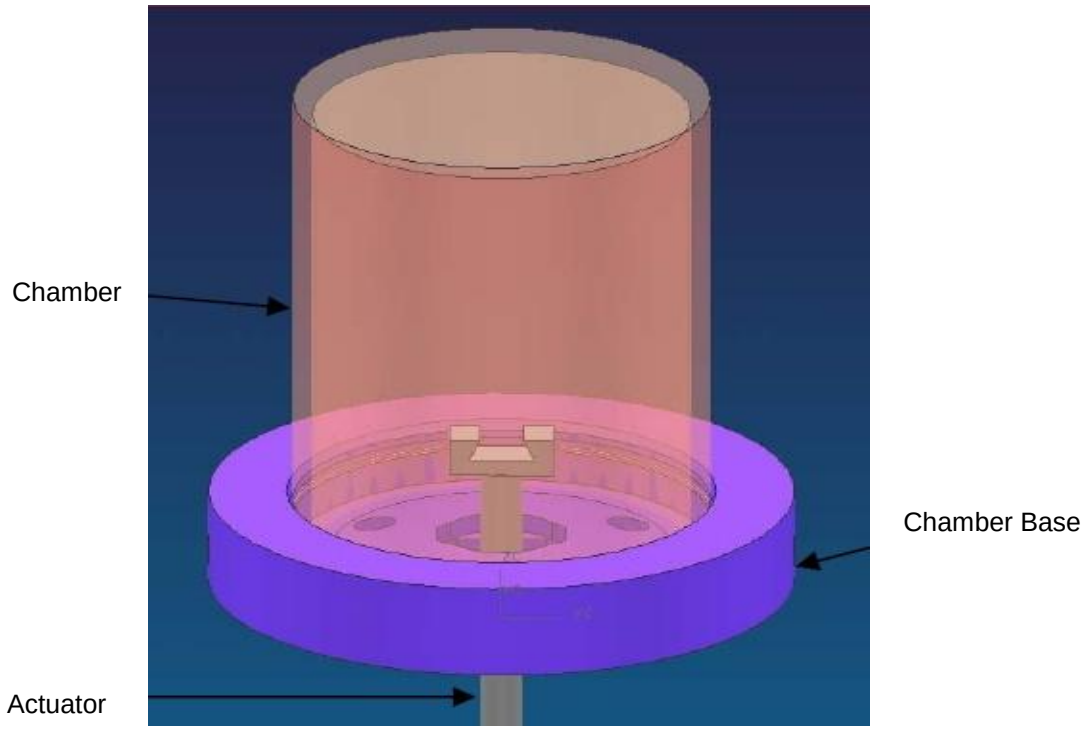

Figure 3.1 Design of the humidity chamber enclosing the DMA tension clamps.

3.3.2 Sample Mounting and Equilibrium

Uniaxial tensile specimens were cut in the machine direction from the GoreSelect 57 membranes using a scalpel. Typical width of the specimens tested was about 2.5 mm, as determined with a measuring light microscope. Typically the width would be measured at the top, middle and bottom sections of the strip to select the portion which showed less variation. The specimen was inserted in the tension clamps (TA Instruments) making sure that it was mounted parallel to the axis of the instrument. The gage length of the sample clamped in the grips was typically around 15-16 mm. Before the start of a test, the humidity chamber was equilibrated to a set temperature. A calibrated HMT 337 dew point sensor with a tolerance of ±1% in humidity measurements (Vaisala, Vantaa,

Finland) was used during all the hygrothermal tests to provide a direct indication of relative humidity within the environmental chamber. This sensor was placed just outside of the chamber in the outlet tube in such a way that it measured the dew point of the air coming out of the chamber. The DMA furnace was heated first to reduce water condensation. Moisture was introduced once thermal equilibrium was reached, and after 20 min of soak time, the test started. For stress relaxation tests, the membrane samples were subjected to 0.5% strain to evaluate the behavior in what is believed to be the linear viscoelastic region of the material response[1]. A preload of 1 mN (corresponding to about 20 kPa of stress) was applied to the sample to ensure that the membrane remained taut, but at the same time was small enough that the sample did not creep significantly. The stress relaxation tests typically would run for two minutes. The tests were run from 40-100°C and 30-90% relative humidity (RH) (except at 40°C, tests were conducted from 50-90% RH). Typically temperature was held constant and humidity was increased by 10% until the maximum desired humidity was achieved. The temperature would then be increased by 10°C and the relaxation test was repeated. After each relaxation test, the sample was allowed to recover for about 30 minutes before the next test began. This was accomplished by letting the instrument return to zero displacement. This does not necessarily mean strain in the sample goes to zero, however; due to bucking, the sample should nominally have zero stress. During the recovery time, the sample would be subjected to an increased humidity level to speed up the recovery process. Since the membrane was assumed to behave linear viscoelastically, no permanent damage was

[1] Isochronal stress-strain plots based on relaxation tests conducted at various strain levels showed that the material starts to behave nonlinearly at about 1%. Thus 0.5% was thought be a strain level well below this limit and stress relaxation experiments were performed at this strain level. The work is unpublished at this point.

anticipated during various tests. To validate out claim, we conducted a strain-recovery experiment in which a membrane sample was subjected to seven strain loading cycles at 80°C/70% RH condition, and were subjected to a recovery period of 30 minutes. The sample showed full recovery after each cycle. A membrane specimen would typically be used for tests conducted at various humidity levels at a given temperature.

A doubly-shifted hygrothermal master curve can be constructed in three different ways. Hygral master curves can be constructed using a reference humidity (RH_{ref}) and data collected at individual specified temperatures. Then a hygrothermal master curve can be constructed using a reference temperature (T_{ref}) and shifting all the hygral master curves originally constructed. The second approach involves construction of a thermal master curve using thermal shift factors and a reference temperature (T_{ref}); and then constructing a hygrothermal master curve by shifting the thermal master curves using hygral shift factors using a reference humidity (RH_{ref}). The third approach involves shifting the modulus data independently. This approach eliminates the need to do the shifting in a two-step process. More about this method will be discussed later in the paper. A hygrothermal master curve was constructed for GoreSelect 57 using the first approach discussed above; using relaxation modulus data collected over a range of temperature and humidity conditions. The first approach is used throughout the paper unless otherwise stated. However, a hygrothermal master curve produced using the second approach is shown later in the section to emphasize the point that both the approaches are valid and give rise to a similar master curve. The temperature was varied from 40°C-90°C in 10°C increments and RH was varied from 30-90% in 10% increments, except for 40°C, for which RH was varied from 50%-90%. The reference

temperature and RH were taken to be 70°C and 30%, respectively. A discussion of the construction of the master curve will follow in a later section. Because water content within the polymer, rather than relative humidity of the air, is expected to control the viscoelastic properties of the membrane, the effect of humidity over a range of temperatures can be encompassed into λ a common water content metric for ionic materials. Determined from the mass uptake, λ is defined as the number of water molecules per sulfonic acid site of the membrane [2]. An empirical formula to estimate λ at a given set of RH and T conditions is given by [118]:

$$\lambda = \left(1 + RH^2 \times 0.00002325 \times \frac{(T-30)}{30}\right) \times \left(0.00001422 \times RH^3 - 0.00189737 \times RH^2 + 0.13414 \times RH\right) \quad (4)$$

where T and RH refer to the temperature in degrees Celsius and percent relative humidity, respectively. The hygrothermal master curve was then validated using long term stress relaxation tests at 70°C for 5000 minutes and at 90°C for 3000 minutes, both conducted at 30% RH.

3.4 Results and Discussion

The tensile relaxation modulus, E(t), shown in Figure 3.2 was obtained at various humidity levels from 30 to 90% and at 50°C, a representative temperature used to illustrate the procedure. The material was assumed to be hygrorheologically simple, allowing for shifting the relaxation moduli obtained at different humidity levels to the reference condition at 30% RH. The relaxation data overlapped well at different humidities, suggesting the applicability of the time moisture superposition principle, as is shown in Figure 3.3.

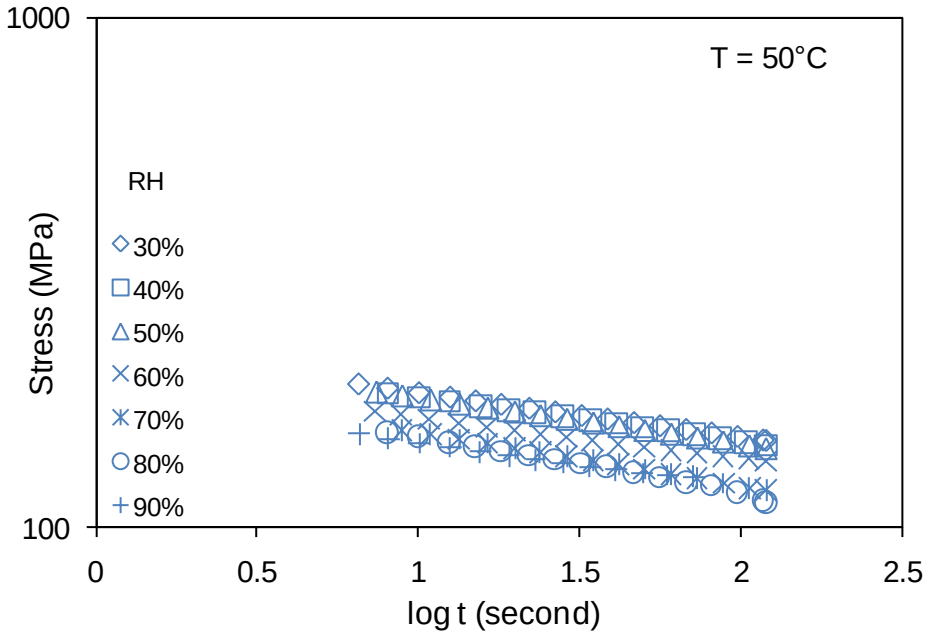

Figure 3.2 The relaxation moduli obtained at 50°C and various relative humidities.

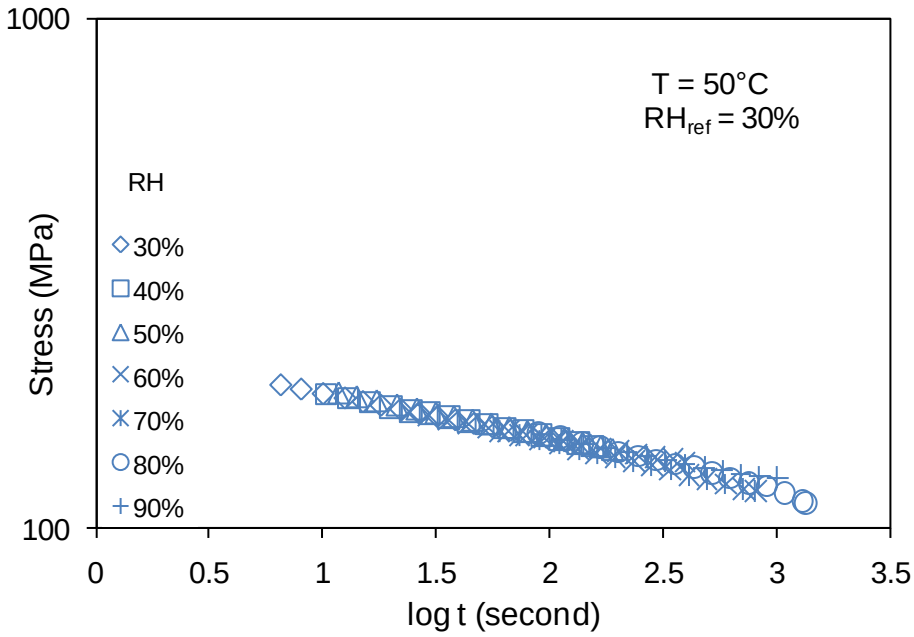

Figure 3.3 A typical hygral master curve of the tensile relaxation modulus at 50°C, referenced to 30% relative humidity.

Once these hygral master curves were obtained using hygral shift factors, a_H, developed at each test temperature, the hygral master curves were shifted using thermal shift factors,

a_T , to form a smooth hygrothermal master curve involving all of the data. The doubly-shifted hygrothermal master curve for the tensile stress relaxation modulus of GoreSelect 57 is shown in Figure 3.4. The thermal shift factors, shown in Figure 3.5, are for reference conditions of 70°C and 30%RH corresponding to λ = 2.77. The WLF equation fits the thermal shifting factors well except for temperatures below the α-transition temperature of the membrane (T_α), which is about 70°C at 30% RH. Page et al. [119] and Osborne et al. [120] investigated the molecular origins of the thermal transitions and dynamic mechanical relaxations of Nafion membranes using various characterization techniques. Molecular level information from their study supports the assignment of the β- relaxation to the genuine glass transition (T_g) of Nafion and the α-relaxation to the onset of long-range mobility of chains/side chains via a thermally activated destabilization of the electrostatic network. The α-transition temperature also depends on the water content. The authors did a small study to understand the effect of humidity on T_α, and found that the depression in T_α over the range of interest (dry-90% RH) is about 20°C. The WLF constants deviate significantly from the universal values. Although the Arrhenius relation is more appropriate [56, 116] for temperatures below T_α, it has been found to have a poor fit in this case. The well known WLF and Arrhenius equations are given by Equation 5 and Equation 6 respectively:

$$\log a_T = \frac{-C_1(T - T_g)}{C_2 + (T - T_g)} \quad . \tag{5}$$

$$\log a_T = -\frac{2.303E^*}{R}\left(\frac{1}{T_0} - \frac{1}{T}\right) \tag{6}$$

where C_1 and C_2 are WLF constants, while E^* refers to the activation energy of the primary transition corresponding to the reference temperature T_0 (or T_α) in the Arrhenius equation [116]. The corresponding hygral shift factors are shown in Figure 3.6. The relaxation modulus decreased monotonically with an increase in humidity. This kind of phenomenon is commonly observed with increasing temperature in a viscoelastic material. Thus it can be concluded that the humidity has the same kind of effect as the temperature, although is less pronounced. This fact can be understood by comparing the temperature and moisture shift factors. Over the range of conditions examined in this study, the span of the hygral shift factors in this study was about 1.5 (30-90% RH), while the thermal shift factors spanned about 5.5 (40-100°C). Averaged over the conditions studied, the viscoelastic acceleration associated with a 10% increase in RH is equivalent to about 0.25°C increase in temperature. Similarly, a unit increase in λ produces shifts comparable to about a 0.3°C increase in temperature. The phenomenon reported by Bauer *et al*. [102], that higher humidity apparently induced an anti-plasticization effect in Nafion® N117 was not observed during this study, although reasons for the discrepancy are not clear.

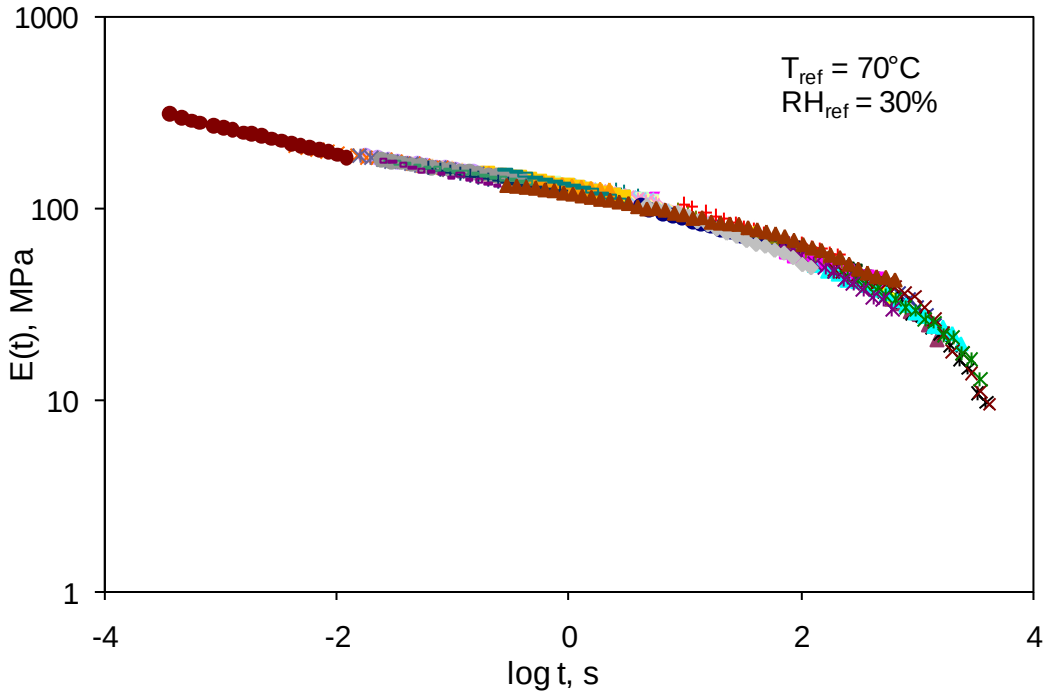

Figure 3.4 Hygrothermal master curve of the tensile relaxation modulus of GoreSelect 57 at reference temperature and relative humidity conditions of 70°C and 30%RH, respectively.

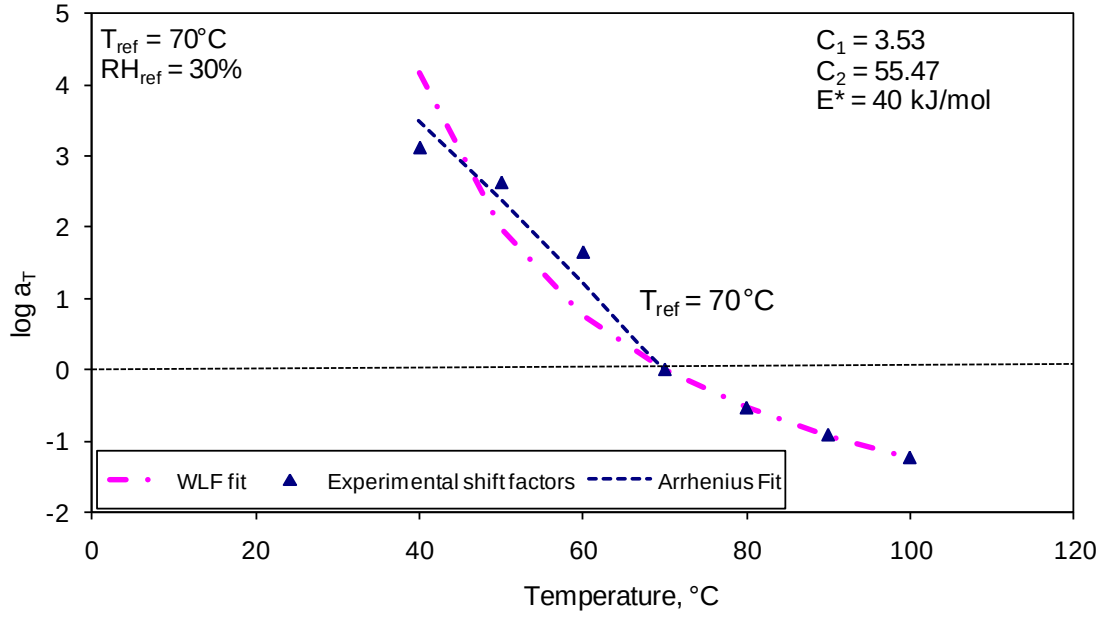

Figure 3.5 Thermal shifting factors at reference temperature of 70°C fit using WLF equation and Arrhenius equation.

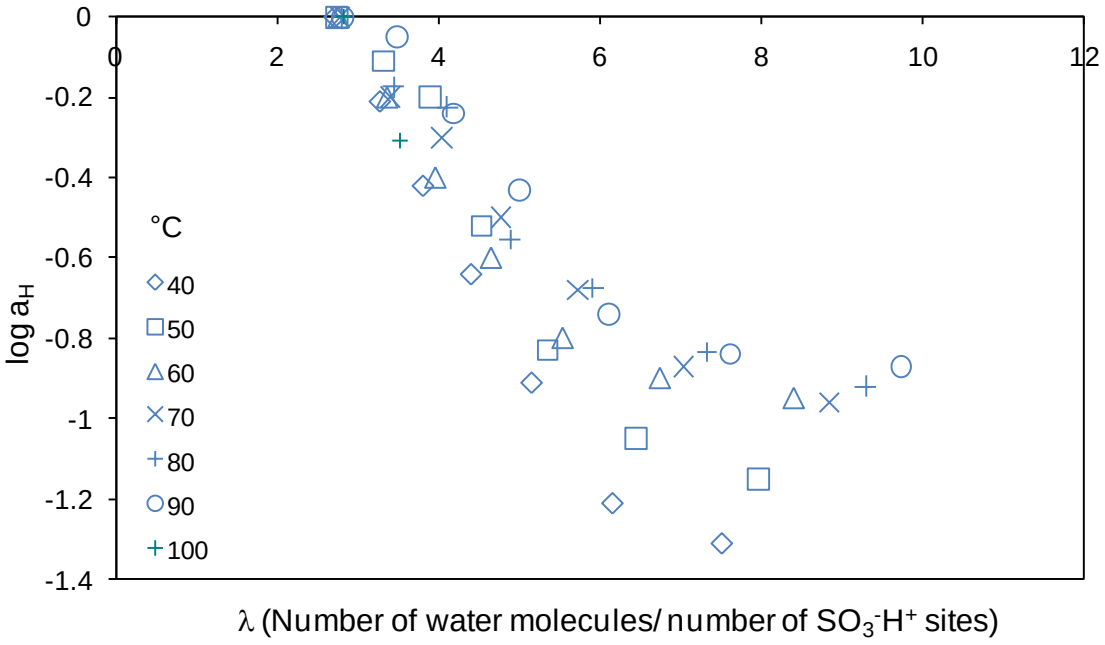

Figure 3.6 Hygral shift factors (a_H) at various temperatures for a reference relative humidity of 30%.

It can be seen from Figure 6 that the hygral shift factors depend on temperature. The shift factors can be fit using a simple quadratic expression:

$$\log a_H = A(\lambda - c)^2 + B \qquad (7)$$

where A and B are parameters that depend on temperature and c is the reference value of λ. The dependence of these constants on temperature has been established and is shown in Figure 3.7. Higher temperature may increase 'A' but appears to increase 'B'.

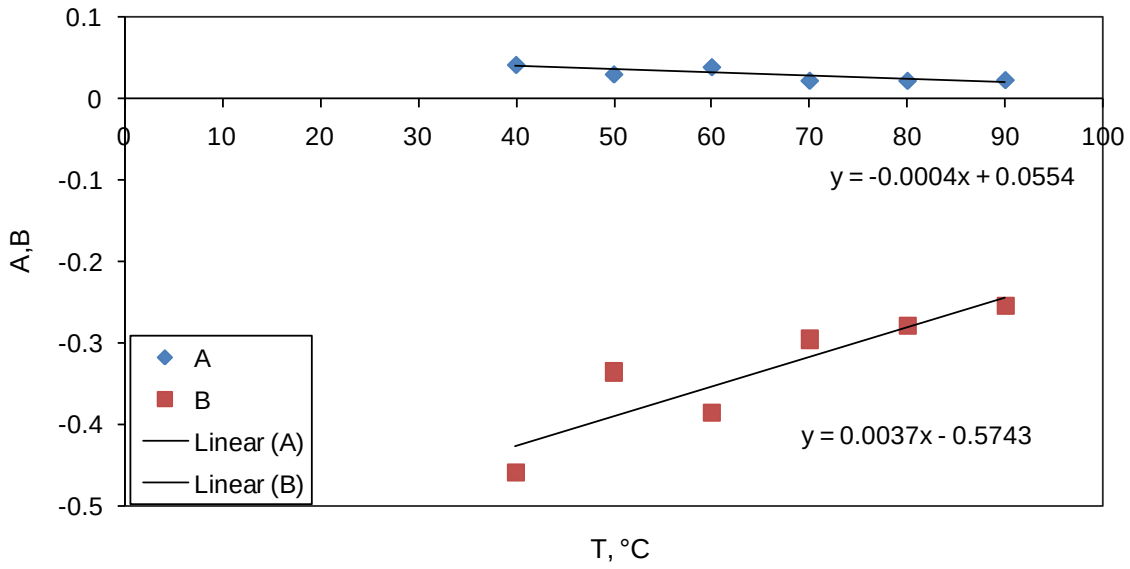

Figure 3.7 Dependence of A and B; the parameters in a quadratic expression for hygral shift factors on temperature.

Based on the expressions of A and B, the mathematical relationship of hygral shift factors in terms of λ can be established and is given by:

$$\log a_H = (-0.0004T + 0.0554)(\lambda - 3)^2 + (0.0037T - 0.5743) \qquad (8)$$

Higher temperature is seen to decrease the values of these constants, suggesting that at these temperatures which are of most interest to PEM fuel cell operation, hygral shift factors are not as strongly dependent on temperature. For potential use in finite element analysis of the membranes, the hygrothermal master curve was fit using a Prony series with nine terms given by:

$$E(t) = E_\infty + \sum_{n=1}^{9} E_n \cdot e^{-\frac{t}{\tau_n}} \quad \text{..... (9)}$$

where E_∞, E_n and τ_n are the material constants to be fit. The "Solver" function in Microsoft® Excel™ was used to fit the stress relaxation data to calculate the Prony series

parameters. The Prony series coefficients are shown in Table 3.1 and the fit is shown in Figure 3.8. The value for E_∞ was chosen to be 3 MPa, consistent with the results obtained from the longer term validation tests.

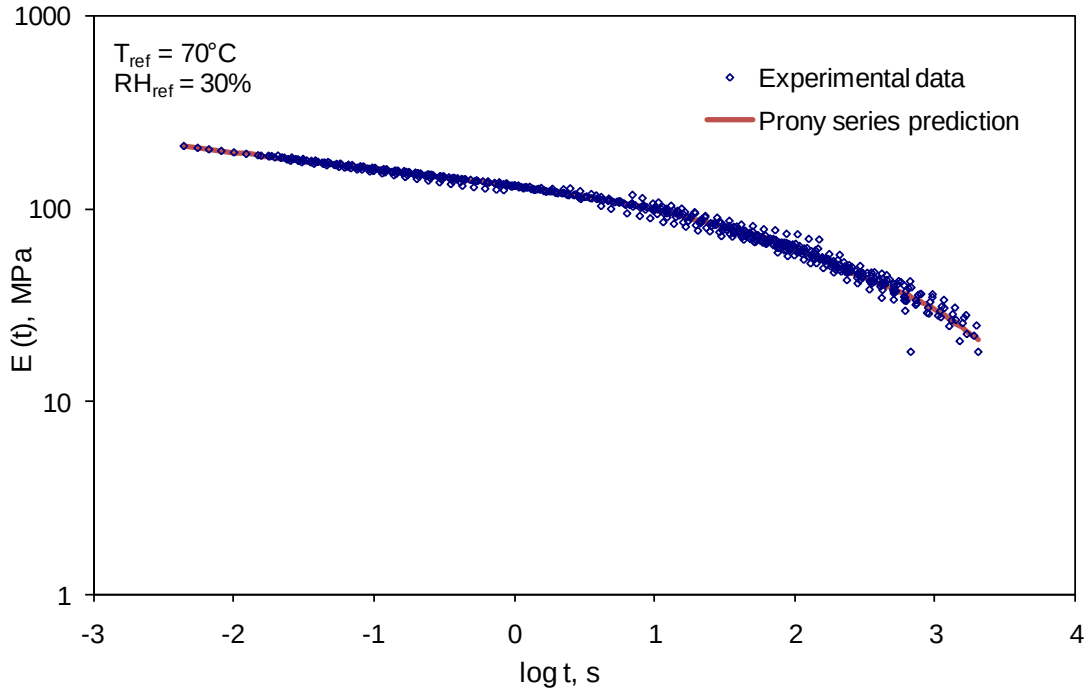

Figure 3.8 The Prony series fit for a hygrothermal stress relaxation of GoreSelect 57 at reference conditions of 70°C and 30% RH.

Table 3.1 The Prony series coefficients to fit the hygrothermal stress relaxation data of GoreSelect 57.

n	log τ_n	E_i (MPa)
1	-3	109.73
2	-2	47.77
3	-1	33.66
4	0	24.76
5	1	36.45
6	2	37.21
7	3	31.99
8	4	17.07
9	5	0

As mentioned earlier, a hygrothermal master curve can also be constructed using the second approach, i.e. thermal shift followed by the hygral shift. It was observed that the process of construction of a hygrothermal master curve is path independent, in that comparable results were obtained by reversing the order of shifting. A third approach would be to construct a master curve using shift factors obtained without partitioning them into temperature or humidity shift factor contributions. In other words, the individual short term data would simply be shifted to form a smooth master curve in one single step. A Prony series fit of the master curve obtained from the independent shift is shown with blue line in Figure 3.9. Such independent shift factors are functions of both temperature and water content, and should yield the same shift in time as the combined hygral and thermal shifts would. Figure 3.9 shows a comparison of Prony series obtained from all the three methods, and Table 3.2 shows the comparison of the Prony series coefficients. The total shift in each of the approaches is approximately 5 decades.

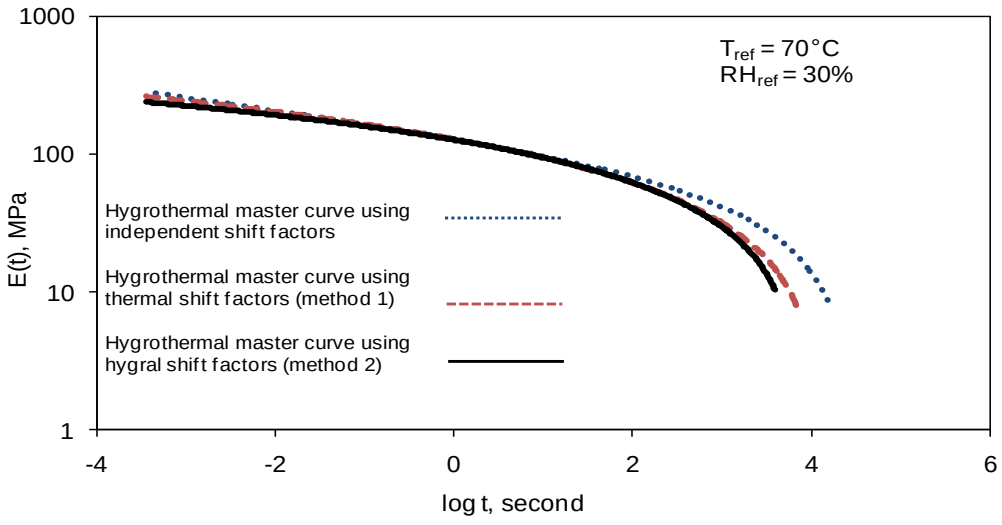

Figure 3.9 Comparison of Prony series fit for the three methods to construct the hygrothermal master curve of the tensile relaxation modulus.

Table 3.2 The Prony series coefficients to fit the hygrothermal stress relaxation data of GoreSelect 57 using three methods.

n	log τ_n	E_i (MPa)		
		1st Method	2nd Method	Independent shift
1	-3	109.73	109.43	103.01
2	-2	47.77	46.87	42.71
3	-1	33.66	33.87	35.74
4	0	24.76	25.65	33.96
5	1	36.45	33.61	26.63
6	2	37.21	35.88	37.28
7	3	31.99	29.54	17.93
8	4	17.07	23.01	35.44
9	5	0	3.15E-05	0

Prony series coefficients from various methods match very well at shorter times deviate somewhat at longer times, however; one should bear in mind that the method to shift the modulus data is somewhat subjective and would vary depending on how well the fit seems to one's eyes. In spite of the fact that the master curve construction process remains somewhat subjective, the Prony series solutions are quite comparable. Thus if one were to decide which method to choose to construct a master curve, the decision would be arbitrary and would be based on individual choice. Any of these methods would yield a similar hygrothermal master curve. However, the longer term validation tests have shown that the first method (using thermal shift factors) seems to shift the relaxation data better than the other methods as evidenced by a better match with the long term stress relaxation modulus. The long term stress relaxation validation has been described in the next section.

3.4.1 Validation of hygrothermal master curve and shift factors

The hygrothermal master curve constructed was validated using a longer term stress relaxation test. The idea behind a long term transient stress relaxation test is that

the stress relaxation modulus should closely match with that from the hygrothermal master curve over all time periods of interest. This procedure gives confidence in the master curve. If run for sufficiently long time, the long term test may extend the data beyond the time scale of the master curve. A Q800 DMA was used in a tensile mode, and the membrane was subjected to a strain of 0.5% for 5000 minutes at 70°C and for 3000 min at 90°C. Both tests were conducted at 30% RH. These tests were conducted twice to make sure that testing procedure and results were consistent. The stress relaxation modulus obtained from a long term test was compared with the hygrothermal master curve obtained from the first method. Figure 3.10 shows the plot of the master curve and the longer term stress relaxation modulus data. The stress relaxation modulus obtained from the longer term tests shows better agreement with the hygrothermal master curve obtained from shift methods 1 and 2 than independent method. Thus the long term data validates the hygrothermal master curve. Multiple validation tests confirm that at sufficiently longer times, the relaxation modulus reaches the plateau value, known as the equilibrium modulus. The value of equilibrium modulus is found to be around 3-3.5 MPa.

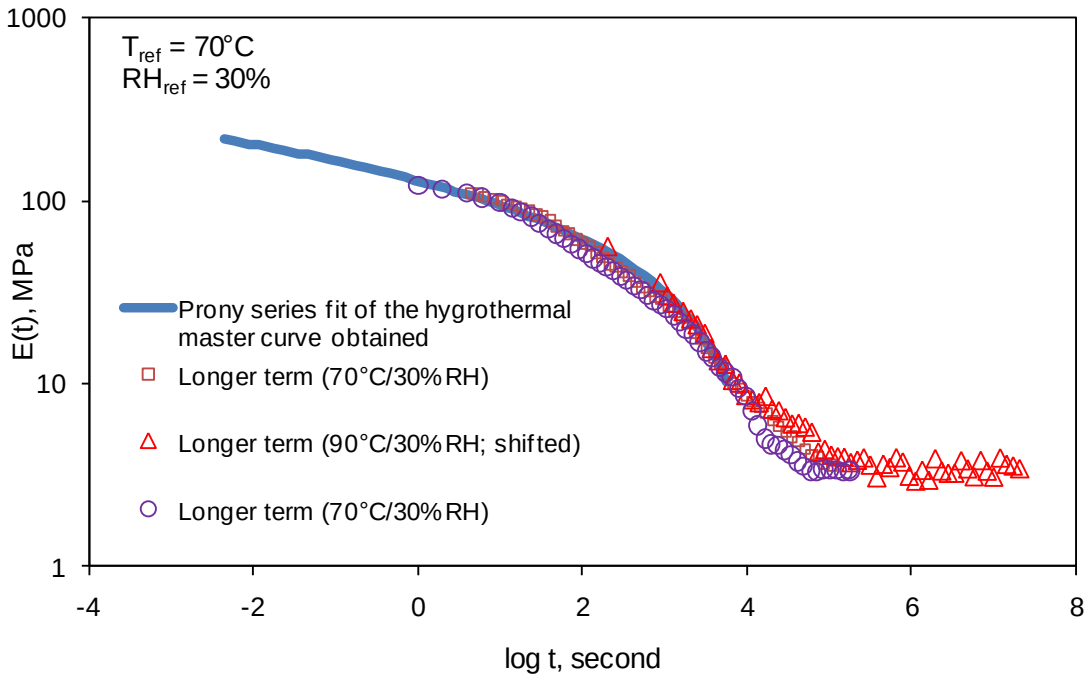

Figure 3.10 Hygrothermal master curve obtained from shifting hygral master curves using thermal shift factors (method 1) of GoreSelect 57 compared with long term validation relaxation data at 70°C and 90°C/30% RH.

3.5 Summary and Conclusion

The viscoelastic properties of GoreSelect 57 were characterized using a DMA modified to accept a humidity chamber. The tensile relaxation moduli of the GoreSelect 57 membrane were obtained from stress relaxation tests conducted at temperatures from 40-90°C and relative humidities ranging from 30-90%. At each test temperature, the relaxation modulus data at various humidities were shifted using hygral shift factors (a_H) form a hygral master curve. The hygral master curves at various temperatures were then shifted using thermal shift factors (a_T) to form a hygrothermal master curve. The success of shifting the data horizontally along the time axis suggests that the time temperature moisture superposition principle is applicable. The hygrothermal master curve was presented in terms of a Prony series with 10-terms excluding the equilibrium

modulus term. The coefficients of the Prony series will later be used in finite element modeling. Increasing humidity at a given temperature reduced the stiffness of the membrane and has a similar effect as higher temperature on other viscoelastic materials. However, the effect of humidity is not as pronounced as that of temperature. Overall hygral shift for the range of testing conditions was about 1.5 decades, while the thermal shift was about 7 decades. Thermal shift factors show the WLF behavior above T_{ref} of the membrane. Hygral shift factors are fit by a quadratic expression in water content and show slightly more variance than thermal shift factors. The hygrothermal master curve was also constructed using an alternative approach with the use of thermal shift factors followed by the hygral shift factors. Both the approaches yield a similar master curve with comparable shift factors. Thus the process of constructing a hygrothermal master curve was found to be "path independent". Hygral shift factors were found to depend on temperature. A third method to generate a master curve was devised using just one shift factor. The master curves generated by three methods were compared using Prony series fit and coefficients. These methods yielded similar looking master curves. The master curve derived from hygral shift followed by temperature shift (method 1) was then validated using a long term stress relaxation test at 70°C and 90°C. The long term data matches nicely with the master curve constructed using method 1, suggesting validity of shift factors. It also showed the modulus plateau at longer times to be about 3 MPa.

3.6 Acknowledgement

The authors would like to express appreciation to the General Motors Corporation for supporting this work, as well as Institute of Critical Technology and Applied Science (ICTAS) and the Engineering Science and Mechanics Department at Virginia Tech for providing additional support and facilities. We would like to acknowledge the

contribution of Soojae Park, Jarod Ewing, and Gerald Fly for initiating this work and building the equipment and to Cortney Mittelsteadt for helpful discussions. Finally, we would like to acknowledge the helpful discussions with TA Instruments concerning retrofitting their DMA to accept the humidity chamber.

CHAPTER 4: Linear Hygrothermal Viscoelastic Characterization of Nafion® NRE211 Proton Exchange Membrane

Manuscript prepared for Journal of Membrane Science

4.1 Abstract

When a proton exchange membrane (PEM) fuel cell is placed in service, hygrothermal stresses develop within the PEM and change dramatically as the internal environment changes with operating conditions. Knowing the viscoelastic constitutive properties of PEMs is necessary for making hygrothermal stress predictions in the transient temperature and humidity environments of operating fuel cells. The tensile relaxation modulus of a commercially available proton exchange membrane, Nafion® NRE 211, was obtained over a range of humidity levels and temperatures using a commercial dynamic mechanical analyzer (DMA). A special humidity chamber was built in the shape of an inverted cup that could enclose the tension clamps of the DMA instrument. Preconditioned humid air was then introduced into this chamber at the specified temperature and relative humidity. Transient stress relaxation tests were conducted under dry and humid conditions at various temperatures and humidity levels. Thermal and hygral master curves were constructed and then used to construct a hygrothermal master curve using the time temperature moisture superposition principle. Horizontal shifts in the master curve suggested the applicability of time temperature moisture superposition. The hygrothermal master curve was fit using a 10-term Prony series and validated using longer term stress relaxation tests. To validate stress relaxation experiments, transient creep tests were conducted at various temperatures at a fixed RH condition. The creep compliance master curve was constructed noting the thermal shift

factors. The thermal shift factors obtained matched well with those obtained from relaxation tests. Short term and long term creep compliance was converted into stress relaxation modulus using a well-known viscoelastic conversion formula, and compared with the relaxation modulus obtained under identical conditions. Good agreement was found between the two datasets. It was found during the investigation that the relaxation master curve under dry conditions did not superimpose with the master curve obtained at elevated humidity conditions. It was evident that relaxation data at 2% RH at the test temperatures was not superposable with the master curves obtained at higher relative humidity (10% < RH< 90%) at the temperature range 70°C < T< 90°C. This so called "dry-humid transition" was found to be triggered at around 2-5% RH levels (corresponding to $\lambda = 0.5\sim0.6$) at temperatures 70-90°C. Dynamic tests were run under dry conditions to determine the α-transition temperature of Nafion® NRE211. The stress relaxation modulus was found to match quite well with the dynamic storage modulus within the experimental window. Longer term relaxation tests were conducted to validate the dry relaxation master curve. Significant discrepancy was found between the short term and longer term relaxation modulus, and was attributed to the physical aging (densification of amorphous phase) in the ionomer and/or irreversible morphological changes in the membrane.

Keywords: Proton exchange membranes, polymer electrolyte membranes, viscoelastic characterization, hygral and thermal shift factors, mechanical durability, hygrothermal stresses, dynamic mechanical analyzer, Nafion® NRE 211, stress relaxation, time temperature moisture superposition principle, doubly-shifted master curve, dry-humid transition, physical aging

4.2 Introduction

Proton exchange membrane fuel cells (PEMFC) have been a consistent focus of research in the automotive industry and for portable power applications, where they have received major attention from various private and government organizations as potentially cleaner and more efficient power sources [93, 94]. However, there are a number of concerns that the fuel cell industry needs to address before the full potential of PEMFCs is realized. According to US Department of Energy targets for the year 2010, PEM-based fuel cells for transportation applications should perform reliably for 5000 hours at operating temperatures ranging from -40°C to 80°C [9, 121]. This imposes stringent conditions on the desired performance characteristics and integrity of automotive fuel cells. When a fuel cell is placed in service, the proton exchange membrane (PEM) must prevent the reactant gases from mixing, yet remain sufficiently hydrated to allow protons to flow freely through the membrane, which requires adequate hydration. Moisture and temperature changes induce significant hygrothermal strains, which, under the constrained boundary conditions imposed on membranes by compression within the fuel cell stack, induce significant in-plane stresses in the PEM. These mechanical stresses vary widely with internal operating environment, and are believed to lead to damage and eventual membrane failure allowing reactant gases to crossover through pinholes [95, 122]. Predicting the hygrothermal stresses in membranes and thus developing a more complete understanding of durability still presents a challenge for commercialization of the fuel cell. Accurate constitutive characterization of the PEM is essential for making stress predictions in the transient humidity and temperature environment of an operating fuel cell. An understanding of these

hygrothermal stresses in the PEM is important for developing life prediction models to estimate durability and improve fuel cell operation.

Extensive work has been published on the effect of moisture and temperature on polymers, composites and adhesives [56, 108, 114, 116, 123, 124]. These studies have shown that moisture frequently accelerates viscoelastic behavior through plasticizing the polymer, in a manner analogous to an increase in temperature, and can be described by a time temperature moisture superposition principle.

Pinhole formation, due to various types of stresses and leading to premature failure of the fuel cell, is reported in the literature [95-98, 122, 125, 126]. The formation of pinholes is complicated and not fully understood, however pinholes could result from the effects of mechanical stresses in a constrained membrane subjected to hygrothermal cycles and chemical dissolution of the ionomer [125]. Thus it becomes necessary to accurately characterize these stresses in order to gain fundamental understanding of PEM durability. Lai et al. [95, 122, 125] proposed a stress model that accounts for PEM viscoelasticity and hygrothermal expansion. They measured the creep compliance of a Nafion® NR111 membrane using a dynamic mechanical analyzer (DMA) at various temperatures and relative humidities (RH). Preliminary data suggested that creep compliance master curves could be determined by horizontally shifting the compliance curves at various temperatures and RHs. Bauer et al. [102] measured the mechanical properties of the Nafion® 117 membrane at elevated temperatures and higher humidity conditions using a DMA, and concluded that in general water acts as a plasticizer. Eisenberg et al. [103] reported the loss tangent as a function of water content of the PEM. Incorporating inorganic fillers and crosslinking agents was proposed to enhance

mechanical durability at higher temperatures by reducing the swelling in the PEM [100, 104]. These membranes showed improved tensile mechanical properties at room temperatures, however, their durability at higher temperatures was questioned [102]. Bauer et al. [104] and Young et al. [105] reported improved mechanical properties of dry Nafion® 117 by adding inorganic fillers and found higher stiffness and lower tangent values as compared to Nafion® 117 at elevated temperatures. Patankar et al. [112, 127] studied the effect of temperature and moisture on the viscoelastic properties of Gore-Select® 57, a expanded poly-tetrafluoroehtylene (PTFE) reinforced PEM, using stress relaxation experiments. Satterfield and Benziger [128] conducted tensile stress-strain and stress relaxation experiments on Nafion of equivalent weight 1100 from 23-100°C at 0-100% relative humidity. Their study concludes that elastic modulus of Nafion decreases with increase in water activity. They also observed that at temperatures above 90°C, hydrated membranes are stiffer than dry membranes and at low humidity levels, stress in the membrane approaches zero at about 10^3-10^4 s. Similar observations were made by Majsztrik et al. [129]. They developed an apparatus to measure creep and strain recovery in an environmentally controlled apparatus. Their results showed that water plasticized Nafion at lower temperatures, but acts to stiffen the membrane at or above 90°C. This stiffening of the membrane is much more dramatic than observed by Bauer et al. [102] and Gittleman et al. [130]. Majsztrik et al. pointed out that environmental control is not only critical but also crucial at high temperature, and that there has not been sufficient control over the environmental conditions in mechanical testing of Nafion. Environmental control is also critical to the relaxation processes in Nafion. Yeo and Eisenberg [45] reported that even a small amount of water increased the stress relaxation

rate in Nafion 1365. They also pointed out that time temperature superposition broke down with the addition of water, especially at longer times. This behavior was attributed to water plasticization of ionic domains in Nafion, and possibly triggering an alternate relaxation mechanism when introduced into the completely dry Nafion. Liu et al. measured stress relaxation under ambient conditions and under water at two strains [6]. They observed that in the case of the submerged sample, stresses and the relaxation rates were lower as compared to those observed under humid conditions. Uan-zo-li [27] investigated the effects of structure, humidity and aging on mechanical behavior of Nafion ionomers, and concluded that the majority of the properties of these membranes were controlled by the formation and growth of the ionic clusters. Dillard et al. [111, 131] took a different approach to characterize the pinhole formations by studying the time-dependent crack propagation using the knife slit test. They constructed fracture energy master curves based on values recorded at various temperature and humidity conditions.

The mechanical response of a PEM subjected to fuel cell cycles has been extensively studied, and models involving stress-strain behavior of membranes and membrane electrode assemblies (MEA) have been reported in the literature [13, 98, 125, 132-139]. Weber and Newman [98] studied the stresses associated with constraint in a simple 1-D model. Tang et al. [13, 137, 138] used a finite element model to incorporate hygrothermal stresses induced in a membrane due to thermal and humidity changes in a cell assembly. They assumed the membrane to be perfectly linear elastic. A viscoelastic stress model proposed by Lai et al. [95, 122, 125] assumes the membrane to be hygrothermorheologically simple, and uses the relaxation master curve obtained for Nafion® NR 111 as an input parameter in the model. Park et al. [140] analyzed the

hygrothermal stress state in a biaxially constrained membrane under transient temperature and humidity conditions. Based on measured tensile relaxation modulus and hygral/thermal expansion coefficients, they developed and proposed a transient hygrothermal viscoelastic constitutive equation. Solasi et al. [134] applied the constitutive properties obtained for a wide variety of thermal and humidity levels in a finite element model to study through-thickness and in-plane behavior of an MEA. In-plane expansion/shrinkage mechanical response of the constrained membrane as a result of changes in hydration and temperature was studied in uniform and non-uniform geometries and environments. A similar in-plane elastic-plastic model was also used for in-plane numerical modeling of RH-induced strain in an MEA in a constrained configuration. In a recent paper, Solasi et al. [135] proposed a two-layer viscoplastic model for a constrained membrane that consists of an elastoplastic network in parallel with a viscoelastic network (Maxwell model). This model separates rate-dependent and rate-independent behavior of the material.

Page et al. [119] and Osborne et al. [120] investigated the molecular origins of the thermal transitions and dynamic mechanical relaxations of Nafion® membranes using various characterization techniques. They claimed that several studies reported in the literature on the thermal transitions and mechanical relaxations are based on limited DMA results and are contradictory at times. Molecular level information from their study supports the assignment of the β- relaxation (~ -20°C) to the genuine glass transition (T_g) of Nafion and the α-relaxation (~100°C) to the onset of long-range mobility of chains/side chains via a thermally activated destabilization of the electrostatic network.

.

4.2.1 Hygrothermorheologically simple material

Polymers are time and temperature dependent in the sense that increasing temperature effectively reduces the time required for molecular motion to take place. This leads to shifts of viscoelastic response of material in log time with increase in temperature, according to the well known time temperature superposition principle (TTSP). When all relaxations are accelerated by equal amounts for a given increase in temperature, the temperature shift factors are functions of temperature only and the polymer is referred to as a thermorheologically simple material (TSM) [50, 51]. For a TSM, a change in temperature is equivalent to a uniform shift of behavior on a log time or log frequency axis. For a thermorheologically complex material (TCM), the curves may not overlap (may indicate material complexity) or different sections of the material response may shift by different amounts for a given temperature change (may be expected if different molecular relaxations represent processes controlled by different activation energies) [53, 66, 82]. Thus if temperature shift factors are not consistent across the various relaxation modes, the polymer may be referred to as a TCM [53, 66, 82]. It has been noted that a material can behave as a TSM within a narrow experimental window, but fail to do so over a wider range [50]. Similarly, if a hygrothermal master curve can be formed by shifting the modulus data horizontally along the time axis, as the hygral and thermal shift factors are functions of humidity (water content, λ) and temperature only, respectively and vertically to account for the entropic and density changes; the material may be referred to as hygrothermorheologically simple material (HTSM). For a HTSM the reduced time may be written as:

$$t' = \int_0^t \frac{d\xi}{a_H[\lambda(\xi)] \cdot a_T[T(\xi)]} \tag{1}$$

where a_H and a_T refer to hygral and thermal shift factors, respectively.

As mentioned earlier, the definition of a HTSM dictates hygral and thermal shift factors to be functions of humidity (or equivalently water content, λ) and temperature only, respectively. However, in this research, it was found that hygral shift factors showed a strong dependence on water content and weak dependence on temperature if the hygrothermal master curve was formed by constructing hygral master curves first, followed by thermal shifts, i.e. $a_H = f(\lambda, T), a_T = f(T)$. On the other hand, if the hygrothermal master curve was formed by constructing thermal master curves followed by hygral shifting, thermal shift factors showed a stronger dependence on temperature, and weaker dependence on water content, i.e. $a_H = f(\lambda), a_T = f(T, \lambda)$. More on this will follow in the discussion section. Also the dependence of humidity on thermal shift factors progressively becomes weaker as temperature increases. In a practical sense, the effect of a weaker dependence of hygral shift factors on temperature works in favor of fuel cell manufacturers, who are often interested in a relatively narrow temperature range (60-90°C) during fuel cell operation. At such temperatures, around and above the α-relaxation temperature of Nafion, there is sufficient mobility for chains to move around as a result of higher fractional free volume, and the viscoelastic processes are dominated by temperature rather than humidity.

4.3 Experimental Procedure

The material tested in this study was DuPont™ Nafion® NRE 211 (referred to as NRE 211 henceforth), 25μm thick perfluorosulfonic acid (PFSA) membranes reportedly produced by a casting process. A TA Instruments™ Q800 dynamic mechanical analyzer (DMA) was used in tensile mode to conduct transient stress relaxation and dynamic

experiments on small membrane samples cut in the machine direction. Membrane samples with an average length (between the clamps) to width ratio of five to six were used. Typical specimen widths ranged from 2.2-2.8 mm. A light microscope was used to accurately measure the sample width. Typically the width was measured at the top, middle and bottom sections of the film to select the part of the film which showed less variation. The most uniform section of the film was then clamped in the tensile fixture of the DMA machine. Typically the gage length was around 15-16 mm, as measured by the DMA machine.

To conduct tests at various humidity levels, a humidity chamber was built to enclose the tension clamps yet fit within the nearly closed DMA temperature chamber without affecting the DMA drive unit [127]. Humidified air was supplied at the desired temperature and humidity level using a Fuel Cell Technologies™ gas humidification system. A Vaisala™ dew point sensor (HMT 337) was used during all the hygrothermal tests to provide a direct indication of relative humidity within the environmental chamber. This sensor was placed just outside of the chamber in such a way that it measured the dew point of the air exhausting from the chamber. For hygrothermal tests, the DMA furnace and the base of the humidity chamber were preheated to reduce any condensation of water. Humid air was introduced once thermal equilibrium was reached, and after an additional 20 minutes soak time, the test was started.

The approach taken for acquiring stress relaxation data was to test the membrane samples at a given temperature over a range of relative humidities from 10-90% in 10% intervals. Upon completion of the humidity range, the temperature was raised by 10°C in preparation for collecting the next dataset. A new specimen was used for each increment

in temperature, while the same specimen was used for the relaxation tests conducted at a given temperature for humidity increments. The tests were conducted for temperatures ranging from 40-90°C. The typical test duration for each condition was 2 minutes, followed by a 20 minutes recovery time at each humidity level. After the test was complete, the drive motor would return to its initial position, leaving slack in the elongated sample. Due to this slack, the stresses in the sample would nominally be zero, although the strains would be non-zero. For each new humidity test at a given temperature, the sample length was automatically re-zeroed by the machine prior to applying the strain. The relaxation modulus was obtained by straining the sample to 0.5%. In order to obtain hygral shift factors at substantially higher humidity levels, tests were also conducted at 95% RH at temperatures 70-90°C. At lower temperatures, higher humidity led to substantial water condensation, rendering the data questionable. In addition, longer term stress relaxation tests were conducted at 70°C/30% RH for 5000 minutes and 90°C/30% RH for 3000 minutes to validate the hygrothermal master curve.

In order to validate the results obtained from the relaxation experiments, creep compliance data was obtained following the similar procedure as observed during relaxation tests. The membrane specimens were subjected to temperatures 40-90°C and 50% RH. Stress corresponding to 80 mN (~90 kPa) was applied to induce creep strains following hygral equilibration in the chamber. Creep compliance master curve was constructed while noting the thermal shift factors. Creep compliance data obtained at 70-90°C at 50% RH was then converted to relaxation modulus using a simple linear viscoelastic transformation [56], which was then compared with relaxation modulus obtained under identical conditions. A longer term creep test was conducted at 90°C/30%

RH for about 1600 minutes with stress of about 90 kPa. In order to explore the effect of mechanical (stress/strain) history on sensitive viscoelastic properties, the membrane specimen was subjected to a creep at 90°C/10% RH for about 12 hours using a stress of about 26 kPa, followed by relaxation experiment at 90°C/30% RH using 0.5% strain for about 3000 minutes (This is merely a side-study and has not been discussed in this paper. Details of this study can be found in Appendix 1).

Stress relaxation tests were also conducted under dry conditions. A compressed dry air tank was used to supply dry air to the humidity chamber. The test parameters were the same as described earlier. Longer term relaxation tests were also conducted at 90°C and 120°C for over 2000 minute under dry conditions and plotted against a short term thermal master curve under dry conditions. In order to understand the differences observed between the long term relaxation modulus and the short term modulus obtained using TTSP, a physical aging study was performed. A membrane specimen, after equilibrating at 90°C for 15 minutes, was subjected to a stress relaxation test at 60°C for 5 minutes at 0.5% strain under dry conditions. Then it was equilibrated at 40°C for about 90 minutes. This sequence was repeated 5 times and the modulus measured. Cyclic dynamic tests were conducted under dry conditions to determine the α-relaxation temperature of NRE 211. The loss modulus

(E'') obtained from single frequency (1Hz) temperature ramp (40-150°C) dynamic tests was used as the criterion to determine the transition. Dynamic tests were also conducted under nominally dry conditions in a multi frequency-temperature ramp mode to construct a thermal master curve, where temperature was stepped from 50-95°C at 0.1, 0.3, 1, 3, 10, 30 and 100 Hz.

Due to the significant differences observed between relaxation master curves obtained under dry and humid conditions, it was decided to conduct the stress relaxation tests at low RH levels to find out the humidity level at which this so called 'dry-humid' transition takes place. The tests were conducted at 2% and 5% RH levels at 60-90°C. The following gives a summary of experiments performed during this research:

- Stress relaxation tests at 10-90% RH at temperatures 40-100°C, at 95% RH at temperatures 70-90°C, under dry conditions at temperatures 40-130°C, and at 2% and 5% at 60-90°C. Creep compliance tests at 50% RH from 40-90°C. (discussion under **'transient hygrothermal tests'**)
- Longer term validation tests to validate stress relaxation master curve constructed under humid and dry conditions. (discussion under **'validation of master curve'**)
- Dynamic tests under dry conditions (discussion under **'dynamic tests'**)

4.4 Results and Discussion

4.4.1 Transient hygrothermal tests

4.4.1.1 Stress relaxation tests

Two approaches used to construct the master curves are illustrated in Figure 4.1. One of the approaches involved constructing a hygral master curve at a given temperature noting humidity shift factors (a_H), and then shifting the hygral master curves at various temperatures noting temperature shift factors (a_T) to construct a hygrothermal master curve. The other approach involved construction of a thermal master curve at a given RH using thermal shift factors (a_T), and then shifting thermal master curves at various RHs using hygral shift factors (a_H). Patankar et al. [127] discussed the approaches mentioned

above and constructed a doubly-shifted master curve and fit it with Prony series for Gore-Select® 57 proton exchange membrane. They found that both the first and second approaches give similar master curves; however, the first method results in a master curve that matches more closely with the longer term stress relaxation data used for validation. They also discussed a third approach in their paper, in which each relaxation response was shifted independently to form a master curve, providing only a combined hygrothermal shift factor, (a_{TH}). They had less success independently shifting the relaxation modulus data. The first approach is used throughout this paper. Figure 4.2a shows the stress relaxation modulus results collected at various humidity levels at a representative fixed temperature (80°C), and the corresponding hygral master curve is shown in Figure 4.2b. Figure 4.2b also highlights sections of the hygral master curve that are discussed in detail later in the paper. The hygral master curve at 80°C clearly shows that relaxation modulus data collected at RH of 2% and under dry conditions do not superimpose with the data collected at and above 5% RH level, suggesting that there is a 'humidity switch' which triggers the membrane to behave differently at very low humidity level. At such low humidity levels, the TTMSP seems to fail. More on this will follow in the section of 'dry-humid transition'. Current section explains the construction of a hygrothermal stress relaxation master curve of relaxation modulus data collected at and above 10% RH level at various temperatures. Even though relaxation modulus data collected at 5% RH level superimposes, the discussion will follow later in the paper in order to maintain consistency.

Hygral master curves were constructed at each of the test temperatures. Shifting all the hygral master curves while noting the thermal shifts resulted in a hygrothermal

master curve, which is shown in Figure 4.3. The water content (λ), which is defined as the number of water molecules per sulfonic acid site [141] of the membrane at the given RH and T, is believed to be more meaningful than RH, which merely reflects the ratio of water to the saturated state of air. An equation to approximate λ for Nafion at a particular T and RH is given by [130]:

$$\lambda = \left(1 + RH^2 \times 0.00002325 \times \frac{(T-30)}{30}\right) \times \left(0.00001422 \times RH^3 - 0.00189737 \times RH^2 + 0.13414 \times RH\right) \quad (2)$$

where RH is the percent relative humidity and T is the temperature in degrees Celsius. This relationship has been used throughout this paper to estimate λ. The hygral shift factors (a_H) as a function of λ are plotted in Figure 4.4a, and the temperature shift factors (a_T) are plotted in Figure 4.4b. These shift factors can also be combined into hygrothermal shift factors assuming the shifting procedure is done independently (as shown in case of GoreSelect 57 in chapter 3). Figure 4.5 shows the independent shifts.

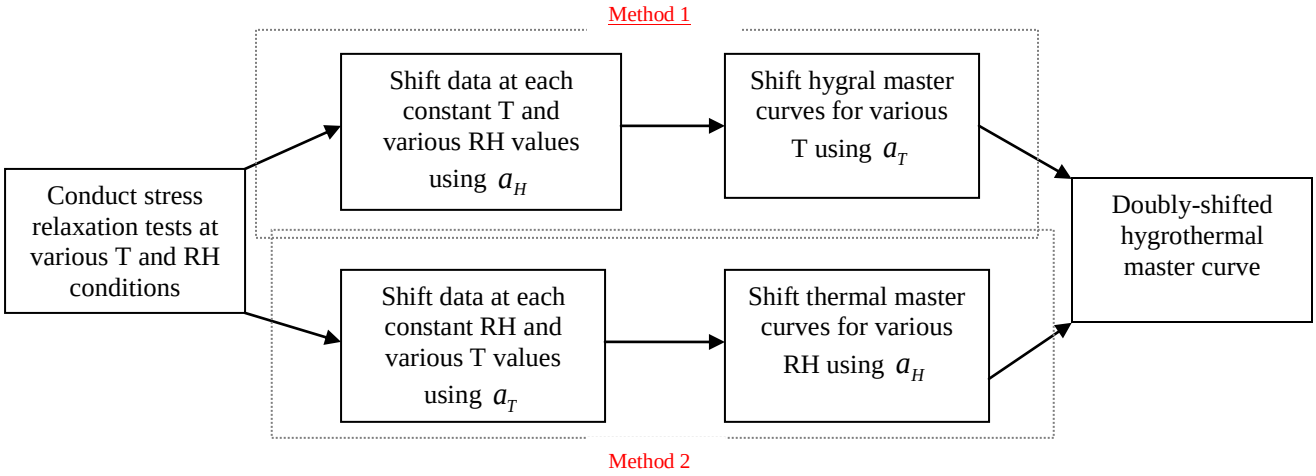

Figure 4.1 Schematic diagram showing two different approaches to construct a hygrothermal master curve.

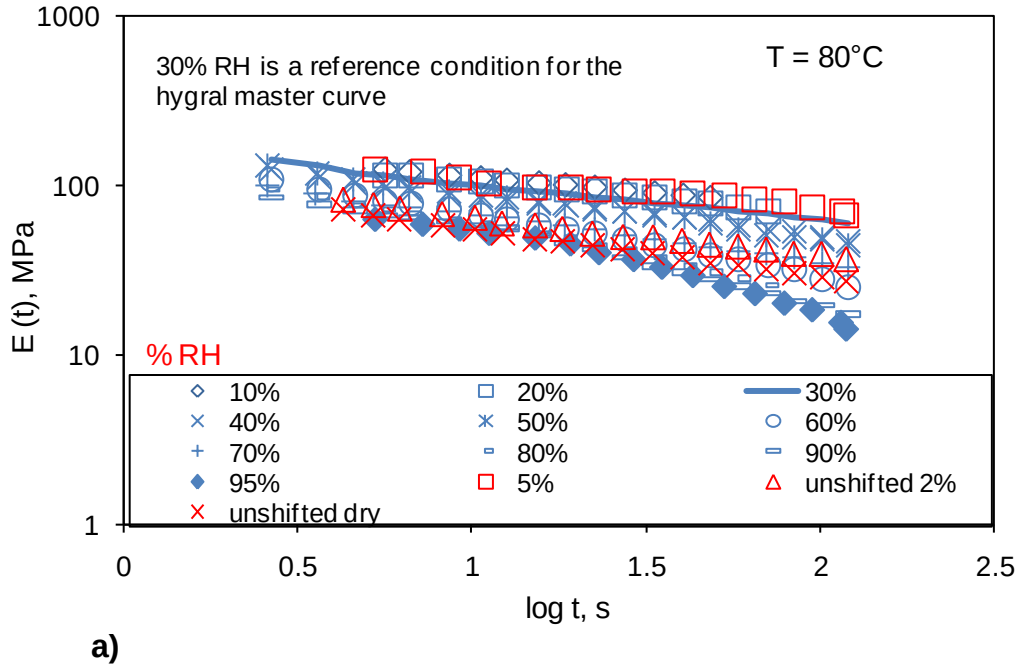

a)

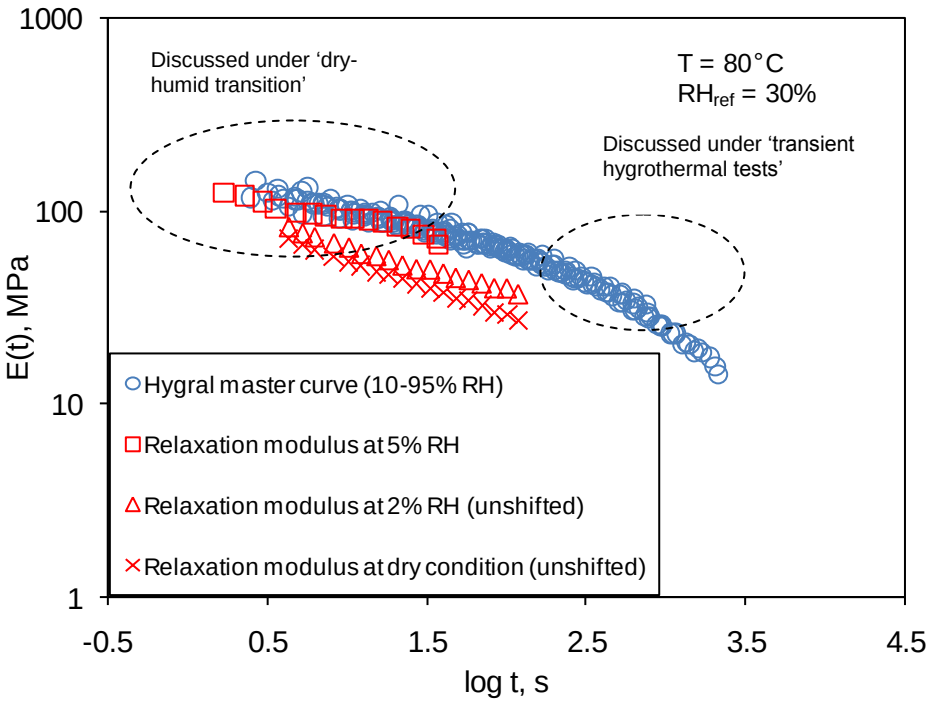

b)

Figure 4.2 Stress relaxation results for NRE 211 obtained at 80°C. a) Relaxation modulus for several humidity levels, b) Hygral stress relaxation master curve shifted to a reference humidity of 30%.

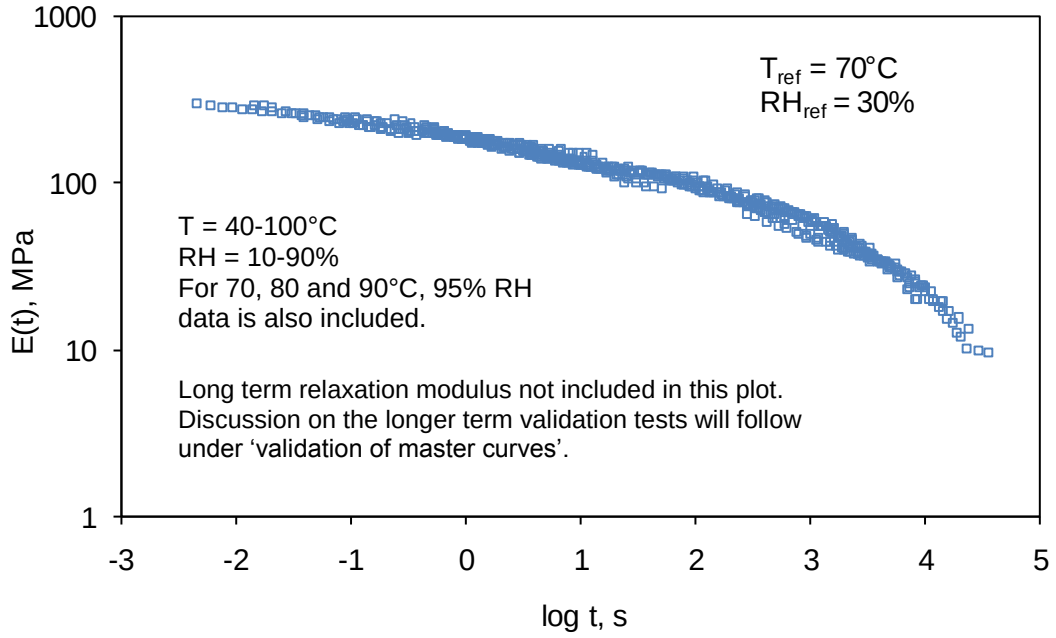

Figure 4.3 Doubly-shifted hygrothermal stress relaxation master curve of NRE 211 at a strain of 0.5% and shifted to a reference temperature of 70°C and reference humidity of 30%.

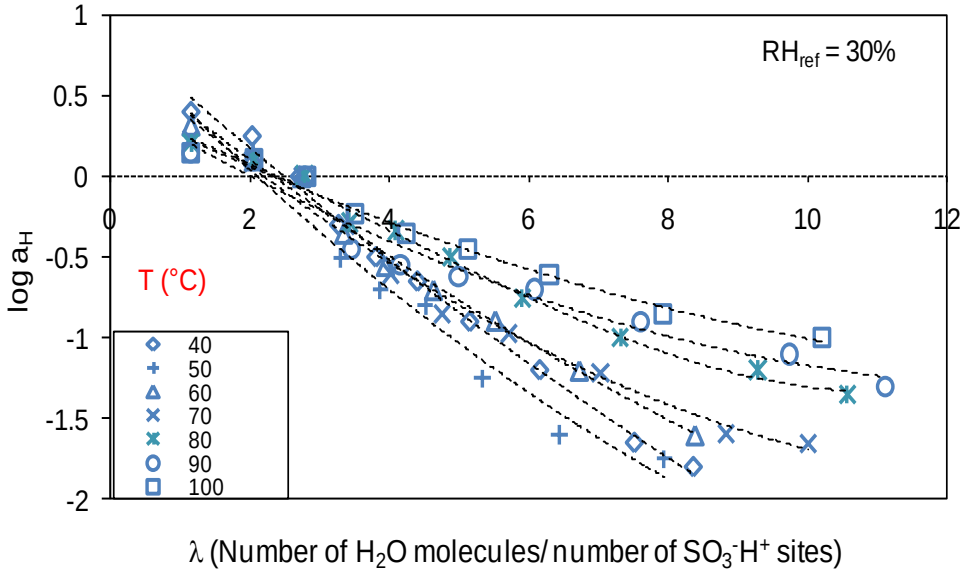

a)

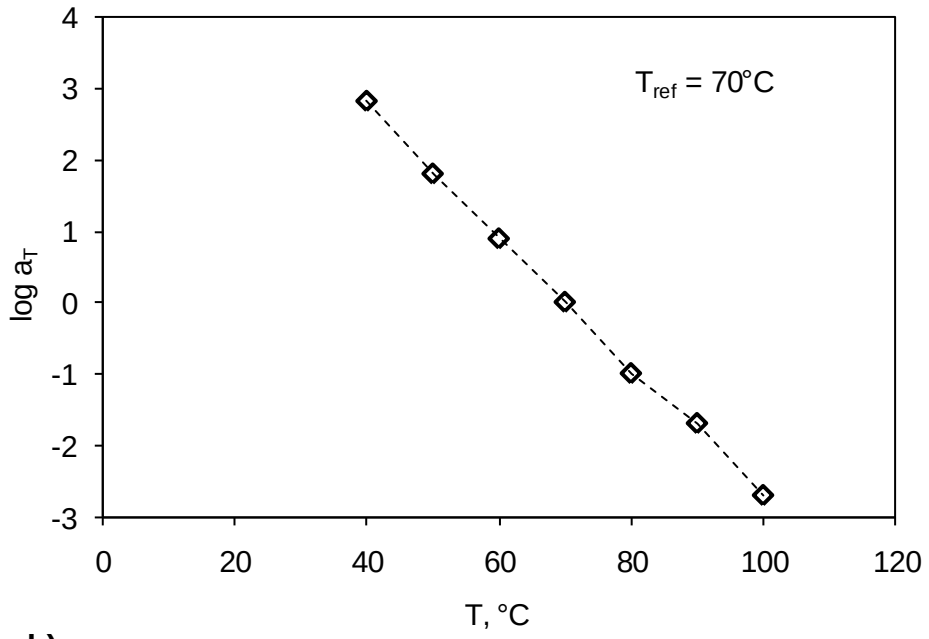

b)

Figure 4.4 The shift factors obtained for stress relaxation of NRE 211. a) Hygral shift factors at various temperatures, b) thermal shift factors.

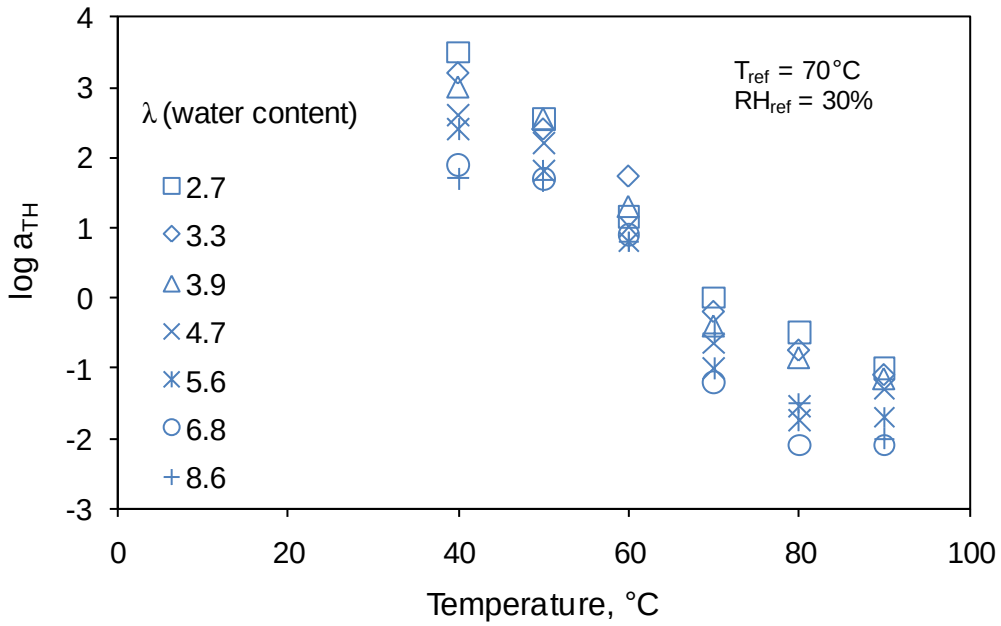

Figure 4.5 The hygrothermal shift factors for stress relaxation of NRE 211 plotted as a function of temperature at various water content levels (the values reported for water content are mean values for the RH span at a given temperature).

The overall temperature shift over the specified temperature range is about 6 decades; on the other hand, the maximum humidity shift is only about 2. Hygral shift factors spread out in a consistent fashion, clearly indicating that they are also functions of temperature. The humidity shifts cover a broader range at lower temperatures, suggesting that humidity plays a more important role in determining viscoelastic properties at lower temperatures than at higher temperatures. This is probably not too surprising considering the amount of free volume the chains have at high temperatures. At high temperatures, the 'inherent material clock' of the polymer is accelerated such that adding humidity does not change the viscoelastic properties as much as would be experienced at lower temperatures. The humidity shifts can be approximated using a quadratic equation such as $\log a_H = A\lambda^2 + B\lambda + C$ where *A*, *B* and *C* are linear functions of temperature. The functions *A*, *B* and *C* can then directly be used in a finite element program.

The stress relaxation master curve presented in Figure 4.3 was fit using a 9-term Prony series. Prony series parameters will be used in subsequent work for stress predictions using finite element programs. The Prony series is expressed as:

$$E(t) = E_\infty + \sum_{i=1}^{9} E_i e^{-\frac{t}{\tau_i}} \qquad (3)$$

where E_∞ represents the equilibrium modulus. Many crosslinked polymers display a relaxation modulus that approaches some equilibrium modulus at sufficiently long times [56, 116]. In the case of ionomers, ionic regions serve as physical crosslinking sites. If temperature, moisture or strain influences the equilibrium modulus in a different way than the transient modulus, it is possible to form a smooth master curve for the transient modulus, but not for the total modulus [114]. However, no such difficulty was

encountered in the master curves produced herein. The value of E_∞ was determined to be 3 MPa based on the results obtained from the longer term validation tests discussed later in this paper. The Prony series coefficients are given in Table 4.1.

Table 4.1 The Prony series coefficients for the stress relaxation master curve generated for NRE 211 strained to 0.5 % and expressed at reference conditions of 70°C and 30% RH.

i	E_i (MPa)	$\log \tau$ (s)
1	65.85	-2
2	44.6	-1
3	62.43	0
4	46.55	1
5	32.62	2
6	45.02	3
7	29.53	4
8	11.79	5
9	1.89	6
	3	∞

An apparent activation energy E* for a viscoelastic relaxation process may be obtained from the slope of a plot of log a_T as a function of reciprocal absolute temperature according to the Arrhenius equation [116]:

$$\log a_T = -\frac{2.303E^*}{R}\left(\frac{1}{T_0} - \frac{1}{T}\right) \tag{4}$$

Such a plot ideally yields a straight line with a slope proportional to E^* and an intercept equal to the reciprocal of T_0, the reference temperature. Such a plot is shown in Fig 4.6. The well-known Arrhenius equation is used to capture secondary transitions in a polymer and is often applicable for temperatures below T_g, and is often used to distinguish between the primary and secondary transitions [116]. Even though Nafion shows a glass transition at -20°C [120], and hence is well above the glass transition temperature for the current study, the thermal shift factors can be fit well using a simple Arrhenius expression. This is not unusual, as many researchers claim that superposition manifests

itself from molecular behavior, and therefore formulate equation based on the activation energy [56, 116]. Therefore, various relaxations can be based on activation energy. The activation energy corresponding to the transition is about 39 kJ/mol.

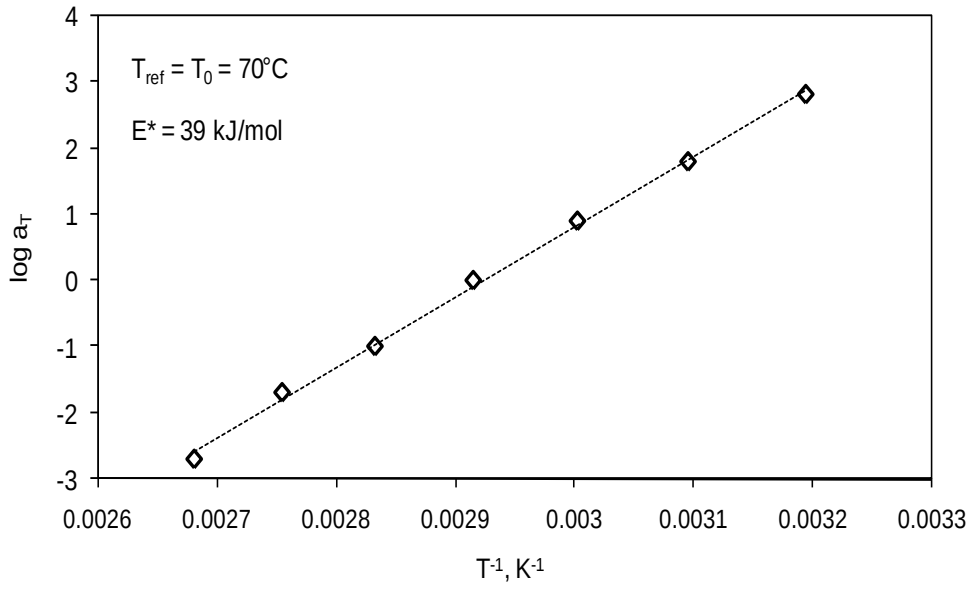

Figure 4.6 Arrhenius plot for NRE 211 showing a straight line for temperature shift factors plotted against reciprocal temperature.

4.4.1.1 Creep tests

Creep tests were conducted to support the validity of the relaxation measurements. The thermal shift factors obtained from constructing the creep compliance master curve should be comparable with the thermal shift factors obtained from the relaxation master curve; also stress relaxation modulus and creep compliance are transformable [50, 56] as long as the membrane specimen is linearly viscoelastic. Figures 4.7a and 4.7b show the creep compliance data obtained at 50% RH from 40-90°C, and creep compliance master curve, respectively. Figure 4.8 shows the thermal shift factors obtained from the creep compliance master curve, compared with those obtained from stress relaxation master curve shown in Figure 4.5.

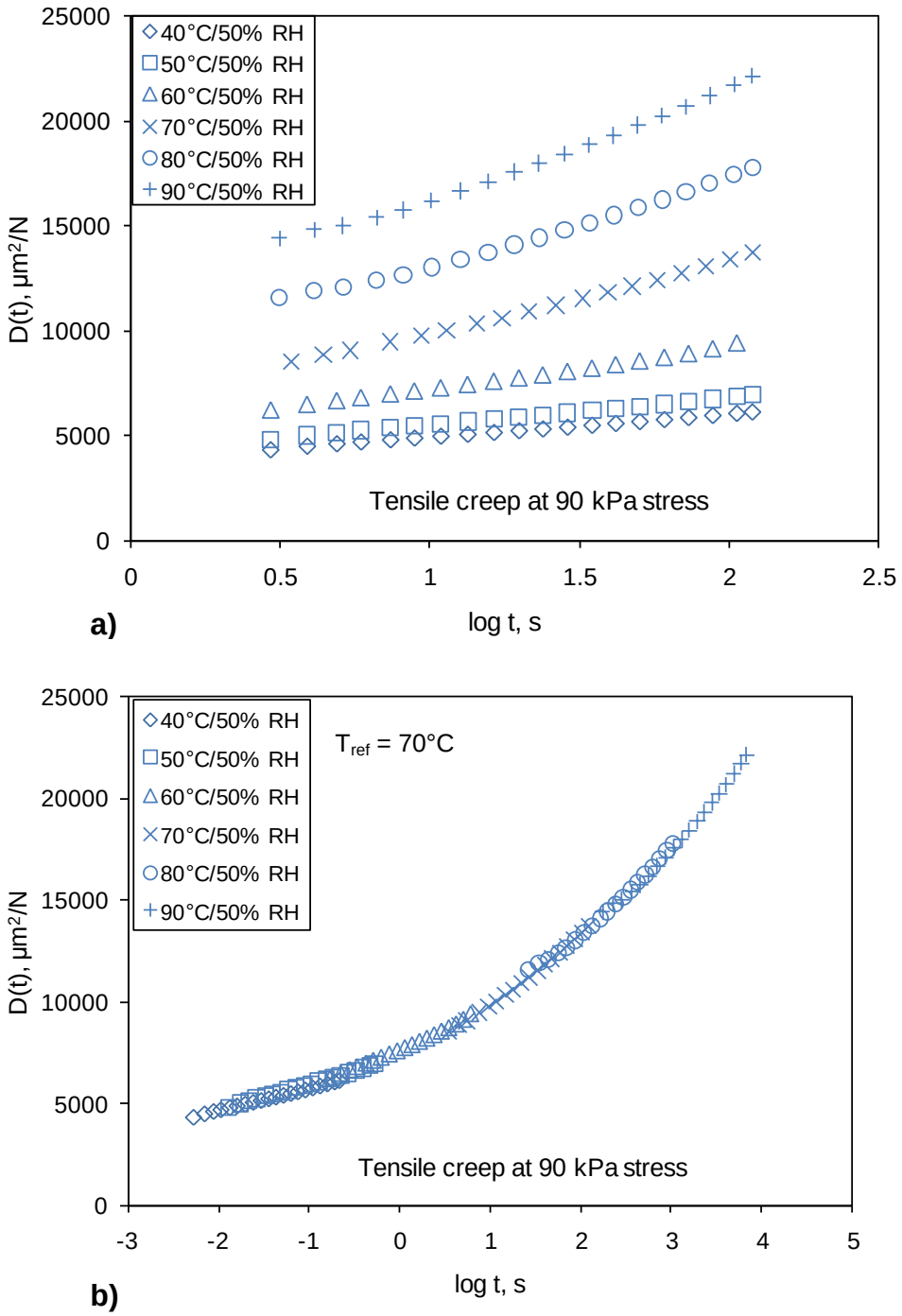

Figure 4.7 Tensile creep compliance for NRE 211 at 50% RH. a) Creep compliance of NRE 211 obtained at 50% RH for temperatures, b) Creep compliance master curve at reference temperature of 70°C.

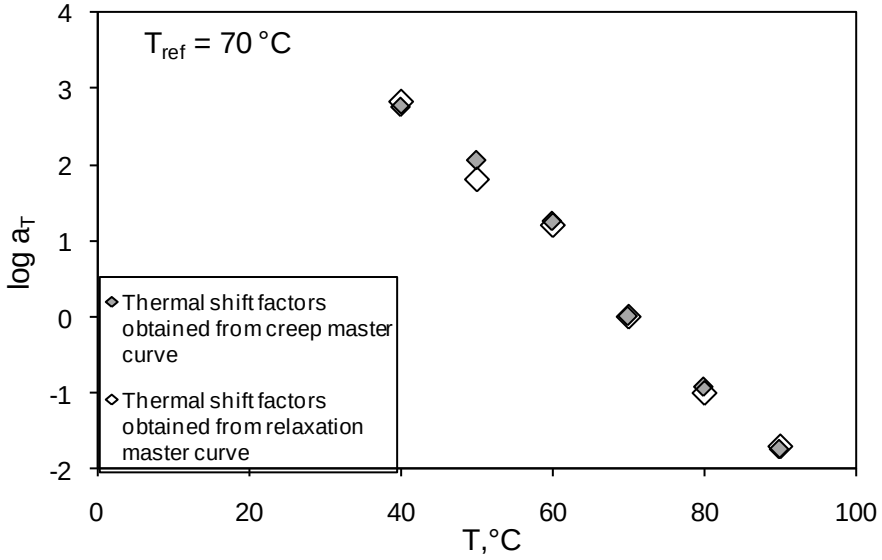

Figure 4.8 The thermal shift factors obtained from creep master curve at 50% RH from 40-90°C, compared with those obtained from stress relaxation of NRE 211 under identical conditions as a function of temperature.

It is clear that the thermal shift factors obtained from both the transient viscoelastic tests are quite similar. In order to check whether creep compliance and stress relaxation modulus are consistent through the conversion interrelationship, creep compliance obtained at 70-90°C/50% RH was converted to relaxation modulus using a simple power law conversion [56]

$$E(t) = \frac{\sin m\pi}{m\pi} \frac{1}{D(t)} \tag{5}$$

where m is the slope on log-log scale and is always taken as a positive number. Figure 4.9 shows a comparison of the relaxation modulus obtained by converting the creep compliance and that obtained directly from the relaxation experiments. These two results agree within 6-8%. Such good accuracy lends confidence not only in the procedure, but also the experimental results obtained with creep and relaxation experiments.

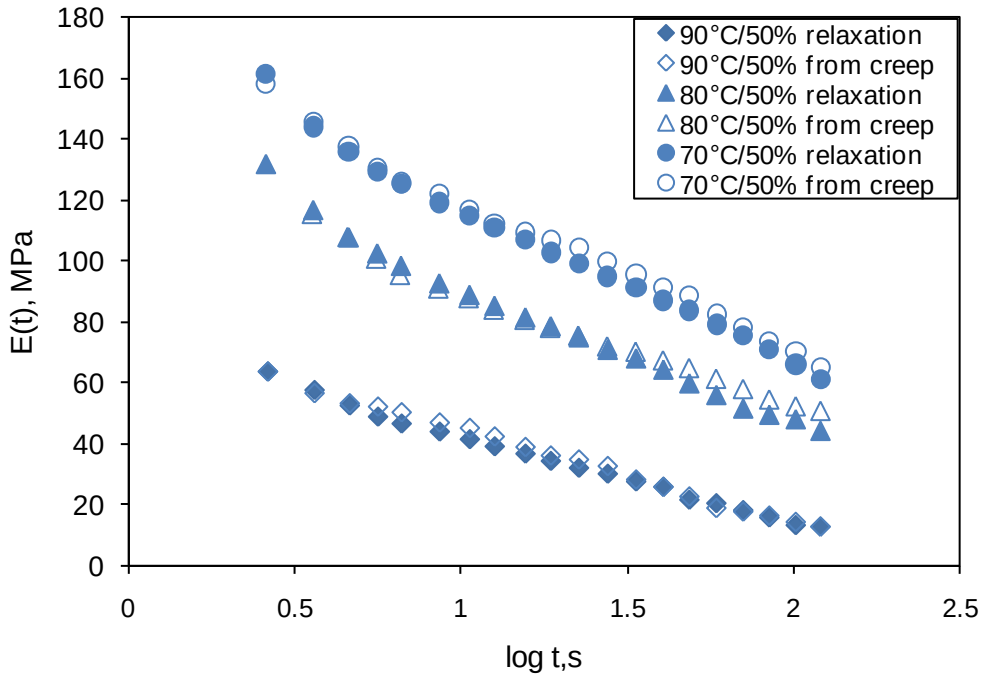

Figure 4.9 Stress relaxation modulus of NRE 211 obtained at 70, 80 and 90°C/50% RH is compared with that obtained by converting creep compliance using a simple conversion relationship.

4.4.2 Transient stress relaxation tests under dry conditions

Transient stress relaxation tests were conducted on NRE 211 under dry conditions to see the differences between dry and hygrothermal master curves. Bauer et al. [102] reported that Nafion® 117 showed different dynamic mechanical properties under humid and dry conditions. Motivated by these differences, additional tests were conducted to explore the differences in viscoelastic properties under dry and humid conditions. Stress relaxation tests were conducted at temperatures from 40-130°C under dry conditions. The relaxation moduli obtained at various temperatures were shifted to a reference temperature of 70°C recording the thermal shift factors. The TTSP master curve thus obtained was then compared with the existing hygrothermal master curve referenced at 70°C / 30% RH. Not only were the shapes of the master curves different, but the thermal shift factors were also found to be different. Moreover, relaxation moduli obtained under

dry conditions was not superposable with the hygrothermal master curve. This clearly indicates NRE 211 behaves quite differently under humid and dry conditions. It was shown earlier that relaxation modulus data obtained at RH levels as low as 10% are superposable with the hygrothermal master curve. Thus somewhere between dry and 10% RH the membrane ceases to follow time temperature superposition, suggesting that the material is different, likely due to morphological changes within the membrane. More on the transition between dry and humid stress relaxation master curves will be discussed later in the paper. A comparison of dry and hygrothermal master curve is shown in Figure 4.10. In a subsequent figure (Figure 4.14), the thermal shift factors are shown along with the ones obtained from dynamic tests, and are compared with those obtained from the hygrothermal master curve.

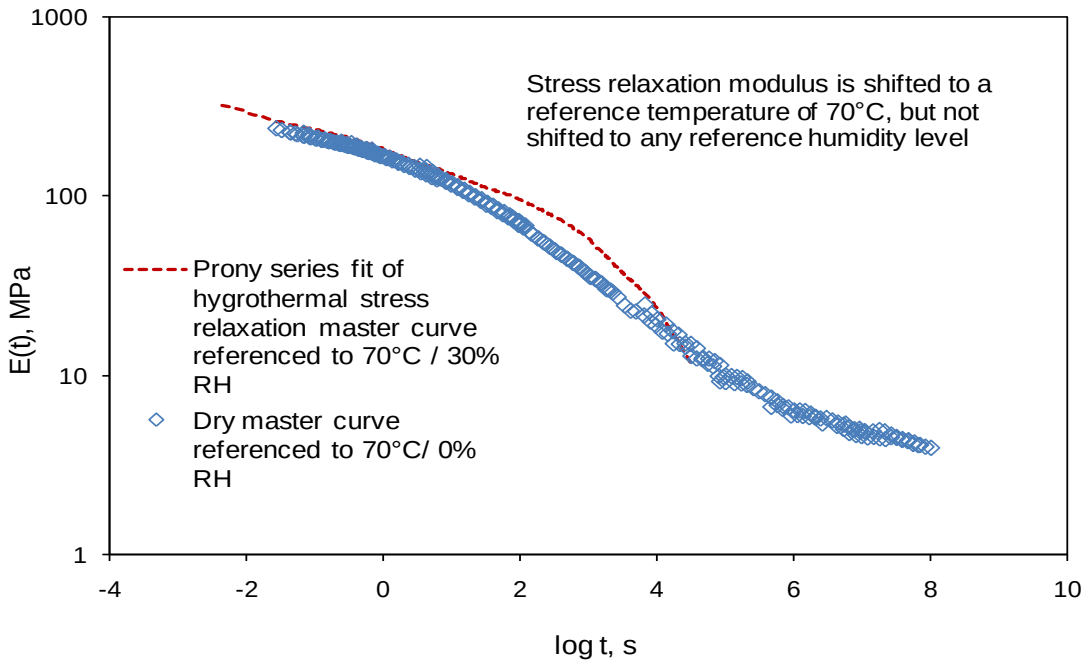

Figure 4.10 Hygrothermal master curve for NRE 211 (referenced at 70°C/30% RH) compared with relaxation master curve under dry conditions (referenced at 70°C).

4.4.3 Dry-humid transition

As Figure 4.10 shows, the hygrothermal master curve and the relaxation master curve obtained for dry conditions have different shapes. A later figure will show that master curves obtained under dry and humid conditions show different thermal shift factors. Thus relaxation tests were conducted at RH levels of 2% and 5% at temperatures of 60-90°C. The relaxation modulus obtained at 5% RH shifted along the existing hygral master curves at these temperatures, but the data at 2% RH did not. The relaxation modulus at 2% RH and under dry condition (less than 1%) at 70-90°C has been shifted assuming the shift is given by the quadratic expression given in context of Figure 4.4 ($\log a_H = A\lambda^2 + B\lambda + C$). It is also clear from Figure 4.11 that relaxation modulus data at 60°C shifts well even at a very low humidity level. This suggests that the TTSP begins to fail at dry conditions and some temperature above 60°C, in the sense that a smooth hygral master curve cannot be formed by shifting the relaxation modulus data obtained at all the humidity levels. The transition is more distinct at 80°C and 90°C. Figure 4.11 shows this transition at the abovementioned temperatures. One hypothesis is that when enough moisture is present in the membrane, Columbic forces between water molecules and sulfonic acid groups dominate, resulting in higher modulus. Further study is required to support this claim. Figure 4.12 shows this transition in terms of the hygral shift factors. It shows the hygral shift factors as shown in Figure 4.4, as well as the ones which might actually be used to superimpose the relaxation data at dry and 2% RH at 70-90°C.

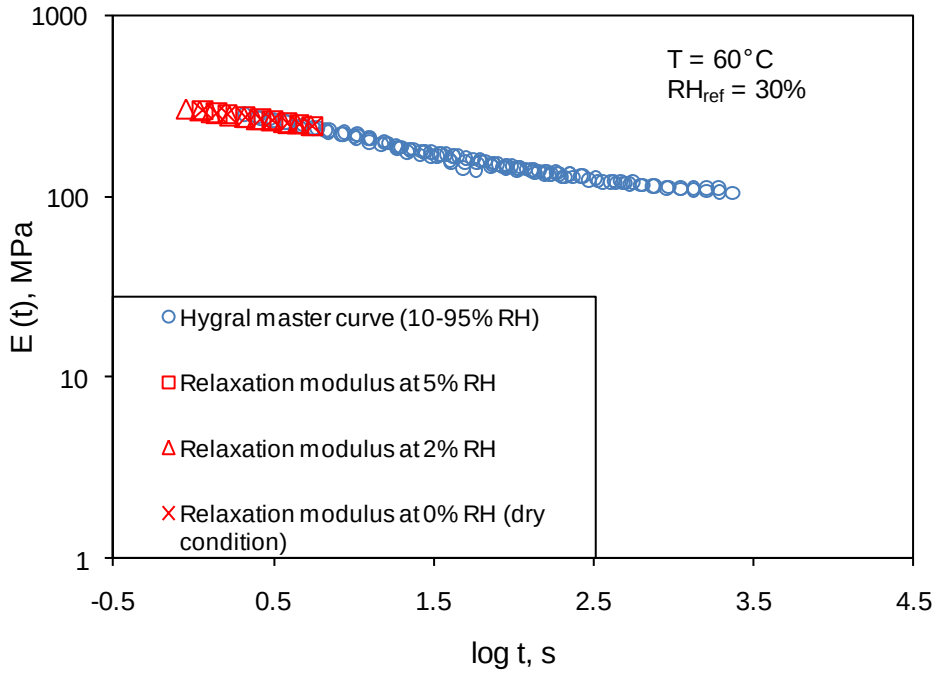
1000
100
10
1
E (t), MPa
T = 60°C
RHref = 30%
Hygral master curve (10-95% RH)
Relaxation modulus at 5% RH
Relaxation modulus at 2% RH
Relaxation modulus at 0% RH (dry condition)
-0.5
0.5
1.5
2.5
3.5
4.5
log t, s

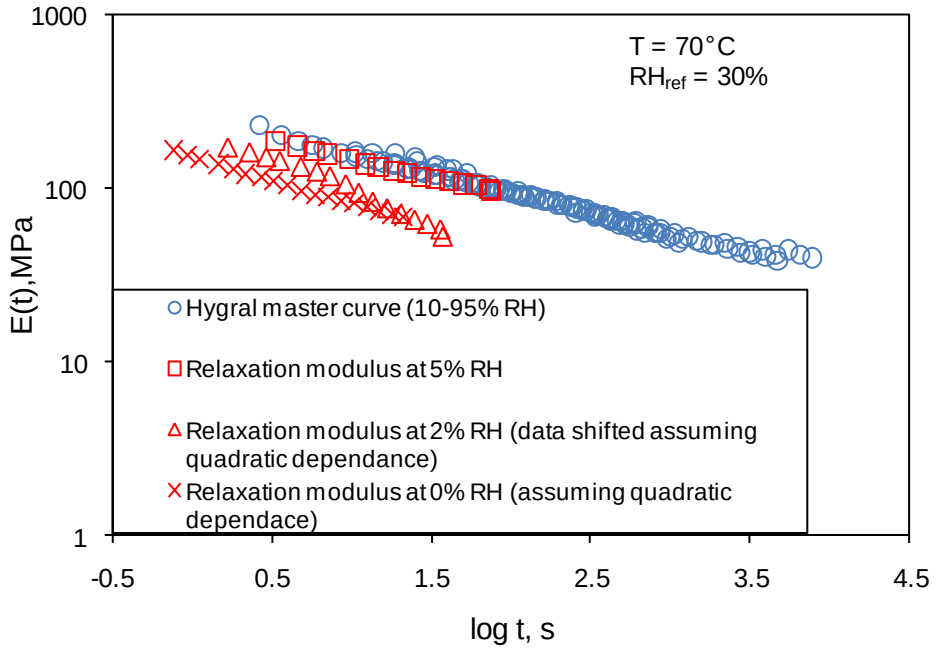
1000
100
10
1
E(t),MPa
T = 70°C
RHref = 30%
Hygral master curve (10-95% RH)
Relaxation modulus at 5% RH
Relaxation modulus at 2% RH (data shifted assuming quadratic dependance)
Relaxation modulus at 0% RH (assuming quadratic dependace)
-0.5
0.5
1.5
2.5
3.5
4.5
log t, s

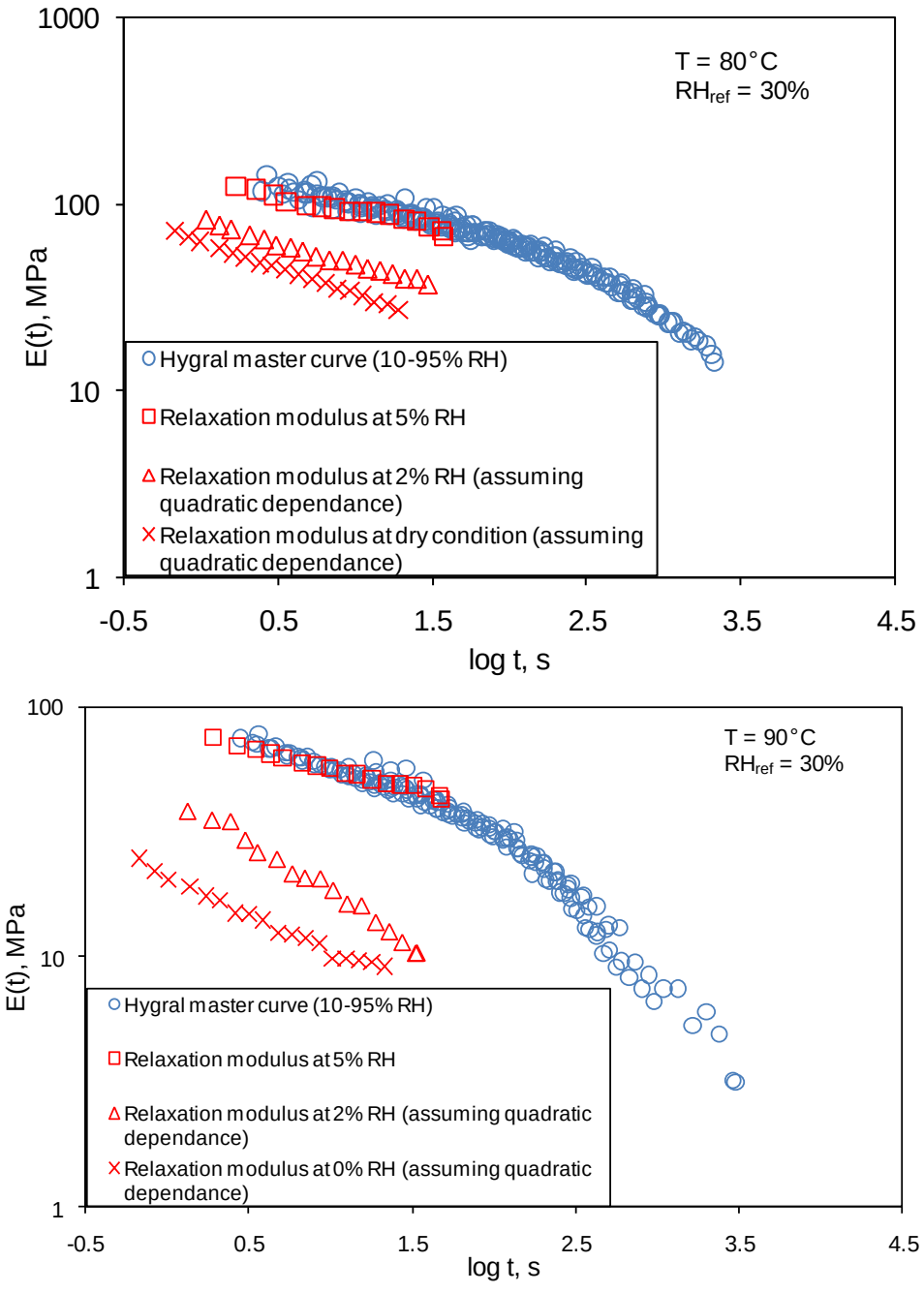

Figure 4.11 Hygral stress relaxation master curves at 60-90°C, clearly showing transition at around RH = 2-5%, corresponding to λ ~ 0.5-0.6, at temperature above 60°C.

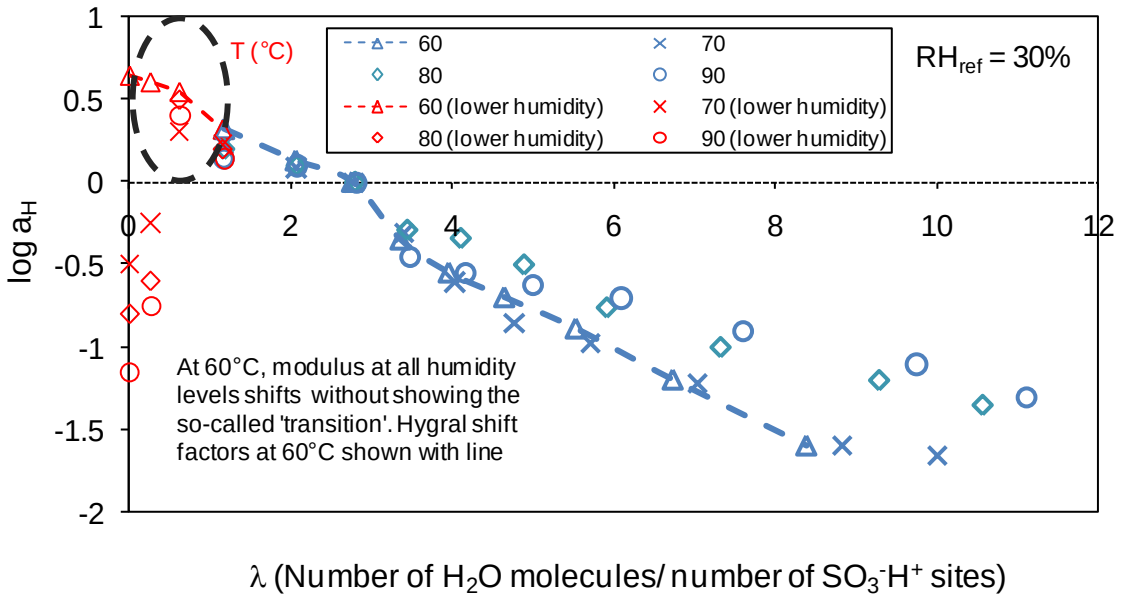

Figure 4.12 Hygral shift factors at 60-90°C, clearly showing transition at around RH = 2-5%, corresponding to λ ~ 0.5-0.6, at temperature above 60°C.

In this section, we try to explain the phenomenon observed and reported above. It is evident that temperature and water content are amongst the important driving forces (perhaps strains and stresses as well, which are not discussed here) dictating the viscoelastic behavior of Nafion. We argue that when these physical conditions drive ordered phase separation, the elastic modulus of Nafion increases and the relaxation process slows down. On the other hand, when ionic domains are in the disordered state, the elastic modulus decreases and the relaxation process is accelerated [128]. It is also evident that water plasticizes Nafion in general; and the large decrease in modulus of Nafion around 70-80°C under dry conditions is also well known. Eisenberg [49] provides an explanation for this transition on the basis of balance between the electrostatic energy to form clusters of sulfonic acid groups and the entropic elastic energy to draw the

sulfonic acid groups together. At about 70-80°C (near the α-relaxation temperature of Nafion [119, 120]), the entropic contributions of the elastic energy dominate over the electrostatic interactions. The sulfonic acid groups cluster by a combination of polar interactions and hydrogen bonding. As the temperature is increased above the critical temperature (under dry conditions, at 70-80°C), the sulfonic acid domains become miscible in the PTFE matrix reducing the modulus. On the other hand, water-acid interactions stabilize the phase-separation to a much higher critical temperature.

As known, sulfonic acid groups are strongly hydrophilic, while the PTFE matrix is hydrophilic. Benziger et al. [128] claim that with absorption of water, the bonding energy within the ionic clusters increases, thereby increasing the critical transition temperature to higher temperature. The absorption of water can also drive the miscible systems to phase separate. At dry conditions, the dipole interactions bind the sulfonic acid cites together. Adding a small amount of water into the clusters allows the hydrogen bonding between the sulfonic acid groups, which increases binding energy [102].

4.4.4 Validation of master curves

The hygrothermal master curve constructed was validated using longer term stress relaxation tests. Longer term relaxation modulus data gives confidence in the master curve if it is in good agreement with predictions, as it should ideally closely match the hygrothermal master curve over all time periods of interest. If run for a sufficiently long time, the long term test may extend the data beyond the time scale of the master curve. The stress relaxation moduli obtained from the longer term tests were compared with the hygrothermal master curve. Figure 4.13 shows a plot of the master curve and the longer term stress relaxation modulus data from two tests. The longer term stress relaxation modulus is seen to match quite well with the hygrothermal master curve, and even extend

beyond it, ultimately showing a plateau that appears to be an equilibrium modulus at about 3 MPa.

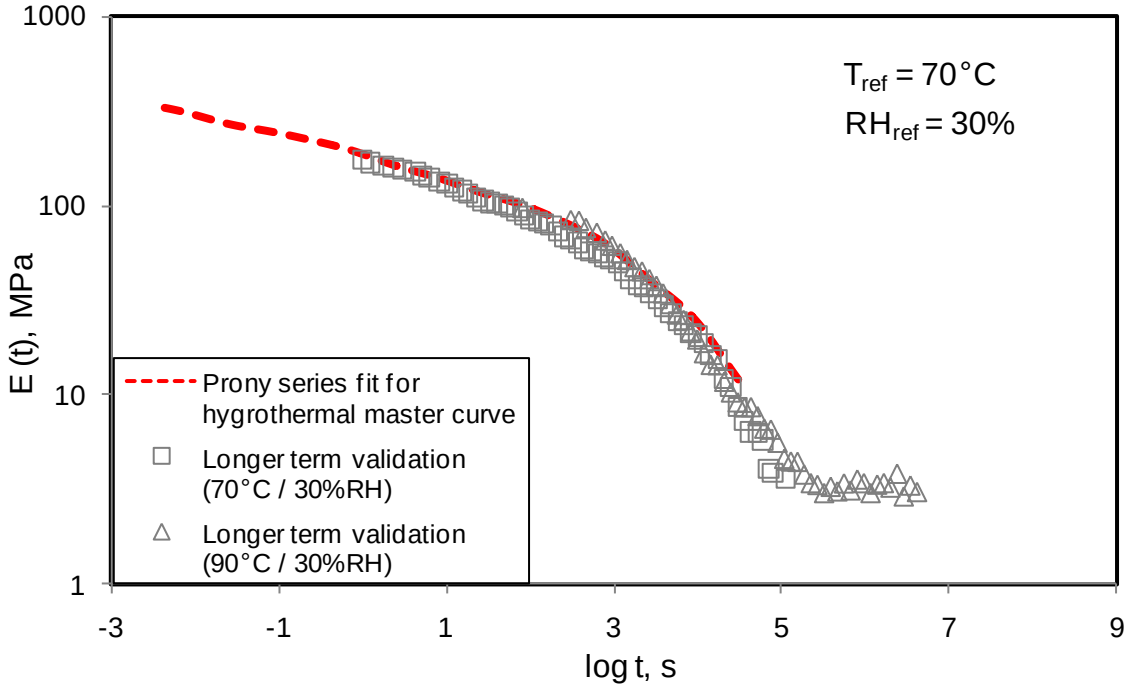

Figure 4.13 Hygrothermal master curve for NRE 211 compared with two longer term stress relaxation tests conducted at 70 and 90°C, at 30% RH. The 90°C /30% RH data was shifted to 70°C /30% RH reference condition using previously shown shift factors.

Besides longer term relaxation tests, longer term creep tests were also conducted in order to see if creep compliance shows an obvious plateau in the same time region that corresponds to about 3 MPa of relaxation modulus. It was evident from the results that the creep compliance hit the plateau at about 1400 s, consistent with the plateau location seen in case of relaxation modulus. Also the plateau compliance is about 0.34 MPa^{-1} which when converted to relaxation modulus would correspond to about 3 MPa, consistent with the longer term relaxation modulus.

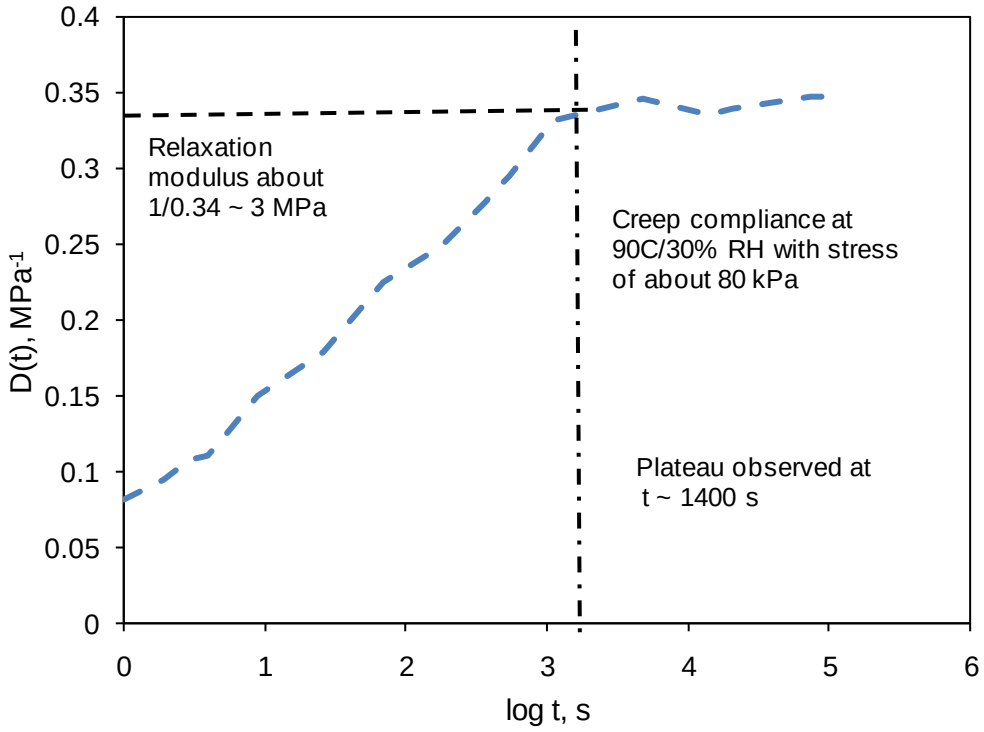

Figure 4.14 Longer term creep compliance of NRE 211 at 90C/30% RH with 80 kPa stress. Evident plateau matches well with the results obtained from longer term stress relaxation tests.

Longer term stress relaxation moduli obtained under dry conditions at 90°C and 110°C are compared with the TTSP master curve in Figure 4.15. The longer term modulus deviates significantly from the short term TTS master curve. Traditionally the modulus at high temperature needs to be corrected with a vertical shift which corresponds to $\left(\frac{T\rho}{T_0\rho_0}\right)$. The vertical shift has been taken into account, but is not significant enough to justify the difference in moduli obtained from short term and long term tests. Interestingly enough, Figure 4.13 (which represents results for a hydrated sample) does not show the presence of physical aging and/or irreversible morphological changes in the membrane. The apparent difference in moduli could be due to significant densification of the amorphous phase in semicrystalline Nafion, as explained and cited by Struik [73, 142,

143] and by Marand et al. [144] in case many semicrystalline polymers. Although mechanism proposed by Marand et al. is different than that proposed by Struik, both claim to observe physical aging above T_g in semicrystalline polymers. In order to explore whether Nafion ages under dry conditions, Nafion was subjected to aging followed by stress relaxation for 5 cycles. For every subsequent cycle, the relaxation modulus was found to be higher than the previous cycle. In order to confirm the existence of physical aging, the modulus was measured after rejuvenating the membrane specimen at 90°C. It was observed that the modulus recovered and was found to be consistent with that obtained from non-aged specimen. Time-aging time master curve was constructed for the relaxation modulus of Nafion, and is shown in Figure 4.16. Typically observed horizontal and vertical shifts were applied while constructing such master curve. This phenomenon can be explained on the basis of formation of secondary crystallites around the α-relaxation temperature of Nafion which act as crosslinking sites for rest of the amorphous phase resulting in higher modulus. Another possible explanation might have to do with irreversible morphological changes in the membranes that have not been understood fully at this point. Such morphological rearrangement may result in better packaging of ionic domains thereby resulting in strengthening of dynamic network as a function of time. Further study is required to claim the validity of either explanation.

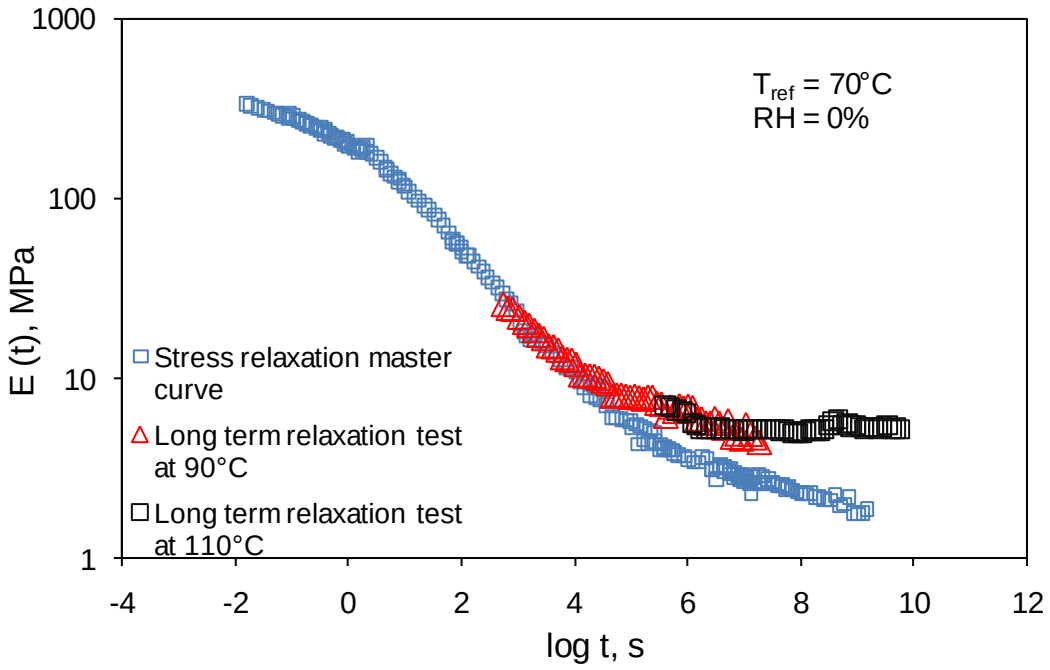

Figure 4.15 Dry master curve for NRE 211 (referenced at 70°C) compared with longer term relaxation modulus under dry conditions at 90°C and 110°C for over 7 decades. Note that 90°C and 110°C relaxation modulus data were shifted to 70°C reference temperature using the shift factors shown in Figure 4.19.

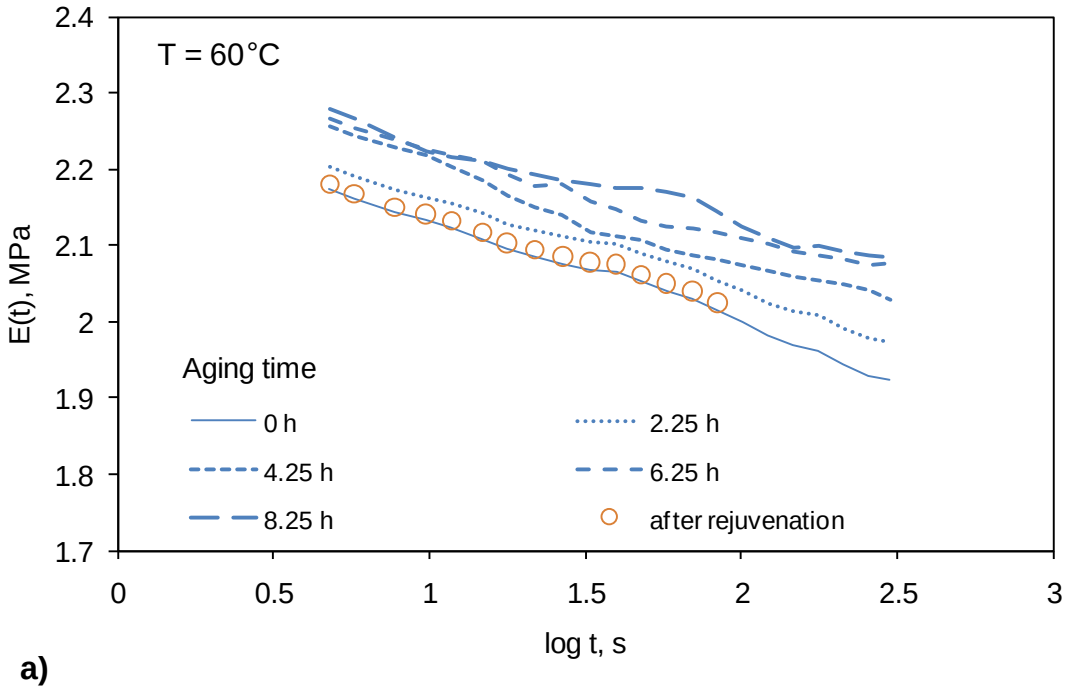

a)

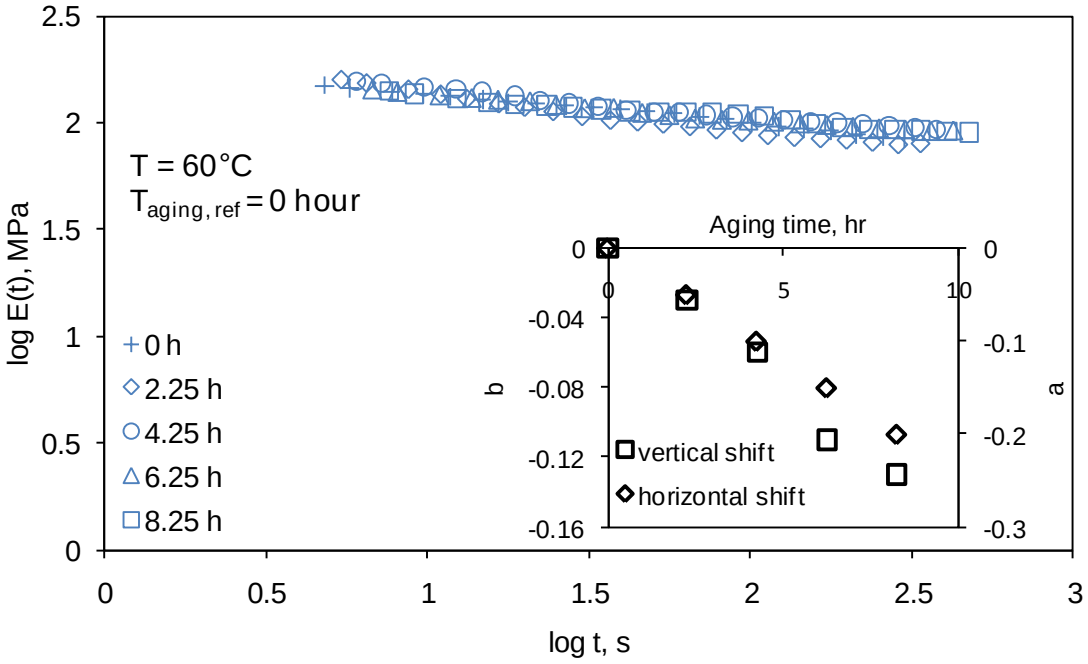

b)

Figure 4.16 Evidence of physical aging in Nafion NRE 211. a) Stress relaxation modulus obtained after aging the membrane for various time intervals at 60°C, b) Time-aging time master curve constructed for the stress relaxation modulus at 60°C for Nafion NRE 211. The necessary horizontal and vertical shifts are shown as inset.

4.5 Dynamic tests

Dynamic tests were conducted to complement and validate the transient stress relaxation procedure under dry condition. Nafion NRE211 was subjected to a dynamic loading under nominally dry conditions to obtain storage ($E^{'}$) and loss ($E^{''}$) moduli, as well as $\tan\delta = \frac{E^{''}}{E^{'}}$. The peak of the loss modulus was used as the criterion to define the α-transition in NRE 211. Figure 4.17 shows the dynamic response of NRE 211. The loss modulus shows a peak at around 80°C; which corresponds to the α-relaxation of Nafion. Osborne and Moore [120] used a peak in tan δ (at about 85-90°C) in the H-form of Nafion to characterize the α-relaxation. Thus our observation matches reasonably well with the results reported by Osborne and Moore.

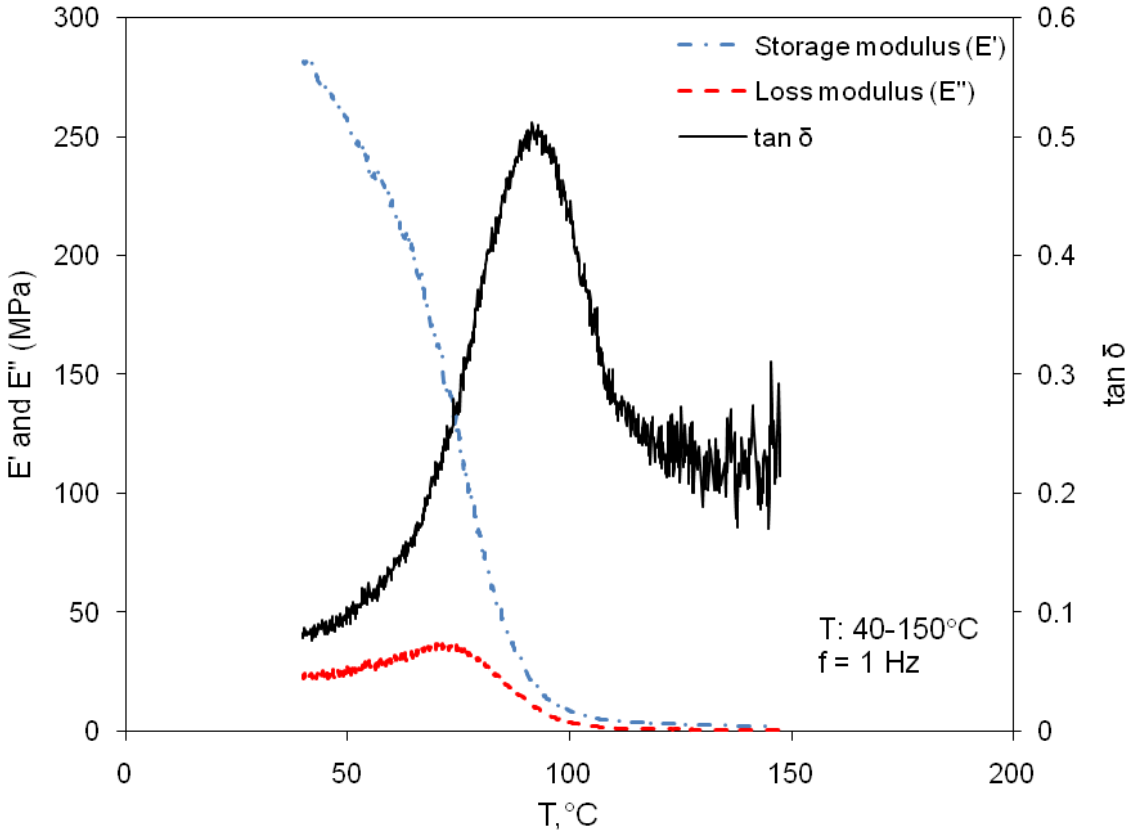

Figure 4.17 Dynamic test performed on NRE 211 under dry conditions showing storage and loss modulus as well as tan δ.

Dynamic tests were also conducted in multi-frequency, temperature ramp mode and a storage modulus master curve was constructed using reduced frequencies. The master curve and corresponding temperature shift factors are shown in Figure 4.18. The thermal shift factors obtained from dynamic tests are under dry conditions and are significantly greater than those obtained from the hygrothermal master curve. Again, appropriate vertical shifts have been added to account for a change in modulus with temperature. These shift factors match closely with the thermal shift factors obtained

from stress relaxation tests under dry conditions. The thermal shift factors for humid conditions were found to be quite different than for dry conditions, especially above the α-transition. A similar observation has also been made by Bauer et al. [102]. This phenomenon can be explained using the underlying understanding of fractional free volume. Moisture accelerates the viscoelastic properties of hydrophilic polymer like Nafion in a similar fashion temperature does. When experiments are conducted under transient humidity environment, the effect of moisture and temperature is combined to change the fractional free volume in a polymer. Moisture tends to increase the free volume in the material making more space to mobilize the polymer chains. At higher temperature, the thermal effect does not need to do as much to accelerate the processes as it otherwise would with not as much free volume in absence of moisture. Thus water acts as an internal plasticizer. Figure 4.19 shows a comparison of thermal shift factors obtained under humid and dry conditions.

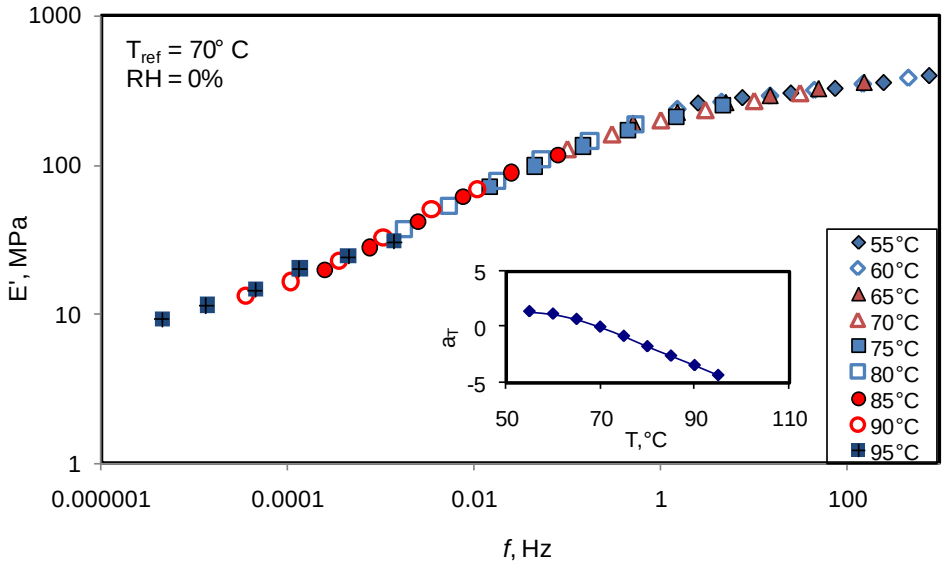

Figure 4.18 Storage modulus (E') master curve as a function of reduced frequency obtained under multi-frequency, temperature ramp mode.

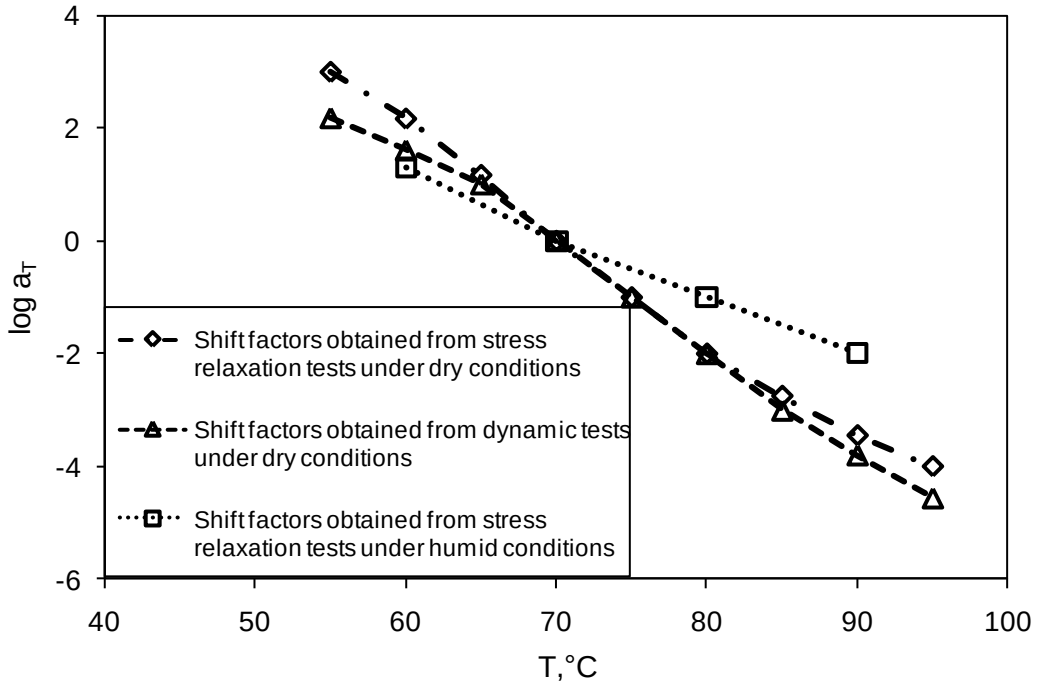

Figure 4.19 Comparison of thermal shift factors obtained under dry and humid conditions.

Dynamic data can also be used to validate the Prony series fit of the stress relaxation data. Dynamic storage modulus can be written in terms of Prony series coefficients as [56, 116]:

$$E(\omega) = \sum_{n=1}^{9} \frac{E_i \omega^2 \tau_i^2}{1 + \omega^2 \tau_i^2} \qquad (6)$$

E_i and τ_i are the Prony series coefficients obtained from fitting the Prony series to the stress relaxation master curve constructed under dry conditions. Storage modulus (E') obtained from multi-frequency tests conducted at 70°C is compared with that predicted from Equation (3), and is shown in Figure 4.20. Within experimental error, the modulus obtained from dynamic tests matches well with that predicted from the Prony series fit for a stress relaxation master curve.

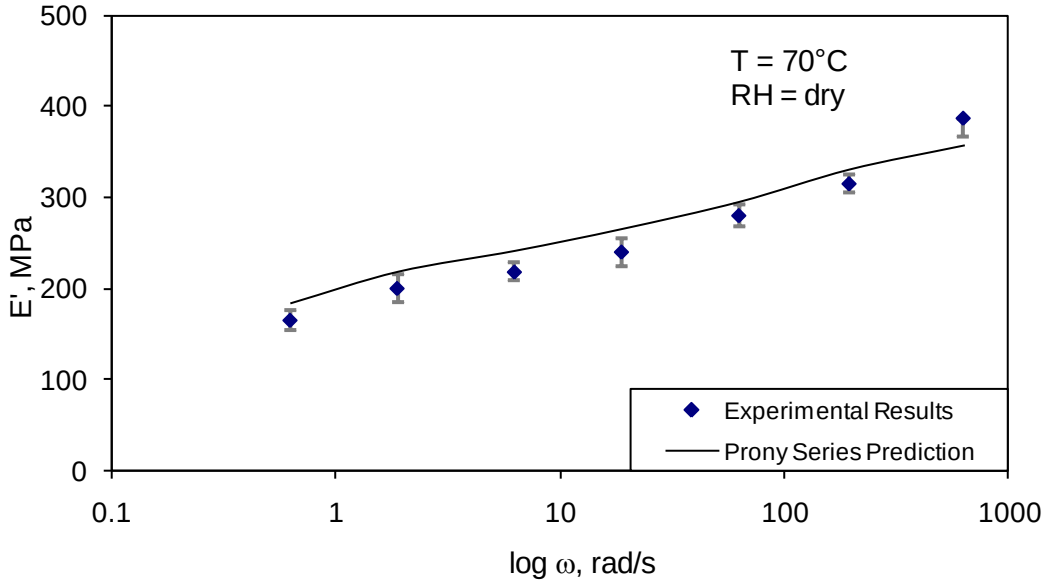

Figure 4.20 Storage modulus from dynamic test compared with that predicted from Prony series parameters obtained from stress relaxation tests under dry conditions.

In constructing the master curves, we have incorporated the vertical shifts that correspond to a temperature change and density change. The vertical shift of less than a tenth of a decade was required to account for a humidity change from dry-90% RH. We have not included submerged stress relaxation tests in this paper. Such tests are underway. In case of submerged tests, significant vertical shifts would be required, as Nafion absorbs significant amount of water under immersed conditions. The Prony series coefficients obtained from the hygrothermal relaxation master curve have been incorporated in a stress prediction program (not discussed in this paper) [140], and results obtained from numerical simulations matched closely with the experimental results.

4.6 Summary

Transient stress relaxation tests were conducted at a strain of 0.5% on NRE 211 membrane samples for the following test conditions: 10-90% RH at temperatures 40-

100°C, at 95% RH at temperatures 70-90°C, under dry conditions at temperatures 40-130°C, and at 2% and 5% RH at 60-90°C. The data from each test temperature was shifted to form a smooth hygral master curve at various RH levels using humidity shift factors. All hygral master curves obtained at different temperatures were then shifted using temperature shift factors to get a smooth doubly-shifted hygrothermal master curve. The success of the horizontal shifting of the data suggests the applicability of the time temperature moisture superposition principle. Appropriate vertical shifts were added to construct the master curves. Temperature shift factors assume the shape of Arrhenius-type behavior. Humidity shift factors are spread out at higher water content values and show higher moisture dependence at lower temperatures. The stress relaxation master curve was accurately fit with a 9-term Prony series for subsequent use in finite element software. The hygrothermal master curve was validated with longer term stress relaxation tests and 70°C and 90°C at 30% RH. The longer term relaxation modulus matches well with the master curve, suggesting the validity of the shift factors, as well as the experimental procedure. The equilibrium modulus plateau seen at longer times was about 3MPa. Creep compliance was measured at 40-90°C/50% RH and was seen to form a smooth creep master curve. The thermal shift factors obtained were consistent with those obtained from stress relaxation master curve. Creep compliance at 70-90C/50% RH was converted to stress relaxation modulus using a simple power law interconversion. The converted stress relaxation modulus matched closely with relaxation modulus experimentally obtained at identical conditions. Longer term creep test was conducted at 90°C/30% RH to see if the test showed any compliance plateau at all. Creep compliance

showed a plateau at about 0.34 MPa^{-1}, consistent with stress relaxation modulus plateau at about 3 MPa

The storage modulus obtained from the dynamic tests under dry conditions was compared with the stress relaxation modulus obtained from transient tests under dry conditions and good agreement was found between the two. Longer term stress relaxation modulus at 90°C showed a significant deviation with the master curve under dry conditions, suggesting the possibility of some morphological changes within the membrane or physical aging in Nafion. No such phenomenon was observed in case of longer term stress relaxation tests under humid condition. This may suggest that water acts to rejuvenate the membrane, and retards the aging process. There could be irreversible morphological changes in the membrane leading to this behavior.

Dry and hygrothermal master curves not only have different shapes with dry modulus dropping much more rapidly at higher temperatures; but also have different thermal shift factors. Relaxation modulus at a humidity level of 5% shifted along the hygral master curve at temperatures 70-90°C, but failed to shift at 2% RH and dry conditions. This indicates a possible 'humidity transition' in which the membrane ceases to conform to the time temperature moisture superposition principle. Accurate information regarding the viscoelastic behavior of proton exchange membranes may be useful in determining the resulting stress state in constrained fuel cell operating conditions, and its effect on membrane life and durability.

4.7 Acknowledgement

The authors would like to express appreciation to the General Motors Corporation for supporting this work, as well as the Institute for Critical Technology and Applied

Science (ICTAS) and the Engineering Science and Mechanics Department at Virginia Tech for providing additional support and facilities. We thank Cortney Mittelsteadt for helpful discussions. We would also like to acknowledge the Macromolecules and Interfaces Institute at Virginia Tech for fostering interdisciplinary research in the field of fuel cells.

CHAPTER 5: Nonlinear Viscoelastic Characterization and Modeling of Proton Exchange Membranes

Manuscript prepared for Mechanics of Time-Dependent Materials

5.1 Abstract

When a proton exchange membrane (PEM) fuel cell (PEMFC) is placed in service, significant hygrothermal stresses develop in the constrained membrane due to the transient humidity and temperature operating environment. Our previous work which characterized the viscoelastic response of the membrane in order to predict stresses was based on the assumption of linear viscoelasticity. However, nonlinear viscoelastic effects are likely to play an important role in damage localization and in the neighborhood of stress concentration sites such as cracks and layer termination sites. Such nonlinear effects should be investigated and modeled in order to assess their effect on predictions of life and durability of the membrane. In this work, a commercially available PEM, Nafion® NRE 211 (DuPont) was subjected to various stress levels at two different temperatures under dry conditions. The well-known Schapery uniaxial single hereditary integral model was found appropriate to capture nonlinearity induced in these membranes. The material parameters developed were subsequently used in a numerical prediction scheme developed to predict the strain response to stress inputs. The model was validated by comparison with additional test results involving more complex loading profiles. Good agreement between experimental data and model predictions was observed over a range of stress, and stress ramp rates.

Keywords: Proton exchange membranes, polymer electrolyte membranes, fuel cell, nonlinear viscoelastic characterization, Schapery model, Nafion, durability

5.2 Introduction

Proton exchange (or polymer electrolyte) membrane (PEM) fuel cells (PEMFCs) have received considerable attention from various government and private organizations interested in developing more efficient energy conversion systems for portable, automotive, and stationary applications. PEMFCs offer significant advantages in terms of energy and power density, higher efficiency, and cleaner power [2]. However, the durability of the PEM still poses a significant concern that must be addressed before the potential of PEMFCs can be realized. Constrained by the stack compression in a fuel cell, substantial in-plane hygrothermal stresses develop in the membranes as moisture and temperature vary during operation. These stresses are believed to significantly affect the durability of the membrane. Investigating the mechanical response of membranes subjected to simulated fuel cell cycles has been extensively studied and models involving stress-strain behavior of membranes and membrane electrode assemblies (MEA) have been reported in the literature [13, 125, 132, 134, 135, 139, 140, 145]. Weber and Newman [98] studied the stresses associated with constraint in a simple 1-D model. Tang et al. [13, 138] used a finite element model to incorporate hygrothermal stresses induced in a membrane due to thermal and humidity changes in a cell assembly. They assumed the membrane to be perfectly linear elastic. A viscoelastic stress model proposed by Lai et al. [122, 125] assumes the membrane to be hygrothermorheologically simple, and uses the relaxation master curve obtained for Nafion® NR 111 as an input parameter in the model. Park et al. [140] analyzed the hygrothermal stress state in a biaxially constrained membrane under transient temperature and humidity conditions. Based on measured

tensile relaxation modulus and hygral/thermal expansion coefficients, they developed and proposed a transient hygrothermal viscoelastic constitutive equation. Solasi et al. [134] applied the constitutive properties obtained for a wide variety of thermal and humidity levels in a finite element model to study through-thickness and in-plane behavior of an MEA. In-plane expansion/shrinkage mechanical response of the constrained membrane as a result of changes in hydration and temperature was studied in uniform and non-uniform geometries and environments. A similar in-plane elastic-plastic model was also used for in-plane numerical modeling of RH-induced strain in an MEA in a constrained configuration. In a recent paper, Solasi et al. [135] proposed a two-layer viscoplastic model for a constrained membrane that consists of an elastoplastic network in parallel with a viscoelastic network (Maxwell model). This model separates rate-dependent and rate-independent behavior of the material. Our previous work in this area was based on characterizing the hygrothermal viscoelastic properties of membranes and predicts the stresses using linear viscoelastic stress model [112, 113, 127]. But the assumption of linear viscoelasticity may not be valid under a variety of conditions, such as damage localization and stress concentration sites. Local stresses in such regions may be too high to push the membrane to behave nonlinearly. Accurately understanding these stresses is not only important for durability and life concerns, but it can also serve to know the limits of the existing linear viscoelastic stress model.

To date, very few nonlinear viscoelastic characterization and modeling studies on PEMs have been reported in the literature. Thus, we discuss a very popular nonlinear viscoelastic model (which has been used in this study as well); the Schapery model and its implementation in various problems. Based on irreversible thermodynamics, Schapery

[78, 80, 81, 83, 84] formulated a universal nonlinear viscoelastic model. This model assumes the nonlinear stress dependent behavior of a material that may be characterized in a manner similar to the traditional TTSP used for linear viscoelastic materials. The stress dependence is shown by a systematic compression or expansion of the time scale. Schapery has provided a review of experimental results, and has presented the theoretical results for a variety of nonlinear viscoelastic materials such as nitrocellulose films, fiber-reinforced phenolic resin and polyisobutylene to name a few. He has validated his theory with the characterization of additional viscoelastic materials and states that the constitutive equations are suitable for use in engineering stress analysis. Smart and Williams [85] compared Schapery's method to the modified superposition principle (MSP) and to the Bernstein-Kearsley-Zapas (BKZ) theory [86]. The MSP theory separates creep behavior into time dependent and stress dependent parts. It is simple to implement, but the predicted stress output based on input strain history is poor. Dillard et al. [146] while studying nonlinear response of graphite/epoxy composites, compared Schapery's model to several nonlinear theories, including MSP. They claim that Schapery's method produces the most accurate results. They also maintain that this method retains its applicability when given complex loading histories. Popelar et al. [91] analyzed a comprehensive dataset obtained from stress relaxation and constant strain tests conducted on amino-based epoxy adhesive. The relaxation datasets are used to develop the nonlinear model, and the nonlinear response is characterized by Schapery's model. At low strains, the nonlinear model based on relaxation data predicts the stress-strain response in agreement with the experimentally measured response. The discrepancies at higher strain rates are possibly due to viscoplastic effects that are not incorporated into

the model. A special case of the Schapery model is the 'free-volume' approach by Knauss and Emri [88, 89]. The underlying assumption is that the free volume, although not explicitly defined in the papers, controls the molecular mobility, directly affecting the time scale of the material. Instead of using the Doolittle equation, which the abovementioned theories used, Shay and Carruthers [90] used a thermodynamic equation of state to establish the interrelation between temperature, specific volume and pressure. Popelar and Liechti [91, 92] while studying epoxy-based structural adhesives, proposed a distortion-modified free volume theory, which takes into account the distortional effects in the inherent time scale of the material along with the dilatational effects. Payne et al. [147] present a methodology to characterize the nonlinear viscoelastic behavior of thin films (such as polyethylene) using a dynamic mechanical approach. Stress-dependent behavior in high altitude scientific balloons, induced by large stresses was studied. They used dynamic oscillatory tests, which produce predictions consistent with the results of traditional creep tests. Wilbeck [148] studied the nonlinear viscoelastic characterization of thin polyethylene films. He attempted to predict the stress state in the film given the individual strain and temperature histories. After studying the dependence of the film on the loading history Wilbeck determined that the polyethylene film behaves, and consequently should be modeled as a nonlinear viscoelastic material.

Although there are various formulations proposed to model nonlinear viscoelastic behavior, Schapery's model has been extensively applied for both isotropic and anisotropic materials. Numerical integration formulations within a finite element (FE) environment to model nonlinear viscoelastic behavior have been studied extensively. Henriksen [149] used Schapery's nonlinear constitutive model and developed a recursive

numerical integration algorithm. In their work, a Prony series form is required to express the transient compliance in order to allow for a recursive form of the hereditary integral. Higher stresses were believed to induce nonlinearity in a material. Roy and Reddy [150] used a similar approach and formulated a numerical integration method for the Schapery model coupled with moisture diffusion and used for 2D FE modeling of adhesively bonded joints. Lai and Bakker [151] modified the Henriksen recursive algorithm in order to include nonlinear effects due to temperature and physical aging by using a reduced-time function. The constitutive formulation was used to model experimental tests with PMMA. Touati and Cederbaum [152] presented a numerical scheme to obtain the nonlinear stress relaxation response from nonlinear creep response in the form of discrete data. They further extended this idea for nonlinear viscoelastic characterization and analysis of orthotropic laminated plates [153]. Li [154] developed a FE procedure to analyze nonlinear viscoelastic response for anisotropic solid materials subjected to mechanical and hygrothermal loading. The time increment was assumed smaller and stress was assumed to vary linearly over this short time increment. The hereditary stresses were obtained from the material properties, time increment, strains and stresses from the previous step. Yi et al. [155, 156] developed a FE integration procedure to analyze nonlinear viscoelastic response of composites subjected to mechanical and hygrothermal loading. Different problems in laminated composites such as interlaminar stresses, bending and twisting of composites, were solved using this FE method. Haj-Ali and Muliana [157] presented a numerical integration scheme for the nonlinear viscoelastic behavior of isotropic materials and structures. The Schapery 3D nonlinear viscoelastic material model was integrated within a displacement- based FE environment.

We have used a well-known and widely used Schapery model of nonlinear viscoelasticity to model the nonlinear response of proton exchange membranes in this paper. The Schapery model contains several stress dependent functions characterizing nonlinearity. In order to obtain these nonlinear parameters, data reduction techniques on creep/recovery datasets are routinely run; however, the development of reliable methodology for data reduction is still a subject of debate [158]. The model contains the following stress-dependent terms: material functions (g_0, g_1, g_2) which represent the vertical shift in transient creep compliance to account for nonlinearity and stress-induced shift factor (a_σ) representing the horizontal shift along the time axis, which acts to accelerate the internal material clock in a way analogous to the thermal shift factor. Lou and Schapery described a methodology to define the nonlinear parameters assuming power-law time dependence [159]. If the creep response does not obey a power-law, a Prony-series representation of creep compliance must be used, as suggested by Tuttle and researchers [160, 161]. The model also includes a viscoplastic strain term, which may be represented in the form employed by Zapas-Crissman [162].

In this paper, we explore the nonlinear viscoelastic behavior of Nafion® NRE 211 (referred to as NRE 211 henceforth), which has become the benchmark standard for proton exchange membranes. We establish the onset of nonlinearity in NRE 211, evaluate the nonlinear parameters used in the Schapery model using data reduction techniques, and develop a nonlinear viscoelastic model applicable to a PEM fabricated from NRE 211. Results from the analysis are validated by running various stress profiles and comparing with experimental data. Throughout the analysis, we have used a Prony series representation of the creep response of NRE 211, as the Kelvin-Voigt kernel is quite

amenable to the hereditary integral used in the model. Since all the test cases were run in a DMA, certain limitations were imposed on the stress or temperature levels to which the membrane samples could be subjected. For example, it was not possible to run a creep/recovery test at 10 MPa stress at temperatures above 70°C, as the large strains reached the limit of travel thereby effectively stopping the DMA quickly, making any kind of reduction procedure impossible.

5.3 Theory

5.3.1 Isochronal stress-strain plots

Polymers, being time-dependent, result in a nonlinear stress-strain curve for a constant strain rate test. Isochronal stress-strain plots generated from either creep or relaxation tests give a basis to establish linearity in polymers. For linear viscoelastic materials, the isochronous (meaning "the same time") response is linear, but the effective modulus drops with time so that the stress-strain curves at different times are separated from one another. When a viscoelastic material behaves nonlinearly, the isochronal stress-strain curves begin to deviate from linearity at a certain stress (or strain) level [70].

5.3.2 Constitutive model

A general nonlinear theory of viscoelasticity developed by Schapery presented constitutive equations for multiaxial loading, which were later modified for the case of uniaxial loading [159]. The constitutive equation for uniaxial loading is given by

$$\varepsilon(t) = g_0 D_0 \sigma(t) + g_1 \int_0^t \Delta D(\psi - \psi') \frac{d\left(g_2 \sigma(\tau)\right)}{d\tau} d\tau + \varepsilon_{vp}(t, \sigma) \qquad (1)$$

where D_0 and $\Delta D(\psi)$ are the time independent and time dependent components of the creep compliance, respectively. The reduced time variables, ψ and ψ' are defined by

$$\psi = \psi(t) = \int_0^t \frac{dt'}{a_\sigma} \text{ and } \psi' = \psi(\tau) = \int_0^\tau \frac{dt'}{a_\sigma} \quad (2)$$

Here g_0, g_1, g_2 are stress-dependent material properties, and a_σ is the stress-dependent time scaling factor (also known as stress shift factor). These factors have been shown to be a function of stress, temperature [91, 92, 163-165], but may also depend on humidity. In the present study, we have not considered humidity, so the stress shift factor becomes a function of stress and temperature only (We recognize that humidity is an important factor in PEM stress modeling and should be considered in future work). If the applied stress is sufficiently small, $g_0 = g_1 = g_2 = a_\sigma = 1$ and Equation (1) becomes the stress-strain relationship (Boltzmann integral) for a linear viscoelastic material. The transient creep compliance during loading can be expressed as a Prony series

$$\Delta D(\psi) = \sum_{n=1}^{N} D_n \left(1 - \exp\left(\frac{\psi}{\tau_n}\right)\right) \quad (3)$$

where D_n are constants and τ_n are the retardation times. A good approximation to experimental data may be obtained if the retardation times are spread uniformly over the logarithmic time scale, typically with a factor of ten between them. On the linear scale, acceptable fits are typically obtained with 1-2 elements per decade. Another way of looking at the Prony series form is the representation of a system with a series of spring and dashpots in parallel (Kelvin-Voigt form). The last term in Equation (1), which represents the viscoplastic strain accumulated during a loading-unloading cycle, is a function of time, applied stress and temperature. Each of the g parameters defines a nonlinear effect on the compliance of the material. The factor g_0 defines stress and temperature effects on the instantaneous elastic compliance and is a measure of the

stiffness variation. The transient compliance factor g_1 has a similar meaning, operating on the creep compliance component. The factor g_2 accounts for the influence of loading rate on creep and depends on stress and temperature. The factor a_σ is a time scale shift factor. This factor is, in general, a stress and temperature dependent function and modifies the viscoelastic response as a function of temperature and stress. Mathematically a_σ shifts the creep data parallel to the time axis to form a time-stress superposition master curve. These coefficients required for describing material behavior were determined from data collected during the creep/recovery experiments across a range of temperatures and stresses. Brinson and Brinson [70] discuss the time temperature stress superposition (TTSSP) to predict the long term properties of polymers, and how TTSSP can be used in conjunction with the Schapery model. The uniaxial constitutive model has been adopted from Haj-Ali and Muliana [157]. They also present an elaborate 3-D formulation; however, since our experimental data was uniaxial (obtained using tension clamps in a DMA), a simpler 1-D model was used for modeling purposes. The recursive formulation can be obtained by splitting the hereditary integral into two time-steps; namely 0 to $t-\Delta t$ and $t-\Delta t$ to t. Details of the formulation can be found in the paper by Haj-Ali and Muliana [157] and have been discussed to some extent here. The readers are encouraged to consult the paper for further information.

The Schapery uniaxial form expressed by Equation (1) contains a compliance term, function of the reduced time; which can be expressed using a Prony series as:

$$\Delta D(\psi) = \sum_{n=1}^{N} D_n \left(1 - \exp\left[-\lambda_n \psi(t)\right]\right) \tag{4}$$

where N is the number of terms, D_n of t is the n[th] coefficient of the Prony series, and λ_n is the reciprocal of the n[th] retardation time. Substituting Equation (4) into Equation (1) leads to an expression, which can further be modified to assume the form of recursive integration:

$$\varepsilon(t) = g_0 D_0 \sigma(t) + g_1 g_2 \sum_{n=1}^{N} D_n - g_1 \sum_{n=1}^{N} D_n q_n(t) \tag{5}$$

where

$$q_n(t) = \int_0^{t-\Delta t} \exp[-\lambda_n(\psi - \psi')] \frac{d(g_2\sigma)}{d\tau} d\tau + \int_{t-\Delta t}^{t} \exp[-\lambda_n(\psi - \psi')] \frac{d(g_2\sigma)}{d\tau} d\tau \tag{6}$$

A reduced time increment is given by:

$$\Delta\psi(t) \equiv \psi(t) - \psi(t - \Delta t) \tag{7}$$

Assuming that the term $g_2\sigma$ is linear over the current time increment Δt and that the shift factor is not a function of time:

$$q_n(t) = \exp[-\lambda_n \Delta\psi(t)] q_n(t - \Delta t) + (g_2(t)\sigma(t) - g_2(t - \Delta t)\sigma(t - \Delta t)) \frac{1 - \exp[-\lambda_n \Delta\psi]}{-\lambda_n \Delta\psi} \tag{8}$$

The total current strain as a function of nonlinear functions and applied stress can be obtained as:

$$\varepsilon(t) = \left[g_0(t)D_0 + g_1(t)g_2(t)\sum_{n=1}^{N} D_n - g_1(t)g_2(t)\sum_{n=1}^{N} D_n \frac{1-\exp[-\lambda_n \Delta\psi(t)]}{\lambda_n \Delta\psi(t)} \right]\sigma(t)$$
$$- g_1(t)\sum_{n=1}^{N} D_n \left[[\exp[-\lambda_n \Delta\psi(t)]]q_n(t-\Delta t) - g_2(t-\Delta t)(1-\exp[-\lambda_n \Delta\psi(t)])\frac{\sigma(t-\Delta t)}{\lambda_n \Delta\psi(t)} \right]$$
$$\equiv \overline{D}(t)\sigma(t) - f(t)$$

(9)

$$f(t) = g_1(t)\sum_{n=1}^{N} D_n \left[q_n(t) - g_2(t)\sigma(t)\frac{1-\exp[-\lambda_n \Delta\psi(t)]}{\lambda_n \Delta\psi(t)} \right]$$

(10)

The above equations allow for the incremental strain calculation for a time increment Δt, which is then added to the total strain from the previous time step $(t-\Delta t)$. The additional viscoplastic term can be incorporated through the reduced time (t/a_σ).

5.3.3 Evaluation of model parameters using creep/recovery data

A typical loading-unloading profile is given in Figure 1. Stress, given by $\sigma = \sigma_0[H(t) - H(t-t_1)]$ where $H(t)$ is the Heaviside step function, is applied for a particular time (t_1) and then removed, allowing the sample to recover until the end of the test. Correspondingly, creep strain is measured in the sample for $t \le t_1$ and then recovery strain is observed at times $t > t_1$. Substituting the expression for stress into Equation (1) yields the creep strain

$$\varepsilon_c(t) = g_0 D_0 \sigma_0 + g_1 g_2 \Delta D\left(\frac{t}{a_\sigma}\right)\sigma_0 + \varepsilon_{vp}(t,\sigma) \qquad 0 < t < t_1$$

(11)

During the recovery period, strain is

$$\varepsilon_r(t) = g_2\left[\Delta D\left(\frac{t_1}{a_\sigma} + t - t_1\right) - \Delta D(t - t_1)\right]\sigma_0 + \varepsilon_{vp}(t_1, \sigma) \qquad t > t_1 \tag{12}$$

Using the Prony series representation of creep compliance shown in Equation (3), the creep strain (Equation 11) and recovery strain (Equation 12) can be written as [158]

$$\varepsilon_c = D_0 g_0 \sigma_0 + g_1 g_2 \sigma \sum_m D_m \left(1 - \exp\left(-\frac{t}{a_\sigma \tau_m}\right)\right) + \varepsilon_{vp}(t, \sigma) \tag{13}$$

$$\varepsilon_r = g_2 \sigma \sum_m D_m \left(1 - \exp\left(-\frac{t}{a_\sigma \tau_m}\right)\exp\left(-\frac{t - t_1}{\tau_i}\right)\right) + \varepsilon_{vp}(t, \sigma) \tag{14}$$

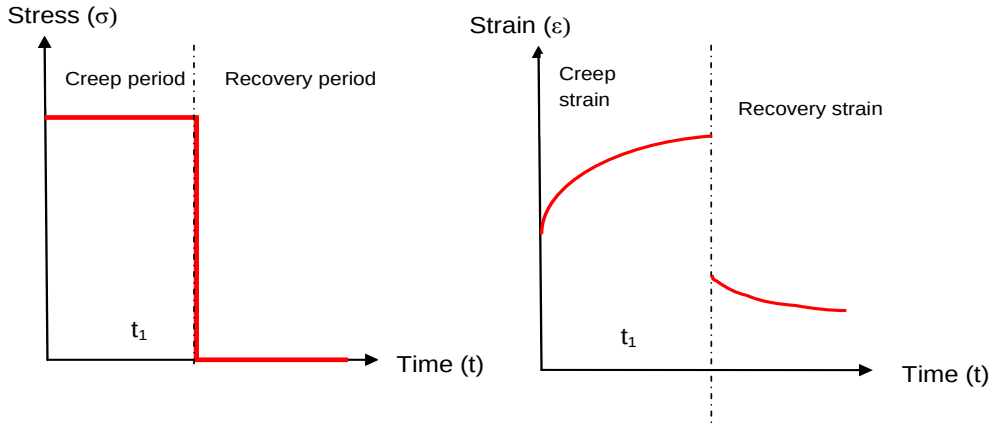

Figure 5.1 Creep and creep recovery behavior: a) Stress input and b) strain output for a creep test followed by a recovery period.

Zaoutsos et al. [166, 167] have devised an elaborate numerical scheme to calculate the nonlinear parameters using a power-law formulation for transient creep compliance. For a detailed derivation, readers are encouraged to refer to the papers cited above. Using Levenberg-Marquardt least square methods (abbreviated as the LMA henceforth) [168], the recovery test data for each recovery experiment can be fit to obtain the stress-induced

shift factor (a_σ). Even though a Prony series formulation is amenable to the nonlinear Schapery modeling, it often lends itself to extensive numerical reduction scheme to obtain the nonlinear parameters. In this work, we use the nonlinear parameters obtained using a simpler power-law formulation as a first guess to seed the LMA. The LMA are then used to optimize the nonlinear parameters which are generated using a Prony series formulation.

5.3.4 Viscoplastic strain

If the reduction procedure does not fit the creep/recovery data well and/or there happens to be a permanent set, one should use the viscoplastic term. Researchers traditionally use the Zapas-Crissman viscoplastic model in reduction of the creep and recovery data [146, 154, 160, 161, 169, 170]. This model adds a viscoplastic strain to the elastic and viscoelastic strains in the form of a power law in stress and time [162]

$$\varepsilon_{vp} = C\left\{\int_0^t \sigma(\tau)^P \, d\tau\right\}^q \tag{15}$$

The viscoplastic parameters, *C*, *P*, and *q*, are found from fits to viscoplastic strain versus stress and creep data. According to their definitions, the parameters *C* and *P* should be stress independent but temperature dependent; however, depending on how the time dependence of the viscoplastic strain is determined, *q* could be stress and temperature dependent. For a step-input of stress for a certain period of time, the integral from 0 to t becomes t and the viscoplastic strain becomes

$$\varepsilon_{vp}(t,T,\sigma) = \left\{C(T)\sigma^{P(T)}t\right\}^{q(\sigma,T)} \tag{16}$$

The time dependence in the Zapas–Crissman model is normally a source of difficulties during the data reduction [163]. It is recommended for its estimation that *q* to be treated

as a “linear” parameter, only a function of temperature, and determined from fits to linear creep data and then fixed for subsequent fits to nonlinear data [160, 161]. Boyd [160, 161] discusses the disadvantages behind this rationale and proposes a simpler power law form of viscoplastic strain

$$\varepsilon_{vp}(\sigma) = (Ct)^q \sigma^{P.q} \tag{17}$$

We have used a power-law form of the model in this paper, and have found it to work reasonably well. Boyd also claims that the Zapas–Crissman model does not lend itself to master-curve modeling because the viscoplastic component is a function of time rather than reduced time [171]. However, we observed that the parameter is indeed a function of reduced time, at least for the temperature/time conditions tested. It has been argued that the viscoplastic strain cannot be directly measured during the test since viscoelastic strains are still developing simultaneously. However, after strain recovery, the remaining irreversible strain corresponding to the loading period may be measured [158, 172, 173]. We remain skeptical about this idea, as this would suggest that loading which yields linear viscoelastic response must have some viscoplastic response as well (as there would be some unrecovered linear viscoelastic strain at this time).

5.4 Experimental

A TA Instruments Q800 dynamic mechanical analyzer (DMA) was used in tensile mode to conduct transient stress relaxation and creep/recovery experiments on small membrane samples. A long, narrow membrane sample with an average length to width ratio of five to six was used along with the dynamic mechanical analyzer fit with the humidity chamber designed. Patankar et al. [127] has described the construction of this chamber and how the humidity is controlled and measured. Typical width and length of

various specimens used for testing varied between 3.5-4 mm and 20-21 mm respectively. A light microscope was used to accurately measure the sample width. Typically the width would be measured at the top, middle and bottom sections of the film to select the part of the film which showed less variation. The uniform section of the film was then clamped in the tensile fixture of the DMA machine. The length between the clamps was accurately measured by the DMA machine prior to each loading event. The properties of Nafion depend strongly on temperature and moisture, and even a slight change in humidity can change the properties significantly as shown by Bauer et al. [102] and Benziger et al. [128, 129]. They have shown that very low water activities (~ 1% RH) can result in more than a magnitude change in the elastic modulus and the creep rate at 90°C. In addition, the rate of water absorption and desorption is such that it can take up to 10^5 s for a sample to equilibrate to changes in RH from 1% RH to 0% RH. Considering the strong dependence of Nafion on moisture, the RH in the chamber was carefully monitored. Before the start of each test, the sample chamber was purged with dry air (fed directly from a tank containing compressed dry air) for about 2 hours at a flow rate of about 300-500 sccm. Throughout the test, the chamber was fed with dry air and the dew point of air coming out of the chamber was carefully monitored. It was noted that the dew point recorded at the chamber outlet corresponded to a chamber relative humidity (at the least temperature) of less than 1% RH.

In order to construct the isochronal plots for NRE 211, creep experiments were conducted at various stress levels; including 0.5, 1, 2, 3, 5, 10, 11, 12, 15, 25 MPa for 1 hour under dry conditions at 40°C. To evaluate the nonlinear Schapery parameters, creep and creep recovery tests were conducted at 40 and 70°C. At 40°C, the membrane samples

were subjected to stress levels of 0.1, 0.5, 1, 2, 3, 5 and 10 MPa. At 70 °C, the membrane samples were subjected to all the stress levels mentioned above except 10 MPa, because a stress of 10 MPa induced excessive strain (typically above 80%), and as a result the drive shaft would reach its limit and the DMA would stop quickly without providing useful data. Typically the samples were subjected to creep for 60 minutes, followed by a recovery period of 60 minutes. At 70 °C, creep and recovery tests were run for a period of 30 minutes. In order to evaluate the viscoplastic term (Zapas-Crissman function), creep/recovery tests were run as long as 3 hours in order to determine the time-dependence of the viscoplastic term. The viscoplastic term was evaluated at 40 and 70°C only, as at higher temperatures, such long term tests were not feasible even under moderate stress levels, as the strain was too large for the DMA, shutting it down quickly. In this study, the nonlinear Schapery model was first developed in C++, and later coded in FORTRAN so it could be coupled with the finite element software, ABAQUS® as a user-defined material model (abbreviated as UMAT). To validate the model, strains were measured for several step-stress tests conducted at 40 and 70°C, and the predictions from the model were matched against the experimental data.

5.5 Results and Discussion

As mentioned earlier, nonlinear viscoelastic stresses are likely to play a critical role in assessing the life and durability of the membrane. We now present steps taken to develop a nonlinear model. These steps are illustrated in Figure 5.2, which also helps understand the sequential progression of this paper.

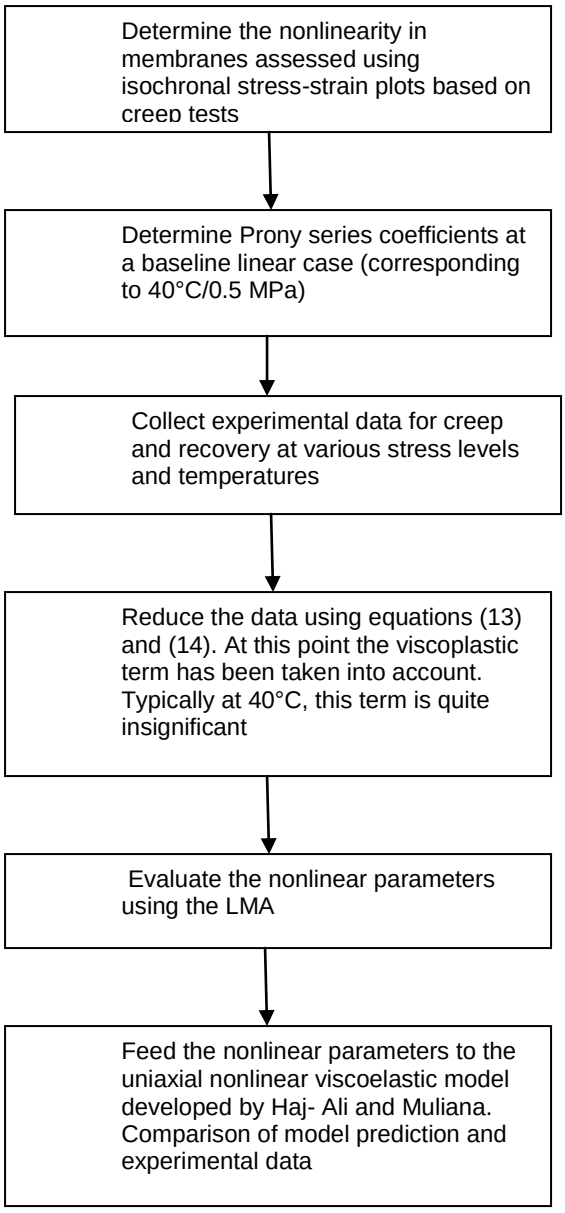

Figure 5.2 Steps taken toward developing the model.

5.5.1 Determination of the onset of nonlinearity

PEMs in an operating fuel cell experience complex stress profiles depending on temperature and humidity conditions. Thus it becomes important to know the onset of nonlinearity for PEMs, as then one can decide whether a linear viscoelastic model is accurate enough for hygrothermal stress prediction in membranes.

Thus, first step is to determine the stresses which would cause the membrane to behave nonlinearly. Isochronal stress-strain plots based on creep tests were generated to observe the onset of nonlinearity under dry conditions. Figure 3 shows such an isochronal stress-strain plot generated at 40°C. It can be seen that nonlinearity occurs at low stress levels (~3MPa), and at relatively low strain levels (~2-4%) under dry conditions. PEM-based fuel cells typically operate at 60-90°C, and anywhere between dry and 100% RH to liquid water. Depending on the temperature/RH condition in an operating fuel cell, the onset of plasticity/nonlinearity could be at lower strain levels (corresponding to dry conditions and lower temperature) or higher strain levels (higher RH levels and higher temperature). This suggests that PEM stress-prediction programs based on linear viscoelasticity [122] may not be sufficiently accurate under certain conditions. The membrane response could be different under hydrated condition. There is some indication that membranes under hydrated condition may very well exceed the mentioned strain limits before it becomes nonlinear; however, the work is unpublished at this point. Similar response was observed at other temperatures, although, tests at lower temperatures required higher strains before the membrane became nonlinear. PEMs in an operating fuel cell experience complex stress profiles depending on temperature and humidity conditions, and it is not possible to measure the amount of stresses in a membrane in a live fuel cell. Thus it becomes important to know the onset of nonlinearity for PEM in operating fuel cells ex situ, as then one can decide whether a linear viscoelastic model is sufficient for hygrothermal stress prediction in membranes.

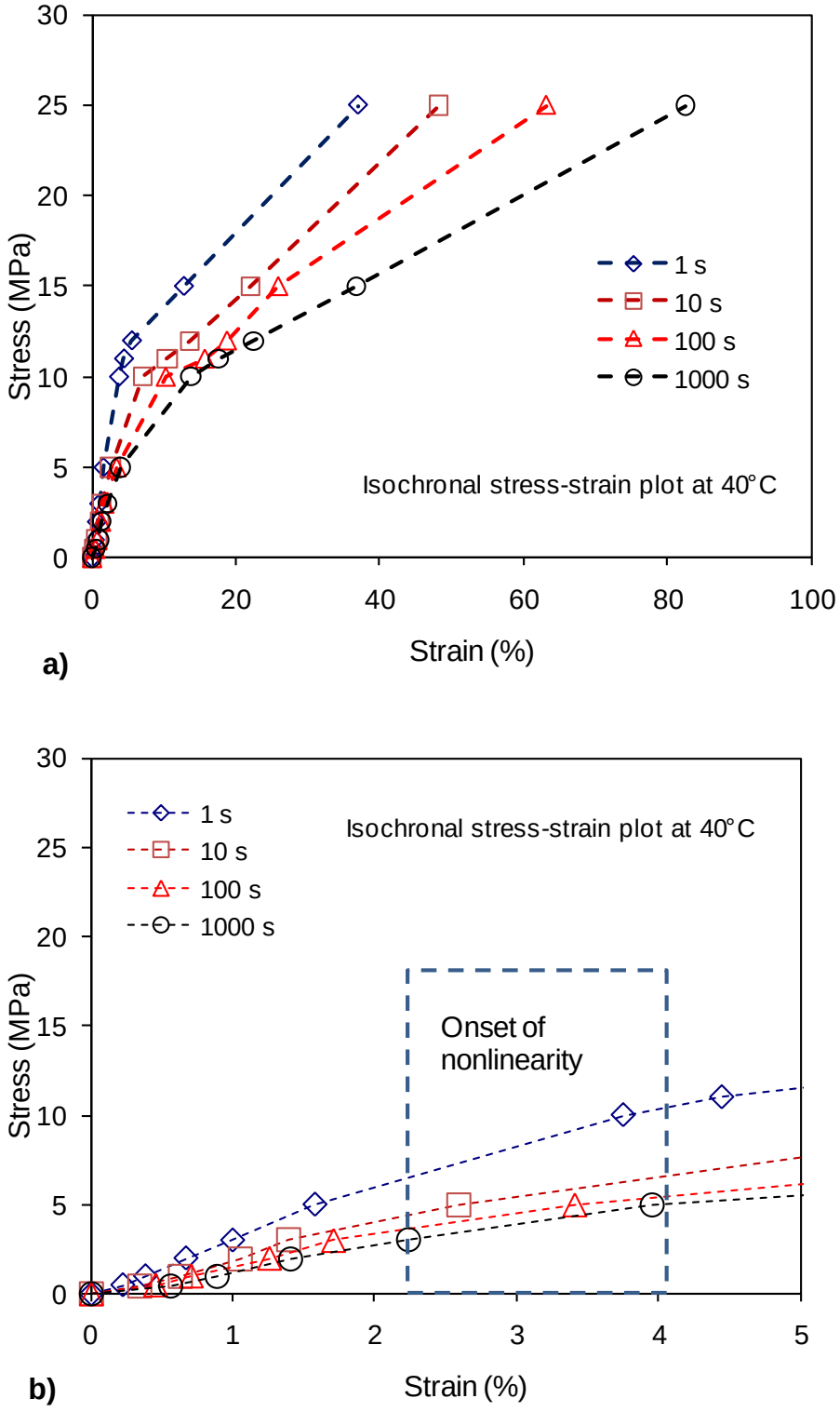

Figure 5.3 Isochronal stress-strain plot generated from creep tests for NRE 211 at 40°C under dry condition. a) Overall stress-strain plot with stress levels up to 25 MPa shown, b) the onset of nonlinearity indicated in the plot, and is found to be around 2-4% strain level.

5.5.2 Nonlinear parameter evaluation

5.5.2.1 Prony series development

The nonlinear parameters can be evaluated using a data reduction method applied to creep/recovery data at various stress level using Equation (13) and (14). The fit to the creep/recovery data is based on a Prony series fit of creep compliance measured at 0.5 MPa stress level, shifted to a reference temperature of 40°C. Note that the required thermal shifts (a_T) and minor vertical entropic shifts have already been accounted for in the reference master curve; therefore, the D_i terms represent the compliance coefficients over the entire temperature range at the reference stress. Any nonlinearity induced at high stress levels can then be incorporated using the nonlinear factors. Table 5.1 shows the Prony series coefficients along with retardation times. This certainly helps in getting a better fit to experimental data. Once the Prony series parameters are obtained, these can then be used to obtain the nonlinear parameters.

Table 5.1 Coefficients in Prony Series obtained by constructing a thermal master curve at 0.5 MPa.

i	log τ (s)	D_i (MPa^{-1})
1	0	3.00E-03
2	1	1.00E-06
3	2	7.00E-04
4	3	1.40E-03
5	4	1.60E-03
6	5	1.00E-02
7	6	1.00E-02
8	7	6.40E-02
9	8	2.80E-02
10	9	4.50E-01

5.5.2.2 Data reduction and the viscoplastic Zapas-Crissman term

The experimental data was used in conjunction with the LMA to determine Schapery parameters required to fit the creep and recovery data. It has been reported that

the Zapas-Crissman parameter does not lend itself to master curve modeling since the viscoplastic strain is a function of time rather than reduced time, thus invalidating the shifting used in the viscoelastic model, and leading to instability at longer times [163]. In contrast, our results suggest the Zapas-Crissman viscoplastic term was indeed a function of reduced time, wherein the reduced time was incorporated through a_σ, as given by

$$\varepsilon_{vp}(\sigma) = \left(C \frac{t}{a_\sigma} \right)^q \sigma^{P.q} \tag{18}$$

The viscoplastic strain is the residual strain remaining in the membrane specimen when the viscoelastic strain is fully recovered which would occur only in the limit of infinite time. This residual strain at the end of a long recovery experiment at a given temperature/stress condition will be a good first estimate of the viscoplastic strain. We measure the creep/recovery strain by optimizing the fit by adding the viscoplastic term. At low temperature, the viscoplastic strain was found to be quite small, while at higher temperature and/or stress levels, the strain was found to be substantial. Figure 5.4 shows the creep/recovery data obtained for NRE 211 at a few temperature/stress conditions. The membrane specimens were allowed to recover for over 6000 minutes to improve the estimate of the viscoplastic strain.

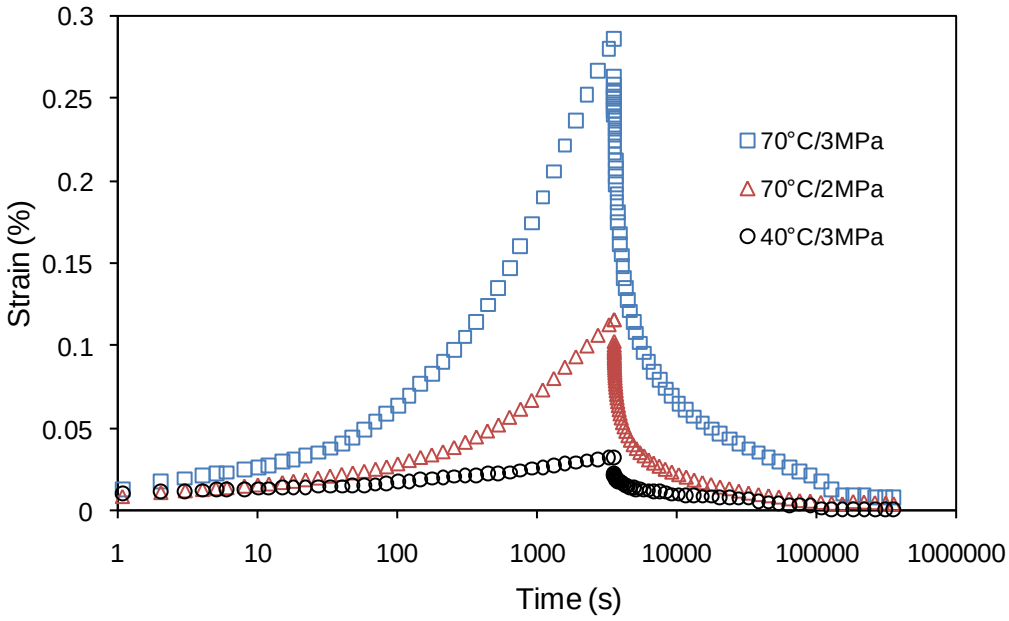

Figure 5.4 Creep/recovery data generated from creep tests conducted at a few temperature/stress conditions for NRE 211. The residual strain at the end of recovery (over 6000 minutes) provides a first guess as the viscoplastic term.

Obviously higher temperature induces more viscoplastic strain. It is also clear that higher stress levels and longer times induce significant viscoplastic strain. Thus when the tests were conducted to validate the model at 40°C, lower stress levels and shorter times did not yield any significant viscoplastic strain and hence the parameter was not considered in modeling. However, when more complex profiles were run for longer times and at high stresses, the viscoplastic term had to be incorporated in the model. For the sake of maintaining continuity, we present the viscoplastic parameters and constants C, *q*, and *P* later after discussing the nonlinear parameter evaluation.

Having discussed the viscoplastic Zapas-Crissman parameter, we move to on to discuss the data reduction procedure to obtain the nonlinear parameters. To do so, one must determine the base linear case, which corresponds to the stress level where the TTSP master curve can be formed, and also where the strain in the membrane is still

small enough that the membrane obeys linear viscoelasticity. Figure 5 shows a plot of creep/recovery data at 40°C at 0.5 MPa stress level along with the model fit (to remind readers, the model fit for this case or any other case discussed henceforth for the creep/recovery datasets is given by Equation (13) and (14) with the viscoplastic strain term given by Equation (17)). This happens to be a linear viscoelastic baseline case, with all the nonlinear parameters set to unity. Obviously at these conditions of temperature and stress, the viscoplastic strain is zero. Figure 5.6 shows the creep/recovery data at 40°C, under various stress-loading conditions, and Figure 5.7 shows recovery data fit with a model. It can be seen that the model, described by Equations (13) and (14) through the use of the nonlinear parameters, fits quite well with the data. In Figures 5.5-5.7, for the sake of simplicity, the legends say "model fit", but essentially it describes the fit obtained by using Equations (13) and (14). The baseline case (linear case) was chosen to be 0.1 MPa in this case.

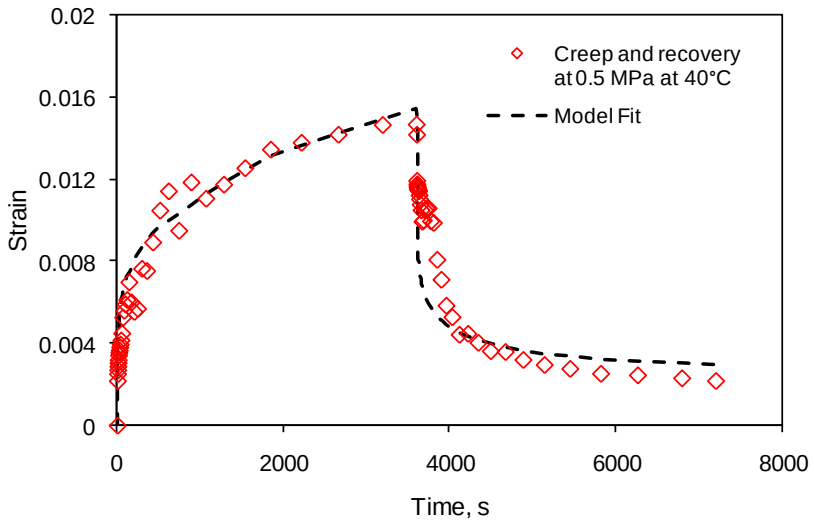

Figure 5.5 Creep/recovery data obtained on NRE 211 at 40°C under 0.5 MPa stress. The test ran for 2 hours; 1 hour creep followed by 1 hour of recovery period. This also happens to be the baseline linear viscoelastic case with all the nonlinear parameters set to unity.

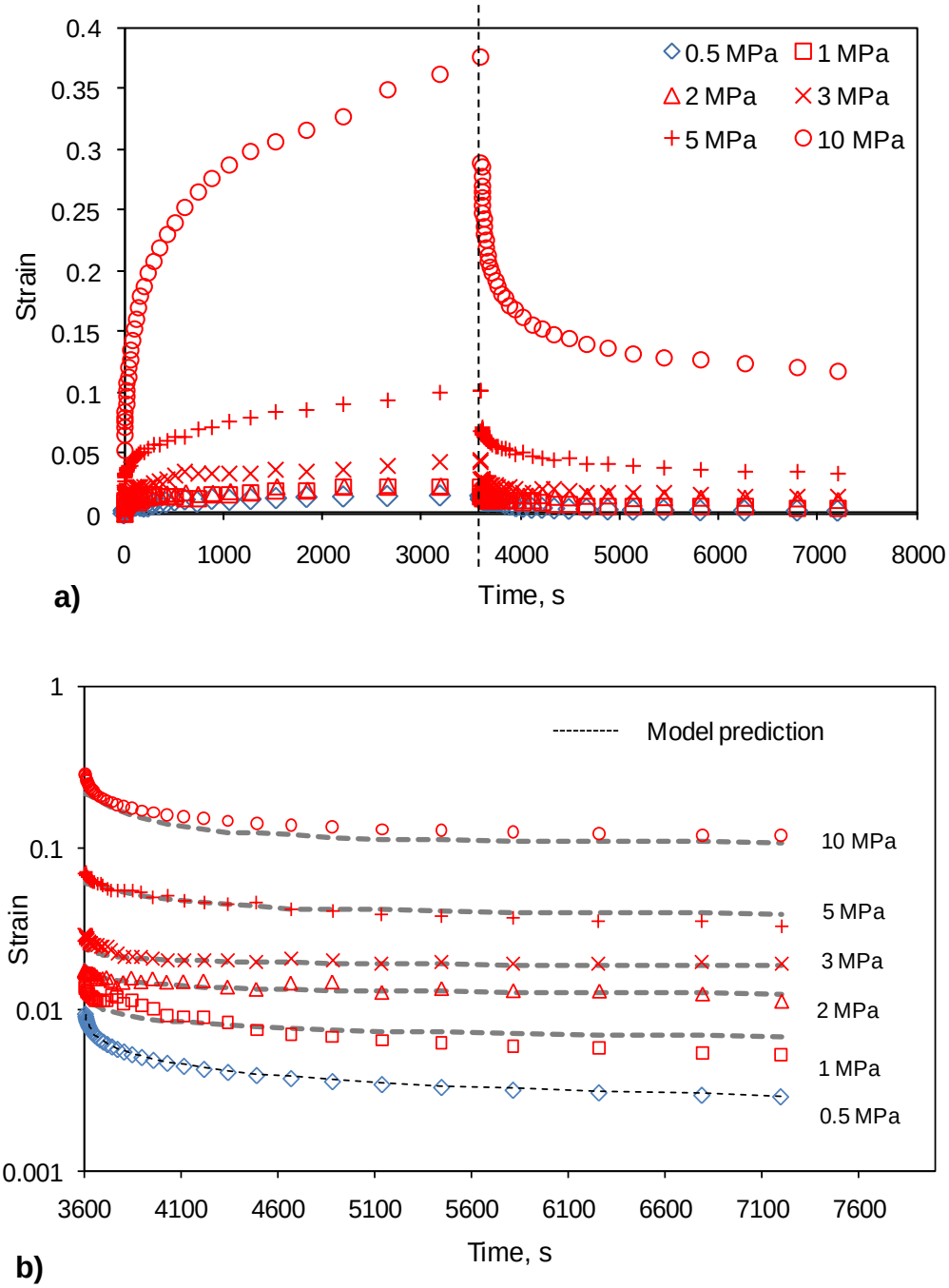

Figure 5.6 Creep/recovery data obtained on NRE 211 at 40°C under various stress levels and model fit. The tests ran for 2 hours; 1 hour creep followed by 1 hours of recovery period. 0.5 MPa is the baseline linear viscoelastic case. a) Creep/recovery data, b) Recovery data is fit with a model. A linear case is also shown as a reference.

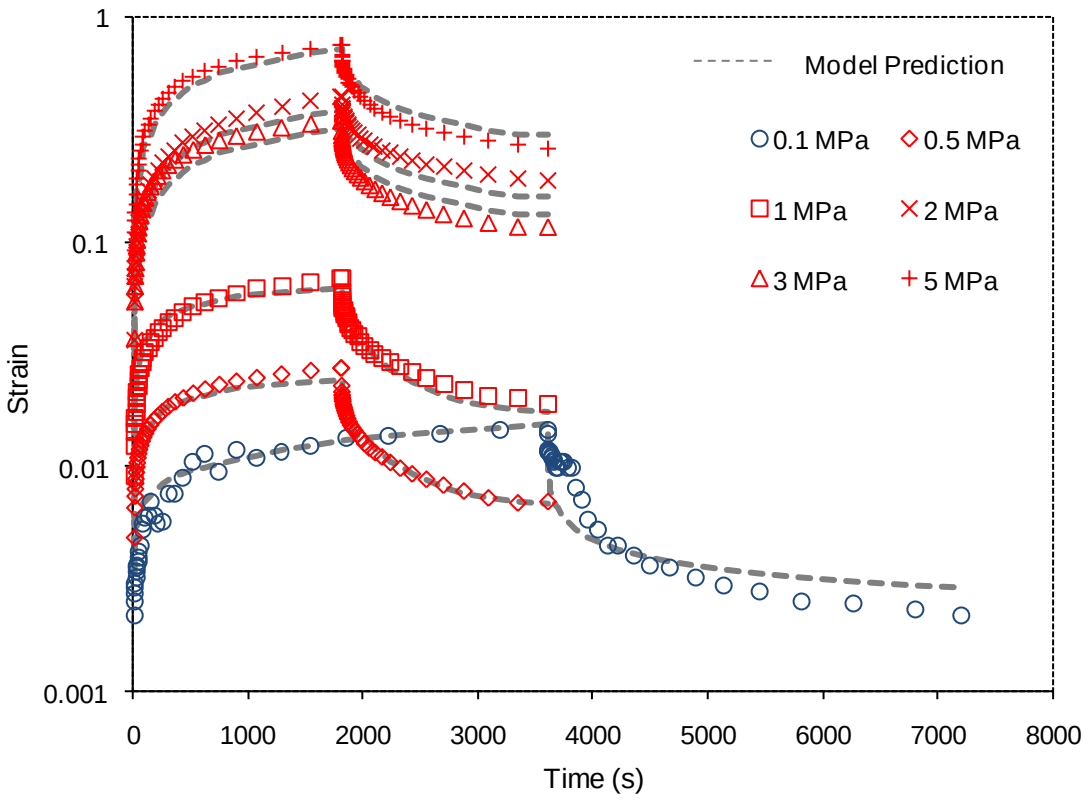

Figure 5.7 Creep and creep recovery data at various stress levels at 70°C. The baseline case (0.1 MPa stress level) runs for 2 hours; 1 hour creep and 1 hour recovery period. The data is fit with a model.

Figure 5.8 shows the nonlinear parameters obtained at 40 and 70°C and several stress levels. These experimentally obtained nonlinear parameters are seen to obey different second order polynomials in stress at 40°C and 70°C. At 40°C, the parameters seem to be in order and follow a particular pattern; however no such statement can be made for the parameters obtained at 70 °C. Also the g_0 term at various temperatures seems to show an expected trend: an increase in instantaneous compliance at higher temperatures. No such observation can be made for the other parameters, however. Tests at other temperatures and stress levels need to be conducted to get some sort of relationship between the nonlinear parameters, stress and temperature. Figure 5.9 and 5.10 show the Zapas-Crissman parameter at 40 and 70°C at various stress levels and times. As a summary,

Table 5.2 shows the various nonlinear parameters at different stress levels and temperatures.

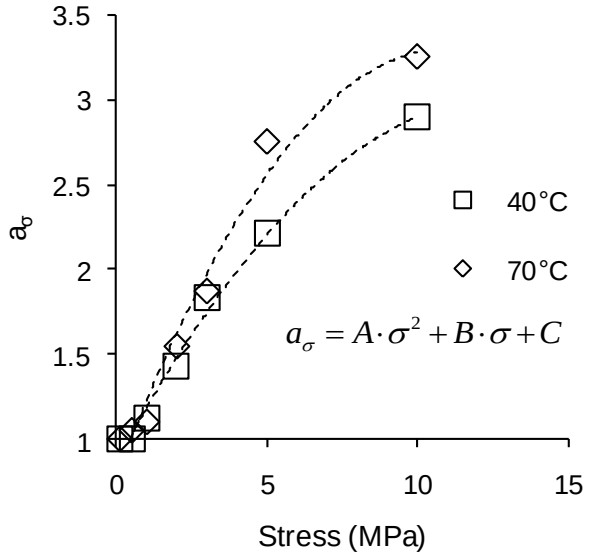

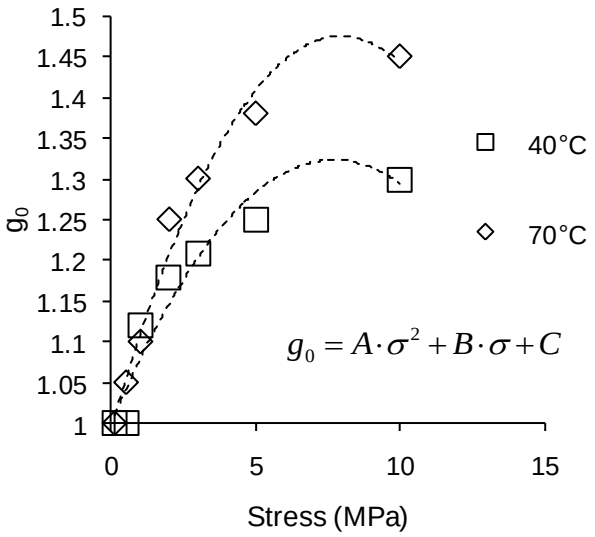

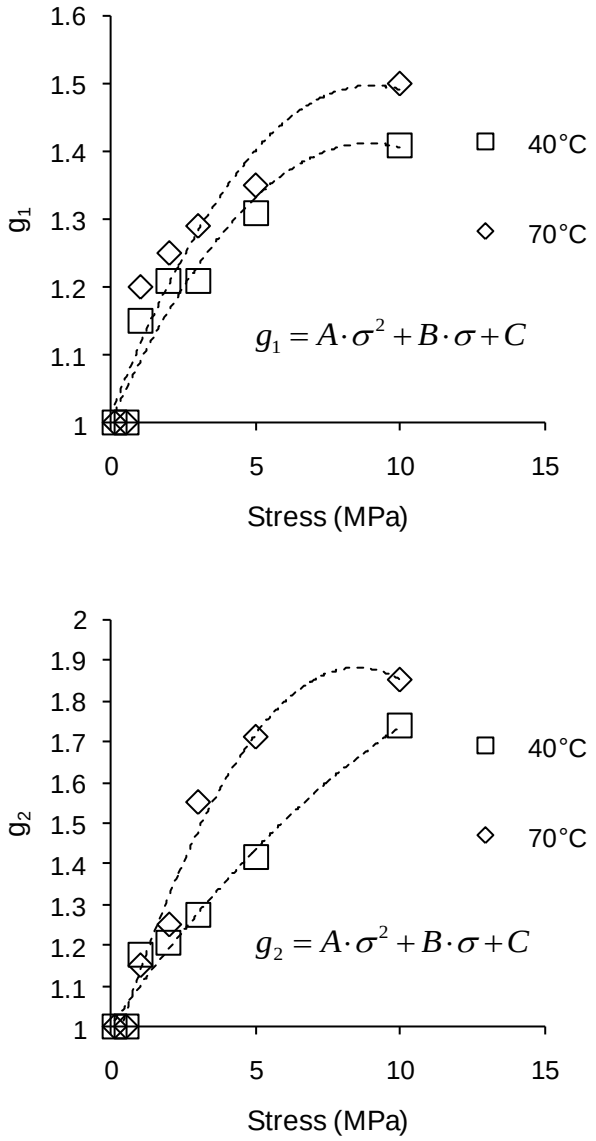

Figure 5.8 Nonlinear parameters calculated at 40 and 70 °C.

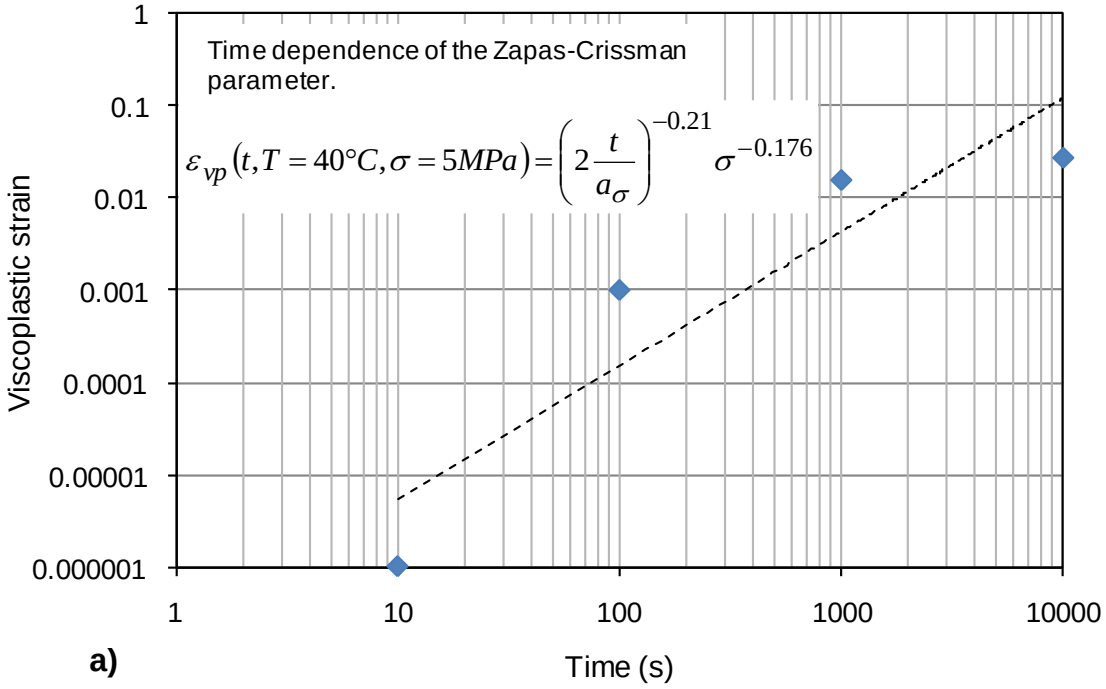

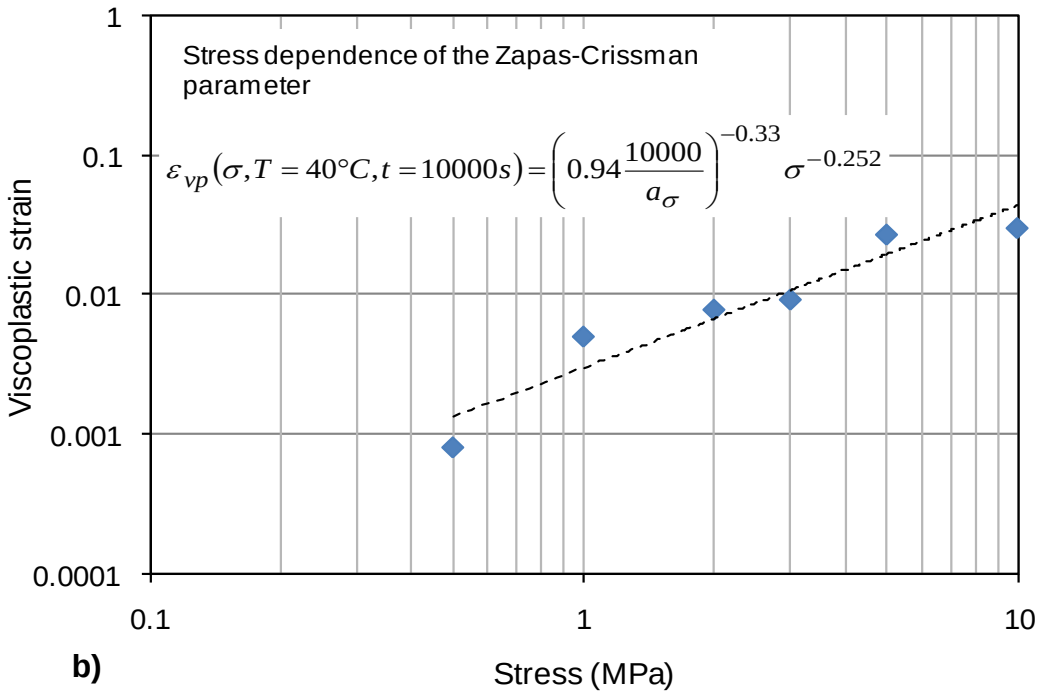

Figure 5.9 The viscoplastic Zapas-Crissman parameter at 40°C developed. a) As a function of time; b) As a function of stress.

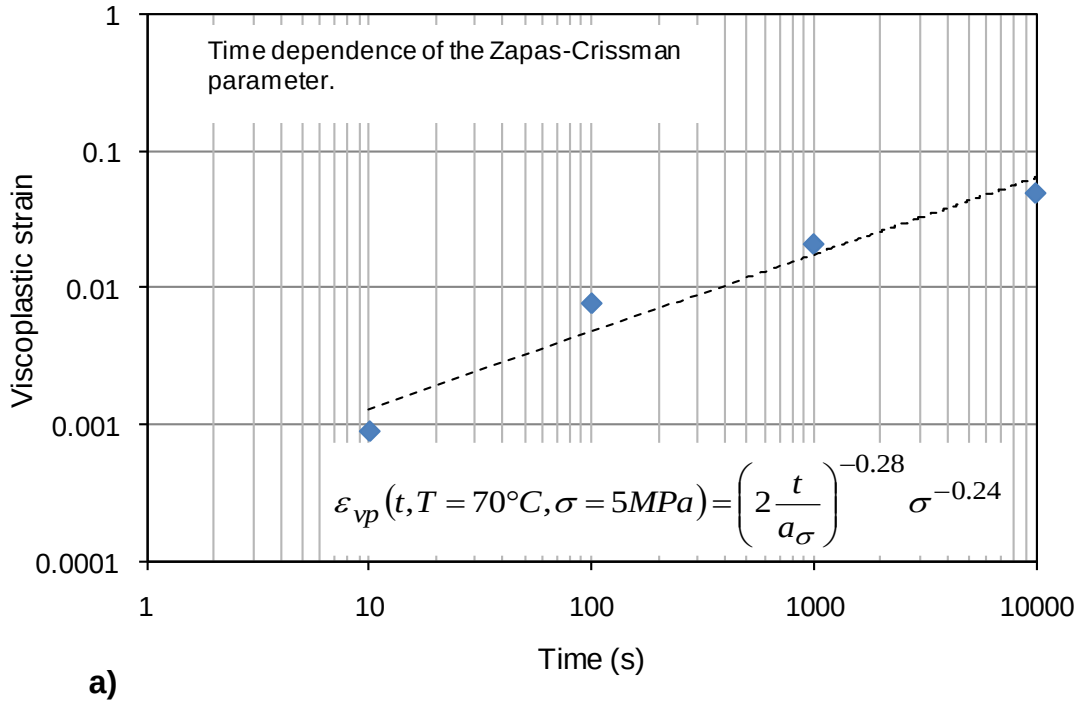

a)

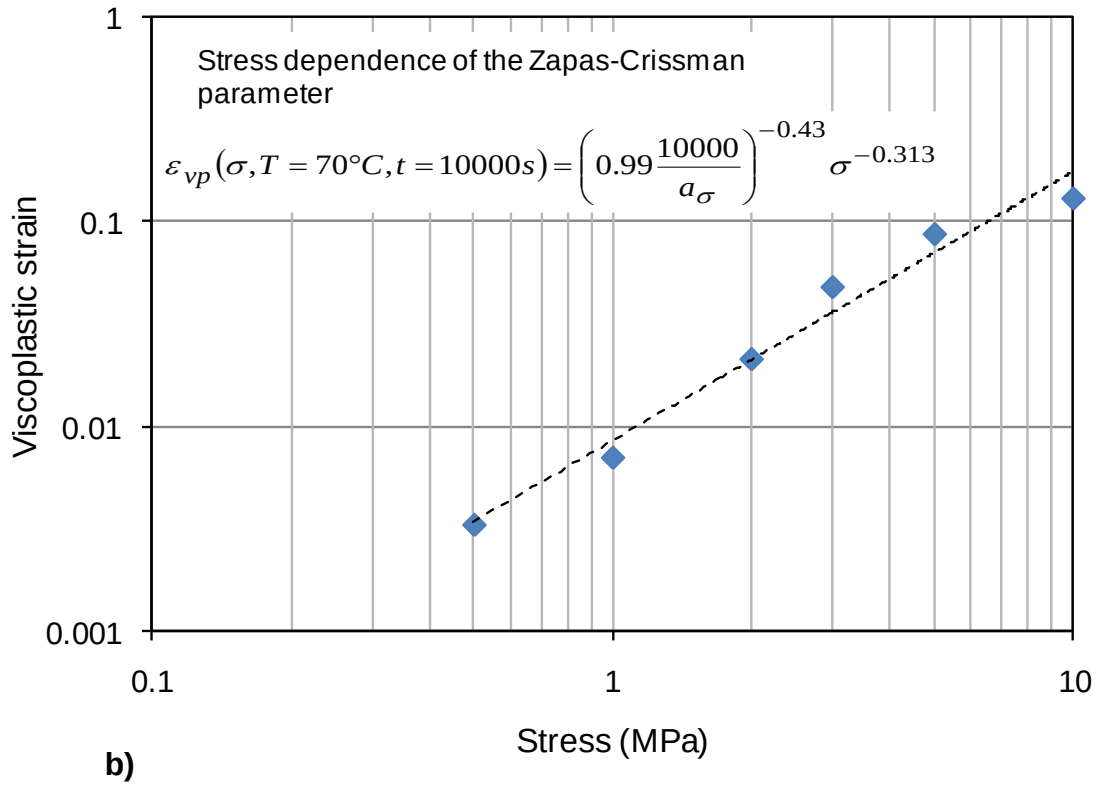

b)

Figure 5.10 The viscoplastic Zapas-Crissman parameter at 70°C developed. a) As a function of time; b) As a function of stress.

Table 5.2 Nonlinear parameters at various temperatures and stress levels.

40°C				
Stress (MPa)	g_0	g_1	g_2	a_σ
0.1	1	1	1	1
0.5	1	1	1	1
1	1.12	1.15	1.17	1.12
2	1.18	1.21	1.2	1.43
3	1.21	1.21	1.27	1.83
5	1.25	1.31	1.41	2.21
10	1.3	1.41	1.73	2.9

70°C				
Stress (MPa)	g_0	g_1	g_2	a_σ
0.1	1	1	1	1
0.5	1.05	1	1	1.05
1	1.11	1.2	1.15	1.12
2	1.25	1.25	1.25	1.54
3	1.3	1.29	1.55	1.87
5	1.38	1.35	1.71	2.25
10	1.51	1.5	1.85	3.25

5.5.3 Validation of nonlinear model

A finite element nonlinear uniaxial viscoelastic Schapery model proposed and developed by Haj-ali and Muliana was used in this study [157]. The nonlinear parameters and Prony series used in the model have already been discussed in the previous section of the paper. We have seen that second order polynomials are sufficient to calibrate the stress-dependent nonlinear parameters. The stress that determines the linear response limit is about 3 MPa at 40°C under dry conditions, and the polynomial stress-dependent parameters are calibrated up to a stress level of 10 MPa at 40°C, and up to 5 MPa at 70 °C. Thus step-stress validation tests are run at stress level of 5 MPa and lower. Accuracy and convergence is not guaranteed beyond this stress level. In order to

determine the initial time increment to simulate a stress-step input, a parametric study needs to be conducted in examine the effect of different initial time increments on the instantaneous material response with varying load levels. The initial time increment size can affect the accuracy of the results and a large time increment may lead to a diverged solution [157]. In order to avoid sluggishness in the program without compromising the accuracy of the results, it was decided to use time-increments in the range of 10^{-2}-10^{-3} s. After the UMATs were written for ABAQUS®, the model initially developed in C++ was mainly used as another tool for verification. Results, based on stress-step input, obtained from both the models have been found to be consistent with one another. Defining and implementing four nonlinear parameters in a model makes it complex and unwieldy at times. It would be interesting to note the effect of the vertical shifts defined by the g terms in the model. This can easily be done by assuming all the g terms to be unity and the only nonlinearizing factor is the stress-induced shift factor. It has been observed that for the cases of step-stress increase, the response in strain is about 15-20% off if all the 'g' terms are assumed unity. Figures 5.11 and 5.12 show the following results for step-increase stress input; experimental strain values, Schapery uniaxial model (formulated in C++) prediction, ABAQUS® prediction (UMAT), prediction assuming all the g terms unity, and a linear viscoelastic response assuming all the nonlinear terms (including the stress shift factor) are unity. The input stress function is shown as an inset. For such input profiles running for short duration, the viscoplastic strain was not an issue. It is for those tests which ran for prolonged times, viscoplastic strain had to be taken into account for. One should include the viscoplastic term in the analysis if the test runs for a longer time, or the temperature is high, or both. Figure 5.13 shows the model prediction for a cyclic

loading profile wherein step stress profile of 5MPa-2MPa was cycled 5 times. It is evident that the model is robust and accurately predicts strains for a given cyclic loading profile. Although the experimental strain values are somewhat erratic, the model still predicts strain values within reasonable (few percents of the experimental results) error limits.

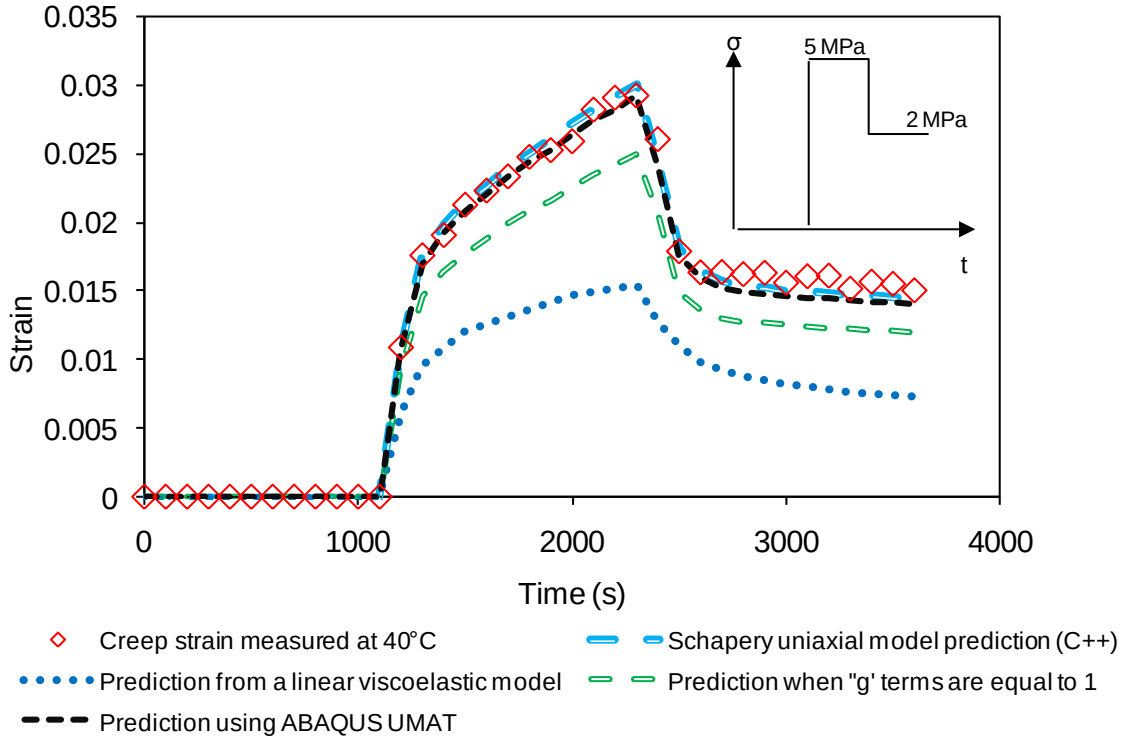

Figure 5.11 Nonlinear viscoelastic Schapery model validation for step increase in stress at 40°C. Following responses are shown: experimental strain values, Schapery uniaxial model (formulated in C++) prediction, ABAQUS prediction (UMAT), prediction assuming all the 'g' terms unity, linear viscoelastic response.

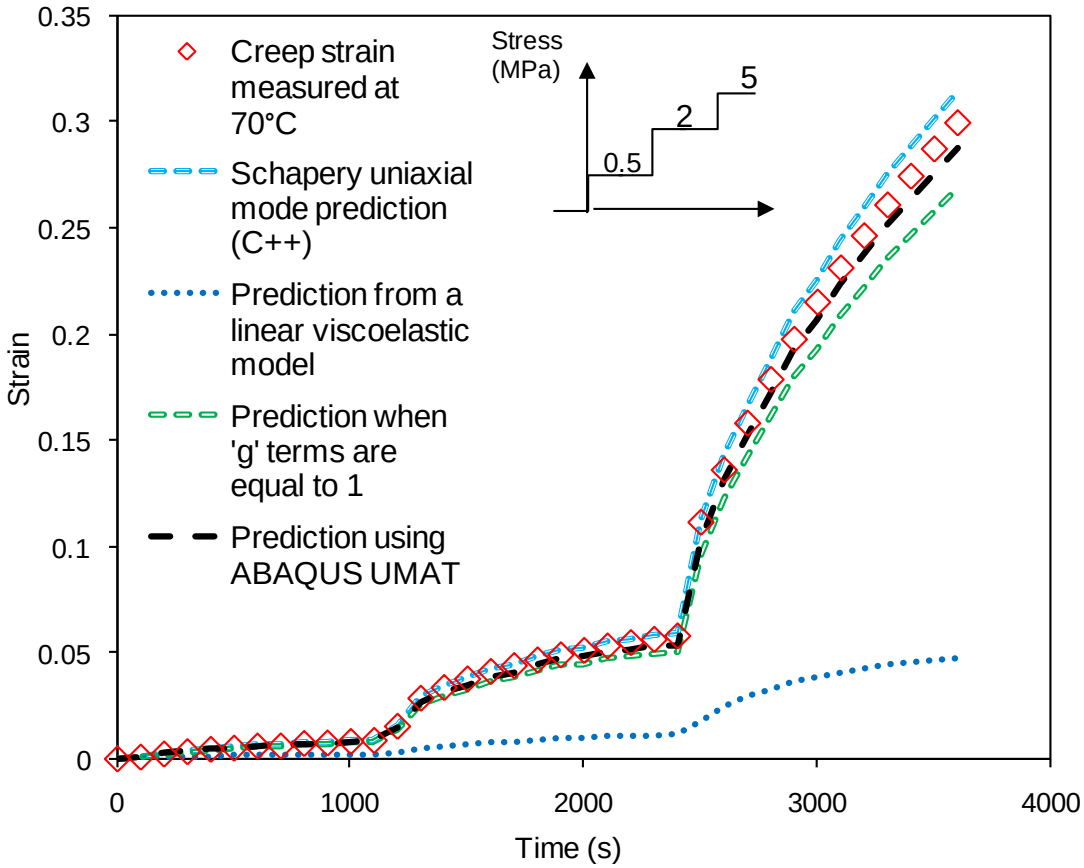

Figure 5.12 Nonlinear viscoelastic Schapery model validation for step increase in stress at 70°C. Following responses are shown: experimental strain values, Schapery uniaxial model (formulated in C++) prediction, ABAQUS prediction (UMAT), prediction assuming all the 'g' terms unity, linear viscoelastic response.

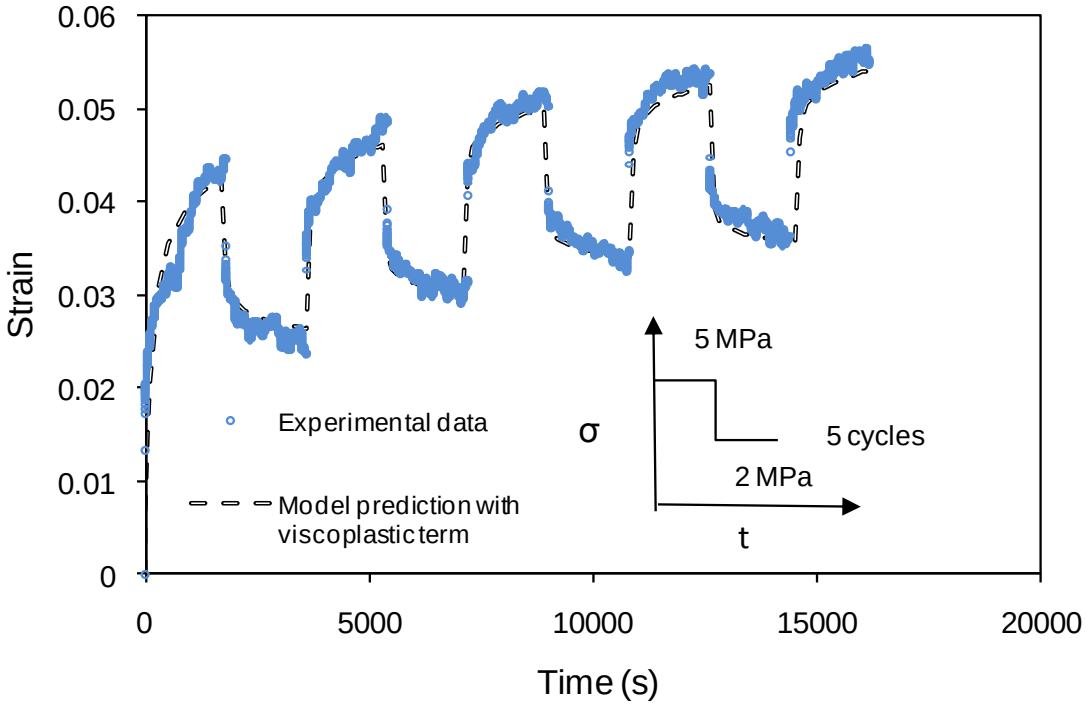

Figure 5.13 Nonlinear viscoelastic Schapery model validation for step increase in stress at 40°C. Following responses are shown: experimental strain values, model with viscoplastic strain given by the Zapas-Crissman parameter, and model without viscoplastic strain included.

Following Figure 5.14, it can be seen that the model predicts accurate strain response for a given stress input for about 15000 s at 40°C under dry condition. A membrane stacked in a fuel cell assembly is expected to function for at least a few years, will be subjected to complex temperature and humidity profiles, and hence will obviously experience much complex stress patterns in its lifetime. Since the humidity effects are not considered in the model, it will be hard to predict the stability and accuracy of the model when the membrane is subjected to complex humidity and temperature profiles. At 40°C under dry conditions, the model is expected to remain stable. At 70°C, the accuracy of the model will severely be compromised if the membrane is subjected to stresses more than 5 MPa. Also the viscoplastic strain will set in quickly even after a few cycles, and will build up after each cycle. The nonlinear factors, presumably the function of humidity, may

significantly change, as the humidity is expected to accelerate the material clock analogues to the temperature and stress. Thus the interplay of humidity, stress and temperature will determine if the model will remain accurate. Another interesting consequence of the humidity and thermal cycles on the membrane is resetting its "internal material clock". Exact conditions are yet to be known at this point, presumably above α-transition temperature (~100°C). So it is likely that one may not need to consider nonlinear viscoelastic effects if the membrane is subjected to temperatures higher than α-relaxation. However, the aim of this study was to formulate the framework of nonlinear viscoelastic model. Therefore, other complicated issues, such as a few discussed above, have not been considered yet and will be dealt with in future.

5.6 Summary and Conclusions

Proton exchange membranes used in fuel cell applications cease to be linearly viscoelastic at small stress/strain levels under dry conditions. The isochronal stress-strain plots, obtained by running creep tests at various stress levels at different temperatures, suggest that typically above 3 MPa stress level, (about 2-4% strain level) under dry conditions at 40°C, the membrane no longer remains linearly viscoelastic. There is likelihood that under humid condition, this limit may be pushed to higher strain levels. Existing models that assume the membrane to be linearly viscoelastic may not be appropriate for use under high stress/strain conditions, as they may produce erroneous results. The objective of this paper was to develop a methodology and a nonlinear viscoelastic model which can later be used to include other temperature, stress and humidity conditions.

The well-known Schapery model, which represents a single integral constitutive equation for uniaxial stress-strain, was found to be quite useful to describe nonlinear viscoelastic behavior of NRE 211. The model contains four nonlinear parameters (g_0, g_1, g_2 and a_σ), which were determined by running a number of creep/recovery tests at various stress levels and for different temperatures. A baseline stress level at which the membrane still remained linearly viscoelastic was determined at each of the temperatures. The creep/recovery strains were fit assuming that the transient creep compliance could be represented as a Prony series referenced at 40°C and at 0.5 MPa. An algorithm known as Levenberg-Marquardt nonlinear least squares algorithms in C/C++ was used to fit the creep and recovery data. During the fitting procedure, it was also observed that, the membrane developed permanent viscoplastic strain, $\varepsilon_{vp}(t,\sigma,T)$ at longer times and at high temperatures. This strain, normally given by the Zapas-Crissman model, is dependent on the actual time and not on reduced time and thus cannot be incorporated directly in the master curve construction. The nonlinear parameters and viscoplastic strains were obtained at various temperature and stress levels.

The nonlinear uniaxial finite element Schapery model was developed in C++ and later as an UMAT, so it could be implemented in ABAQUS. Various stress-step profiles were run in order to check the validity of the model and consistency among the two programs. Strains observed matched quite well those predicted by the models.

5.7 Acknowledgement

The authors would like to express appreciation to the General Motors Corporation for supporting this work, as well as the Institute for Critical Technology and Applied Science (ICTAS) and the Engineering Science and Mechanics Department at Virginia

Tech for providing additional support and facilities. We also acknowledge the contributions of Soojae Park, Jarrod Ewing, and Gerald Fly for initiating this work and building the equipment and to Cortney Mittelsteadt for helpful discussions. We would also like to acknowledge the Macromolecules and Interfaces Institute at Virginia Tech for fostering interdisciplinary research in the field of fuel cells.

CHAPTER 6: Characterizing Fracture Energy of Proton Exchange Membranes using a Knife Slit Test

Manuscript prepared for Journal of Polymer Science: Part B Polymer Physics

6.1 Abstract

Pinhole formation in proton exchange membranes (PEM) may be thought of as a process of flaw formation and crack propagation within membranes exposed to cyclic hygrothermal loading. Fracture mechanics is one possible approach for characterizing the propagation process, which is thought to occur in a slow, time-dependent manner under cyclic loading conditions, and believed to be associated with limited plasticity. The intrinsic fracture energy has been used to characterize the fracture resistance of polymeric material with limited viscoelastic and plastic dissipation, and has been found to be associated with long term durability of polymeric materials. Insight into this limiting value of fracture energy may be useful in characterizing the durability of proton exchange membranes, including the formation of pinhole defects. In an effort to collect fracture data with limited plasticity, the knife slit test was adapted to measure fracture energies of PEMs, resulting in fracture energies that were two orders of magnitude smaller than obtained with other fracture tests. The presence of a sharp knife blade reduces crack tip plasticity, providing fracture energies that may be more representative of the intrinsic fracture energies of the thin membranes. An environmental chamber was used to enclose the slitting process, so experiments at elevated temperatures and moisture levels could be conducted. Three commercial PEMs were tested to evaluate their fracture energies ($\mathcal{G}_c$) at temperatures ranging from 40-90ºC and humidity levels varying from dry to 90% RH

using a humidification system. Experiments were also conducted with membrane specimens immersed in water at various temperatures. The time temperature moisture superposition principle was applied to generate fracture energy master curves plotted as a function of reduced cutting rate based on the humidity and temperature conditions of the tests. The shift with respect to temperature and humidity suggests that the slitting process is viscoelastic in nature. Also such shifts were found to be consistent with those obtained from constitutive tests such as stress relaxation. The fracture energy seems to depend somewhat more strongly on temperature than on humidity. The master curves seem to converge at the lowest reduced cutting rates, suggesting similar intrinsic fracture energies, but diverge at higher reduced cutting rates to significantly different fracture energies. Although the relationship between G_c and ultimate mechanical durability has not been established, the test method may hold promise for investigating and comparing membrane resistance to failure in fuel cell environments.

Keywords: Proton exchange membranes (PEM), fracture energy, intrinsic fracture, knife slit test, durability of proton exchange membranes

6.2 Introduction

Polymer electrolyte membrane fuel cells (PEMFCs) have received considerable attention from various government and private organizations in the quest to develop a cleaner source of energy for stationary, portable, and automotive applications. However, there are still barriers to overcome before realizing the full potential of PEM fuel cells. Thermal and humidity cycles experienced during operation impose significant mechanical stresses within membranes, which are constrained against in-plane deformation by the fuel cell stack compression through the catalyst and gas diffusion

layers. The most important function of the membrane is to allow protons to pass through while preventing the flow of electrons and reactant gas cross-over. Through-thickness pinholes may form in PEMs because of the cyclic stresses induced by changes in temperature and humidity, resulting in gas cross-over that leads to localized mechanical and/or chemical degradation that may ultimately result in failure of the fuel cell. The formation of a pin-hole can be visualized in terms of crack initiation and propagation, suggesting that a fracture mechanics approach might be useful in understanding and characterizing membranes [111]. In this study three commercial perfluorinated sulfonic acid (PFSA) membranes are compared: the homogeneous recast DuPont™ Nafion® NRE 211 (simply referred to as NRE 211 in the paper henceforth), the homogeneous extruded Ion Power™ Nafion® N111-IP (referred to as N111-IP), and the composite Gore™ Gore-Select® 57 (referred to as Gore-Select 57) membranes, which are reinforced with expanded poly(tetrafluoroehtylene) (ePTFE). The failure mode and crack morphology of the samples have been investigated using cross-sectional micrographs and reported elsewhere [125]. Figure 6.1 shows typical micrographs of these three commercially available PEMs, removed from a humidity cycling fixture [125]. A range of failure features can be seen in these micrographs; apparent brittle cracks associated with small crack opening and the absence of permanent material deformation can be seen in Figures 1a and 1d and more ductile cracks associated with large crack opening and evidence of permanent deformation can be seen in Figure 1b and 1d. These apparently brittle and ductile crack formation and propagation can be caused by different stress levels and environmental conditions. Observations based on these micrographs lead us to believe that there are no features that are associated with mechanical overload (such as necking

or plastic deformation). Also the micrographs reveal that the cracks are perpendicular to the plane of the membrane, suggesting that the cracks are driven by in-plane tensile loads. The presence of a number of cracks of different dimensions suggests that these cracks are propagated gradually and not catastrophically. The devised fracture test, knife-slit test confines the plastic zone to the thickness of the membrane, which helps capture the fracture features are that generally observed in these micrographs.

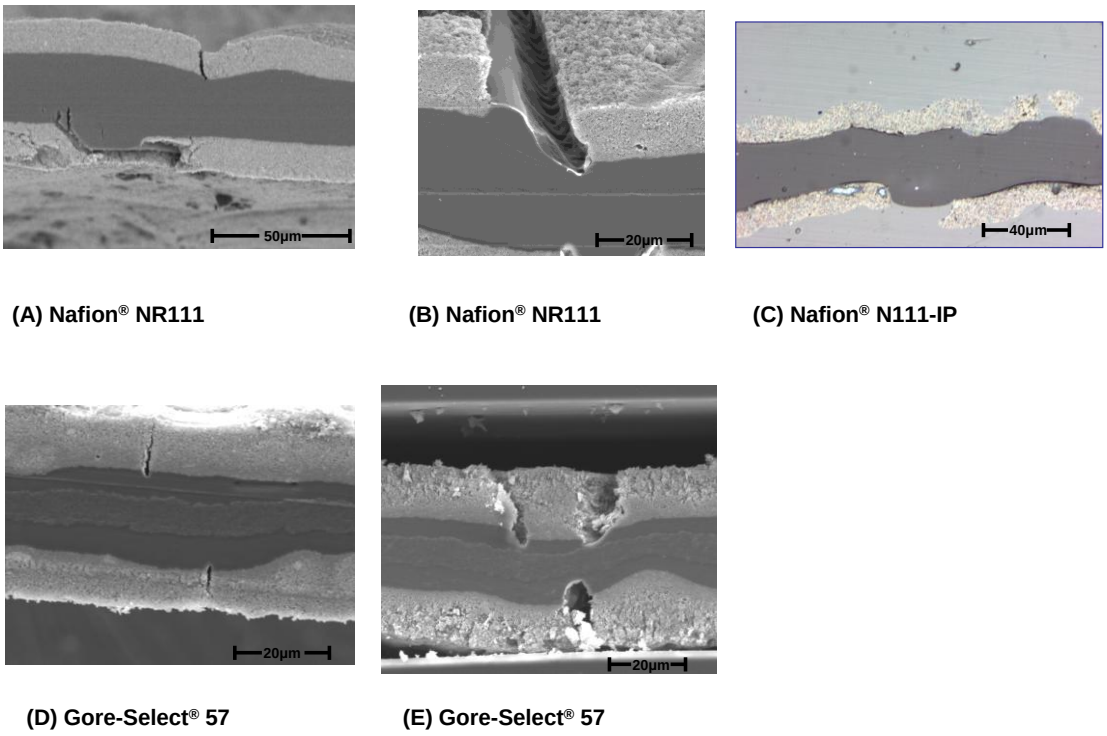

Figure 6.1 Micrographs of three commercially available PEMs after they were removed from a humidity cycling fixture [125].

Previous work reported several techniques for measuring the fracture energy, or resistance to crack propagation, of PEMs, including the double-edge notch test (DENT), trouser tear test, and knife slit test [131]. Significantly lower values of fracture energy

were seen in the case of the knife slit test due to the use of a sharp microtome blade, which greatly reduced crack tip plasticity. The significant reduction in observed fracture energy was associated with a smaller plastic zone ahead of the crack tip, which was believed to be of the order of the membrane thickness (≈ 25μm). By lowering the plastic dissipation, the intrinsic fracture energy of the material, which is the limiting fracture energy at vanishingly small propagation rates, could perhaps be approached. By reducing the visco-plastic deformation at the crack tip, useful insights about crack propagation can be gained, potentially relevant to the more brittle fracture earlier observed [111, 131].

6.3 Experimental Technique

The knife slitting fixture used in this study was based on a modified form of the fixtures used by Lake and Yeoh [174] and Gent et al. [175, 176]. The fixtures described by Lake and Yeoh, and Gent were capable of characterizing the fracture resistance of thin polymeric sheets under varying ratios of cutting and tearing. Gent and co-workers reported that by optimizing the angle between the two legs of the specimen and the angle at which the knife is oriented with respect to the uncut portion of the specimen, the frictional losses during the cutting process were minimized. They tested elastomeric and thermoplastic specimens and found that, although a sharp blade effectively reduces the plastic zone ahead of crack tip and maintains a sharp crack tip in elastomers, it is not as effective at limiting the plastic blunting that occurs in ductile thermoplastic films [175, 176]. Nonetheless, the presence of a sharp blade can significantly reduce plastic deformation and the excessive tear energies that may occur in thermoplastic films.

Dillard et al. [111] modified the original design and eliminated the pulleys and associated frictional effects. This Y-slit test, however, resulted in a changing angle of the

legs as the knife progressed, complicating the analysis. Further modifications were made in the design, which can be found in the paper by Li et al. [131]. They discussed an improvement of the knife slitting fixture to eliminate the geometrical change and subsequent effects during cutting, ensure consistent crack propagation rate, and simplify the analysis. In the new knife-slit fixture, the relative positions of the knife and the pins that support the membrane are fixed. Thus a fixed geometry is maintained as the membrane is cut by passage over the knife (Leica #818 microtome blade), which is mounted to an Interface Forces ULC load cell (0.5N). The two legs of the membrane pass over guide pins and are attached to the moving crosshead of an Instron 4505 universal testing machine, which pulled the membrane against the knife at a cutting speed that is equivalent to the crosshead rate, since the loads were so small that extension of the cut legs was insignificant. Figure 6.2 and 6.3 show a schematic illustration of the geometry of the fixture, and the frame close-up, respectively. Although quite similar to the fixtures used by previous researchers, friction of the pulleys (or pins in this case) is not a problem in this design since the load cell directly measures the force on the cutting blade.

Figure 6.4 shows the dimensions and geometry of the membrane specimens used for the experiments. An aluminum template, used to cut specimens out of a membrane sheet, had a slit of the desired length to initiate the precrack in the specimen. A sharp blade was used to cut the edges and to create a precrack. To reduce waste of the expensive membrane, inexpensive polyester film leaders with overall width of 12.5 mm and length of about 210-215 mm were cut. A small piece of membrane of length slightly greater than the uncut section (about 95 mm) with a precrack of about 6 mm was cut. The

polyester leaders were attached to the cut legs of the membrane and passed over guide pins, allowing the knife to cut the membrane.

One of the advantages of this fixture is that since the knife does not move at all, it can be enclosed in an environmental chamber. The chamber can be heated and moist air can be introduced. The chamber was insulated with polystyrene foam and heated with a silicon rubber-coated resistance heater. The humidity was controlled using a dual channel humidifier supplied by the Fuel Cell Technologies Inc™ (Albuquerque, NM). A Vaisala humidity sensor (HMT 337, Vintaa, Finland) was used to monitor the humidity in the chamber. It was observed that if the chamber was placed higher than the humidifier, there was significant condensation of moisture in the tubes and in the chamber. To reduce condensation, the humidifier was placed at least at the same height as the chamber. The membranes were tested at temperatures of 40-90°C. At each temperature, various humidity levels and cutting levels were employed to measure the fracture energies. Typically temperature was held constant and humidity was increased in 10% increments until the maximum desired humidity was achieved. The temperature was then increased by 10°C and the tests repeated. A single membrane sample was used for all the cutting rates employed at given temperature and RH. At each increased humidity level, a new membrane sample was used. At each temperature/ relative humidity test condition, the membranes were tested with cutting rates of 0.1, 1, 10, 50, 100 mm/min. For the GoreSelect 57 and N111-IP membranes, only dry and 50% relative humidity levels were employed. The fixture was flexible enough to accommodate testing specimens in controlled temperature/humidity conditions as well as specimens immersed in water at controlled temperatures. In order to conduct tests in submerged conditions, a recirculating

water bath (Thermo Scientific, Neslab RTE 7) was used to pump water at the desired test temperature into the chamber. The water bath had a capability to circulate water at sub-ambient conditions as well. The tests were conducted at 1, 10, 23, 40, 50, 60, 70, 80, and 90°C at cutting rates of 0.1, 10, 50, 100 mm/min. Even though the cutting rates 0.1 and 10 mm/min are two decades apart, it was found that the fracture energy data obtained at 10 mm/min cutting rate was superimposable with the data obtained at 0.1 mm/min cutting rates. Thus, in order to save time, the experiments were not conducted at a cutting rate of 1 mm/min. The PEMs membranes tend to float on the surface of water. In order to keep them immersed, a small weight of 15 mg was attached to the end of membrane, and subsequent calculations were done taking this dead weight into account.

Lake and Yeoh [174] discussed the equations of cutting and tearing energy based on simple equilibrium of body forces, assuming there is no straining in the membrane.

$$C = \frac{\langle P \rangle}{h} \tag{1}$$

$$T = \frac{2L(1-\cos\theta)}{h} = \frac{(\langle P \rangle + W)}{h\cos\theta}(1-\cos\theta) \tag{2}$$

$$G_{slit} = \mathrm{C} + \mathrm{T} = \frac{\langle \mathrm{P} \rangle + W(1-\cos\theta)}{\mathrm{h}\cos\theta} \tag{3}$$

where C is cutting energy; T is tear energy; G_{slit} is the total slit energy; L is the pulling force in each leg; $\langle P \rangle$ is the average cutting force; W is the tearing weight hanging under the uncut ligament; θ is the cutting (splay) angle; and h is the thickness of the membrane. In determining the above fracture energies, the width of the crack surface is taken to be

equal to the thickness of the membrane, h by previous researchers. Figure 6.2 shows a schematic diagram of the knife-slit experiment.

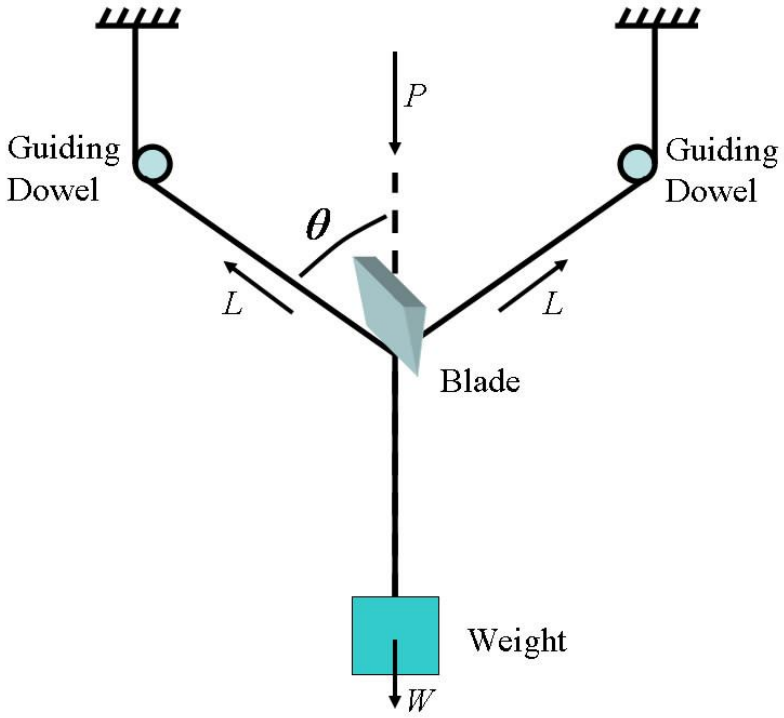

Figure 6.2 Schematic illustration and equilibrium diagram of knife-slit test. The blade and the guiding dowels remain stationary relative to one another (all moving downward at the same velocity), such that during the cutting process, the cutting angle θ remains constant [131, 177].

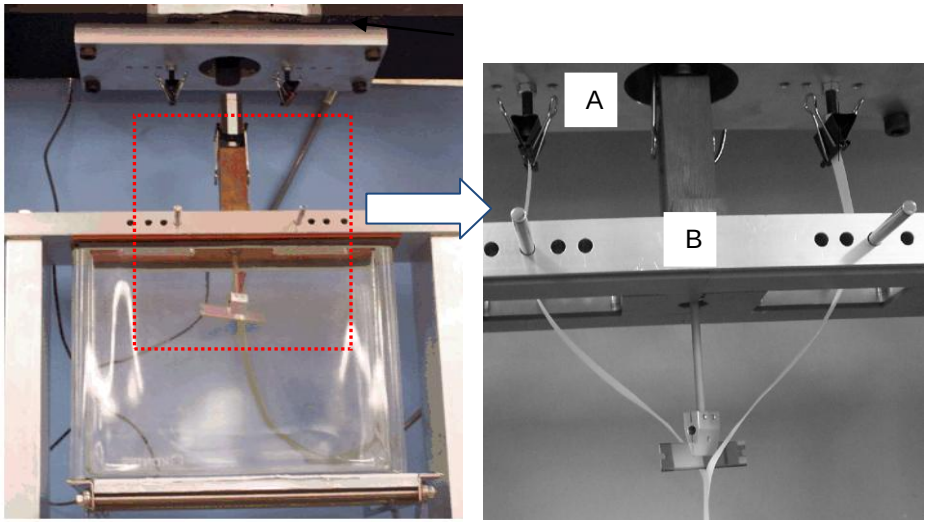

Figure 6.3 The test fixture used in the study. The figure on left is a full view of the fixture. The figure on right is a close-up of the fixture where 'A' refers to the stationary beam, while 'B' refers to the moving beam of the fixture. By placing the guiding pins in different holes, tests at different angles can be conducted. The small load cell is mounted inside the top hole and attached to the support.

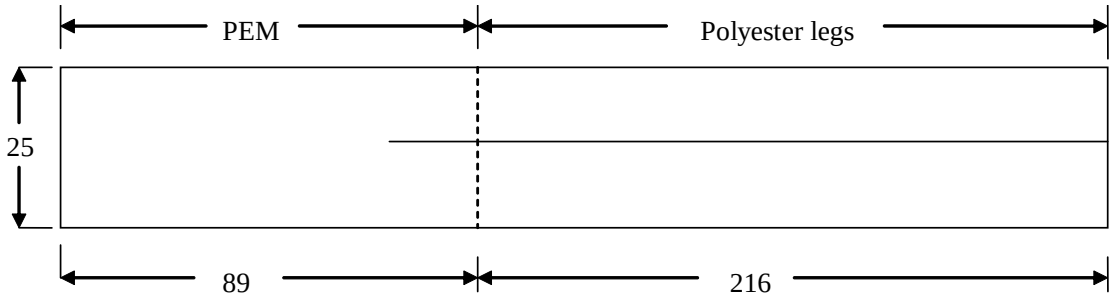

All dimensions are in mm.

Figure 6.4 The modified slitting specimen with polyester leaders attached to the membrane to reduce waste.

6.4 Results

6.4.1 Load traces and micrographs

Figure 6.5 shows typical load traces for NRE 211 membrane tested at a fixed cutting rate of 50 mm/min, at various temperatures and under dry condition. Representative load traces in Figure 6.5 show a steady state nature of this test and fixture, as well as their ability to distinguish various load levels under different test conditions.

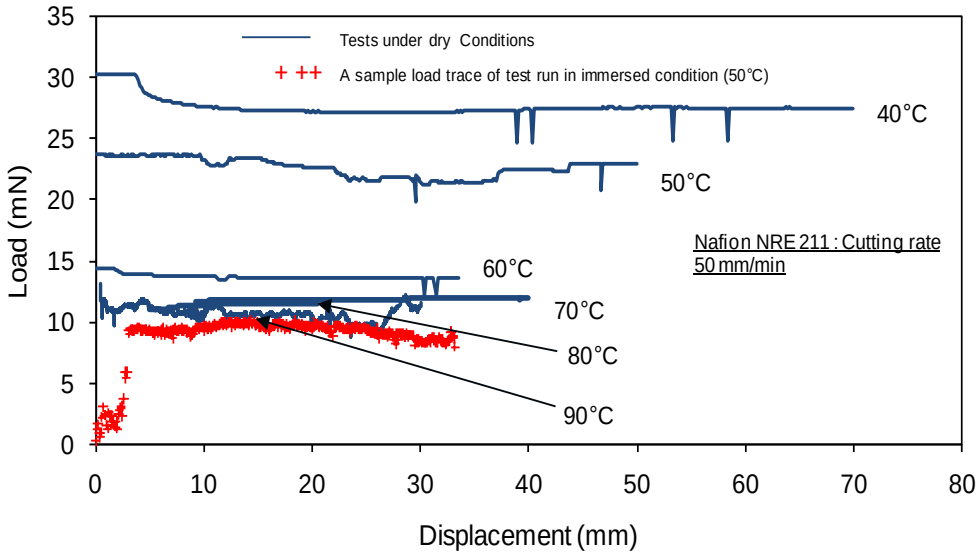

Figure 6.5 Typical load-displacement curve for Nafion NRE 211 specimen tested under dry conditions at various temperatures, at a cutting rate of 50 mm/min. For comparison, a load trace of sample cut at the same cutting rate and at 50°C under immersed condition is also shown in red.

Overall, the curves show that the forces recorded during the tests were relatively constant, although occasional interruptions occur, perhaps due to stick-slip propagation. The average force during a given cutting process was calculated ignoring the initial and ending regions of the load trace. The average force during each test was used to calculate the cutting, tearing, and total slitting energies following Equations 1-3.

Cut membrane edges were evaluated using optical and scanning electron microscopy (SEM) to get an idea of the width and texture (whether smooth or rough) of the fractured surface. The SEM images showed differences in texture along the cut surface of the membrane. The samples were then mounted in epoxy on edge, so that the cut edge profile could be observed using optical microscopy. A ratio of length of the cut edge profile to membrane thickness was calculated. A 90° cut, with no edge deformation should yield a ratio of 1. At various other angles of the knife with respect to the membrane, this ratio would be higher. Initially the knife was placed at 45° angle with respect to the plane of the uncut membrane specimen in order to reduce friction. But later it was found that more consistent data could be obtained if the knife was mounted at an angle close to 90° with respect to membrane. Therefore all further tests were conducted using this configuration. Fracture energies measured by planning the blade at 45° or 90° with respect to membrane specimen did not alter the results. Figure 6.6 shows a schematic of how the imaging was done; and Figure 6.7a and 6.7b show a scanning electron micrograph and optical micrograph of NRE 211 sample fractured at the cutting rate of 1 mm/min at 40°C respectively. The fracture width can be calculated using the images obtained from optical microcopy and SEM. In Figure 7b), the edge of the membrane is about 20° with respect to the perpendicular line (this would correspond to a

straight cut). Using trigonometric results ($\cos 20° \approx 0.94$), it can be seen than the fracture width observed in SEM images is about 94% of the actual fracture width. For example if the fracture width (as observed in Figure 7a) is 25.5µm, the actual width should be about 25.5/0.94 µm, or about 27µm. Based on other images obtained, the fracture width was seen to lie between 25 to 29µm. Such widths are comparable to the actual membrane thickness (25.4µm), and therefore the equations proposed earlier (Equations 1-3) are valid for further analysis.

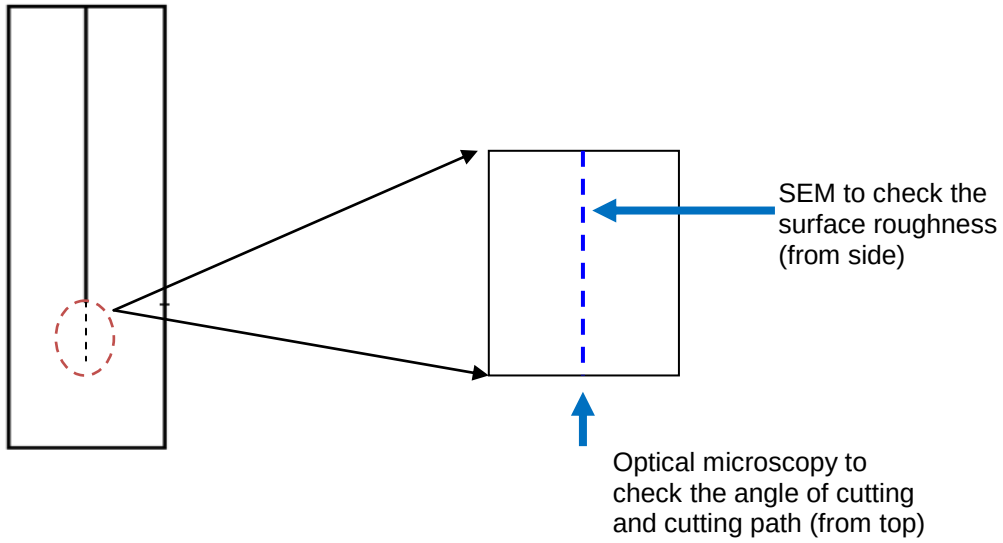

Figure 6.6 A schematic showing the use of SEM and optical microscopy to observe the surface roughness and crack propagation angle and smoothness.

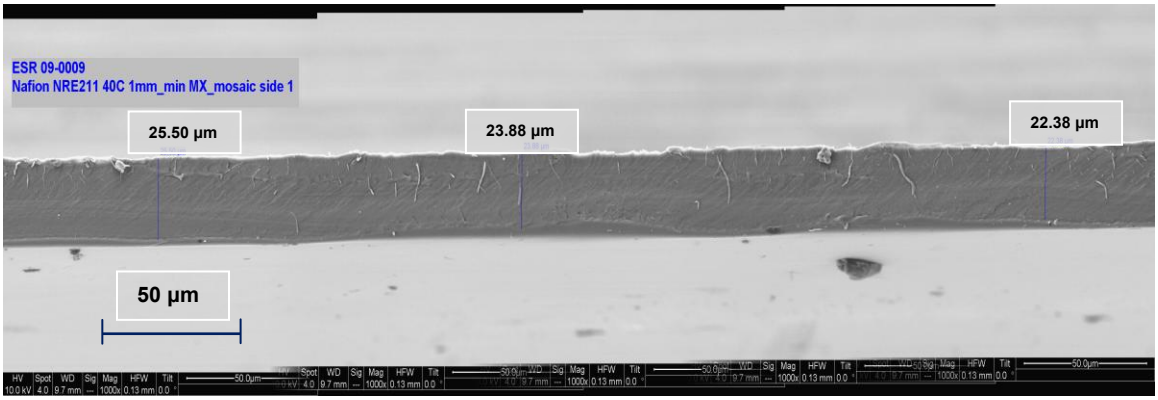

a)

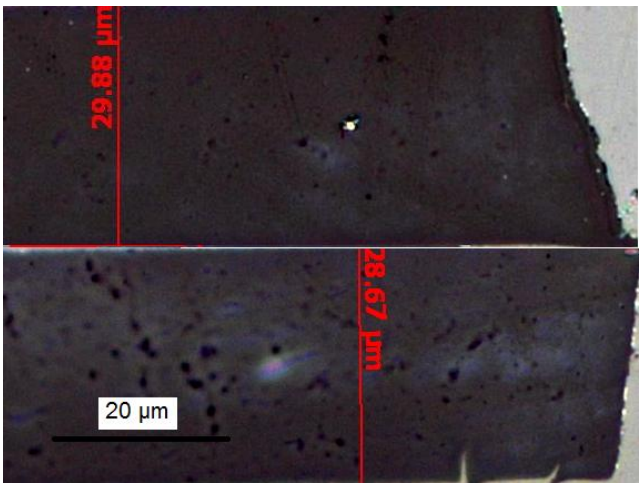

b)

Figure 6.7 Optical and SEM imaging of the fracture membrane surface. a) SEM image of the fracture surface of Nafion NRE 211 cut at 1mm/min tested under dry conditions at 40°C, b) Optical micrograph showing the shape of the cutting path.

6.4.2 Fracture energy master curve

Polymers are time and temperature dependent in general and often obey the time temperature superposition principle (TTSP) [56]. Extensions of this principle to include the plasticizing effects of diluents such as water have been used [108, 124]. Ionomeric PEMs are especially sensitive to humidity levels and sorbed moisture. We assume PEMs follow the time temperature moisture superposition principle (TTMSP) [112, 178]. Patankar et al. [112, 178] conducted stress relaxation experiments to measure the relaxation modulus of GoreSelect 57 PEM at various temperatures and humidity conditions using a dynamic mechanical analyzer fit with a humidity cup. Thermal and hygral master curves were then constructed to construct a so called 'hygrothermal master curve'. Grohs et al. [179] used a pressure loaded blister test to measure the biaxial strength of GoreSelect 57 PEM over a range of time and temperatures under nominally

dry conditions. Biaxial strength master curves were then constructed using TTSP, and associated thermal shift factors showed a good agreement with those obtained from stress relaxation experiments conducted by Patankar et al. [112, 127]. We extend the technique of TTMSP to fracture energies obtained from slitting various membranes at a range of temperature and humidity conditions.

We now present a methodology for construction of a fracture energy master curve for NRE 211. A similar method has been applied to construct a fracture energy master curve for GoreSelect 57 and N111-IP. Figure 6.8 shows the fracture energy obtained at various humidity levels at 40°C. The fracture energies measured at various humidities compare well, and were found to lie within 95% with those reported by Li et al. [131]. Recording hygral shift factors (a_H) at this temperature, a hygral master curve for fracture energy is constructed. All such hygral master curves at various other temperatures are then combined to form a hygrothermal master curve for fracture energy recording the thermal shift factors (a_T) (shown in Figure 6.9). The thermal and hygral shift factors noted are shown in Figure 6.10. The fracture energy master curves for N111-IP and GoreSelect 57 are shown later for consistency in the discussion. Again NRE 211 membrane was characterized at various humidities, while N111-IP and GoreSelect 57 were characterized for fracture energy only under dry and 50% RH conditions, as the tests were much quicker and still gave sufficient data to construct hygrothermal master curves for fracture energy with respect to reduced cutting rate. One should note that fracture and strength master curves often exhibit more scatter than is typical for master curves of constitutive data, which is often gathered in a more continuous fashion. The constitutive data is typically representative of the average of the bulk properties of

polymeric materials and thus is less influenced by material non-uniformity and defects. On the other hand, fracture properties are dependent on material non-uniformity and defects. Defects on a local scale can affect the strength and fracture properties and bring about more scatter in data. Also for a material such as PEM, that is extremely sensitive to both temperature and humidity, a slight variation in either temperature and/or humidity may cause slightly different results leading to added scatter in the data. It was observed that at lower temperatures and higher cutting rates (typically 50 and 100 mm/min), the variation in the force recorded and subsequently the fracture energy was about 5-10%. The fracture energy master curve shown in Figure 6.9 was plotted considering the maximum scatter observed during the experiments.

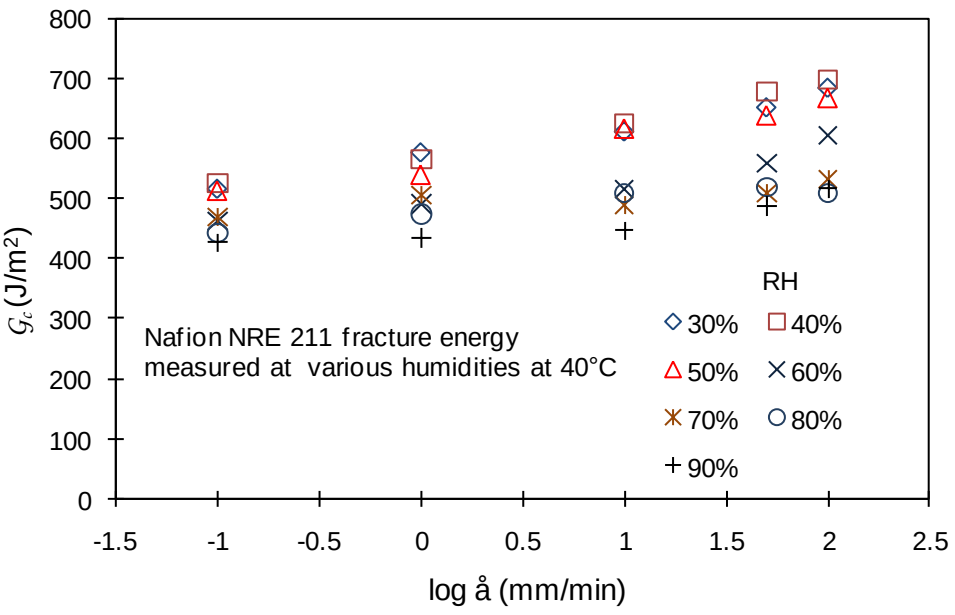

Figure 6.8 The fracture energy recorded for Nafion® NRE 211 tested at 40°C for various cutting rates and relative humidities (30-90% RH).

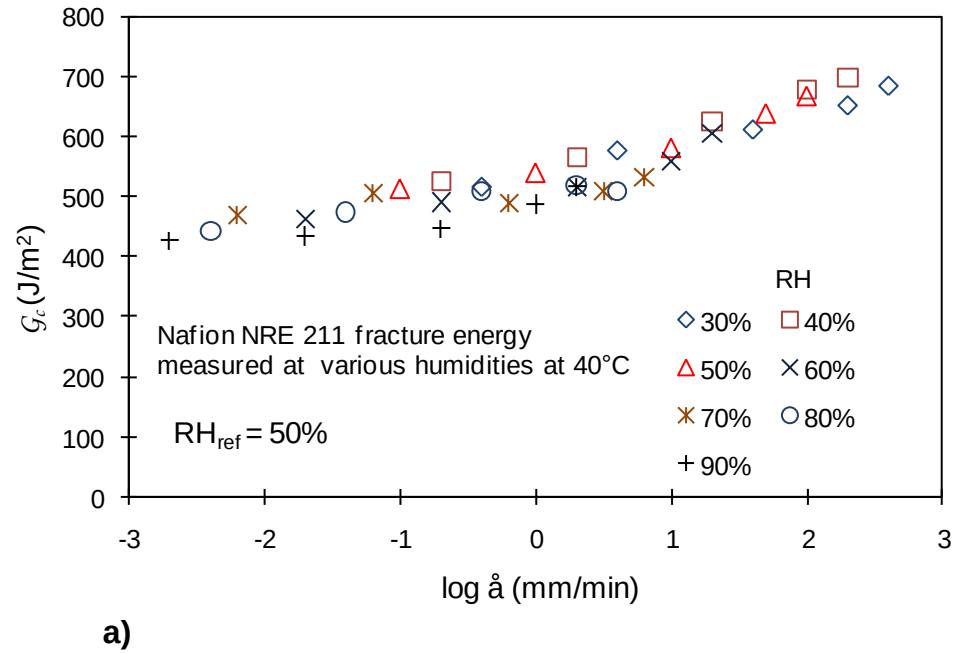

a)

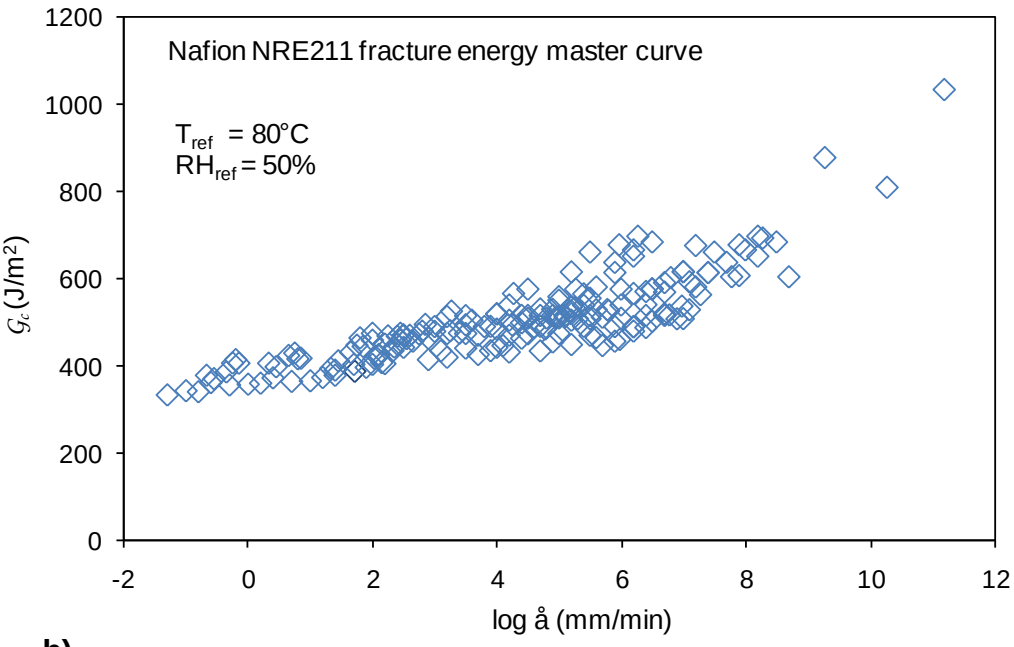

b)

Figure 6.9 Fracture energy measured for NRE 211. a) Hygral master curve of fracture energy recorded for NRE 211 tested at 40°C for various cutting rates and relative humidities (30-90% RH), b) hygrothermal master curve for fracture energies obtained by shifting all the hygral curves at various temperatures noting the thermal shift factor.

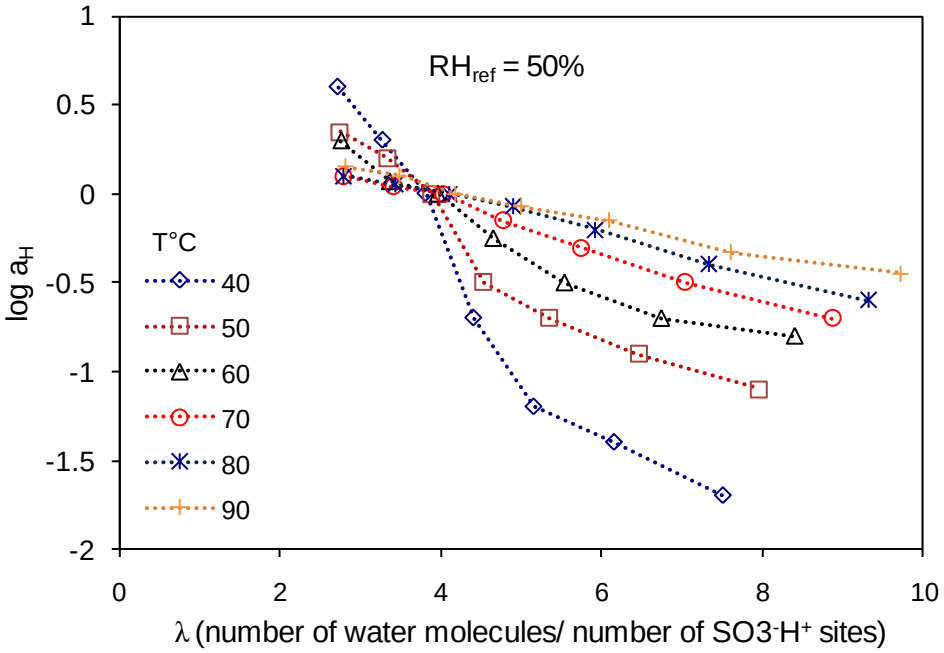

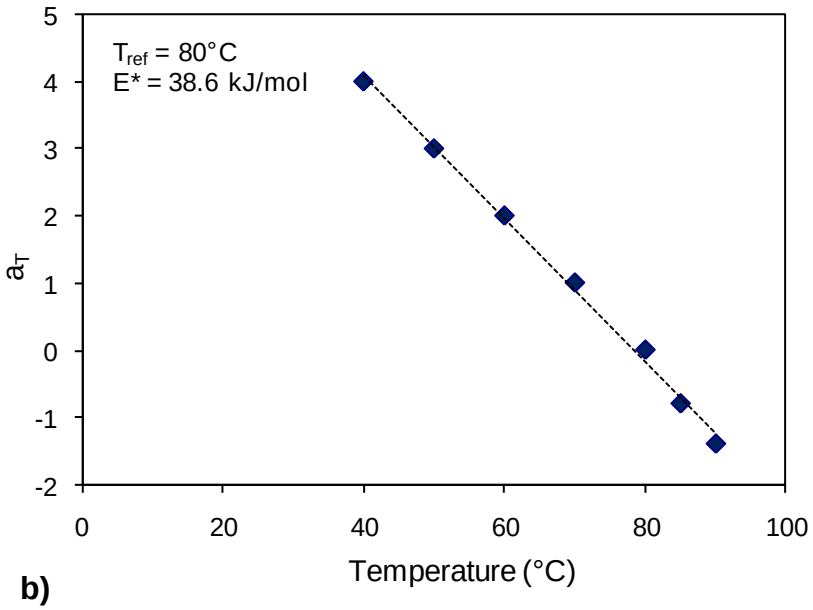

Figure 6.10 Shift factors for Nafion NRE 211. a) Hygral shift factors; and b) thermal shift factors for a doubly-reduced fracture energy master curve for NRE 211 tested at various temperatures, humidities and cutting rates. Thermal shift factors follow Arrhenius type behavior.

While plotting the hygral shift factors, the term "water content (λ)" instead of % RH is used, because water content within an ionomer, rather than relative humidity of the air, is expected to control the viscoelastic properties of the membrane. The effect of humidity over a range of temperatures can be encompassed into λ, a common water content metric for ionomers. Determined from the mass uptake, λ is defined as the number of water molecules per sulfonic acid site of the membrane [2]. An empirical formula to estimate λ at a given set of RH and temperature conditions for un-treated Nafion membranes is given by [118]:

$$\lambda = \left(1 + RH^2 \times 0.00002325 \times \frac{(T-30)}{30}\right) \times \left(0.00001422 \times RH^3 - 0.00189737 \times RH^2 + 0.13414 \times RH\right) \quad (4)$$

where T and RH refer to temperature in °C and % RH respectively.

The hygral shift factors appear to be affected by temperature. A similar trend was observed in our previous study dealing with measuring the constitutive properties of GoreSelect 57 membranes [127]. It is clear that higher temperatures reduce the dependence of hygral shift factors on temperature. This phenomenon can be explained on the basis of free volume theory. The fractional free volume in a polymer is expressed as [116]:

$$f = f_g + \alpha \Delta T + \beta \Delta \lambda \quad (5)$$

where f_g corresponds to the free volume at the glass transition temperature. The fractional free volume increases linearly above the glass transition temperature with the coefficients of thermal and hygral expansions α and β, respectively. At low temperature,

there is not enough fractional free volume to allow polymer chains to become mobilized and hence even small amounts of moisture act as a strong plasticizer (this fact is apparent from the shape of the WLF plot), thereby increasing the mobility of the chains significantly. At high temperature, there is significant mobility present as a result of high fractional free volume. Therefore additional of water does not significantly increase the mobility as it would at lower temperatures. Under this condition, moisture has less effect toward facilitating the mobility of polymer chains to any further extent, and thus has less effect on viscoelastic properties at higher temperatures. As a result, moisture acts as a weaker plasticizer. This idea provides a clue to the systematic arrangements of the hygral shift factors from lower to higher temperatures.

It can be seen that the fracture energy decreases at higher temperature and relative humidity, and increases with faster cutting rate. The same trend was seen with the N111-IP and GoreSelect 57 membranes. Considering that the most relevant temperature and RH ranges affecting membrane durability within an operating fuel cell are 60°C < T < 90°C and 10% < RH < 100%, the effect of both humidity and temperature needs to be carefully examined. By extrapolation, it can be seen that both hygral and thermal shifts for the given operating conditions would be about 2-3 decades. Thus in the temperature range that is most important to fuel cell operation, the fracture energy shows a similar dependence on temperature and relative humidity. The fracture energies at various temperatures and humidity conditions, seen as a function of cutting rate, seem to shift well. Furthermore, the principles of viscoelasticity dictate certain attributes to the process of the master curve construction. The master curve should be smooth, the shift factors reasonable, and the shift factors obtained from one viscoelastic process applicable to the

other physical processes [56]. Figure 6.11 shows a comparison of the thermal shift factors obtained from stress relaxation and knife slitting processes. The TTMSP appears to be applicable to the fracture energy of the PEMs, confirming that the process of slitting is viscoelastic in nature. It is intriguing to note that the thermal shift factors obtained from stress relaxation tests are consistent with time dependent durability data obtained from two separate tests; namely a fracture test such as the knife slit test and a strength test such as the pressure-loaded blister test discussed by Grohs et al. [179]. The rate and temperature dependence for these fracture energies and times to burst are both consistent with the rate, temperature, and moisture dependence of the relaxation modulus, suggesting the usefulness of a viscoelastic framework for examining and modeling fuel cell membrane durability.

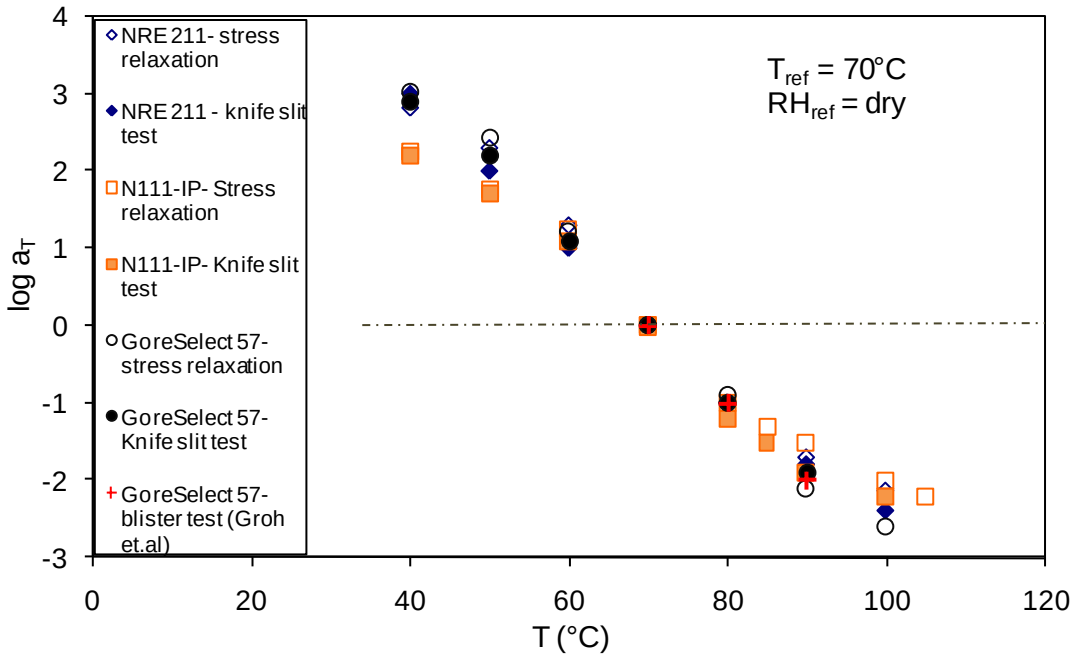

Figure 6.11 Comparison of temperature shift factors for Nafion NRE 211 and Ion Power N111-IP, and GoreSelect 57 obtained from stress relaxation and knife slitting tests.

6.4.3 Durability considerations

For comparison purposes, only fracture energies of the three membranes obtained under dry and 50% RH are considered. For convenience, hygral shift factors are not plotted here, but total hygral shift at any temperature for any of these membranes from dry to 50% RH is not more than a decade. The fracture energies obtained at vanishingly slow reduced cutting rates (i.e. at high temperatures and humidity levels) may approach the intrinsic fracture energy of the membranes. We do not claim to observe a plateau at lower reduced cutting rates, as the fracture energies are seen to decrease for many decades at the lower end of the flattening master curve with a small change in slope; a comparison of the master curves should ideally provide information about their relative intrinsic fracture energy values. For a given amount of fracture energy (or crack driving force) around both ends of the master curve, NRE 211 has significantly higher crack propagation rates than N111-IP, and therefore it may have poorer durability. This is in agreement with the humidity cycling tests results reported [125]. This may also suggest that cast membranes (such as NRE 211) may have poorer durability when compared with extruded membranes (such as N111-IP) in general. On the other hand, GoreSelect 57 appears to have higher fracture energy or lower crack propagation rates as compared with both NRE 211 and N111-IP membranes. However, this is not consistent with humidity cycling test results reported by Lai and Dillard [125]. The increased fracture resistance may be attributed to the tough extrudate polytetrafluoroethylene (ePTFE) layer used in the composite Gore membranes. The failure mode analysis showed that the Gore membrane failed by crack propagation in the ionomer layers instead of cracking through ePTFE layer. However, the knife slit test, which drives a crack through composite layers of Gore membrane, does not truly measure the fracture energy of an ionomer layer. This

may explain the anomaly in the durability ranking seen between fracture toughness obtained from the slit test and humidity cycling test results. The master curves have flatter slopes at lower reduced cutting rates, but have significantly different slopes (GoreSelect 57 and N111-IP being higher than NRE 211) at higher reduced cutting rates, cutting rates at a given value of fracture energy may be significantly different. For example, at a given fracture energy value, the reduced cutting rates associated with NRE 211 and N111-IP could differ as much as 2-4 decades. This suggests faster pinhole formation and propagation in NRE 211 as compared with N111-IP. It may be interesting to study other types of films and membranes to examine if chemistry and/or processing conditions of the polymer change the intrinsic value of fracture energy.

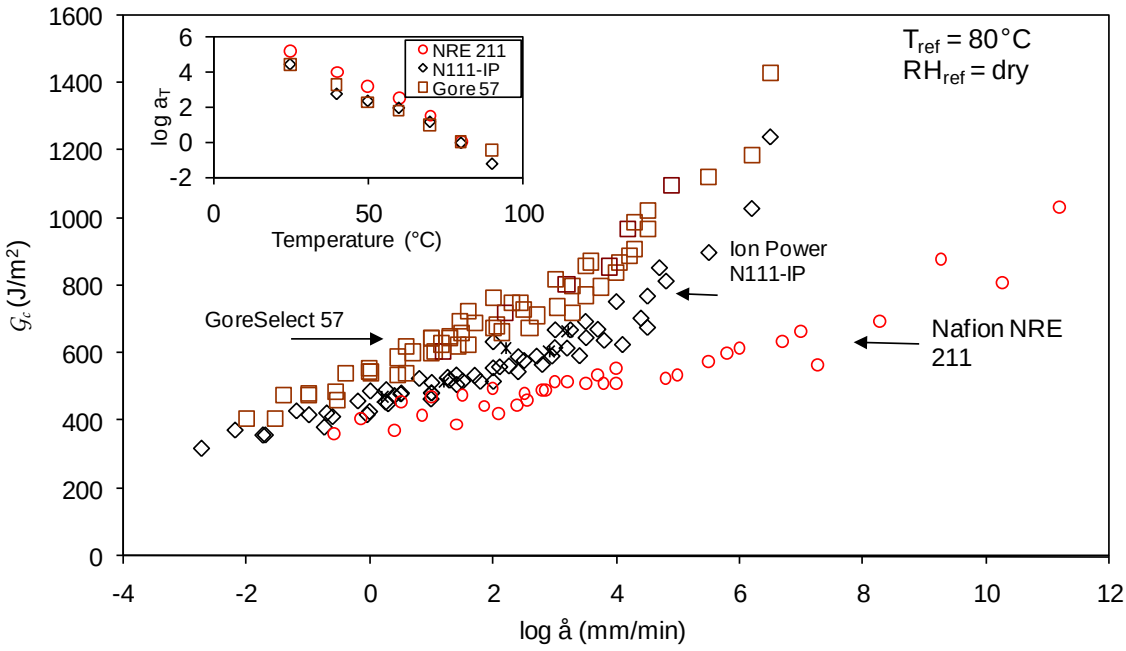

Figure 6.12 Comparison of master curves generated from shifting the fracture energy values at various temperature and humidity conditions for NRE 211, N111-IP, and GoreSelect 57.

6.4.4 Immersed Tests

In most polymers, water acts as a plasticizer [56]. Thus, under immersed conditions, hydrophilic polymers such as PEMs swell significantly, thereby presumably

allowing one to better approach the intrinsic fracture energy, which is the amount of energy required to break a given amount of bonds at vanishing rates. Thus, one may not consider the swelling in the thickness direction, as this does not change the number of bonds broken through the thickness. On the other hand, due to in-plane swelling, there are fewer bonds that are cut at a given crosshead rate. Therefore we thought it was appropriate to correct the crosshead rate for moist specimens due to the significant swelling. The swelling in the cutting direction was assumed to be about 15% based on Nafion NRE 211 product information [180], and the cutting rate was taken to be 85% of the crosshead rate. To be consistent, we have applied such crosshead correction to other humidity conditions as well, but since the correction is not large, it has not been discussed in this paper.

Only Nafion NRE 211 was tested under immersed conditions at various temperatures. Figure 6.13 shows the fracture energy obtained at various temperatures under immersed conditions, and shifted to form a fracture energy master curve (thermal shift factors shown as inset). The data appears to shift well, following consistent thermal shift factors (Figure 6.14). PEM fuel cells undergo humidity cycling from dry to equilibrium with moist air to equilibrium with liquid water during cell operation. Thus it is of interest to see if there is a clear and smooth transition from humid to wet condition. We do not discuss this subject in a great detail in this paper, but try to understand a "humid-wet transition" in a viscoelastic sense. In order to see if the hygral shift factors under immersed conditions are even possible to obtain, we tried to construct the hygral master curves of fracture energy at two temperatures (50 and 80°C) using the data obtained at the following humidity condition: dry, 50% RH, 90% RH and immersed.

Figure 6.15 shows the un-shifted fracture energy data obtained at the above conditions. It was clear that the data obtained in immersed conditions could not be shifted to form a consistent master curve, even after applying necessary vertical shifts. One may need data at higher humidity levels such as 95-100% RH in order to see if it would then shift with the data obtained under immersed conditions to form a hygral master curve.

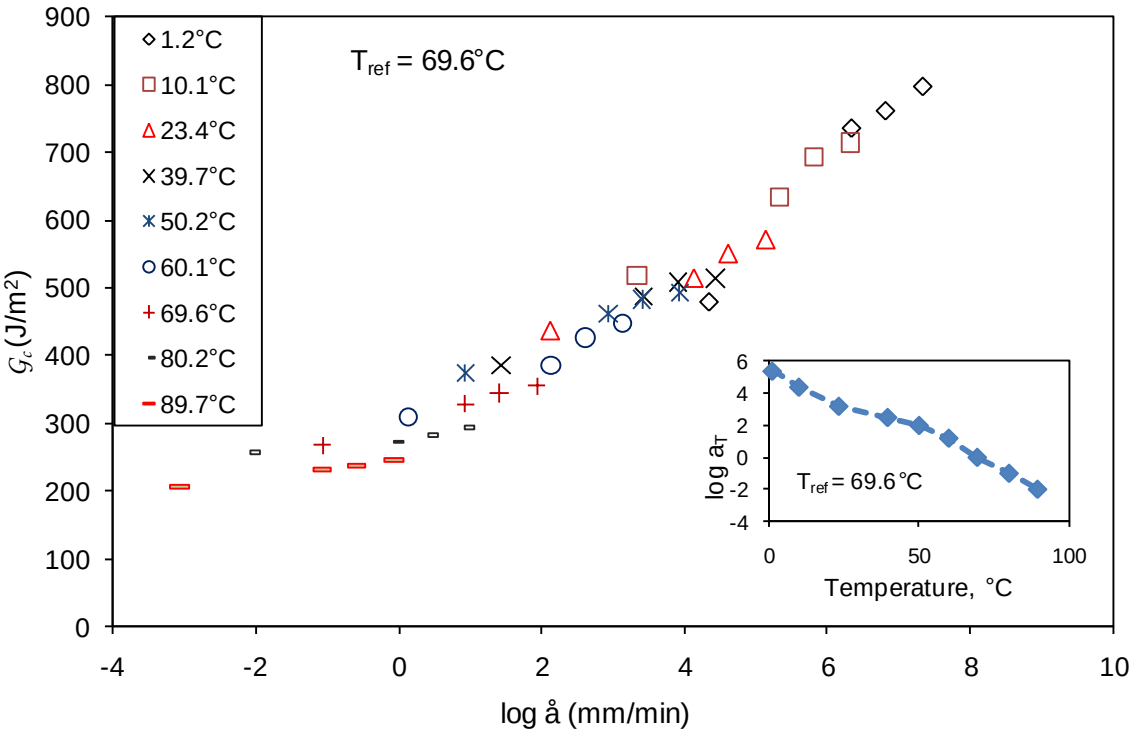

Figure 6.13 Fracture energy master curve for Nafion NRE 211 specimen tested at various temperatures and cutting rates, tested under immersed conditions. The thermal shift factors are shown as the inset.

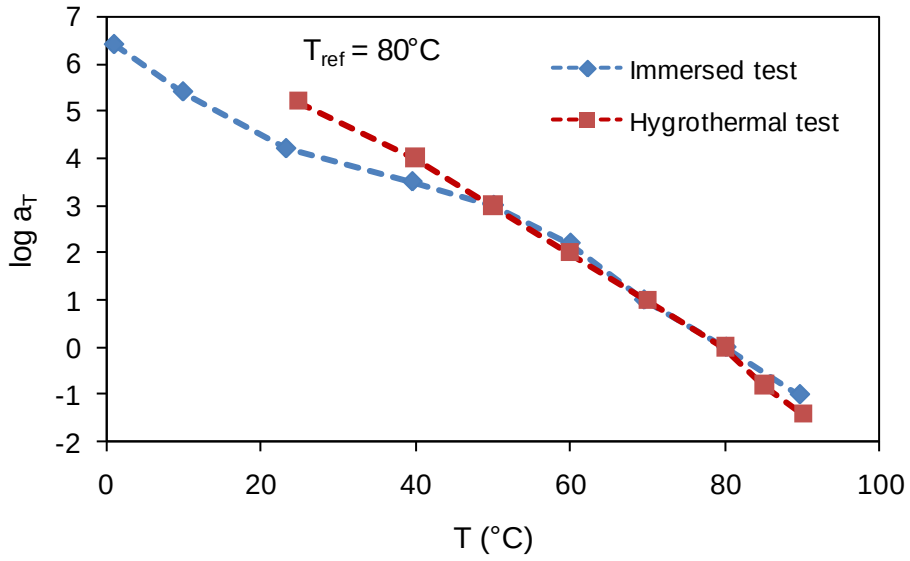

Figure 6.14 The thermal shift factors obtained from hygrothermal and immersed knife slitting tests conducted on Nafion NRE211 at various temperatures.

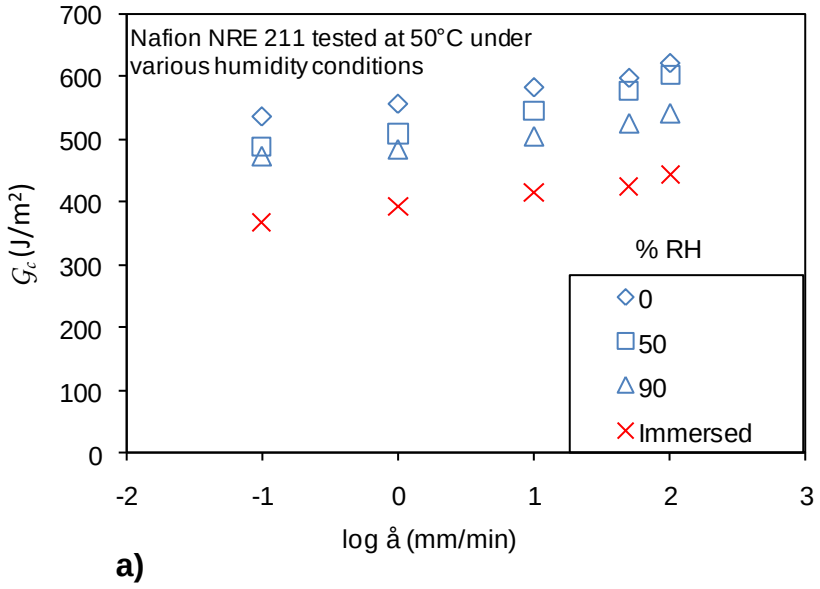

a)

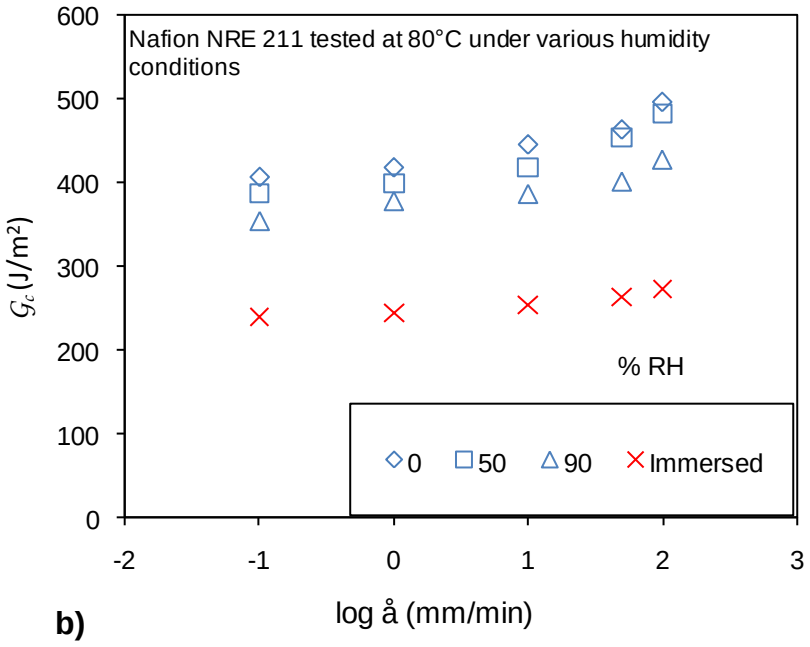

Figure 6.15 The fracture energy data for NRE 211 obtained under dry, 50%, 90% and immersed conditions at a) 50°C; b) 80°C. Clearly, the hygral shift factors under immersed conditions cannot be obtained as there would be a gap in the master curve.

6.5 Summary and Conclusions

The knife-slitting study initiated earlier was extended to other membranes in this study. The test fixture had the capability to perform knife-slit tests on thin membranes with limited plasticity. At small reduced cutting rates, the plastic dissipation is minimized and we may approach intrinsic fracture energy of the PEMs, which in turn may help us understand the process of apparently more brittle fractures that have been observed in failed membranes removed from operating fuel cells. Nafion NRE 211, Ion Power N111-IP and GoreSelect 57 membranes were tested at various temperatures, humidities, and cutting rates. The fracture energy associated with the process was doubly shifted using temperature and humidity shift factors to construct the master curve. The shift with respect to temperature and humidity suggests that the slitting process is viscoelastic in

nature. The thermal shift factors were compared with those obtained from transient stress relaxation tests conducted on these membranes. Good agreement was found between the thermal shift factors obtained from two different physical processes. The effect of humidity on fracture energy as evidenced from the hygral shift factors is not as significant as temperature. The effect is even less pronounced at higher temperatures, which are most relevant to fuel cell operations. Thus pinhole formation and propagation at high temperatures can be more influenced by temperature than humidity. The master curves for the three materials were then compared and were found to converge at low cutting rates, which may suggest that these membranes have similar intrinsic fracture energy. The fracture energies at higher cutting rates, which may be thought of in terms of fracture toughness, seem to show different behavior for the three membranes. The N111-IP and GoreSelect 57 membranes have higher fracture energies at a given cutting rate as compared to NRE 211. Or in other words, at a given fracture energy value, the corresponding reduced cutting rate for Nafion NRE 211 could be 10-100 times faster than those associated with N111-IP or GoreSelect 57 membranes. The tests were also conducted under immersed conditions as water; known to plasticize most polymers, was thought to help better approach the intrinsic fracture energy. Although we do not claim to have observed the fracture energy plateau (rate-independence), a very gradual decrease in fracture energy over a few decades of reduced cutting rates was observed. This may be an indication of approaching the intrinsic fracture energy. The immersed tests were successfully conducted at various temperatures and the fracture energy associated with the slitting process was shifted using thermal shift factors. The thermal shift factors obtained from the hygrothermal and immersed slitting tests were quite comparable. This

suggests that irrespective of testing conditions temperature influences the viscoelastic fracture energy in a similar fashion, especially at higher temperatures. We believe the knife-slitting test can be used as a tool to evaluate the durability of various PEMs.

6.6 Acknowledgment

The authors would like to express appreciation to the General Motors Corporation for supporting this work, as well as the Institute for Critical Technology and Applied Science (ICTAS), the Engineering Science and Mechanics Department, and the Macromolecules and Interfaces Institute (MII) at Virginia Tech for providing additional support and facilities.

CHAPTER 7: Effect of Water-pretreatment on Viscoelastic Properties of Proton Exchange Membranes

Manuscript prepared for Journal of Membrane Science

7.1 Abstract

Researchers investigating various properties of proton exchange membranes (PEM) often pretreat the membranes in order to remove low molecular weight impurities from the membranes and erase thermal and morphological history. Such pretreatments may involve boiling the membrane in deionized water, hydrogen peroxide, or various acids to mention a few. These pretreatments have been shown to change the physical properties of the membranes such as mass uptake, proton conductivity, and Young's modulus etc. The effects of such pretreatments on the viscoelastic properties of pretreated membranes have not been studied extensively, yet this time-dependent behavior may be important in assessing membrane durability. Our previous work has dealt with measuring the viscoelastic properties of untreated (as-received) membranes, in part because fuel cell manufacturers would prefer to use such materials in the stack assembly process. In this paper we investigate dynamic and transient viscoelastic properties under dry conditions after these membranes were subjected to pretreatment (preconditioning) in deionized water at several temperatures. The tensile relaxation modulus of a commercially available proton exchange membrane, Nafion® NRE211, was obtained over a range of temperatures using a commercial dynamic mechanical analyzer (DMA). The stress relaxation master curve was constructed recording the thermal shift factors (a_T) at various temperatures. Storage $\left(E^{'}\right)$ and loss moduli $\left(E^{''}\right)$ were obtained by subjecting tensile membrane samples to oscillatory dynamic loading. A very unusual viscoelastic

behavior was observed as a result of transient and dynamic loading. For membranes pretreated at 80°C and in boiling water, both the storage and relaxation modulus was found to increase with increase in temperature up to a certain temperature (~90°C) and then decrease with increase in temperatures above this temperature. Possible morphological changes when the membrane was exposed to water might have triggered the unusual viscoelastic behavior. The effect of pretreatment on hygral strains induced as a function of relative humidity (RH) was also investigated. These studies suggest that pretreatment by immersion in water at several different temperatures can significantly change the viscoelastic properties of proton exchange membranes. Besides the treated membranes, the hygral strains induced in as-received membranes as a function of RH were also measured. Successful measurement of the hygral strains using a dynamic mechanical analyzer (DMA) provides a new tool for measuring this important piece of constitutive properties.

Keywords: Pretreatment, Nafion® NRE 211, water immersion, hygral strains, morphological changes, dynamic mechanical analyzer, time temperature superposition, viscoelasticity

7.2 Introduction

Proton exchange membrane fuel cells (PEMFC) offer considerable potential for electrical power applications, including, automotive and portable applications. Their potential for providing a cleaner power source with high power density and high efficiency offers attractive advantages over traditional power sources [94]. However, there are a number of concerns that the fuel cell industry must address before the full potential of PEMFCs is realized. According to US Department of Energy targets for year 2010, PEM-based fuel cells for transportation applications should perform reliably for

5000 hours at operating temperatures ranging from -40°C to 80°C [9]. This requirement imposes stringent durability concerns on a fuel cell. Of various components, the durability of the proton exchange membrane is of prime concern, as it must prevent the reactant gases from mixing, yet allow protons to flow freely through the membrane. Several papers in last few years have focused on the durability aspect of proton exchange membranes through mechanical characterization [6, 13, 27, 96, 102, 104, 122, 127-130, 133, 137-139]. Most of these papers discussed some form of pretreatment before testing the mechanical properties of PEMs. The rationale behind treating the membrane before conducting any tests is to attempt to make the membrane free from any low molecular weight impurity and to erase any thermal and morphological history it may have. Few papers discuss conducting experiments on as-received samples without any form of pretreatment [95, 112, 122, 127]. This distinction is quite important in the sense that when membranes are used in commercial fuel cell assemblies, they may likely not be pretreated. Thus there is a potential for discrepancy if the mechanical, morphological or viscoelastic properties of pretreated membranes are used to assess durability of as-received membranes in fuel cell stacks.

Our previous work dealing with hygrothermal viscoelastic characterization was based on tests conducted on untreated PEMs, and has shown that PEMs behave as hygrothermorheologically simple materials, thereby allowing hygral master curves at various temperatures to superpose on each other giving rise to a hygrothermal master curve [113, 127]. Thus the morphology of the membranes after they are processed may be amenable to time temperature moisture superposition principle, and durability of untreated (as-received) PEM can be assessed within the framework of viscoelasticity as

described by Lai et al. [125]. The goal of this study is to establish the effect of treatment on the important viscoelastic properties of pretreated membranes, and to determine whether the properties of treated PEMs are amenable to the time temperature moisture superposition principle.

Recent work by Majsztrik et al. [129] and Satterfield el al. [128] focused on viscoelastic creep and relaxation properties of Nafion membranes, respectively. They used a pretreatment on Nafion membranes which included boiling sequentially in 3% hydrogen peroxide, deionized water, sulfuric acid, and deionized water. Majsztrik et al. [129] conducted tensile creep test on Nafion under various temperature and humidity conditions, and found that waster plasticized Nafion at low temperature and stiffened it higher temperature. At 90°C, the creep rate of Nafion decreased by a factor of 100 between 0% and 85% RH. Satterfield et al. [128] measured the tensile stress-strain and relaxation properties of Nafion under variety of temperature and humidity conditions. They had similar observations as reported by Majsztrik et al. They found that at room temperature, the elastic modulus decreases with water activity, but at temperatures ≥ 90°C, hydrated membranes are stiffer than dry membranes. These findings were not consistent with Bauer et al. [102], which could be attributed to environmental control. They concluded that temperature, absorbed water, and imposed strain alter the microstructure of Nafion, inducing ordering transitions. They claim that a loss of microphase order reduces the elastic modulus and results in stress relaxation modulus approaching zero after 10^3-10^4 second.

There are a few studies comparing the properties of treated and untreated membranes. Tang et al. [13] compared the effect of pretreatment on mechanical

properties of Nafion®112 membranes. They reported Young's modulus at 50% RH for both treated and as-received membranes and claimed that as-received membranes had a higher modulus. Their pretreatment procedure involved boiling membrane samples in hydrogen peroxide, sulfuric acid and deionized water. Zawodzinski et al. [25, 28, 181] claim that pretreatment removes the low molecular weight impurities, thereby increasing the conductivity of the membrane. Also boiling helps promote creation and growth of hydrated ionic clusters, which lead to an increased water content. The morphological rejuvenation or reorganization of the membrane along with the formation of ionic clusters, is responsible for the higher water content of pretreated samples. A recent interesting paper by Alberti et al. [182] describes kinetics of water-uptake of Nafion membranes after different thermal and hygrothermal treatments. They found that the kinetics of water-uptake is the result of two different processes: a fast process that is attributed to the time to reach osmotic equilibrium necessary for diffusion of water within the membrane, and a slow process that is associated with slow conformational changes in Nafion with temperature. This observation is consistent with the diffusion process into a glassy polymer. Typically above the glass transition temperature (T_g), only the former is present, while below the T_g, both the mechanisms are present [56]. The irreversibility of the hydration process with temperature was also investigated by Alberti et al. [182] and was attributed it to the conformational changes.

In this paper, we discuss the effect of pretreatment on viscoelastic properties of Nafion, as well as the hygral strain induced as a function of RH and how pretreatment affects both the aspects.

7.3 Experimental Procedure

The material tested in this study was DuPont™ Nafion® NRE 211 (referred to as simply Nafion henceforth), 25μm thick perfluorosulfonic acid (PFSA) membranes reportedly produced by a casting process. Nafion membranes were pretreated by submerging in deionized water at three different temperatures; namely 60, 80 and 100°C for 2 hours, followed by drying in a vacuum oven for about 12 hour at 80°C with vacuum applied. A TA Instruments™ Q800 dynamic mechanical analyzer (DMA) was used in tensile mode to conduct transient stress relaxation and dynamic (steady state oscillation) experiments on small membrane samples. The DMA was also used to measure hygral strains induced in membrane samples as indicated by the change in length. Membrane samples with an average length (between clamps) to width ratio of five to six were used. Typical specimen widths ranged from 3.5-4 mm. A light microscope was used to accurately measure the sample width. Typically the width was measured at the top, middle and bottom sections of the film to select the part of the film which showed less variation. The most uniform section of the film was then clamped in the tensile fixture of the DMA machine. Typically the gage length was around 20-21 mm, as measured by the DMA machine. In order to conduct tests at various humidity levels, a humidity chamber was built to enclose the tension clamps yet fit within the nearly closed DMA temperature chamber without affecting the DMA drive unit. Details of this unit can be found in the paper by Patankar et al. [127]. Humidified air was supplied at the desired temperature and humidity level using a Fuel Cell Technologies™ gas humidification system. A Vaisala™ dew point sensor (HMT 337) was used during all the hygrothermal tests to provide a direct indication of relative humidity within the environmental chamber. This sensor was placed just outside of the chamber in such a way that it measured the dew point of the air

exhausting from the chamber. For hygrothermal tests, the DMA furnace and the base of the humidity chamber were preheated to reduce any condensation of water. Humid air was introduced once thermal equilibrium was reached, and after an additional 20 minute soak time, the test was started.

All transient stress relaxation and dynamic tests were conducted under dry condition. A compressed dry air tank was used to supply dry air to the humidity chamber. The tests were conducted for temperatures ranging from 40-100°C. The typical test duration for each condition was 2 minute, followed by a 20 minute recovery time at each temperature. During the recovery mode, the drive motor would return back to its initial position, leaving slack in the elongated sample, and hence the stresses in the sample would nominally be zero, although the strains would be non-zero. The relaxation modulus was obtained by straining the sample to 0.5%. Oscillatory dynamic tests were conducted under dry conditions to determine the α-relaxation temperature of Nafion [119, 120]. The loss modulus $\left(E''\right)$ obtained from single frequency (1 Hz), temperature ramp (40-150°C, 2°C/min heating rate) dynamic tests was used as the criterion to determine the transition.

In order to measure the hygral strain induced in membrane samples as a function of humidity, a test protocol was first established using as-received samples. The Membranes tested in this study were Nafion®NRE 211 and Gore®Select™ 57. It was important to apply a small amount of preload during the test so that the sample would just remain taut without inducing significant creep in the sample, hence reducing possible error in measurement. Initially a preload of 0.2 mN was applied, but was found to give erratic data; as such small preload might have approached the resolution limit of the

DMA. Therefore, all future tests involving measurement of hygral strain were conducted using a preload force of 0.5 mN, which seemed to give consistent data. To validate our claim that 0.5 mN would not induce any significant mechanical strain in the sample, a creep test was performed at 80°C/0% RH using a stress that corresponds to a load of 0.5 mN (~ 5kPa). Mechanical strain induced due to this preload was measured and found to be quite negligible (~0.3-0.7% of the hygral strains).

At a given temperature, the humidity was stepped from dry-90% RH. The membrane sample was allowed sufficient time to equilibrate; this time depends upon the humidity level. After hygral equilibrium was established, the humid air was flushed out with dry air at the same temperature. Once the hygral strain returned to zero (suggesting that the shrinkage and swelling mechanisms appear reversible), humid air at higher RH level was introduced into the chamber. To measure the coefficient of hygral expansion, CHE for as-received membranes, the relative humidity was stepped from 30-90% RH with the increments of 10%. The original membrane length was measured under dry conditions as this would give a reference condition based on which the hygral strains induced at other RH conditions would be measured. The experiments were performed at 40-80°C. At a given temperature, the RH was stepped up until it reached 90% and then stepped down to dry conditions. The average of strains recorded during humidity step-up and step-down processes at a given RH was taken as the hygral strain at that particular RH.

7.4 Results and Discussion

7.4.1 Viscoelastic properties of treated membranes

In order to explore the effect of pretreatment on viscoelastic properties of Nafion, transient stress relaxation tests and oscillatory dynamic tests on specimens under dry conditions were conducted. Figure 7.1 shows the stress relaxation modulus for membrane samples treated at 80°C. The figure is split into two plots to show how the modulus changes with temperature. As temperature increases from 40 to 80°C (Figure 7.1a), the relaxation modulus increases. As temperature increases from 90 to 120°C (Figure 7.1b), the modulus decreases. In the range 80 to 90°C, the modulus remains somewhat constant. The drop in modulus from 90-120°C is quite expected; however, the rise in modulus from 40-80°C is not. Similar behavior was observed for the membranes that were treated in boiling water. Figure 7.2 shows the changes in modulus with temperature for the membranes treated in boiling water. Since the membranes were vacuum-dried for about 12 hours at 80°C, there is no likelihood of trapped water that might escape as temperature rises during the relaxation test. The α-relaxation of Nafion is about 80°C, which corresponds to destabilization of the dynamic network [119, 120]. Some form of morphological rearrangement must be taking place to exhibit this unusual behavior around the α-relaxation. Although it is possible to construct a relaxation master curve where the modulus rises with temperature, such phenomenon is not usually observed in the field of polymer science. If one tried to construct a master curve, the thermal shift factor plot would look the one shown in Figure 7.3. Possible morphological changes leading to strengthening of the dynamic network and thereby leading to higher modulus as temperature goes up might explain this behavior. Another possible explanation stems from the fact that the morphological perturbations (rearrangements of ionic domains and

crystallites) may not have enough time to relax when the membrane is treated for two hours at 80 and 100°C. Higher temperature may reestablish the network by introducing physical crosslinking sites in the form of phase separated crystallites. Also different morphological features may relax differently during a thermal cycle in a DMA, and this might result in higher modulus.

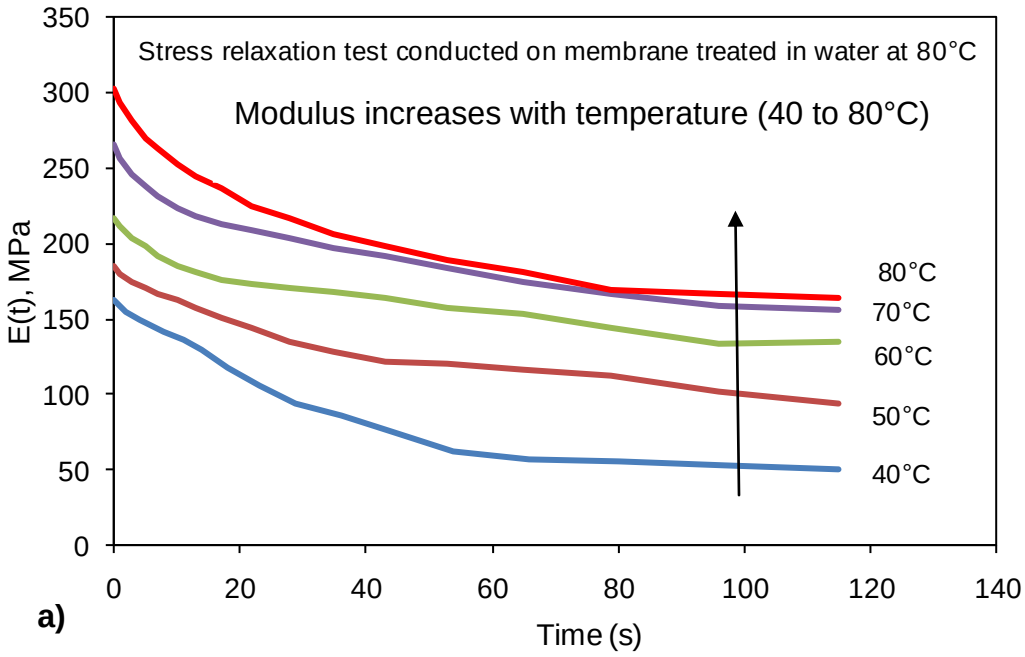

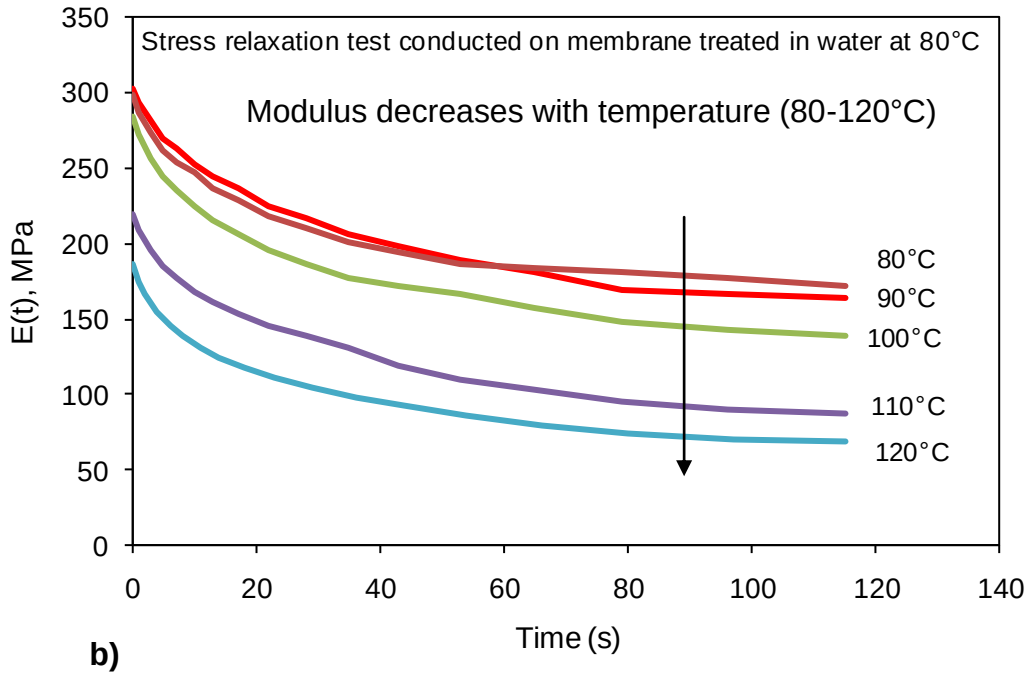

Figure 7.1 Tensile stress relaxation modulus (corresponding to 0.5%) plotted against temperature for the membranes treated in water at 80°C; a) for temperature 40-80°C, and b) from 80-120°C. Modulus rises with temperature in figure a) and drops in figure b).

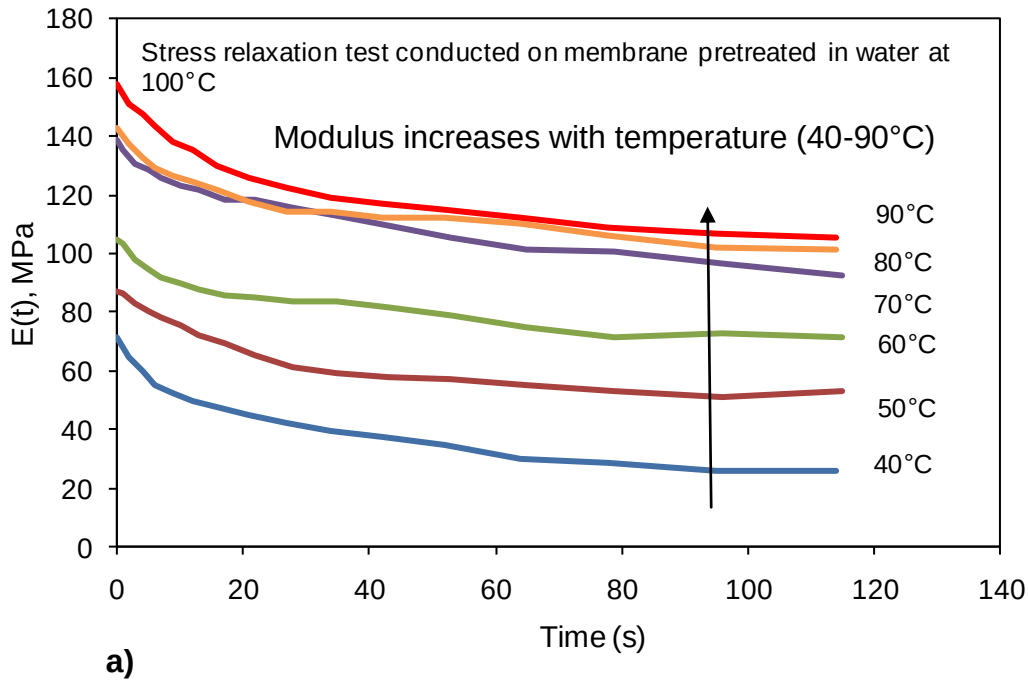

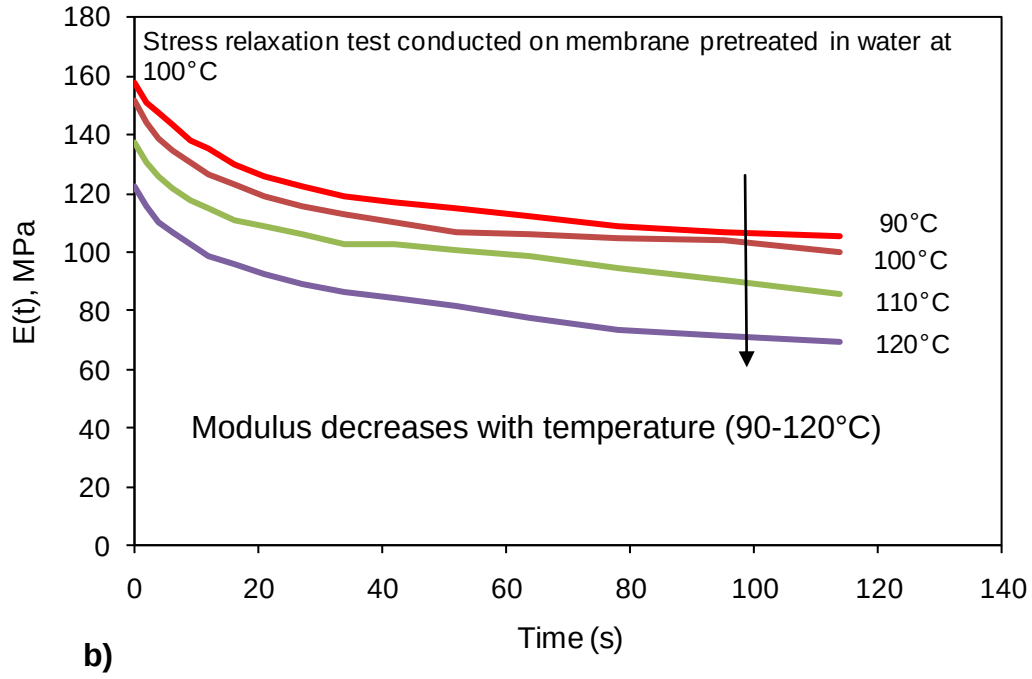

Figure 7.2 Tensile stress relaxation modulus (corresponding to strain of 0.5%) plotted against temperature for the membranes treated in water at 100°C; a) for temperature 40-90°C, and b) from 90-120°C. Modulus rises with temperature in figure a) and drops in figure b).

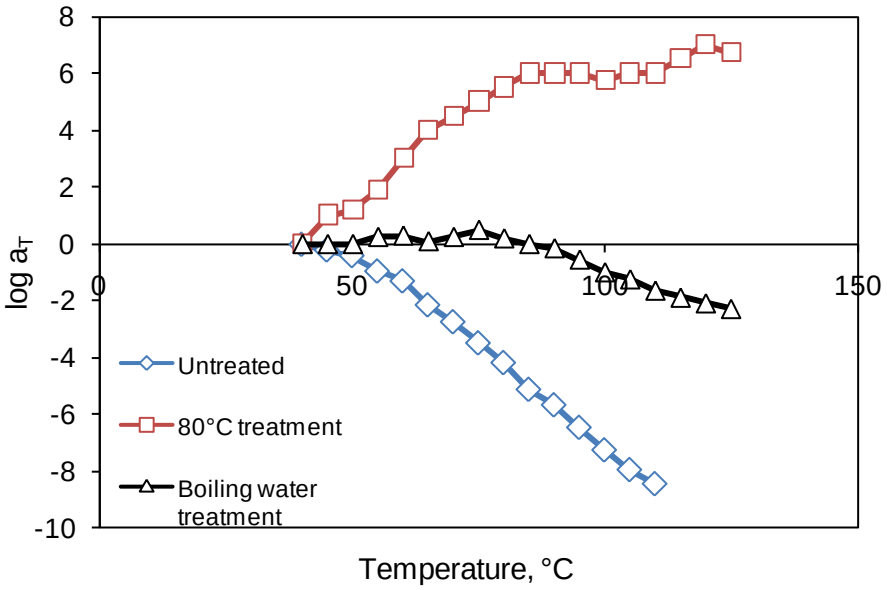

Figure 7.3 Thermal shift factors as a function of temperature plotted for treated and as-received membranes. These shift factors would be obtained if tensile relaxation master curve was to be constructed for membrane samples strained at 0.5%.

Dynamic tests conducted on treated and as-received membranes revealed similar behavior. All the tests were conducted under dry conditions and at 1 Hz. The storage and loss moduli $\left(E^{'}, E^{''}\right)$ and $\tan\delta$ are plotted for the membranes subjected to a temperature ramp (40-150°C) and at 1 Hz frequency. Generally tan δ did not show a peak over this temperature range, so the loss modulus peak was used as the criterion for a transition. Again, as seen in the case of tensile stress relaxation for the membrane treated at 80°C in DI water, the storage modulus clearly increased as temperature rose until about 100°C and then gradually dropped. This observation is consistent with the results from the stress relaxation tests. The storage modulus for the membranes pretreated at 100°C in DI water showed a similar trend as observed in the case of the relaxation modulus obtained from the transient tests. However, the rise in modulus is not as clear. Figures 7.4-7.6 show the plots of the storage modulus, loss modulus and tan δ respectively. Again it is evident from the plots that pretreatment induces some form of morphological changes, exact nature of which unknown at this point, which behave quite differently in a viscoelastic sense. Small angle x-ray scattering (SAXS) analysis was performed on the membranes, but it did not reveal any particularly useful information and hence not included in the discussion here.

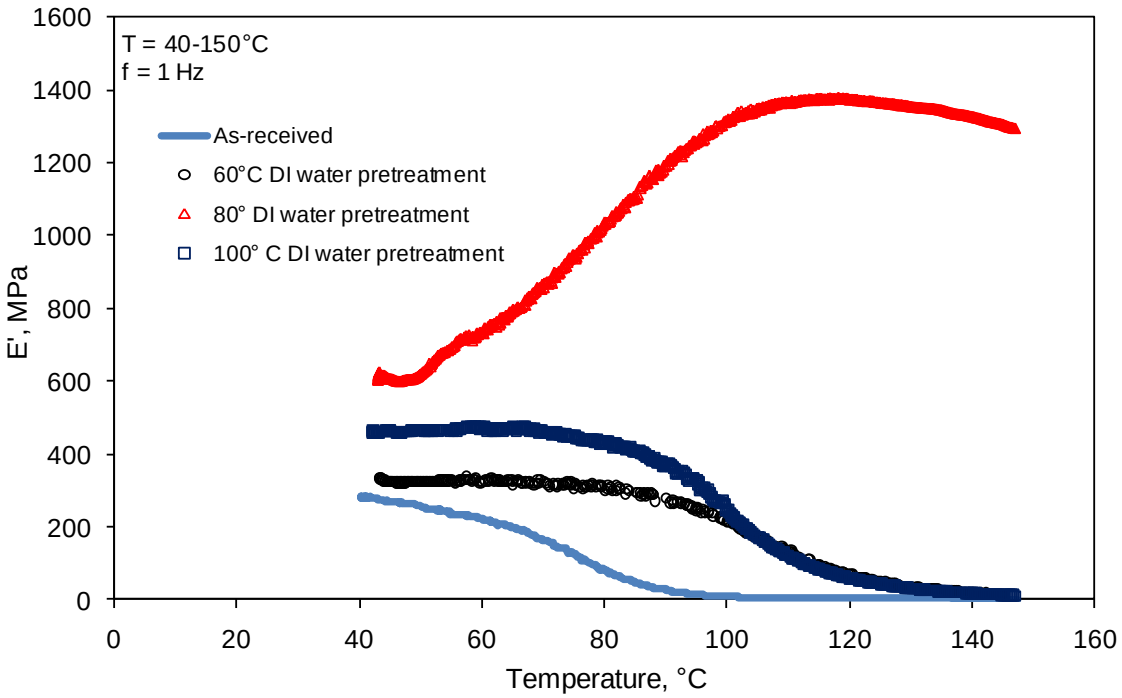

Figure 7.4 The storage modulus obtained for as-received and treated membranes subjected to temperature ramp at 1 Hz frequency.

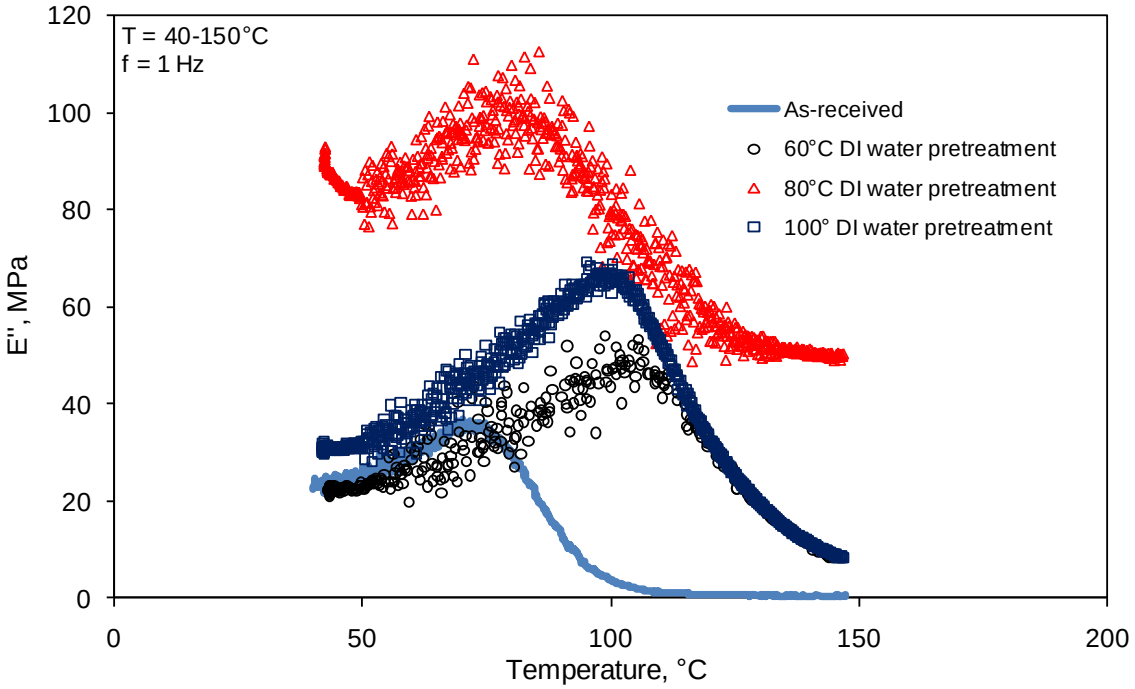

Figure 7.5 The loss modulus obtained for as-received and treated membranes, subjected to temperature ramp at 1 Hz frequency.

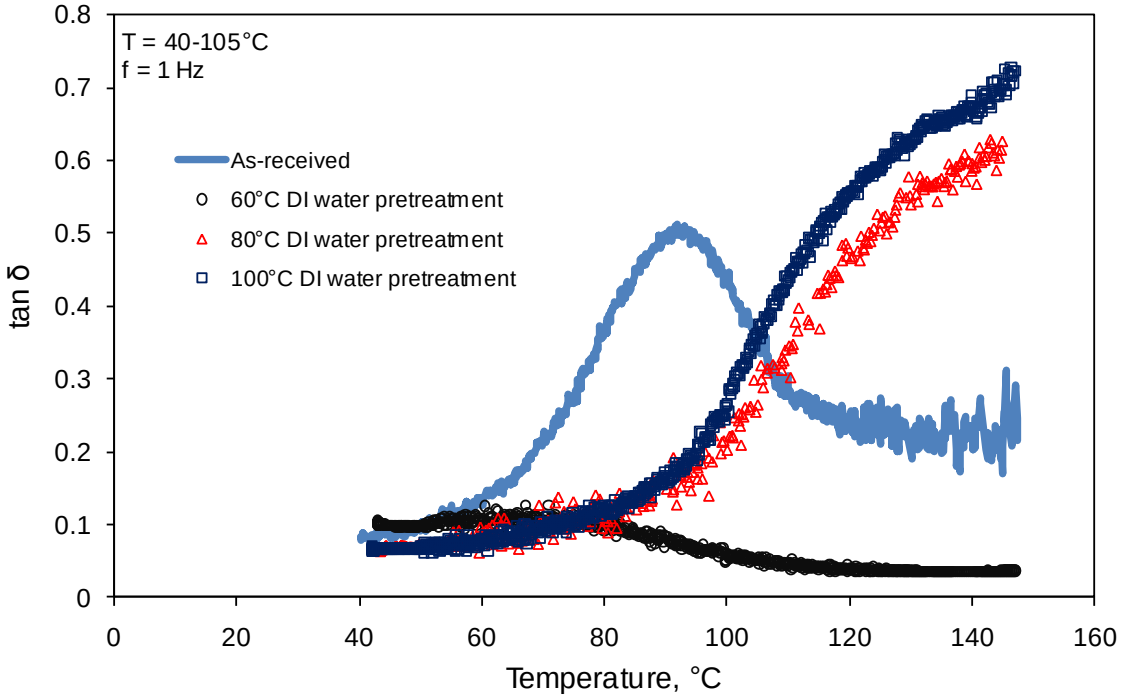

Figure 7.6 tan δ modulus obtained for as-received and treated membranes subjected to temperature ramp at 1 Hz frequency.

The highly unusual behavior observed so far in case of the water-treated membranes may have its origin in the morphological reorganization of ionic and crystalline domains during pretreatment. Gebel et al. [183] proposed a conceptual description for the swelling of an ionomer. In this qualitative model, the dry membrane, considered to contain isolated, spherical ionic clusters, absorbs water. As a result, the clusters swell to hold the pools of water surrounded by ionic groups. As the water content increases, the structural inversion takes place and it resembles a network of connecting ionic domain rods. This model could very well be temperature dependent. Thus temperature may induce similar changes in presence of water. When the membranes are pretreated at 80°C and in boiling water, they may possess features that tend to stabilize until the temperature reaches the α-

relaxation [119, 120] of Nafion. Significant mobility above this temperature would reduce the modulus as expected.

7.4.2. Hygral strain measurement

As mentioned earlier, measurement of the hygral strains at different temperature/RH conditions is just as important as knowing the viscoelastic properties, as both these properties are required to be used in a constitutive stress modeling of PEM. Figure 7.7 shows hygral strain induced at 80°C/30% RH condition. It can be seen that strains developed with 0.2 mN load cell track the ones developed with preload 0.5 mN. However, the data obtained from the 0.2 mN preload is quite erratic. Figure 7.8 shows an example of an RH cycling test conducted at 70°C. Typically at low humidity levels, the equilibrium strain value (corresponds to the plateau) was achieved quite rapidly, but at higher humidity levels, the time to reach this plateau was varied. The higher the temperature and humidity, longer was the time to reach the maximum strain. As stated earlier, the moisture ingression process consists of a kinetic step followed by a thermodynamic step consisting of conformational changes. Interplay of these two different processes will determine the overall rate of ingression of moisture into the membrane. Possible fast swelling of ionic domains with ingression of moisture up to a certain water content level (60% RH), followed by relatively retarded swelling rate at higher moisture content could explain this behavior. It can be seen from Figure 7.8 that for 30-60% RH data, the rate of expansion $\frac{d\varepsilon}{dt}$ appears to be quite similar; while the rate is different for 70-90% RH.

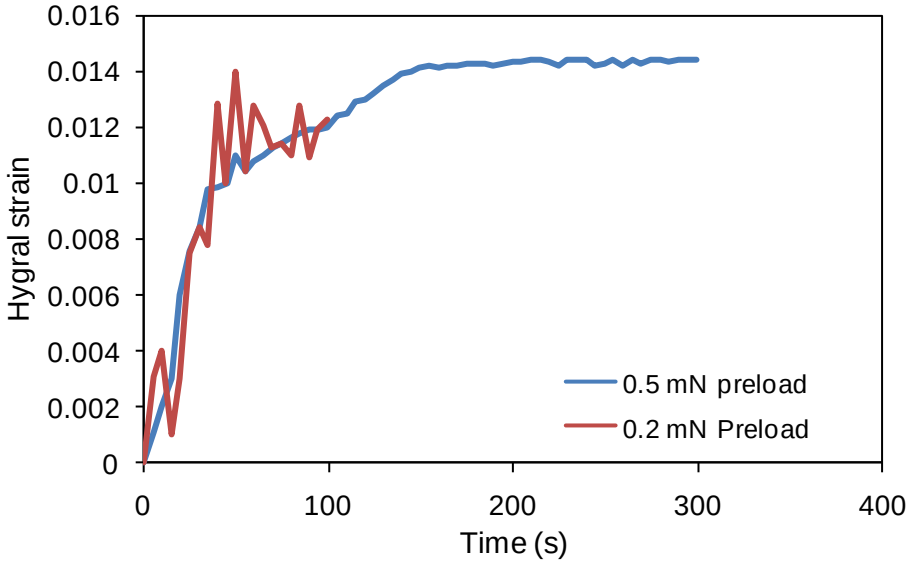

Figure 7.7 Hygral strain induced in the membrane sample at 80°C/30% RH condition as a result of preloads of 0.5 mN and 0.2 mN.

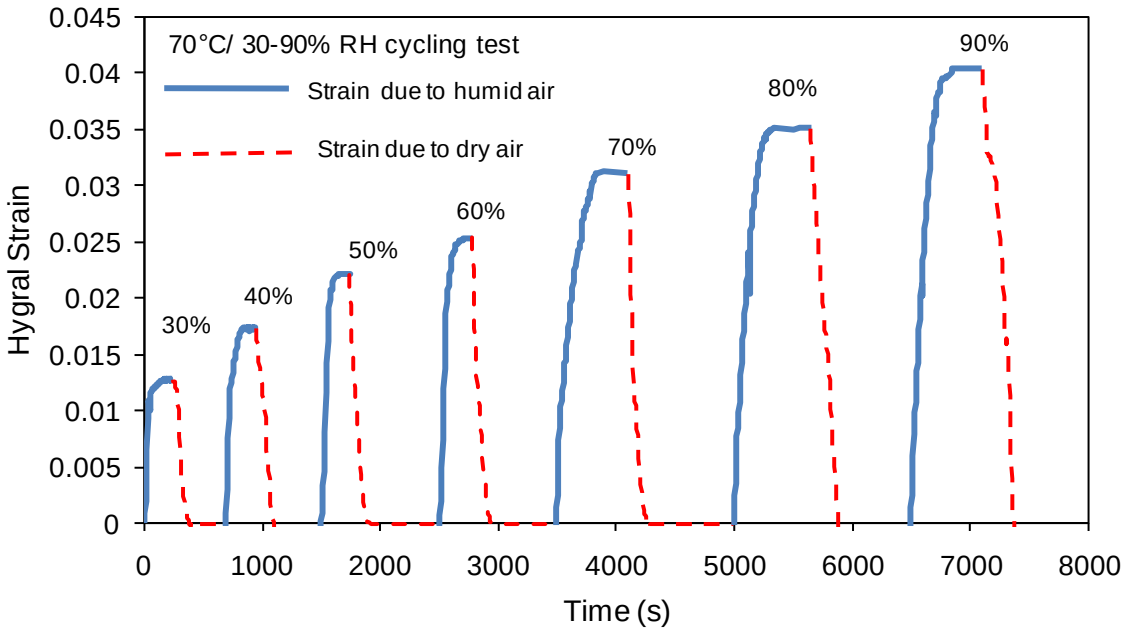

Figure 7.8 Hygral strain induced in the membrane sample at 70°C/30-90% RH conditions. At each humidity level, the plateau observed corresponds to the maximum hygral strain.

Having established that the technique works well to measure hygral strain in the as-received membranes, strains developed in the pretreated membranes were measured.

The average of the strains from three replicates was reported in the plot shown in Figure 7.9, where we show the strains induced due to RH, and not the water content (λ). As the water content within the polymer, rather than relative humidity of the air, is expected to control the viscoelastic properties of the membrane, the effect of humidity over a range of temperatures can be encompassed into λ (defined as the number of water molecules per sulfonic acid site of the membrane at the given RH and T [2]), a common water content metric for ionic materials. In order to measure the coefficient hygral expansion (β), one needs to know the water content at each RH level, which can be measured based on mass uptake. However, we did not measure the mass uptake in this study. Our aim was simply to point out the differences in the strains at given RH levels due to various treatments. It can be seen that treated membranes show higher hygral swelling strains as compared to as-received ones. Figure 7.9 shows hygral strains induced when RH cycling tests were carried out at 80°C, but similar behavior was observed at other temperatures. An interesting point to note is the order in which the recorded hygral strains appear at a given RH in Figure 7.9. The hygral strains at any given RH order sequentially by pretreatment to which the membranes are subjected to. For example, as-received membranes show the least of hygral strains, and the membranes subjected to treatment in boiling water show the maximum amount of hygral strain, while the membranes subjected to 60 and 80°C water-treatment show strains that are intermediate. Such particular sequencing was not observed in the case of transient or dynamic viscoelastic tests.

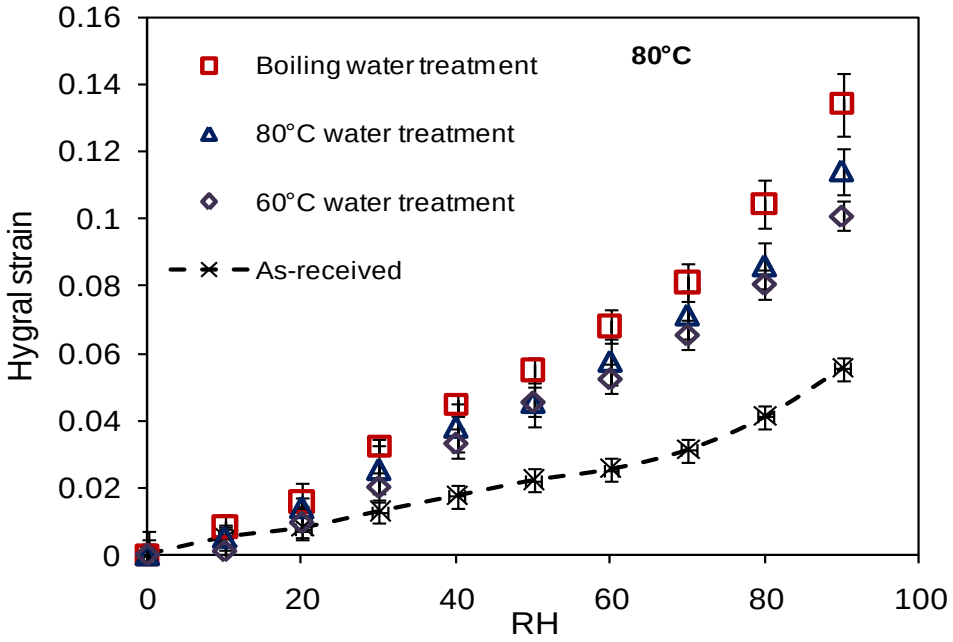

Figure 7.9 Hygral strain induced in the membrane sample at 80°C/0-90% RH conditions, when membrane samples were treated at various temperatures in deionized water.

7.4.3. Coefficient of hygral expansion measurement

Besides the viscoelastic constitutive properties, the other essential property which needs to be measured is the coefficient of hygral expansion (CHE), as both the properties will be required as an input for constitutive stress modeling of membranes constrained in a fuel cell stack. For the stress model discussed by Lai et al. [122] and Park et al. [140] the following polynomial expression for the CHE was assumed

$$\beta = 7.489\times10^{-9}T^{3} - 1.638\times10^{-6}T^{2} + 1.268\times10^{-4}T - 1.517\times10^{-3} \quad (1)$$

where T is the temperature expressed in degree Celsius. The expression was based on the results obtained by measuring the hygral strains induced in Nafion NR 112 at various temperatures and humidity levels [125]. For as-received membranes, the water content as a function of temperature and relative humidity was calculated using the following expression

$$\lambda = \left[1 + RH^2 \cdot 0.00002325 \cdot \frac{(T-30)}{30}\right] \cdot \left[0.00001422 \cdot RH^3 - 0.00189737 \cdot RH^2 + 0.13414 \cdot RH\right] \quad (2)$$

where T and RH are temperature in degree Celsius and relative humidity in per cent respectively [130]. Figure 7.10 shows a representative plot of the hygral strains-water content at 70°C for GoreSelect 57, and Figure 7.11 shows the CHE plotted against temperature and fit with a cubic polynomial. Identical experiments were conducted using NRE 211 membrane and results are plotted in Figure 7.12 and 7.13. Figure 7.14 shows a comparison of the CHE values of GoreSelect 57, NRE 211 and previously reported results on NR 112.

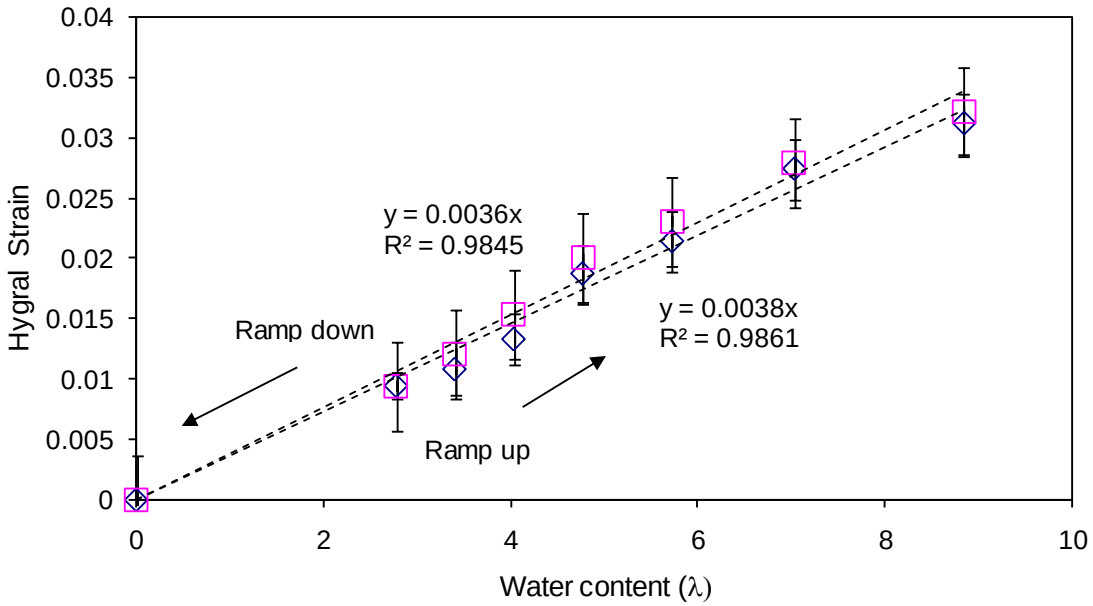

Figure 7.10 Strain in GoreSelect 57 membrane sample as the humidity was ramped up from dry condition to 90% RH (corresponding to water content of 8.84 units) and back down to dry condition at 70°C.

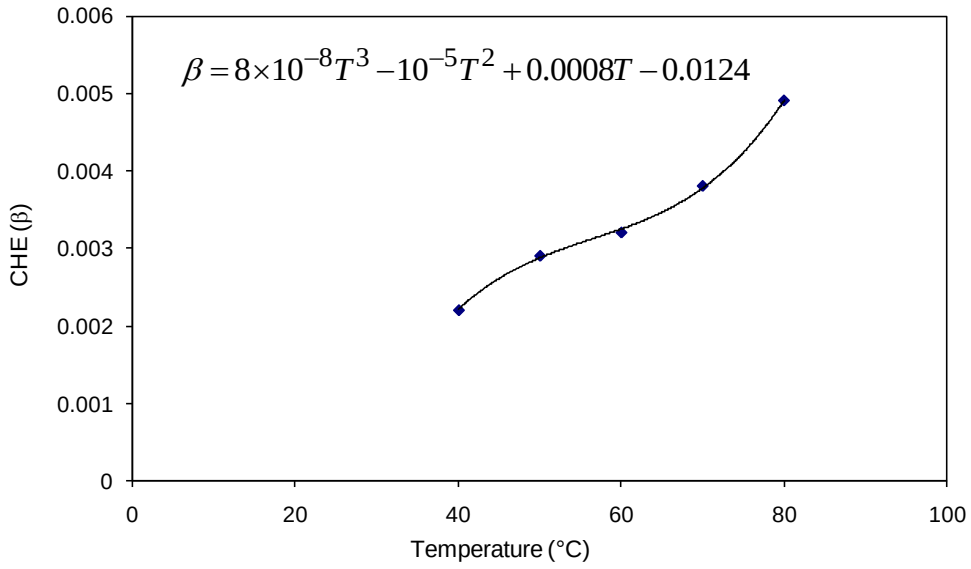

Figure 7.11 Coefficient of moisture expansion plotted against temperature for GoreSelect 57 membrane samples and fit with a cubic polynomial.

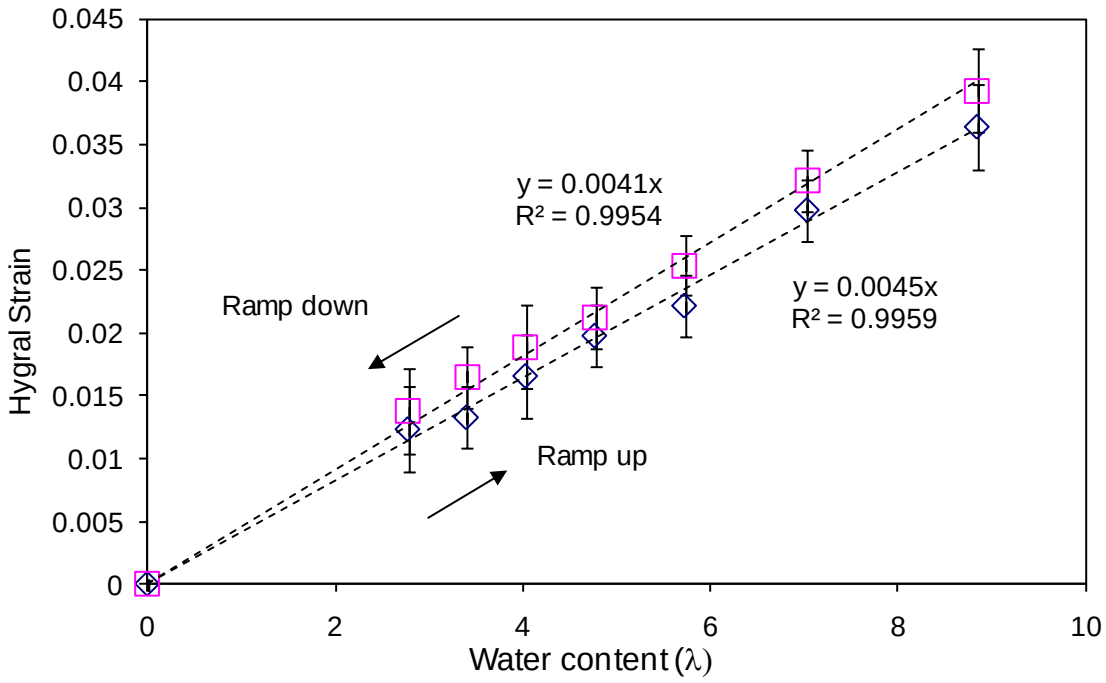

Figure 7.12 Strain in Nafion NRE 211 membrane sample as the humidity was ramped up from dry condition to 90% RH (corresponding to water content of 8.84 units) and back down to dry condition at 70°C.

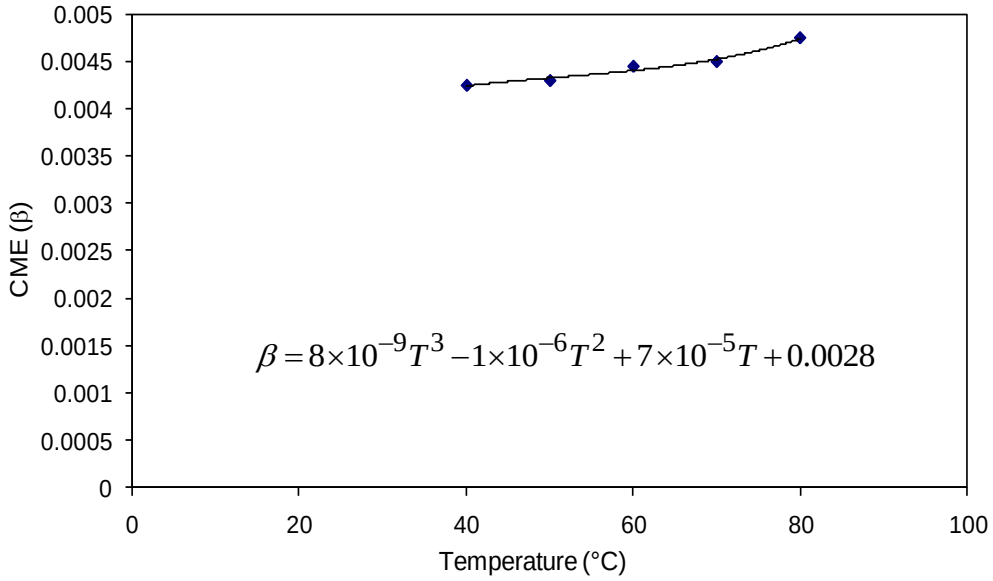

Figure 7.13 Coefficient of moisture expansion plotted against temperature for Nafion NRE 211 membrane samples and fit with a cubic polynomial.

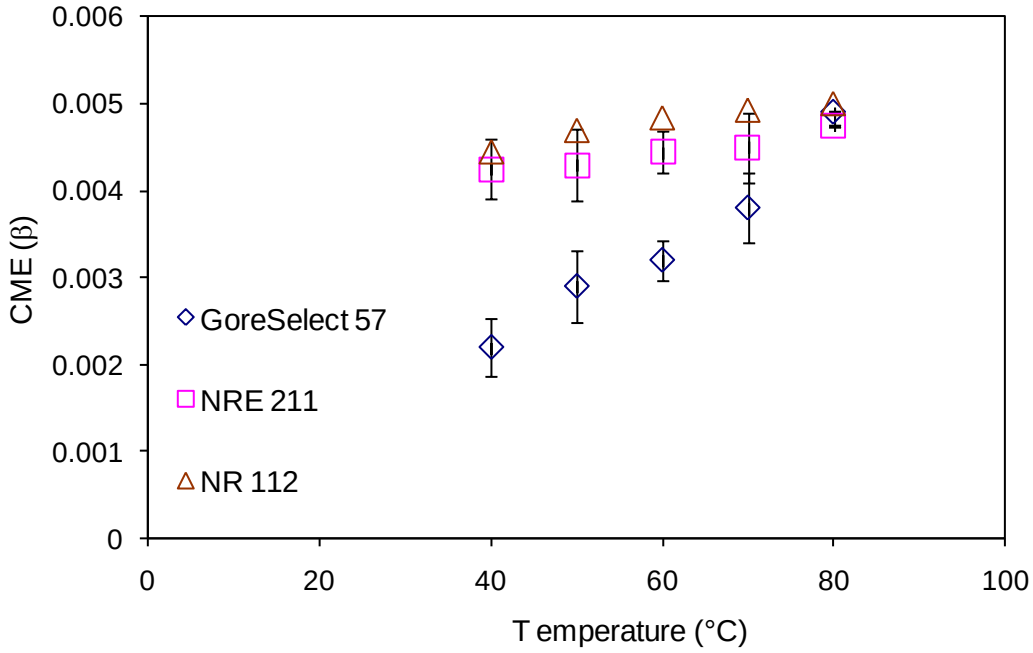

Figure 7.14 Coefficient of moisture expansion plotted against temperature for Nafion NRE 211, GoreSelect 57 and NR 112 membrane samples.

The CHE values for Nafion NRE 211 and NR 112 are quite close to one another at all temperatures under consideration; however, GoreSelect 57 shows a different behavior.

The CHE for GoreSelect 57 is much lower at and below 70°C and then suddenly rises to match those of Nafion materials at 80°C. This is surprising in that the reinforcing layer in the Gore 57 membrane should offer more resistance as temperature is increased and the ionomer becomes softer. Nonetheless, the DMA does appear to be a useful method to characterize the CHE, producing quite consistent results.

7.5 Summary and Conclusions

In order to understand the effects pretreatment might induce in Nafion NRE 211, membrane samples were pretreated at three different temperatures in deionized water (60, 80 and 100°C) followed by drying in a vacuum oven for about 12 hour. These pretreated membranes were then tested in conjunction with as-received membranes to see the differences. It was observed that viscoelastic properties of treated membrane change substantially. In both transient tensile relaxation tests and oscillatory dynamic tests, the modulus was found to increase with increase in temperature for treated samples. This effect is not as pronounced for the samples treated at 100°C, and disappears for the samples treated at 60°C. This leads us to a conclusion that specific morphological rearrangements of ionic and/or crystalline domains which are strengthened at 80°C, and break down if membrane is treated at 100°C. This appears to be a temperature dependent phenomenon as the membranes treated at 60°C did not show this unusual behavior either. The SAXS analysis did not reveal any specific information about the crystalline/ionic domains reorganization.

The effect of moisture in terms of induced hygral strains was measured as a function of relative humidity (RH) at various temperatures. Typically the membranes were subjected to a given RH followed by drying before reintroducing air with higher

RH. A Q800 DMA by TA Instruments successfully measured the hygral expansion of membranes. It was evident that treatment affects the hygral strains in membranes, with as-received membrane showing the least amount of strain under a given set of conditions. This procedure could give a useful information about the coefficient of moisture expansion, which could be used a stress model to predict stresses due to humidity changes developing in the membrane in a live fuel cell. But in order to do that, one needs to know the water content (λ), which has not been measured at this point.

7.6 Acknowledgements

The authors would like to express appreciation to the General Motors Corporation for supporting this work, as well as the Institute for Critical Technology and Applied Science (ICTAS) and the Engineering Science and Mechanics Department at Virginia Tech for providing additional support and facilities. Special thanks to Park Jong Keon for conducting SAXS experiments.

Appendix 1. Effect of Preconditioning on Relaxation Modulus of Nafion® NRE 211

Preconditioning PEMs prior to testing them could have substantial impact on the viscoelastic properties. A collaborative laboratory observed the following protocol prior to conducting stress relaxation experiments on Nafion® NRE 211 (referred to NRE 211 henceforth): preconditioning the membrane specimen with 90°C/10% RH for 12 hours of using a prestress of 0.026 MPa. The results obtained from the relaxation tests conducted after observing this protocol were significantly different than reported in chapter 4. In order to understand the origin of the discrepancy, we observed the protocol mentioned above prior to conducting the relaxation tests. It was observed that almost 1% strain was developed at the end of the preconditioning test. Although this strain is probably not going to be enough to make the membrane behave nonlinearly, the additional strain history might lead to higher modulus observed especially at high temperature. Figure A1.1 shows the effect of preconditioning. It can be seen that the preconditioning protocol may induce significant strain in the membrane sample, and as a result will have a different loading history than the membranes tested without preconditioning. To see whether the strain induced as shown in Figure A1.1 affects the relaxation modulus, a stress relaxation test was conducted at a strain level of 0.5% at 90°C/30% RH for 3000 minute right after the preconditioning. The relaxation modulus from this test was compared with that obtained from conducting relaxation tests using our protocol (90°C/30 minutes, no preload) as reported in chapter 4.

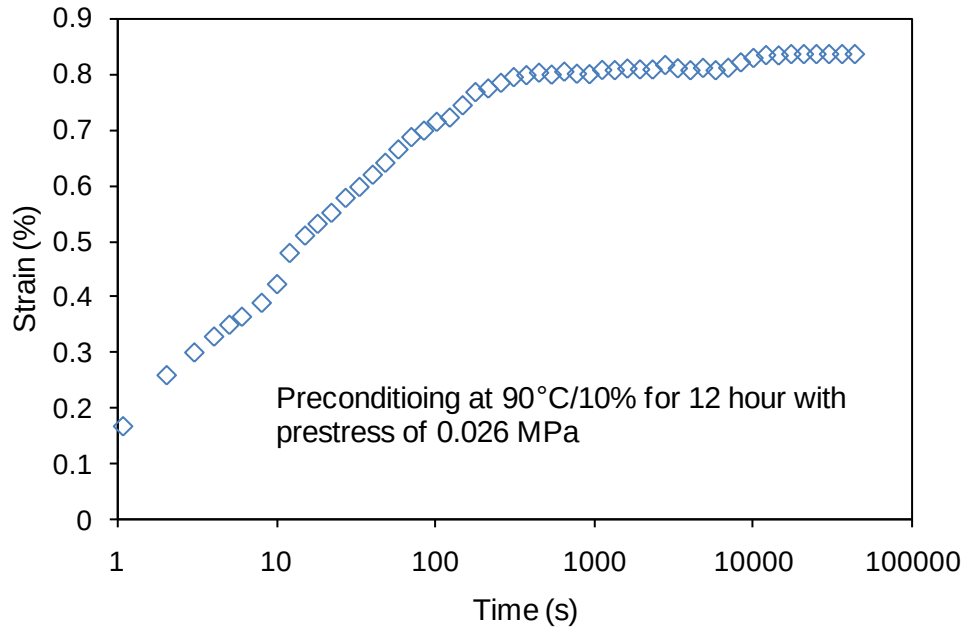

Figure A1.1 Creep strain induced in NRE 211 due to preconditioning at 90°C/10% RH.

Figure A1.2 shows the comparison stress relaxation modulus obtained with and without prior preconditioning. The relaxation modulus has been shifted by 1.9 decades (consistent with the shift shown from 70°C/30% RH to 90°C/30% RH) as reported in Chapter 4. The conditions and other details are shown as inset.

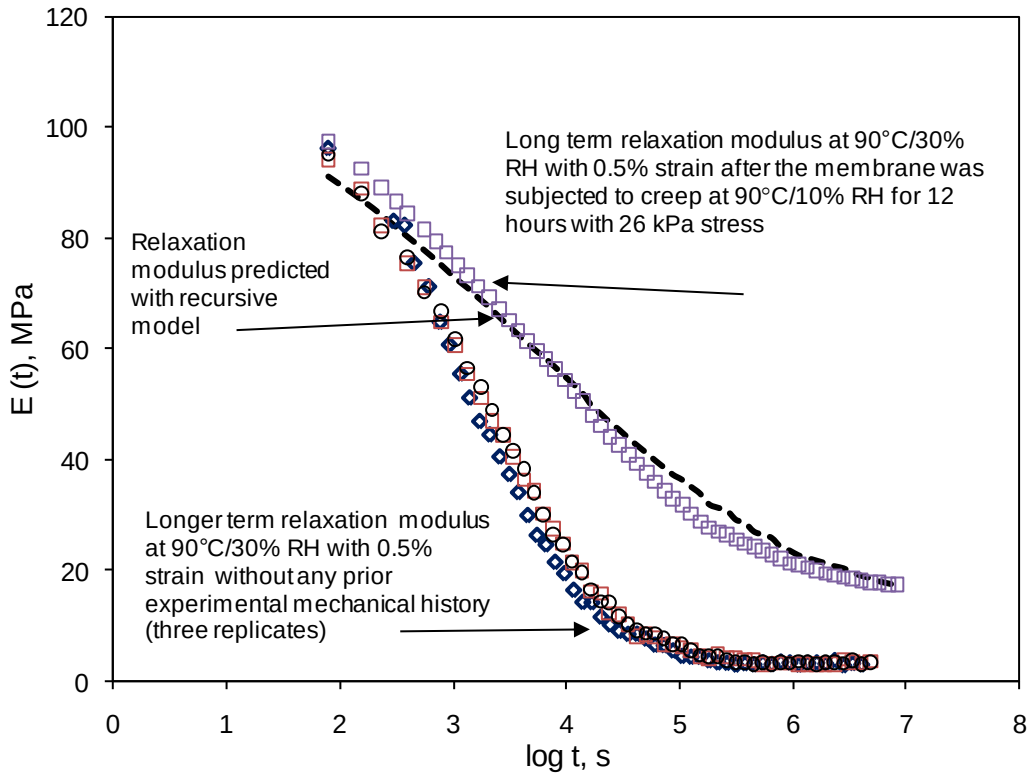

Figure A1.2 A comparison of stress relaxation modulus of NRE 211 obtained at 90°C/30% RH. Clearly preconditioning seems to have increased the modulus.

It is well known in the field of polymer science that any thermal/morphological/mechanical history can affect the subsequent viscoelastic properties measured. Even a small induced strain (~1%) is shown to have drastically increased the modulus especially at longer times. Effect of prior mechanical loading can be captured with Boltzmann hereditary integral as long as the material remains linear viscoelastic. Small strain levels such as 1% strain would probably not be enough for the membrane to behave nonlinearly and hence Boltzmann integral would still be valid [127]. A recursive program was written to capture the effect of strain history. The model predicted relaxation modulus values that match closely with the experimental value observed after preloading.

References

1. Hoogers, G., ed. *Fuel Cell Technology Handbook*. 1st ed. 2002, CRC Press.
2. O'Hayre, R., Suk-Won, C., Oletta, C., and Prinz, F.B., *Fuel Cell Fundamentals*. 2005, New York: John Wiley and Sons.
3. Berger, C., ed. *Handbook of Fuel Cell technology*. 1968, Prentice-Hall: Englewood Cliffs, NJ.
4. Larminie, J., and Dicks, A., *Fuel Cell Systems Explained*. 2000: John Wiley and Sons.
5. Carrette, L., Friedrich, K.A., and Stimming, U., *Fuel Cells-Fundamentals and Applications.* Fuel Cells, 2001. **1**(1): p. 5-39.
6. Liu, D., *Durability Study of Proton Exchange Membrane Fuel Cells via Experimental Investigations and Mathematical Modeling: PhD Dissertation*, in *Macromolecular Science and Engineering*. 2006, Virginia Polytechnic Institute and State University: Blacksburg.
7. Henderson Jr., K.R., *Evaluation of the Effect of Microporous Sublayer Design and Fabrication on Performance and Adhesion in PEM Fuel Cell Assemblies: MS Thesis*, in *Mechanical Engineering*. 2005, Virginia Polytechnic Institute and State University: Blacksburg, Va.
8. Berning, T., *Three-Dimensional Computational Analysis of Transport Phenomenon in a PEM Fuel Cell*. 1997, University of Victoria: Victoria, British Columbia.
9. *Development and Demonstration Plan: Planned Activities for 2003-2010 (Draft 6/3/03), Section 3.4.4*, Department of Energy. p. 7.
10. Wilkinson, D.P., and St-Pierre, J., *Handbook of Fuel Cells - Fundamentals, Technology and Applications*. 2003.
11. Cleghorn, S.J.C., Mayfield, D.K., Moore, D.K., Moore, J.C., Rusch, G., Sherman, T.W., Sisofo, N.T., and Beuscher, U., *A Polymer Electrolyte Fuel Cell Life Test: 3 Years of Continuous Operation.* Journal of Power Sources, 2006. **158**(1): p. 446-454.
12. Mittal, V.O., Kunz, H.R., and Fenton, J.M., *Effect of Catalyst Properties on Membrane Degradation Rate and the Underlying Degradation Mechanism in PEMFCs.* Journal of the Electrochemical Society, 2006. **153**(9): p. A1755-A1759.
13. Tang, Y., Sanatare, M.H., and Karlsson, A.M., *Stresses in Proton Exchange Membrane due to Hygrothermal Loading.* Journal of Fuel Cell Science and Technology, 2006. **3**: p. 119-124.
14. Tarasevich, M., Sadkowski, R.A., and Yeager, E., *Comprehensive Treatise of Electrochemistry*. Vol. 7. 1983, New York: Plenum Press.
15. Davies, D.P., Adcock, P.L., Turpin, M. and Rowen, S.J., *Stainless Steel as a Bipolar Plate Material for Solid Polymer Fuel Cells.* Journal of Power Sources, 2000. **86**(1-2): p. 237-242.
16. Makkus, R.C., Janssen, A.H., de Bruijn, F.A., and Mallant, R., *Use of Stainless Steel for Cost Competitive Bipolar Plates in the SPFC.* Journal of Power Sources, 2000. **86**(1-2): p. 274-282.
17. Wind, J., Spah, R., Kaiser, W., and Bohm, G., *Metallic Bipolar Plates for PEM Fuel Cells.* Journal of Power Sources, 2002. **105**(2): p. 256-260.

18. Schmidt, T.J., Paulus, U.A., Gasteiger, H.A., and Behm, R.J., *The Oxygen Reduction Reaction on a Pt/carbon Fuel Cell Catalyst in the Presence of Chloride Anions.* Journal of Electroanalytical Chemistry 2001. **508**(1-2): p. 41-47.
19. Curtin, D.E., Lousenberg, R.D., Henry, T.J., Tangeman, P.C., and Tisack, M.E., *Advanced Materials for Improved PEMFC Performance and Life.* Journal of Power Sources, 2004. **131**(1-2): p. 41-48.
20. Qiao, J., Saito, M., Hayamizu, K., and Okadaz, T., *Degradation of Perfluorinated Ionomer Membranes for PEM Fuel Cells during Processing with H_2O_2.* Journal of The Electrochemical Society 2006. **153**(6): p. A967-A974.
21. LaConti, A.B., Hamdan, M. and McDonald, R.C., ed. *Mechanism of Membrane Degradation*. Handbook of Fuel Cells - Fundamentals, Technology and Applications. 2001.
22. Stucki, S., Scherer, G.G., Schlagowski, S., and Fischer, E., *PEM water electrolysers: evidence for membrane failure in 100kW demonstration plants.* Journal of Applied Electrochemistry, 2004. **28**(10).
23. Verbrugge, M.W., and Hill, R.F., *Ion and Solvent Transport in Ion-Exchange Membranes.* Journal of the Electrochemical Society, 1990. **137**(3): p. 886-893.
24. Yeager, H.L., and Steck, A., *Cation and Water Diffusion in Nafion Ion Exchange Membranes: Influence of Polymer Structure.* Journal of the Electrochemical Society, 1981. **128**(9): p. 1880-1884.
25. Zawodzinski, T.A., Neeman, M., Sillerud, L.O., and Gottesfeld, S., *Determination of Water Diffusion Coefficients in Perfluorosulfonate Ionomeric Membranes.* The Journal of Physical Chemistry, 1991. **95**(15): p. 6040-6044.
26. Liu, H., Zhou, T., and Cheng, P., *Transport Phenomena Analysis in Proton Exchange Membrane Fuel Cells.* Journal of Heat Transfer, 2005. **127**: p. 1363-1379.
27. Uan-zo-li, J.T., *The Effects of Structure, Humidity and Aging on the Mechanical Properties of Polymeric Ionomers for Fuel Cell Applications*, in *Materials Science and Engineering*. 2001, Virginia Polytechnic institute and State University: Blacksburg.
28. Zawodzinski, T.A., Derouin, C., Radzinski, S., Sherman, R.J., Smith, V.T., Springer, T. E., and Gottesfeld, S., *Water Uptake by and Transport Through Nafion® 117 Membranes.* Journal of the Electrochemical Society, 1993. **140**(4): p. 1041-1047.
29. Weiss, R.A., Sen, A., Willis, C.L., and Pottick, L.A., *Block Copolymer Ionomers: 1. Synthesis and Physical Properties of Sulphonated Poly(styrene-ethylene/butylene-styrene).* Polymer, 1991. **32**(10): p. 1867-1874.
30. Hickner, M.A., *Transport and Structure in Fuel Cell Proton Exchange Membranes: PhD Dissertation*, in *Chemical Engineering*. 2003, Virginia Polytechnic Institute and State University: Blacksburg.
31. Nakamura, K., Hatakeyama, T., and Hatakeyama, H., *Relationship Between Hydrogen Bonding and Bound Water in Polyhydroxystyrene Derivatives.* Polymer, 1983. **24**(7): p. 871-876.
32. McConville, P., and Pope, J.M., *^1H NMR T_2 Relaxation in Ccontact Lens Hydrogels as a Probe of Water Mobility.* Polymer, 2001. **42**(8): p. 3559-3568.

33. Kim, Y.S., Dong, L., Hickner, M.A., Glass, T.E., Webb, V., and McGrath, J.E., *State of Water in Disulfonated Poly(arylene ether sulfone) Copolymers and a Perfluorosulfonic Acid Copolymer (Nafion) and Its Effect on Physical and Electrochemical Properties.* Macromolecules, 2003. **36**(17): p. 6281 - 6285.
34. Gierke, T.D., Munn, G.E., and Wilson, F.C., *The Morphology in Nafion Perfluorinated Membrane Products, as Determined by Wide- and Small-angle X-ray Studies.* Journal of Polymer Science, Part B: Polymer Physics, 1981. **19**(11): p. 1687-1704.
35. Moore, R.B., and Martin, C.R., *Chemical and Morphological Properties of Solution-cast Perfluorosulfonate Ionomers.* Macromolecules, 1988. **21**(5): p. 1334-1339.
36. Starkweather, H.W., *Crystallinity in Perfluorosulfonic Acid Ionomers and Related Polymers.* Macromolecules, 1982. **15**(2): p. 320-323.
37. Mauritz, K.A., and Moore, R.B., *State of Understanding of Nafion.* Chemical Reviews, 2004. **104**: p. 4535-4585.
38. Fujimura, M., Hashimoto, T., and Kawai, H., *Small-angle X-ray Scattering Study of Perfluorinated Ionomer Membranes. 1. Origin of Two Scattering Maxima* Macromolecules, 1981. **14**(5): p. 1309 - 1315.
39. Gebel, G., and Lambard, J., *Small-Angle Scattering Study of Water-Swollen Perfluorinated Ionomer Membranes.* Macromolecules, 1997. **30**(25): p. 7914 - 7920.
40. Gebel, G., and Moore, R.B., *Small-Angle Scattering Study of Short Pendant Chain Perfuorosulfonated Ionomer Membranes.* Macromolecules, 2000. **33**(13): p. 4850 - 4855.
41. de Almeida, S.H., and Kawano, Y., *Thermal Behavior of Nafion Membranes.* Journal of Thermal Analysis and Calorimetry, 1999. **58**(3): p. 569-577.
42. Hodge, I.M., and Eisenberg, A., *Dielectric and Mechanical Relaxations in a Nafion Precursor.* Macromolecules, 1978. **11**(2): p. 289-293.
43. Moore, R.B., and Martin, C.R., *Morphology and Chemical Properties of the Dow Perfluorosulfonate Ionomers.* Macromolecules, 1989. **22**(9): p. 3594 - 3599.
44. Su, S., and Mauritz, K.A., *Dielectric Relaxation Studies of Annealed Short Side Chain Perfluorosulfonate Ionomers.* Macromolecules, 1994. **27**(8): p. 2079 - 2086.
45. Yeo, S.C., and Eisenberg, A., *Physical Properties and Supermolecular Structure of Perfluorinated Ion-containing (Nafion) Polymers.* Journal of Applied Polymer Science, 1977. **21**(4): p. 875-898.
46. de Almeida, S.H., and Kawano, Y., *Ultraviolet-Visible Spectra of Nafion Membrane.* European Polymer Journal, 1997. **33**(8): p. 1307-1311.
47. Deng, Z.D., and Mauritz, K.A., *Dielectric Relaxation Studies of Water-containing Short Side Chain Perfluorosulfonic Acid Membranes.* Macromolecules, 1992. **25**(10): p. 2739 - 2745.
48. Deng, Z.D., and Mauritz, K.A., *Dielectric Relaxation Studies of Acid-containing Short-side-chain Perfluorosulfonate Ionomer Membranes.* Macromolecules, 1992. **25**(9): p. 2369 - 2380.

49. Kyu, T., Hashiyama, M., and Eisenberg, A., *Dynamic Mechanical Studies of Partially Ionized and Neutralized Nafion Polymers* Canadian Journal of Chemistry, 1983. **61**(4): p. 680-687.
50. Haddad, Y.M., *Viscoelasticity of Engineering Materials*. 1995, London, UK: Chapman and Hill.
51. Lakes, R.S., *Viscoelastic Solids*. 1998: CRC Press.
52. Riande, E., Diaz-Calieja, R., Prolongo, M.G., Masegosa, R.M., and Salom, C., *Polymer Viscoelasticity: Stress and Strain in Practice*. 2000, New York: Marcel Deker.
53. Christensen, R.M., *Theory of Viscoelasticity: an Introduction*. 2nd ed. 1982, New York: Academic Press.
54. Tschoegl, N.W., *The Phenomenological Theory of Linear Viscoelastic Behavior*. 1989: Springer-Verlag.
55. Tschoegl, N.W., *Time Dependence in Material Properties: An Overview*. Mechanics of Time-Dependent Materials, 1997. **1**(1).
56. Ferry, J.D., *Viscoelastic Properties of Polymers*. 3rd ed. 1980, New York: John Wiley and Sons.
57. Christensen, R.M., *A Thermodynamical Criterion for the Glass-Transition Temperature.* Transactions of the Society of Rheology, 1977. **21**(163).
58. Doolittle, A.K., and Doolittle, D.B., *Studies in Newtonian Flow. V. Further Verification of the Free-Space Viscosity Equation* Journal of Applied Physics, 1957. **28**(8): p. 901-905
59. Wenbo, L., Ting-Qing, Y., and Qunli, A., *Time-Temperature-Stress Equivalence and its Application to Nonlinear Viscoelastic Materials.* Acta Mechanica Solida Sinica, 2001. **14**(3): p. 195-199.
60. Van Gurp, M., and Palmen, J., *Time -Temperature Superposition for Polymeric Blends* Rheology Bulletin, 1998. **67**(1): p. 5-8.
61. Neilsen, L.E., and Landel, R.F., *Mechanical properties of Polymers and Composites*. 2nd ed. 1994, New York: Marcel Dekker.
62. Ward, I.M., and Hadley, D.W., *An Introduction to the Mechanical Properties of Solid Polymers*. 1998, New York: John Wiley and Sons.
63. Faucher, J.A., *Viscoelastic Behavior of Polyethylene and Polypropylene.* Journal of Rheology, 1959. **3**(1): p. 81-93.
64. Nakayasu, H., Markovitz, H., and Plazek, D.J., *The Frequency and Temperature Dependence of the Dynamic Mechanical Properties of a High Density Polyethylene.* Journal of Rheology, 1961. **5**(1): p. 261-283.
65. Mark, R., and Findley, W.N., *Nonlinear Variable Temperature Creep of Low-Density Polyethylene.* Journal of Rheology, 1978. **22**(5): p. 471-492.
66. Harper, B.D., and Weitsman, Y., *Characterization Method for a Class of Thermorheologically Complex Materials.* Journal of Rheology, 1985. **49**(1): p. 49-66.
67. Miller, E., *Introduction to Plastics and Composites*. 1996, New York: Marcel Dekker.
68. Djoković, V., Kostoski, D., and Dramićanin, M.D., *Viscoelastic Behavior of Semicrystalline Polymers at Elevated Temperatures on the Basis of a Two-*

process Model for Stress Relaxation. Journal of Polymer Science Part B: Polymer Physics, 2000. **38**(24): p. 3239-3246.
69. Onogi, S., Sasaguri, K., Adachi, T., and Ogihara, S., *Time-humidity Superposition in Some Crystalline Polymers.* Journal of Polymer Science, 1962. **58**(166): p. 1-17.
70. Brinson, H.F., and Brinson, L.C., *Polymer Engineering Science and Viscoelasticity: An Introduction*. 2008, New York, NY: Springer.
71. Sperling, L.H., *Introduction to Physical Polymer Science*. second ed. 1992, New York: John Wiley and Sons.
72. Scherer, G.W., *Relaxation in Glass and Composites*. 1986, New York: John Wiley and Sons.
73. Struik, L.C.E., *Physical Aging of Amorphous Polymers and Other Materials*. 1978, Amsterdam: Elsevier.
74. Kovacs, A.J., Aklonis, J. J., Hutchinson, J. M., and Ramos, A. R., *Isobaric Volume and Enthalpy Recovery of Glasses. II. A Transparent Multiparameter Theory*. Journal of Polymer Science: Polymer Physics, 1979. **17**(7): p. 1097-1162.
75. Lee, A., and McKenna, G.B., *Effect of Crosslink Density on Physical Ageing of Epoxy Networks.* Polymer, 1988. **29**(10): p. 1812-1817.
76. Schwarzl, F., and Silverman, A.J., *Time-Temperature Dependence of Linear Viscoelastic Behavior.* Journal of Applied Physics, 1952. **23**: p. 838.
77. Fesco, D.G., and Tschoegl, N.W., *Time-temperature Superposition in Thermorheologically Complex Materials.* Journal of Polymer Science 1971. **35**: p. 51-69.
78. Schapery, R.A. *A Theory of Nonlinear Thermoviscoelasticity based on Irreverible Thermodynamics*. in *The Fifth National Congress of Applied Mechanics* 1966. Minneapolis, MN.
79. Halpin, J.C., *Characterization of Orthotropic (Fiber-reinforced) Polymeric Solids*. 1969, University of Akron: Akron, OH.
80. Schapery, R.A., *Irreversible Thermodynamics and Variational Principles with Applications to Viscoelasticity*. 1962, California Institute of Technology: Pasadena, Ca.
81. Schapery, R.A., *On the Characterization of Nonlinear Viscoelastic Materials.* Polymer Engineering and Science, 1969. **9**: p. 295.
82. Findley, W.N., Lai, J.S., Onaran, K., *Creep and Relaxation of Nonlinear Viscoelastic Materials*. 1989, New York: Dover.
83. Schapery, R.A., *An Engineering Theory of Nonlinear Viscoelasticity with Applications.* International Journal of Solid Structures, 1966. **2**: p. 407.
84. Schapery, R.A. *On a Thermodynamic Constitutive Theory and its Application to various Nonlinear Materials*. in *IUTAM Symposium*. 1968. East Kilbride.
85. Smart, J., and Williams, J.G., *A Comparison of Single-Integral Nonlinear Viscoelastic Theories.* Journal of Mechanics and Physics of Solids, 1972. **20**(5): p. 313-324.
86. Bernstein, B., Kearsley, E.A., and Zapas, L.J., *A Study of Stress Relaxation with Finite Strain.* Transactions of the Society of Rheology, 1963. **7**(1): p. 391-410.

87. Popelar, C.F., Popelar, C.H. and Kenner,V.H., *Viscoelastic Material Characterization and Modeling for Polyethylene.* Polymer Engineering and Science, 1990. **30**(10): p. 577-586.
88. Knauss, W.G., and Emri, I., *Non-linear Viscoelasticity Based on Free Volume Considerations.* Computers & Structures, 1981. **13**: p. 123-128.
89. Knauss, W.G., and Emri, I., *Volume Change and the Nonlinearly Thermo-viscoelastic Constitution of Polymers.* Polymer Engineering and Science, 1987. **27**(1): p. 86-100.
90. Shay, R.M., and Caruthers, J.M., *A New Nonlinear Viscoelastic Constitutive Equation for Predicting Yield in Amorphous Solid Polymers.* Journal of Rheology, 1986. **30**(4): p. 781.
91. Popelar, C.F., and Liechti, K.M., *Multiaxial Nonlinear Viscoelastic Characterization and Modeling of a Structural Adhesive.* Journal of Engineering Materials Technology, 1997. **119**: p. 205-210.
92. Popelar, C.F., and Liechti, K.M., *A Distortion-modified Free Volume Theory for Nonlinear Viscoelastic Behavior* Mechanics of Time-Dependent Materials, 2003. **7**: p. 89-141.
93. Benziger, J.B., and Keverekidis, I.G. *Polymer Electrolyte Membrane Fuel Cell reactors*. in *AIChE Annual Meeting, San Fransisco, CA*. 2003.
94. Bossel, U.G., *Portable Fuel Cell Charger with Integrated Hydrogen Generator*. European Fuel Cell Forum Portable Fuel Cell Conference, Lucerne, 1999: p. 79-84.
95. Lai, Y.-H., Mittelsteadt, C.K., Gittleman, C.S., and Dillard, D.A. *Viscoelastic Stress Model and Mechanical Characterization of Perfluorosulfonic Acid (PFSA) Polymer Electrolyte Membranes*. in *The Third International Conference on Fuel Cell Science, Engineering and Technology*. 2005. Ypsilanti, Michigan.
96. Liu, W., Ruth, K. and Rusch, G., *Membrane Durability in PEM Fuel Cells.* Journal of New Materials for Electrochemical Systems, 2001(4): p. 227-231.
97. Stanic, V. *Mechanism of Pin-hole Formation in Membrane Electrode Assemblies for PEM Fuel Cells*. in *The Fourth International Symposium on Proton Conducting Membrane Fuel Cells, October*. 2004.
98. Webber, A., and Newman, J., *A Theoretical Study of Membrane Constraint in Polymer-Electrolyte Fuel Cell.* AIChE Journal, 2004. **50**(12): p. 3215-3226.
99. Costamagna, P., Yang, C., Bocarsly, A. B. and Srinivasan, S., *Nafion 115/Zirconium Phosphate Composite Membranes for Operation of PEMFCs above 100C.* Electrochimica Acta, 2002. **47**(7): p. 1023-1033.
100. Jorissen, L., Gogel, V., Kerres, J., and Garche, J., *New Membranes for Direct Methanol Fuel Cells.* Journal of Power Sources, 2002. **15**(2): p. 267-273.
101. Yang, C., Srinivasan, S., Arico, A. S., Cretti, P., Baglio, V., and Antonucci, V., *Composite Nafion/Zirconium Phosphate Membranes for Direct Methanol Fuel Cell operation.* Electrochemical and Solid State Letter, 2001. **4**(4): p. A31-A34.
102. Bauer, F., Denneler, S. and Willert-Porada, M. , *Influence of Temperature and Humidity on the Mechanical Properties of Nafion 117 Polymer Electrolyte Membrane.* Journal of Polymer Science, Part B: Polymer Physics, 2005. **43**: p. 786-795.

103. Eisenberg, A., and King, M., *Polymer Physics*, ed. A. Eisenberg, King, M. 1977: Academic Press, NY. 162-169.
104. Bauer, F., and Willert-Porada, M., *Microstructural Characterization of Zr-Phosphate Nafion Membranes for Direct Methanol Fuel Cell Applications.* Journal of Membrane Science, 2004. **233**: p. 141-149.
105. Young, S.K., and Mauritz, K.A., *Dynamic Mechanical Analyses of Nafion/ Organically Modified Silicate Nanocomposite.* Journal of Polymer Science, Part B: Polymer Physics, 2001. **39**(12): p. 1282-1295.
106. Diamant, Y., and Folman, M., *Influence of Dewetting on the Damping Properties of a Filled Polymer System: 1. Static Characterization.* Polymer, 1979. **20**(8): p. 1025-1033.
107. Sumita, M., Shizuma, T., Miyasaka, K., and Ishikawa, K., *Effect of Reducible Properties of Temperature, Rate of Strain, and Filler Content on the Tensile Yield Stress of Nylon-6 Composites Filled With Ultrafine Particles.* Journal of Macromolecular Science, Part B: Physics, 1983. **22**(4): p. 601-618.
108. Emri, I., and Pavsek, V., *On the Influence of Moisture on the Mechanical Properties of Polymers.* Materials Forum, 1992. **16**: p. 123-131.
109. Kohan, M.I., *Nylon Plastics*. 1973, New York: Wiley Interscience.
110. Shepherd, N.E., and Wightman, J. P., *Measuring and Predicting Sealant Adhesion: PhD Dissertation*, in *Chemistry*. 1995, Virginia Polytechnic Institute and State University: Blacksburg.
111. Dillard, D.A., Lai, Y. H., Budinski, M., and Gittleman, C. *Tear Resistance of Proton Exchange Membranes*. in *The Third Internation Conference on Fuel Cell Science, Engineering and Technology*. 2005. Ypsilanti, Michigan.
112. Patankar, K.A., Dillard, D.A., Ellis, M. W., Case, S. W., Lai, Y.H., Budinski, M. and Gittleman, C. *The Effect of Temperature and Moisture on the Viscoelastic Stress Relaxation of the Proton Exchange Membrane (PEM).* in *The Fifth International Conference on Fuel Cell Science, Engineering and Technology*. 2007. New York City, NY.
113. Patankar, K.A., Dillard, D.A., Ellis M.W., Case, S.W., Lai, Y., Budinski, M., and Gittleman, C., *Linear Hygrothermal Viscoelastic Characterization of Nafion® NRE211 Proton Exchange Membrane.* Journal of Membrane Science (in preparation), 2009.
114. Harper, B.D., Rao, J. M., Kenner, V. H. and Popelar, C. H., *Hygrothermal Effects upon Stress Relaxation in a Polyimide Film.* Journal of Electronic Materials, 1997. **26**(7): p. 798-804.
115. Ting, E.C., *Stress-Strain Relations of Thermorheologically Simple Materials Under Finite Deformations.* Transactions of The Society of Rheology, 1970. **14**(3): p. 297-305.
116. Shaw, M.T., and MacKnight, W. J., *Introduction to Polymer Viscoelasticity*. 3rd ed. 2005: Wiley Interscience.
117. Sung, Y., Yu, Z., and Neo, R. *Hygro-thermo mechanical Behavior of Molding Compounds at Elevated Environments*. in *Electronic Components and Technology Conference*. 2004. Singapore.
118. Mittelsteadt, C.K. *Water Uptake and Conductivity of Sulfonated Ionomers: Similarities and Limitations for PEM Fuel Cells*. in *Proceedings ACS Advances in*

Materials for Proton Exchange Membrane Fuel Cell Systems. 2003. Asilomar, CA.
119. Page, K.A., Cable, K.M., and Moore, R.B., *Molecular Origins of the Thermal Transitions and Dynamic Mechanical Relaxations in Perfluorosulfonate Ionomers.* Macromolecules, 2005. **38**: p. 6472-6484.
120. Osborn, S.J., Hassan, M.K., Divoux, G.M., Rhoades, D.W., Mauritz, K.A. and Moore, R.B., *Glass Transition Temperature of Perfluorosulfonic Acid Ionomers.* Macromolecules, 2007. **40**: p. 3886-3890.
121. *US Department of Energy: Cost Analysis of Fuel Cell Systems for Transportation*. Compressed Hydrogen and PEM Fuel Cell System [cited 2004; http://www1.eere.energy.gov/hydrogenandfuelcells/fuelcells/fc_challenges.html].
122. Lai, Y.-H., Mittelsteadt, C.K, Gittleman, C.S., and Dillard D.A., *Viscoelastic Stress Analysis of Constrained Proton Exchange Membranes Under Humidity Cycling.* Journal of Fuel Cell Science and Technology (ASME) (in press), 2008.
123. Flaggs, D.L., and Crossman, F.W., *Analysis of the Viscoelastic Response of Composite Laminates During Hygrothermal Exposure.* Journal Of Composite Materials, 1981. **15**(1): p. 21-40.
124. Knauss, W.G., and Kenner, V.H., *On the Hygrothermomechanical Characterization of Polyvinyl Acetate.* Journal of Applied Physics, 1980. **51**: p. 5131–5136.
125. Lai, Y.-H., and Dillard, D.A., *Mechanical Durability Characterization and Modeling of Ionomeric Membranes*. Handbook of Fuel Cells Volume 5: Advances in Electrocatalysis, Materials, Diagnostics and Durability, ed. A.W. Vielstich, Gasteiger, H., and Yokokama, H. 2009: John Wiley & Sons, Ltd.
126. Webber, A., and Newman, J., *Transport in Polymer-Electrolyte Membranes. I. Physical Model.* Journal of Electrochemical Society, 2003. **150**(7): p. A1008-A1015.
127. Patankar, K.A., Dillard, D.A., Ellis M.W., Case, S.W., Lai, Y., Budinski, M., and Gittleman, C., *Hygrothermal Characterization of the Viscoelastic Properties of Gore-Select® 57 Proton Exchange Membrane.* Mechanics of Time-Dependent Materials 2008. **12**: p. 221-236.
128. Satterfield, M., and Benziger, J., *Viscoelastic Properties of Nafion at Elevated Temperature and Humidity.* Journal of Polymer Science, Part B: Polymer Physics 2009. **47**: p. 11-24.
129. Majsztrik, P.W., Bocarsly, A.B., and Benziger, J.B., *Viscoelastic Response of Nafion. Effects of Temperature and Hydration on Tensile Creep.* Macromolecules 2008. **41**: p. 9849-9862.
130. Gittleman, C.S., Lai, Y. H., Lewis, C., and Miller, D. P. *Durability of Perfluorosulfonic Acid Membranes for PEM Fuel Cells*. in *AIChE*. 2005. Cincinnati, OH.
131. Li, Y., Quincy,J., Dillard, D.A., Case, S.W., Ellis, M.W., Lai, Y-H., Budinski, M., and Gittleman, C., *Characterizing the Fracture Resistance of Proton Exchange Membranes.* Journal of Power Sources 2008. **185**(1): p. 374-380
132. Liu, D., Kyriakides, S., Case S.W., Lesko, J.J., Li, Y., and McGrath, J.E., *Tensile Behavior of Nafion and Sulfonated Poly (arylene ether sulfone) Copolymers and*

its Morphological Correlations. Journal of Polymer Science, Part B: Polymer Physics, 2006. **44**: p. 1453-1465.
133. Satterfield, M., and Benziger, J., *Mechanical Properties of Nafion and Titania/Nafion Composite Membranes for Polymer Electrolyte Membrane Fuel Cells.* Journal of Polymer Science, Part B: Polymer Physics, 2006. **44**(16): p. 2327–2345.
134. Solasi, R., Zou, Y., Huang, X., Reifsnider, K., and Condit, D., *On Mechanical Behavior and in-plane Modeling of Constrained PEM Fuel Cell Membranes Subjected to Hydration and Temperature Cycles.* Journal of Power Sources, 2007. **167**(2): p. 366-377
135. Solasi, R., Zou, Y., Huang, X., and Reifsnider, K., *A Time and Hydration Dependent Viscoplastic Model for Polyelectrolyte Membranes in Fuel Cells.* Mechanics of Time-Dependent Materials, 2008. **12**: p. 15-30.
136. Springer, T.E., Zawodzinski, T.A., and Gottesfeld, S., *Polymer Electrolyte Fuel Cell Model.* Journal of the Electrochemical Society, 1991. **138**(8): p. 2334-2342.
137. Tang, Y., Sanatare, M.H., and Karlsson, A.M. *Stresses in Proton Exchange Membranes due to Hydration-Dehydration Cycles*. in *The Third International Conference on Fuel Cell Science, Engineering, and Technology*. 2005. Ypsilanti, MI.
138. Tang, Y., Sanatare, M.H., and Karlsson, A.M., *An Experimental Investigation of Humidity and Temperature Effects on the Mechanical Properties of Perfluorosulfonic Acid Membrane.* Materials Science and Engineering A, 2006. **425**(1-2): p. 297–304.
139. Zou, Y., *Hygrothermal Mechanical Properties and Durability of Ionomer Membranes*, in *Mechanical Engineering*. 2007, University of Connecticut: Storrs, CT.
140. Park, S., Lai, Y-H., Coupar, T., Patankar, K.A., Case, S.W., Ellis, M.W., and Dillard, D.A., *Transient Hygrothermal Viscoelastic Stress Analysis of Proton Exchange Membranes.* Journal of Power Sources (in press), 2008.
141. Doyle, M., and Rajendran, G., *Handbook of Fuel Cells Volume 3- Fundamentals, Technology and Applications*, ed. W. Vielstich, Gasteiger, H., and Lamm, A. 2003, New York City, NY: John Wiley & Sons.
142. Struik, L.C.E., *The Mechanical and Physical Ageing of Semicrystalline Polymers: 1.* Polymer, 1987. **28**: p. 1521-1533.
143. Struik, L.C.E., *Mechanical Behaviour and Physical Ageing of Semi-crystalline Polymers: 3. Prediction of Long Term Creep from Short Time Tests.* Polymer, 1989. **30**: p. 799-814.
144. Marand, H., Alizadeh, A., Sohn, S., Xu, J., Farmer, R., Prabhu, V., Cronin, S., and Velikov, V. *A Model for the Physical Aging of Semicrystalline Polymers Above T_g: Secondary Crystallization Induced Constraining Effects*. in *ANTEC*. 2001. Dallas, TX.
145. Huang, X., Solasi, R., Zou, Y., Feshler, M., Reifsnider, K., Condit, D., Burlatsky, S., and Madden, T., *Mechanical endurance of polymer electrolyte membrane and PEM fuel cell durability.* Journal of Polymer Science, Part B: Polymer Physics, 2006. **44**(16): p. 2346-2357.

146. Dillard, D.A., Straight, M.R., and Brinson, H.F., *The Nonlinear Viscoelastic Characterization of Graphite/Epoxy Composites.* Polymer Engineering and Science, 1987. **27**(2): p. 116-123.
147. Payne, D.B., Biskup, B.A., Letton, A., and Strganac, T.W. *Viscoelastic Characterization of Thin-Film Materials Using a Dynamic Mechanical Approach*. in *32nd Aerospace Sciences Meeting & Exhibit*. 1994. Reno, NV.
148. Wilbeck, J.S., *Viscoelastic Characterization of Thin Polyethylene Film*. 1981: Wallops Island, Va.
149. Henriksen, M., *Nonlinear Visocoelastic Stress Analysis - a Finite Element Approach.* Computers & Structures, 1984. **18**(1): p. 133.
150. Roy, S., and Reddy, J.N., *A Finite Element Analysis of Adhesively Bonded Composite Joints with Moisture Diffusion and Delayed Failure.* Computers & Structures, 1988. **29**(6): p. 1011.
151. Lai, J., and Bakker, A., *3-D Schapery Representation for Non-linear Viscoelasticity and Finite Element Implementation.* Computational Mechanics, 1996. **18**: p. 182.
152. Touati, D., and Cederbaum, G., *On the Prediction of Stress Relaxation from Known Creep of Nonlinear Materials.* Journal of Engineering Materials and Technology, 1997. **119**: p. 121.
153. Touati, D., and Cederbaum, G., *Post Buckling of Non-linear Viscoelastic Imperfect Laminated Plates Part I: Material Considerations.* Composite Structures, 1998. **42**: p. 33.
154. Li, R., *Non-linear Viscoelastic Stress and Fracture Analyses of Laminated Composites, PhD*. 1997, University of Washington.
155. Yi, S., Hilton, H.H., and Ahmad, M.F., *Non-linear Thermo-viscoelastic Analysis of Interlaminar Stresses in Laminated Composites.* Journal of Applied Mechanics (ASME), 1996. **63**: p. 218.
156. Yi, S., *Finite Element Analysis of Free Edge Stresses in Non-linear Viscoelastic Composites under Uniaxial Extension, Bending, and Twisting Loadings.* International Journal for Numerical Methods in Engineering, 1997. **40**: p. 4225.
157. Haj-Ali, R.M., and Muliana, A.H., *Numerical Finite Element Formulation of the Schapery Non-linear Viscoelastic Material Model.* International Journal for Numerical Methods in Engineering, 2004. **59**: p. 25.
158. Marklund, E., Varna, J., and Wallström, L, *Nonlinear Viscoelasticity and Viscoplasticity of Flax/Polypropylene Composites.* Journal of Engineering Materials and Technology, 2006. **128**: p. 527-536.
159. Lou, Y.C., and Schapery, R.A., *Viscoelastic Characterization of a Nonlinear Fiber-Reinforced Plastic.* Journal of Composite Materials, 1971. **5**: p. 208-234.
160. Pasricha, A., Van Duser, P., Tuttle, M.E., and Emery, A.F. *The Nonlinear Viscoelastic/Viscoplastic Behavior of IM6/5260 Graphite/Bismaleimide*. in *The Seventh International Congress on Experimental Mechanics*. 1992. Bethel, CT.
161. Tuttle, M.E., Pasricha, A., and Emery, A.F., *The Nonlinear Viscoelastic-Viscoplastic Behavior of Im7/5260 Composites Subjected To Cyclic Loading.* Journal Of Composite Materials, 1995. **29**(15): p. 2025-2046.

162. Zapas, L.J., and Crissman, J.M, *Creep and Recovery Behaviour of Ultra-high Molecular Weight Polyethylene in the Region of Small Uniaxial Deformations.* Polymer, 1984. **25**: p. 57-62.
163. Boyd, S.E., *Compression Creep Rupture of an E-glass/Vinyl Ester Composite Subjected to Combined Mechanical and Fire Loading Conditions: PhD Dissertation*, in *Engineering Science and Mechanics*. 2006, Virginia Tech: Blacksburg.
164. Cui, S.-Z., and Wang, S-Y., *Nonlinear Creep Characterization of Textile Fabrics.* Textiles Research Journal, 1999. **69**(12): p. 931-934.
165. Lin, W.S., Pramanick, A.K., and Sain, M., *Determination of Material Constants for Nonlinear Viscoelastic Predictive Model.* Journal of Composites Materials, 2004. **38**(1): p. 19-29.
166. Zaoutsos, S.P., Papanicolaou, G.C., and Cardon, A.H., *On the Non-linear Viscoelastic Behavior of Polymer-Matrix Composites.* Composites Science and Technology, 1998. **58**: p. 883-889.
167. Zaoutsos, S.P., Papanicolaou, G.C., and Cardon, A.H., *Further Development of a Data Reduction Method for the Nonlinear Viscoelastic Characterization of FRPs.* Composites: Part A, 1999. **30**: p. 839-848.
168. Lourakis, M., *Levenberg-Marquardt nonlinear least squares algorithms in C/C++* 2008, http://www.ics.forth.gr/~lourakis/levmar/.
169. Guedes, R.M., Marques, A.T., and Cardon, A.H., *Analytical and Experimental Evaluation of Nonlinear Viscoelastic-Viscoplastic Composite Laminates under Creep, Creep-Recovery, Relaxation and Ramp Loading.* Mechanics of Time-Dependent Materials, 1998. **2**: p. 113-128.
170. Hiel, C., Cardon, A.H., and Brinson, H.F, *Nonlinear Viscoelastic Response of Resin Matrix Composite Laminates*. 1984, NASA Contractor Report. p. 149.
171. Boyd, S.E., *Compression Creep Rupture of an E-glass/Vinyl Ester Composite Subjected to Combined Mechanical and Fire Loading Conditions*, in *Engineering Science and Mechanics*. 2006, Virginia Tech: Blacksburg.
172. Megnis, M., and Varna, J., *Micromechanics Based Modeling of Nonlinear Viscopleastic Response of Unidirectional Composite.* Composites Science and Technology, 2003. **63**(1): p. 19-31.
173. Megnis, M., and Varna, J., *Nonlinear Viscoelastic, Viscoplastic Characterization of Unidirectional GF/EP Composites.* Mechanics of Time-Dependent Materials, 2003. **7**(3): p. 269-290.
174. Lake, G.J., and Yeoh, O.H., *Measurement of Cutting Resistance of Rubber in Absence of Friction.* International Journal of Fracture, 1978. **14**(5): p. 509-526.
175. Gent, A.N., Lai, S.M., Nah, C., and Wang, C., *Viscoelastic Effects in Cutting and Tearing Rubber.* Rubber Chemistry and Technology, 1994. **67**(4): p. 610-618.
176. Gent, A.N., and Wang, C., *Cutting Resistance of Polyethylene.* Journal of Polymer Science Part B: Polymer Physics, 1996. **34**(13): p. 2231-2237.
177. Li, Y., Quincy,J., Dillard, D.A., Case, S.W., Ellis, M.W., Lai, Y-H., Budinski, M., and Gittleman, C. *Using a Knife Slitting Test to Measure the Fracture Resistance of Proton Exchange Membrane*. in *The 4th International Conference on Fuel Cell Science, Engineering and Technology*. 2006. Irvine, CA, USA.

178. Patankar, K.A., Dillard, D.A., Ellis M.W., Case, S.W., Lai, Y., Budinski, M., and Gittleman, C. *Characterizing Viscoelastic Properties of the Proton Exchange Membrane (Gore 57).* in *Society of Experimental Mechanics*. 2007. Springfield, MA.
179. Grohs, J.R., Li, Y., Dillard, D.A., Case, S.W., Ellis, M.W., Lai, Y-H., Budinski, M., and Gittleman, C., *Evaluating the Time and Temperature Dependent Biaxial Strength of Gore-Select(r) series 57 Proton Exchange Membrane Using a Pressure Loaded Blister Test.* Mechanics of Time Dependant Materials (under review), 2009.
180. http://www.fuelcellmarkets.com/content/images/articles/nae201.pdf. *DuPont™Nafion®PFSA Membranes NRE-211 and NRE-212 Perfluorosulfonic Acid Polymer: Product Information*. 2004 [cited.
181. Zawodzinski Jr., T.A., Springer, T.E., Davey, J., Jestel, R., Lopez, C., Valerio, J., and Gottesfeld, S., *A Comparative Study of Water Uptake by and Transport Through Ionomeric Fuel Cell Membranes.* Journal of the Electrochemical Society, 1993. **140**(7): p. 1981-1985.
182. Alberti, G., Narducci, R., and Sganappa, M., *Effects of Hydrothermal/thermal Treatments on the Water-uptake of Nafion Membranes and Relations with Changes of Conformation, Counter-elastic Force and Tensile Modulus of the Matrix.* Journal of Power Sources, 2008. **178**: p. 575-583.
183. Gebel, G., *Structural Evolution of Water Swollen Perfluorosulfonated Ionomers from Dry Membrane to Solution.* Polymer, 2000. **41**: p. 5829-5838.